ACTIVE AND SEMI-ACTIVE CONTROL OF CIVIL STRUCTURES UNDER SEISMIC EXCITATION

by

Enrique E. Matheu

Dissertation submitted to the faculty of the
Virginia Polytechnic Institute and State University
in partial fulfillment of the requirements for the degree of

DOCTOR OF PHILOSOPHY

in

Engineering Mechanics

APPROVED:

M. P. Singh, Chairman

C. A. Beattie

M. R. Hajj

S. L. Hendricks

S. Thangjitham

May, 1997
Blacksburg, Virginia

Keywords: Active control, semi-active control, sliding mode control.

ACTIVE AND SEMI-ACTIVE CONTROL OF CIVIL STRUCTURES UNDER SEISMIC EXCITATION

by

Enrique E. Matheu

Mahendra P. Singh, Chairman

Engineering Mechanics

(ABSTRACT)

The main focus of this study is on the active and semi-active control of civil engineering structures subjected to seismic excitations. Among different candidate control strategies, the sliding mode control approach emerges as a convenient alternative, because of its superb robustness under parametric and input uncertainties. The analytical developments and numerical results presented in this dissertation are directed to investigate the feasibility of application of the sliding mode control approach to civil structures.

In the first part of this study, a unified treatment of active and semi-active sliding mode controllers for civil structures is presented. A systematic procedure, based on a special state transformation, is also presented to obtain the regular form of the state equations which facilitates the design of the control system. The conditions under which this can be achieved in the general case of control redundancy are also defined. The importance of the regular form resides in the fact that it allows to separate the design process in two basic steps: (a) selection of a target sliding surface and (b) determination of the corresponding control actions. Several controllers are proposed and extensive numerical results are presented to investigate the performance of both active and semi-active schemes, examining in particular

the feasibility of application to real size civil structures.

These numerical studies show that the selection of the sliding surface constitutes a crucial step in the implementation of an efficient control design. To improve this design process, a generalized sliding surface definition is used which is based on the incorporation of two auxiliary dynamical systems. Numerical simulations show that this definition renders a controller design which is more flexible, facilitating its tuning to meet different performance specifications. This study also considers the situation in which not all the state information is available for control purposes. In practical situations, only a subset of the physical variables, such as displacements and velocities, can be directly measured. A general approach is formulated to eliminate the explicit effect of the unmeasured states on the design of the sliding surface and the associated controller. This approach, based on a modified regular form transformation, permits the utilization of arbitrary combinations of measured and unmeasured states. The resulting sliding surface design problem is discussed within the framework of the classical optimal output feedback theory, and an efficient algorithm is proposed to solve the corresponding matrix nonlinear equations. A continuous active controller is proposed based only on bounding values of the unmeasured states and the input ground motion. Both active and semi-active schemes are evaluated by numerical simulations, which show the applicability and performance of the proposed approach.

Dedication

All the efforts and hard work involved in the fulfillment of this task I dedicate to my parents and to Yazmin. This work would not have been possible without their love and constant support.

Acknowledgements

I want to express my most sincere thanks to my advisor, Dr. M. P. Singh, for all his help during the time I spent in Blacksburg. His technical guidance and continuous encouragement were vital elements in the completion of this work.

This gratitude also extends to Dr. C. Beattie for his active participation at the most critical times of this endeavor.

Thanks also to Dr. M. Hajj, Dr. S. L. Hendricks, and Dr. S. Tangjitham for serving in my committee and reviewing this dissertation.

I would also like to express my gratitude to some unique people that only in Blacksburg could be found, specially Daniel Liut, Diana Rubio, Caruso Averboch, Gustavo Maldonado, Raul Andruet, and Paul Prato. The moments shared during the past few years will always be cherished.

This research was supported by the National Science Foundation through Grants Nos. BCS-93-01574 and CMS-96-26850. This support is gratefully acknowledged.

Contents

List of Figures

List of Tables

Chapter 1

Introduction

1.1 Control of Civil Structures

The central problem of earthquake engineering is the design of civil engineering structures such that they can withstand the forces and accommodate the deformations that are induced during a seismic event. Obviously, the response of the system can always be limited by providing stronger structural members but in general the system is not designed to fully resist the design forces because this would be uneconomical. Therefore, it has been a common practice to generate more ductile designs, providing the means for adequate energy dissipation through the yielding of individual members and the generation of localized plastic hinges. Therefore, the occurrence of damage during a seismic event is unavoidable in the context of this design philosophy. The problem with this approach is that the permanent deformations in the structure surviving the seismic event may seriously affect its service life, leading to the need for expensive repairs. Therefore, alternative approaches are constantly investigated to produce structural designs that satisfy both safety and economic requirements.

Recently, the attention of the civil engineering community has focused on reducing forces and deformations in structures, through the methods of structural control, to realize

not only safer but also more economical structural designs. Structural control strategies are materialized by special devices which are added to the system to reduce the structural response in order to fulfill multiple objectives. These methods of response reduction can address not only the prevention of total failure or the limitation of damage but also they can be designed to provide comfort to the occupants of the structure. Depending on the mode of operation of these special devices, the structural response control methods can be broadly classified as passive, active and semi-active control approaches.

In the passive control methods, the idea is to deflect the seismic input energy from reaching the dominant modes of the structure by using base isolation or tuned mass dampers and/or to dissipate the vibration energy in localized elements called energy-absorbing devices. Passive control schemes have the advantage of requiring little maintenance. Also, they do not depend on an external power supply to operate. The only problem with passive control methods is their inherent limitations to be fine-tuned for efficient designs against excitations of different characteristics.

The active control methods, on the other hand, reduce the structural response by applying counteracting control forces externally. In active control schemes, sensing devices are used to measure the external disturbance and/or the structural response. This information is fed into the controller which synthesizes the measured quantities and structural parameter information to generate the corresponding control signal. This signal is then input to the actuators which, if driven by an adequate power source, are able to produce the desired control action. The high control authority characteristic of the active control approaches can provide important response reductions even under severe dynamic loads. However, when compared to passive control systems, the complexities and uncertainties associated with active control schemes are much greater. Also, an important issue is the

magnitude of the control forces required to achieve meaningful levels of response reduction, especially in the case of civil structures.

In the semi-active control methods, the counteractive control forces are created by reactive forces in special dampers and/or stiffeners added to the structure. The temporal regulation of the resulting reactive force can be done, for example, by simple opening and closing of fluid passages or by changes in magnetic flux or electrical current, depending on the principle governing the behavior of the device. Semi-active control approaches have the advantage that this force regulation operations usually require a small power source. These methods represent a compromise between fully active control and passive control approaches.

1.2 Literature Survey

In the sequel, a brief description of developments and related works in the areas of passive, active and semi-active control of civil engineering structures is presented.

1.2.1 Passive Control

The most relevant applications of passive control schemes to civil engineering structures are *base isolation systems*, *tuned mass dampers* and *added energy-absorbing devices*. The principle behind base isolation is the increase of the fundamental period of the structure, moving it away from the high energy content region of the seismic input and thus reducing the transmission of energy to the first vibration mode. Base isolation systems generally are constituted by elastomeric bearings or sliding bearings, which are stiff and strong enough to support the vertical loads but quite flexible in the horizontal direction [63]. Besides flexibility, these systems also have important energy absorbing capabilities provided by the high damping of the elastomeric bearings or the frictional behavior of the sliding bearings.

This added damping becomes important to reduce the response in the case of excitations with significative energy in lower frequency ranges [12].

Tuned mass dampers or vibration absorbers basically consist of a moving auxiliary mass attached to the primary structure. The seismic input energy is transformed into kinetic energy of the moving mass, which is properly designed to induce dynamic forces opposing the motion of the primary system. The advantage of this behavior is clearly seen from the frequency response function of the resulting system: an antiresonance effect is generated at the frequency at which the device is tuned and two new smaller resonance peaks appear surrounding this frequency. To further reduce these peaks, the connection of the moving mass to the primary structure is usually provided with energy dissipation characteristics [91]. These devices have found wide application in mechanical engineering for systems subject to narrow band excitations and extensive research has been done to determine the frequency tuning and damping characteristics providing optimum performance [93, 94]. In civil engineering applications, tuned mass dampers are usually tuned to the first natural period of the structural system. Therefore, they are most effective in those situations where the first mode contribution to the response is dominant [75]. This is generally the case for tall and slender structural systems. In the case of earthquake excitations, due to the broader frequency content of the input, the moving-mass effect has been reported not to be very effective; the role played by the damping characteristics of the tuned mass damper then becomes important [92]. Alternative solutions based on the use of multiple tuned mass dampers has been proposed to improve the performance under wide band excitations [30].

Finally, the third form of passive protection is given by added energy-absorbing devices. They are used to induce localized energy dissipation. Some of the most common energy-

absorbing devices are friction dampers, fluid viscous dampers, metallic yielding elements and viscoelastic dampers [63]. Passive approaches have found applications in engineering practice, not only in structural retrofitting but also in new designs. Several examples can be cited illustrating the application of passive protective systems in buildings and bridges [12, 63].

1.2.2 Active Control

As mentioned before, active control schemes reduce structural response by direct application of external counteracting forces. Among the different alternatives suggested to apply the forces required by the control law, the most common ones are the *active tuned mass damper*, the *active mass driver*, the *hybrid mass damper* and the *active tendon system*. The active tuned mass damper is basically a passive tuned mass damper equipped with hydraulic actuators acting between the tuned mass and the primary system [102]. The active operation of the tuned mass damper increases its effectiveness in response reduction with respect to the corresponding passive operation, which is generally tuned to the first structural period. The active mass driver (or proof-mass actuator) consists only of the auxiliary mass connected to the reaction wall of the building only by the actuation system, with no significant passive tuning effect. A hybrid mass damper is a general definition which includes any form of moving-mass-based device that combines active and passive actuation modes. In this sense, the active tuned mass damper could be considered a hybrid device [44]. An interesting hybrid device was proposed by Sakamoto and Kobori [70], consisting of a small active mass driver acting on top of a passive tuned mass damper. In general, the active mass driver is more effective in reducing the contributions to the response of all vibration modes, whereas the hybrid devices are more efficient in neutralizing the participation of those modes at which the passive component is tuned [44]. Finally, the active

tendon system or active bracing system consists of prestressed tendons or structural braces whose tensions are controlled by hydraulic actuators [76].

In general, the development of algorithms for active control has been done quite independently of the characteristics of the actuation devices. In many cases, the algorithms are developed under the assumption of unconstrained availability of the required control actions. Obviously, the dynamic characteristics and limitations of the actuators will influence the performance of the resulting system and some studies have included these effects in the design of the control law. But in general, it is fair to say that in active control strategies the actuation device does not condition or determine the selected algorithm. This fact can be thought, in part, as inherited from other engineering disciplines, such as electrical, mechanical or aerospace engineering, where the practical feasibility of the required control actions may have not been a critical issue. In the case of control of civil structures, however, the practical feasibility is a paramount issue.

As mentioned by Yang and Soong [102], the response control of civil engineering structures is a problem with exceptional characteristics. This is due to the size of the object to be controlled and the uncertain nature of the excitations, which differentiate it from the control problems arising in aerospace, mechanical and electrical engineering. The idea of using some form of control actions to limit the response of civil engineering structures started to emerge back in the early 1960s [41]. But it is in the pioneer paper by Yao [119] in 1972 where the concept of active structural control is clearly formulated. Since at the design stage it is impossible to exactly predict the dynamic disturbances such as ground motion or wind forces, the structure itself must react during to resist these environmental forces. This concept constituted the foundation for the subsequent research developments. In the sequel, the most relevant contributions in the area of active structural control are

classified and briefly reviewed.

Linear Optimal Control: Many of the first control algorithms proposed to be used in civil engineering applications were based on classical results of optimal control theory [10, 52, 67, 98, 99, 120]. In the optimal control problem, the control actions are calculated by minimizing a specified cost or performance index. The performance index is a functional usually expressed in the form of an integral over a given time interval. When the system is linear and the cost is quadratic in the system states and the control signals, the problem is referred to as the linear quadratic regulator (LQR) problem. The determination of the optimal control law can be done using either a variational approach or the method of dynamic programming [40]. The variational technique will lead to a two point boundary value problem whose solution determines the optimal control. On the other hand, dynamic programming will lead to a partial differential equation that must be satisfied by the optimal control, known as the Hamilton-Jacobi-Bellman equation. In both cases, when the system is affected by an external disturbance, the optimal solution is given by a control law in the form of time-varying state feedback and feedforward components. The time-varying feedback must be determined by solving a nonlinear matrix differential equation, known as the Riccati equation. The feedforward component must be obtained by solving a system of first order differential equations with time-varying coefficients and whose forcing term depends on the external excitation. The problem is that the resulting feedforward component of the control is not causal. This differential system must be solved backwards in time, requiring the future knowledge of the disturbance, which is not feasible in the case of an seismic event. As a result of this, the application of optimal control to the problem of control of civil structures subjected to seismic excitation is done suboptimally, without consideration of the external excitation.

Neglecting the external excitation, the optimal control is given only by the feedback component. Note also that even for a time-invariant system, the optimal control law is time-varying, increasing the complexity of the resulting control system. Usually, a time invariant feedback control law is generated by assuming an infinite horizon of the optimization problem. In this case, the determination of a constant feedback gain must be done by solving the steady-state version of the matrix differential Riccati equation, known as the algebraic Riccati equation. The use of an infinite time interval brings into consideration the stability of the resulting controlled system. A solution of the Riccati equation generating an asymptotically stable closed-loop system is guaranteed to exist only if the system satisfies stabilizability and detectability conditions [2]. As mentioned before, in the case of structures subjected to seismic disturbances, the solution provided by the infinite horizon LQR formulation is not a truly optimal approach as it ignores the input excitation terms in the optimization process. Nevertheless this approach has been repeatedly used in the structural control community as a convenient and useful tool to generate stable controllers in both analytical and experimental research.

Observers and Output Feedback: A major drawback of the optimum control law is that it was obtained under the assumptions that all the states are available to generate the control actions. It is, however, unreasonable to expect that the state vector can be measured in their entirety. Usually the available information is arranged in the form of an output vector whose dimension is smaller than the number of states. Therefore, some form of state estimation must be implemented. In general, a full-order observer consists of a model of the original system, excited by the difference between the actual measurements and the estimated measurements. The structure of the observer is defined by a gain matrix which acts as a design parameter and it has to be selected appropriately to achieve some

desired estimation performance. The control law is then based on the estimated states and the resulting closed-loop system has a dimension twice the dimension of the original system. The closed-loop dynamics depends on the selection of the gain matrices defining the control law and the observer. Based on the so-called separation principle, the design of the controller and the observer can be carried out independently of each other [25].

The design of the observer can be performed in some optimal manner, provided that the problem is reformulated in a stochastic setting. In this case, random disturbances and measurement errors are incorporated into the formulation in the form of white noise processes. The resulting stochastic regulator problem is known as the linear quadratic Gaussian (LQG) problem [16]. Under these conditions, the optimal gain matrix for the observer is obtained as the solution of the so-called filter algebraic Ricatti equation. The incorporation of the observer, however, reduces the stability margins considerably when compared to the full state feedback LQR solution. Supposedly optimal estimated-feedback controllers, were often found to give poor performance, or even unstable behavior, in real-world applications because of high sensitivity to modeling errors. Therefore, LQG-based designs could easily fail to work in environments with model uncertainties because of this lack of robustness.

An alternative to the observer-based design for the case of limited measurements is the direct (or static) output feedback approach. In this case, the control actions are directly generated by multiplying the sensor outputs by an appropriately selected gain matrix [4]. The design of this matrix can be performed in some optimal sense by neglecting the external disturbance and minimizing an integral performance index with respect to the initial state of the system. In this case, it was shown by Levine and Athans [48] that the design problem reduces to the solution of a static constrained optimization problem. A special

case of output feedback is represented by direct velocity feedback with collocated sensors and actuators [5]. This means that the measurements are obtained using velocity sensors, whose number is equal to the number of actuators. Under these conditions, it can be shown that a positive semi-definite gain matrix will render a closed-loop system unconditionally stable in the absence of sensor and actuator dynamics.

Modal Control: The large number of degrees of freedom needed to obtain realistic models of engineering structures motivated the so-called modal control approach [3, 55]. This control strategy is concerned with the control of a critical subset of modes of vibration of the structural system, while leaving the remaining (or residual) modes uncontrolled [11]. The critical modes can be regarded as defining a reduced-order subsystem for which an appropriate controller is to be designed [3]. If the equations of motion can be decoupled using the corresponding modal matrix, then the dynamics of the system can be described in terms of two subsystems corresponding to the controlled and residual modes. In this context, the residual subsystem could also be interpreted as representing any unmodeled dynamics with linear characteristics.

As mentioned before, the objective of the modal control strategy is to shape the dynamics of the controlled subsystem. In the so-called coupled modal control approach, this is achieved by directly designing a control vector which is a function of the modal coordinates and/or the modal velocities corresponding to the controlled modes. Another alternative is to further exploit the diagonal structure of the controlled subsystem by defining a decentralized control input such that each component of the control is designed independently to achieve some desirable objective for each corresponding modal coordinate. This approach is called independent modal control or control by modal synthesis [54]. The effectiveness of this last alternative depends on the number of modes to be controlled and the number

of actuators. In most cases, the number of control devices is usually limited by practical and economic reasons. If the number of actuators is smaller than the number of controlled modes, then this approach can not generate a genuine independent modal control scheme, because the control actions recouple the otherwise independent equations of the controlled subsystem. As a consequence of this, the closed-loop system will show some degradation in performance, this effect becoming more pronounced as the number of controllers decreases with respect to the number of controlled modes [55].

In general, the control signal will have the form of a feedback law in terms of the modal coordinates and/or the modal velocities corresponding to the controlled modes. In practical implementations, these modal coordinates usually will be estimated from available measurements but the sensor outputs will be contaminated with information of the residual subsystem. This effect is known as observation spillover. Additionally, once the controller is implemented in the real system, it will not only affect the controlled subsystem but also excites any unmodeled dynamics, represented by residual subsystem. This effect is known as control spillover. These effects, representing interactions with the residual subsystem, may produce serious degradation of performance. The observation spillover effect may even lead to an unstable closed-loop system [4].

Instantaneous Optimal Control: In the control of structures subjected to seismic disturbances, the standard linear optimal control solution is obtained by neglecting the input excitation terms in the optimization process. An approximated approach proposed by Yang and co-workers [100] and known as instantaneous optimal control, attempts to include the effect of the nonstationary disturbance. In this approach, past information regarding the input disturbance is included in the calculation of the control actions. This control method is based on a discrete-time approximation of the system dynamics. This

can be easily done using the transition matrix approach for the case of linear systems, but it can be also extended to nonlinear systems by employing numerical integration techniques. The method is based on the search for a control minimizing an instantaneous performance measure, but this formulation does not seem to render a consistently posed problem. The response of the system is expressed as an approximation for an interval Δt. The optimal control action is obtained using this approximated dynamics as constraint equations. But when $\Delta t \to 0$ and the dynamics of the system is described exactly in terms of differential equations, the solution of the problem becomes trivial because the minimizing control is equal to zero. Therefore, the only way to obtain a nonzero solution is by arbitrarily enforcing $\Delta t \neq 0$ while imposing the dynamic constraints in the form of approximated evolution equations instead of differential state equations.

In Ref. [101] this technique is applied to nonlinear structures by solving the equations of motion by using the Wilson-θ method. The effectiveness of the proposed approach was numerically evaluated for several example structures. The effects of localized inelastic behavior induced by rubber bearings and distributed nonlinearity generated by elastoplastic story stiffness characteristics were investigated. Later, a parametric sensitivity study was conducted to investigate the effect of uncertainties in the efficiency of the control algorithm [103]. The effectiveness of optimal control and instantaneous optimal control was evaluated with respect to changes in the stiffness and damping characteristics of a nominal linear structure subjected to seismic excitation.

Motivated by the fact that these instantaneous optimal control algorithms did not guarantee the stability of the closed-loop system, an improved procedure based on Lyapunov's direct method was proposed by Yang et al. [104] for the determination of the feedback gain matrix . A condition for stability is satisfied if the symmetric feedback gain matrix defining

the control law is obtained as the solution of an associated algebraic Riccati equation. In a follow-up work [105], this formulation is extended to control hysteretic systems with velocity and acceleration feedback. The hysteretic behavior is modeled using the Bouc-Wen model. Assuming that the uncontrolled structure is stable around the zero initial conditions, the nonlinear dynamics is linearized with respect to the initial equilibrium state to obtain a time invariant feedback law.

Predictive Control: Another approach to formulate an optimal control problem is given by the so-called predictive control or receding-horizon control [16]. The basic idea is to consider a continuously moving performance index in which the final time moves along with the evolution of the system. In this approach, at any given time t, one optimizes for a future interval of duration Δt. This types of solutions are very useful when the evolution of the external disturbance can be identified or predicted for a finite future interval Δt. Rodellar and co-workers [65, 66] presented a digital control scheme based on these ideas. In their approach, an optimization horizon is defined for each sampling instant. A discrete-time model is used to predict the response of the system and a sequence of control actions is obtained such that some performance index is minimized. The effectiveness of this approach was evaluated by numerical simulations and experimental verifications.

Nonlinear Optimal Control: An interesting extension of the LQR-based approach is based on the use of a nonlinear performance index [35]. This approach aims to an improved control of the peak responses which usually occur in the initial stages of the seismic motions. The classical LQR approach is effective in controlling the time-averaged norms of the response, but not very effective in controlling the peak response. In this form of nonlinear optimal control, a higher order performance function with higher order

state vector terms more sensitive to higher response values, is used. Several forms of this nonlinear control law have been proposed in the literature. Tomasula et al. [84] used a performance index which is quartic in the states and quadratic in the control actions. The solution is obtained in form of a series expansion and achieves a polynomial feedback form. Numerical simulations using a SDOF system showed that the nonlinear control attains better reduction of peak responses but at the expense of higher control actions, when compared with the linear optimal solution. Soong and his co-workers [96] adopted an heuristic choice of the cost function such that the feedback gain matrix can still be obtained in terms of the solution of a standard Riccati equation. Their effectiveness is demonstrated with analytical and scaled experimental tests on a three story structural model.

In the previous discussions, it has been assumed that there were no bounds on the admissible control values (unconstrained control problem). When the admissible control actions are subject to constraints, the optimal control must be obtained through the application of Pontryagin's minimum principle [40]. This principle states that the optimal control must minimize a scalar function known as the Hamiltonian with respect to any other admissible control action. The application of Pontryagin's minimum principle to the minimization of a quadratic performance index under admissible control constraints will render a nonlinear control law. The optimal solution is obtained in the form of a discontinuous or switching control law, known as bang-bang control [55], and it is characterized by the fact that the control signal stays always on the boundary of the admissible set, taking only the limit prescribed values. Since the presence of the excitation is neglected, the resulting control law is not optimal with respect to the corresponding disturbance rejection problem.

Lyapunov Control: A more convenient way to design a not-necessarily optimal controller in the presence of control constraints is provided by Lyapunov's direct method. In

this approach, the idea is to find a suitable controller that guarantees the stability of the closed-loop system by forcing the time derivative of a proposed positive definite scalar function to be negative definite. The existence of such a function, referred to as a Lyapunov function, is sufficient to guarantee the asymptotic stability of the controlled system. In general, a Lyapunov function is not unique for a given system, and indeed many different such functions can be found for a stable system [7]. An application of these ideas is presented by Wu and Soong [97]. The discontinuous control law is approximated with a continuous function to avoid high-speed switching requirements on the force delivery systems. Experimental tests were conducted on a three story structural model and the results demonstrated again the effectiveness of nonlinear control schemes in reducing peak responses.

Pulse Control: Another approach based on not-necessarily optimal discontinuous control actions is the so-called pulse control approach. Several alternative schemes have been proposed [53, 85, 86] consisting essentially of impulsive actions which are applied to the structure when a specified treshold response is exceeded. These pulse actions are generally applied separated by time intervals which are similar to the fundamental period of the structure. The idea is to break the continuous buildup of kinetic energy mostly associated with the lower modes of vibration of the system. An application to inelastic structures was presented by Reinhorn and co-workers [64]. The structural response is estimated at each time step using the Newmark-β integration algorithm. If the response is forecasted to exceed a given limit, a correcting force is applied. A combined algorithm was proposed by Pantelides and Nelson [60] for control of nonlinear systems. In this approach, both an instantaneous optimal control law and a pulse control scheme are developed by approximating the nonlinear equations of motion in terms of difference equations. When a given structural response quantity surpasses a prescribed limit, the pulses are activated. Below

the treshold level, the control actions are governed by the instantaneous control algorithm.

Neural Network Control: A totally different framework for the formulation of a control algorithm is provided by the so-called learning control methods, which are not based on an explicit mathematical representation of the structural system [36]. In this context, the use of controllers based on neural networks have been proposed by several researchers [23, 36, 95]. Basically, a neural network consists of a large number of interconnected processing units. Each unit receives the information transmitted by connecting units, and these inputs are assigned with different weights. Depending on the summation of the weighted signals being above or below some specified level, an output signal is forwarded to other units in the architecture [95]. In the so-called back-propagation neural networks the processing units are arranged in layers, with no sharing of information within a given layer. For a given pattern of processing units, the final output of the neural network is determined by the weights assigned to the interconnecting pathways. These weights represent the "knowledge" of the neural network and they are assigned through a adaptive process known as learning. The learning process is usually done by repetitive training procedures in which the errors between the target and the network outputs are minimized by regression fitting techniques. A neural control scheme to reduce the response of a nonlinear hysteretic structure was proposed by Faravelli and Venini [23]. The control system is based on two different neural networks that are conveniently trained to learn the forward and the inverse dynamics of the system, such that the appropriate control action can be determined to counteract the effect of the external disturbance.

H_2/H_∞ **Control:** The control system should be able to perform well under modeling and measurement uncertainties which are inevitable in real life practical implementations.

In the case of linear structures, the modeling of the dynamic behavior of the system is frequently done in terms of transfer functions which are obtained as the result of an identification process. Also, external disturbances are often modeled as stochastic processes with a frequency domain description. These representations naturally encourage the definition of performance specifications in the frequency domain [77]. A typical example of these specifications is the requirement of reduction of control authority in high frequency regions where the system's model is usually most uncertain. In this context, frequency domain optimal control techniques such as H_2/LQG and H_∞ approaches constitute a natural framework for the controller synthesis problem. In the H_2/LQG control approach, a vector of controlled or regulated outputs is defined as a linear combination of the system states and the control components. Frequency domain weighting functions can be easily incorporated in the definition of these outputs. The 2-norm of the transfer function between the external disturbance and the regulated output is minimized by selecting an appropriate stabilizing controller. Since it is based on the 2-norm, the resulting solution will provide optimal disturbance attenuation in an averaged frequency sense. An extensive study regarding the application of this approach for civil engineering structures was carried out by Spencer and co-workers. A control strategy based only on absolute acceleration measurements was proposed, and both numerical and experimental verifications were performed to investigate the effectiveness of this frequency domain optimal control technique [21, 77, 78, 79].

In the H_∞ control approach, the transfer function between the disturbance and the regulated output is minimized with respect to the ∞-norm. In this case, the corresponding optimal design represents the best attenuation with respect to the worst case disturbance [79]. This approach based on the ∞-norm minimization provides a guarantee of robust stability, and hence it is also referred to as robust control. The application of this strategy

to building systems was considered by Schmitendorf and Jabbari. Full state feedback and observer based controllers were numerically investigated in [34, 71, 72]. To avoid the time delay associated with on-line computations in the observer based scheme, a direct output feedback strategy was proposed in [73]. Necessary and sufficient conditions for the existence of a stabilizing direct output feedback controller were presented, leading to a controller design scheme in terms of a nonconvex optimization problem. This control strategy was verified experimentally using a three-story reduced scale model [113, 117].

Sliding Mode Control: A quite different type of control strategy is represented by the sliding mode control approach. In this case, an inherently robust controller is designed such that some specified dynamic constraints are introduced in the system. The evolution of the controlled system is characterized by the existence of sliding motions, which can be described as the resulting motion when the system states are constrained to a target manifold in the state space, known as the sliding surface. In general, sliding motions are generated by means of discontinuous control actions. The application of sliding mode control strategies for active control of civil structures has been considered by Yang and co-workers. In Refs. [108, 109, 111, 116] the selection of linear sliding surfaces was carried out using standard design techniques [89]. Several discontinuous controllers were proposed using Lyapunov's direct method. These controllers are based on full state information and they also include a feedforward term to compensate the effect of the external disturbance on the resulting sliding motion. Additionally, an alternative scheme was proposed based only on direct output feedback. In this case, it is considered that only a limited number of measurements is available, with the restriction that collocated velocity sensors are required as a minimum. A continuous controller was also proposed to avoid the undesirable chattering effects induced by discontinuous control actions. The proposed control schemes

were experimentally verified using a reduced scale model [113, 117]. The presence of nonlinearities in the structural model can be considered by imposing the restriction that there is an active device installed in correspondence with each nonlinear story [111]. Because of this assumption of "collocated nonlinearities", the design of the sliding surface can still be carried out by using standard methods. For the controller design, the nonlinearity is considered as a disturbance and its effect is compensated by incorporating the model of the nonlinearity in the control signal. Numerical simulations showed the effectiveness of this approach in achieving seismic response reduction for nonlinear structural systems. Also, the robustness of sliding mode controllers was confirmed by introducing structured perturbations in the system matrices, with no significant performance degradation. The assumption regarding the location of the active devices and the nonlinear structural elements is naturally satisfied in the case of hybrid base-isolation systems equipped with an actuator at base level. Base-isolation schemes consisting of rubber bearings and sliding bearings were numerically and experimentally investigated in [109, 118]. A extension of the standard sliding mode approach was proposed in [113], where a dynamic compensator is added to the control system and the sliding surface is defined in the reduced state space corresponding only to the compensator variables. The motivation behind the inclusion of a compensator was to increase the design flexibility but the numerical simulations did not show any significant advantage of this approach when compared with the standard sliding mode controller.

1.2.3 Semi-Active Control

As mentioned before, in these schemes the counteractive control actions are generated from the motion of the structure as reactive forces. These counteractive reactions are created by proper adjustment of localized stiffness and/or damping characteristics. The main

advantage of these approaches, which makes them specially attractive for application to civil structures, is that the external power required to operate the devices is nominal. No external energy is input into the structure to regulate its motion. Although these methods are called semi-active, the regulation of the reactive control forces is as actively done in these methods as in the active control schemes. Among the different alternative ways proposed to achieve the regulation of mechanical parameters, the most relevant are *semi-active hydraulic dampers*, *variable stiffness devices*, *electro-* or *magneto-rheological dampers* and *semi-active friction devices*. The semi-active hydraulic dampers essentially consist of a hydraulic piston-cylinder arrangement with a control valve mechanism. By opening or closing the valve, different levels of damping forces can be generated. The variable stiffness devices can be idealized as supplementary bracings connected to the primary structure by a locking mechanism. When the connection is locked, the brace becomes effective in adding stiffness to the system, and when the connection is released, this stiffness contribution is suppressed. Electro- and magneto-rheological dampers are devices based on controllable fluids, consisting of suspensions of micron-sized polarizable particles in oil. The material properties of these special fluids can be controlled by applying an electric or magnetic field. Finally, semi-active friction devices are based on sliding surfaces which are subjected to a controllable contact force.

Semi-active control is also referred to as parametric control, as the structural parameters are altered temporally as motion proceeds. Because of these parametric changes the problem is essentially nonlinear, requiring special methods to design the control system. In this case, due to the special features and limitations of semi-active actuation, the development of control algorithms have been essentially device-oriented. In the sequel, a brief description of some semi-active control schemes is presented.

Hrovat and co-workers [29] pioneered the idea of using semi-active devices for control of wind induced vibrations. Based on the concepts developed for semi-active suspension systems, they proposed a semi-active scheme which consisted of a passive tuned mass damper connected to the structure through a variable damper. The proposed algorithm was based on the calculation of the control force as the solution of the associated steady state regulator problem with no excitation. If the so-called passivity constraint is fulfilled, that is the device is not required to give power to the system, then the required force can be generated by the damper. Numerical simulations showed the potential of this semi-active approach for reduction of wind excited structural vibrations.

An extensive experimental research was conducted by Patten and Sack [61, 62, 69] to investigate the application of semi-active dampers to extend the fatigue life of highway bridges. These studies ended successfully with a full scale implementation. The model describing the behavior of the semi-active damper is nonlinear and a heuristic control algorithm is formulated based on the methodology proposed previously by Hrovat [29]. The value of the required optimal control force is calculated using a reduced model of the system. If the passivity condition is satisfied, then the device is commanded to generate the control action. A feedback linearization scheme is proposed in the form of a prefilter. With this prefilter, the behavior of the device approaches a linear viscous dashpot, characterized by a linear relation between the velocity across the actuator and the resulting force output.

Another analytical and experimental investigation leading to the design of an implementable semi-active fluid damper was carried out by Symans and Constantinou [82, 83]. The semi-active device was developed by introducing some modifications on a fluid damper previously designed for passive seismic protection [12]. This damper has the advantage of being specifically designed to act as a linear viscous damper. Two different alternatives

were considered: 1) a bi-state damper controlled by a solenoid valve, able to deliver two extreme damping values and 2) a variable damper controlled by a direct-drive servovalve, able to produce a continuous range of damping values. These studies focused on the identification of the mechanical parameters of the devices. Some experimental tests indicated that it was very difficult to improve the performance obtained with the dampers operating in a fully passive mode.

The formulation of sliding mode control algorithms for semi-active dampers was proposed by Yang and co-workers [108, 111]. Control algorithms are designed for bi-state and continuously variable dampers. Numerical simulations using a three-story scaled building model showed that one active variable damper installed in the first story was effective in reducing the response, but no further comparisons were provided to establish the efficiency of the semi-active operation compared with the corresponding fully passive mode. A hybrid system for seismic protection of bridge structures is proposed in Refs. [108] and [115]. The system consists of rubber bearings and variable dampers which can operate either in a two stage mode or under a continuous damping regulation. In this special cases, in which the semi-active damper must operate with additional passive dissipation devices, the regulation of damping may provide some advantages with respect to a damper with a constant damping coefficient set to its maximum value. This was considered also by Kawashima and Unjoh [39] for the same type of structures, who proposed a heuristic control algorithm to regulate the damping coefficient of a variable damper installed with elastic bearings. In their approach, the semi-active damper operation is a function of the relative displacement between the bridge deck and the supporting piers. At small displacement levels, the damping coefficient is set to large values to reduce the displacement. The same happens for large displacement levels, when the variable damper acts as a stopper. At intermediate levels,

the damping is reduced to facilitate the dissipation of energy in the passive devices.

Kobori and co-workers [43] proposed a control algorithm for application with variable stiffness devices referred to as non-resonant control approach. The idea is to appropriately modify the stiffness characteristics of the building based on the nature of the earthquake. The ground acceleration is processed through several band-pass filters. Each filter approximates the uncontrolled response corresponding to each possible stiffness configuration. Based on the filtered outputs, the algorithm selects a stiffness distribution by evaluating an averaged index. The approach was subjected to experimental verification using a three-story building with variable stiffness devices installed in all floors. This approach, in general, will not lead to a fast switching operation of the semi-active devices because it is based on the change in time of the excitation frequency content. Usually, the system under this type of controlled operation will adopt only one stiffness configuration during the seismic event. This means that the variable stiffness devices are not exploited for energy dissipation and they are only used to reduce the seismic energy input. A similar algorithm based on a moving window analysis of the ground excitation was proposed in Ref. [39] for application in bridge structures. In this approach, the fundamental period of the bridge is changed between two limiting values according to the predominant period of the ground motion.

Another type of control law was proposed by Kamagata and Kobori [37] for bi-state operation of variable stiffness devices. The algorithm consisted of locking the device every time the corresponding deformation crosses zero and unlocking it when this deformation reaches a local peak. An interesting analysis of systems with bi-state stiffness control devices was also presented in Refs. [31, 32]. These studies focused on the dynamic behavior of systems whose mechanical parameters have different values in different conical regions

of the state space. These nonlinear systems are identified as homogeneous systems of order one, which show the input/output scaling property characteristic of linear systems.

Another interesting semi-active control scheme based on variable stiffness devices was proposed by Nemir and co-workers [59]. The algorithm proposed to control these devices aims to redistribute the modal energies within the structural system. In general, it is desirable to extract the energy from the lower modes of vibration and transfer it to higher modes, since these higher modes have better energy dissipation characteristics. At each sampling time, the algorithm determines the stiffness configuration by minimizing a weighted combination of modal kinetic and potential energies. The computation of these modal energies requires knowledge of the full state vector or the implementation of an observer. The simulation studies demonstrated the feasibility of the switching stiffness concept in reducing the structural response.

Active stiffness control was also studied by Yang [106, 108, 110]. A bi-state control algorithm was developed based on the sliding mode control approach. Numerical simulations were carried out to investigate the effectiveness of the approach. A three-story model with a variable stiffness device in the first story was considered and the device was modeled as a switchable supplementary bracing. The stiffness of the added bracing is assumed equal to the first floor stiffness, value probably too high to be considered feasible for practical implementation. The proposed variable stiffness control is able to reduce the displacement-based response quantities, but it is not as efficient in reducing absolute acceleration responses. In particular, the absolute acceleration of the lowest floor seems to be adversely affected by the impulsive effect induced by the release of stiffness during the switching operation demanded by the control law.

The application of electro-rheological dampers for structural control was investigated by

McClamroch and Gavin [50, 51]. These dampers are based on the change of the mechanical properties of the electro-rheological fluid. This special fluid consists of oil-based suspensions of polarizable particles. When subjected to electric fields, the behavior can change from viscous fluid (zero electric field) to semi-solid (maximum electric field). A control law was proposed based on the minimization of the mechanical energy in the structure. Because of the control constraints due to the limited dielectric strength of the suspension, the control law is of the bang-bang type. The resulting control algorithm indicates that those dampers not connected to the ground must operate continuously at maximum electric field. The only possibility of switching behavior is then restricted to any damper installed at the first story. The implementation of this algorithm requires the measurements of only collocated relative and absolute velocities. A three-story small scale model with a ER damper installed at first floor level was experimentally tested to investigate the proposed approach [26]. The behavior of the system with the damper operated passively at minimum (zero) and maximum electric field was compared with the behavior resulting from the switching control law. Under zero electric field, the large damping introduced by the inherent viscous damping characteristics of the device induced a significant reduction of the response, with no substantial modification of the natural frequencies with respect to the original system. The ER damper operated under maximum field originated a stiffening effect, as revealed by an increase of the structural natural frequencies with smaller reduction of acceleration responses. The switching operation induced some improvement in the response reduction, specially in the low frequency region corresponding with the first structural frequency. Higher modes seemed to be affected by the impulsive nature of the control forces produced by the switching algorithm.

The use of magneto-rheological dampers for seismic response reduction was studied by

Dyke and co-workers [22]. The principle behind these devices is similar to the ER dampers, but they show some advantageous characteristics, such as higher yield strengths and less sensitivity to temperature than their ER counterparts. The control law proposed in this study is similar to the suboptimal strategy first proposed in [29] but the optimal control law for this case is obtained in terms of acceleration feedback using a H_2/LQG formulation. Numerical simulations show the effectiveness of the semi-active MR damper in reducing the structural responses.

Semi-active friction devices in the form of controllable sliding bearings were studied for application in hybrid base-isolation systems by Feng and co-workers [24, 58]. The level of friction at the sliding interface is controlled by proper adjustment of the pressure in the fluid chamber of the bearing. Based on the instantaneous optimal control approach, a control algorithm was developed assuming that there is always sliding motion at the frictional interface [24]. The controller dynamics was incorporated by assuming a first order time delay model between the control signal and the fluid pressure. The proposed system was experimentally tested on a reduced scale model. In a follow-up work [58], the effects of sticking/sliding phases in the interface motion are accounted for. In this case, the Bouc-Wen hysteretic model is used to model the behavior of the sliding interface. With this model, the frictional effect is no longer proportional to the sign of the sliding velocity, but it becomes directly proportional to the hysteretic state variable.

The application of the sliding mode control approach to friction controllable sliding bearings was studied by Yang and co-workers [114]. As proposed in [58], a hysteretic model is introduced to model the behavior of the sliding bearings. A continuous sliding mode controller is proposed to avoid undesirable chattering effects. A static output feedback version of the controller was also developed. A 4-story reduced scale building model was used in the

numerical simulations. Both full state feedback and output feedback schemes performed very satisfactorily in reducing the structural responses, in particular for strong earthquakes, when the displacements of the sliding bearings acting passively could be excessive.

1.3 Motivation and Scope

The development of a control law in the form of an effective algorithm is one of the critical factors for the successful implementation of any control system. The effect of the control action must be to improve, and not degrade, the performance of the system being controlled. Additionally, the controller should be robust enough to handle modeling and measurement uncertainties, especially in applications to civil structures as their properties can change with time and their precise quantitative description may not be possible. Also the control scheme should be able to withstand the incomplete and inexact description of the mathematical model of the structure which is caused by the simplifying assumptions that are made in formulating the problem. Such modeling error can be caused by unknown or improperly modeled nonlinearities. Linearization techniques, which are often used to analyze nonlinear systems, are a direct source of modeling errors. As a result, the model used in the design of a control algorithm may be quite different from the real system. All this means that the controller must be able to accommodate not only the differences between the actual and assumed mass, stiffness and damping parameter values but also be able to handle the unmodeled characteristics of the system.

The aforementioned requirements makes the consideration of the sliding mode control approach very attractive for application in civil engineering structures. The central idea of this approach is to enforce a set of linear or nonlinear pre-defined constraints in the state space, referred to as the sliding surface. This is achieved by appropriate control

actions, which in general show some form of discontinuity with respect to the sliding surface. These control actions are designed such that they drive the system toward the sliding surface and then keep it there. The sliding surface is chosen in such a way that the constrained motion, called sliding motion, is stable and has desirable features. It can be shown that sliding motions are not affected by external disturbances, provided that some special conditions regarding the structure of the system (referred to as the invariance conditions) are satisfied [19]. In this case, the behavior of the system under sliding motion corresponds to an unforced reduced order system. Also, it is known that sliding motions show performances that are very robust with respect to structured uncertainties in form of parametric variations [14, 33, 88, 90].

The main purpose of the proposed study is to investigate the application of the sliding mode control approach for the active and semi-active control of civil engineering structures. As mentioned before, the application of this approach to the problem of seismic response control was first proposed by Yang and co-workers very recently in quite a number of publications ([106]-[118]). However, there are some important issues regarding the practical feasibility and design flexibility of the approach that have been not fully investigated. This research will focus on the study of some of these issues, which are crucial for the successful application of the sliding mode approach to massive civil structures. A brief discussion of these points is presented in the sequel.

Feedback Structure: The incentive for the use of a sliding mode controller is to obtain a system whose performance is robust with respect to parametric uncertainties and unknown disturbances. Hence, to be consistent with this philosophy, the controller should have a closed-loop structure, avoiding explicit feedforward components proportional to the external excitation. These types of components may induce drastic degradations in per-

formance in practical situations with time delays. Therefore, the proposed research will investigate the design of controllers with strictly feedback configuration. The only drawback of such configuration is that if the invariance conditions are not satisfied, then the sliding motion will be affected by the external disturbance. Therefore, the reduced-order system representing the system under sliding motion will not behave as a system in free vibration. However, this is not the goal driving the installation of control systems for civil engineering structures. Because of the massive characteristics of the structural system and the limitation of the actuation devices, we must accept the fact that it is not feasible to modify arbitrarily the evolution of the system under ground excitation. The idea is to use the control system just to shape appropriately the resulting dynamics, not to annihilate completely the effects of any external disturbance to achieve complete compensation.

Continuous Controller: The materialization of sliding motions demands the implementation of (classical) sliding mode controllers, whose structure is variable and characterized by some form of discontinuity with respect to the target sliding surface. To eliminate the high frequency demands on the actuation system which are common for this type of switching controllers, a continuous approximation can be introduced for the design of active controllers. The proposed research will explore the design of continuous sliding mode controllers and it will investigate their performance. The disadvantage of such an approximation is that the system will not be able to substantiate an ideal sliding regime, because of the smoothness of the control law. But this is not crucial if the realization of sliding motions is not the ultimate goal for the control system. In this context, the target sliding surface can be used as a design tool. The controller acts in such a way that it encourages the system to reach and stay on the sliding, and we judge the resulting performance as the system constantly tries to reach this target.

Controller Redundancy: Traditionally, it has been considered that the number of controllers should be identical to the number of sliding constraints, to obtain an unambiguous description of the resulting sliding regime. In the context of a design philosophy not centered on the realization of a particular sliding regime, but on the behavior of the system constantly trying to reach the sliding surface (reaching phase), it is interesting to explore the use of redundant controllers. The proposed research will investigate the conditions to obtain a description of sliding motions for cases with control redundancy.

Generalized Sliding Surface: The selection of the sliding surface is, perhaps, the most crucial step in the development of an effective sliding mode controller. Usually, the sliding surface is defined in static form as a set of linear equations in terms of the state variables. This study will explore the use of more general definitions using auxiliary dynamical systems. This type of dynamic sliding surface has been proposed to eliminate chattering in sliding mode controllers for robot manipulators [121]. In the context of control of civil structures, the frequency domain interpretation that can be associated with this dynamic or generalized definition of the sliding surface will add flexibility to the control design problem.

Output Feedback Structure: For practical implementations it may not be feasible to install as many sensors as to measure all the system states. On the other hand, the estimation of unmeasured states through observers may add significant on-line computations resulting in time delays detrimental for the performance of the control system. Therefore, it is always desirable to design a controller which uses directly the information provided by a limited number of sensors. The proposed research will investigate the design of sliding mode controllers with an output feedback structure.

1.4 Research Goals

Based on the preceding section, the following research goals are proposed for this study:

1. Evaluation of the feasibility and effectiveness of active and semi-active control strategies based on the sliding mode control approach. This will be done through numerical simulations using building models corresponding to real size structures, with particular attention devoted to the following points:

   (a) Active control: In this case, the magnitudes of the required control force and associated mechanical power become critical factors for practical implementation. Several sliding mode controllers will be designed and their performance will be evaluated, considering the effectiveness in response reduction and the control demand.

   (b) Semi-active control: Since the control system is designed assuming full control authority, the effect of limited control actions will be evaluated. The influence of the type of device on the resulting performance will be analyzed using two simple models for generation of reactive forces.

   (c) The effect of the following parameters on the effectiveness of the controlled system will be investigated: (1) selection of sliding surface and the parameters which determine this selection, (2) structural characteristics such as predominant frequencies and damping factors, (3) input disturbance frequency and intensity, (4) method of applying control actions.

2. Improvement of design procedures for active and semi-active control strategies based on the sliding mode control approach. Particular emphasis will be given to the following aspects:

(a) Generalized sliding surface: The design flexibility provided by a dynamic definition of the sliding surface will be exploited to enhance the performance of the control system.

(b) Nonlinear control law: The incorporation of nonlinear terms in the control law will be considered to increase the control authority when the system moves away from the sliding surface.

(c) Output feedback: Several design alternatives will be considered and the influence of limited state information will be evaluated by comparing the performance obtained with the corresponding full-state feedback design.

1.5 Organization of Work

Chapter 1: An overview of the different contributions in the area of active and semi-active structural control is presented. The advantages and limitations are briefly discussed, and the motivation behind the proposed application of sliding mode control schemes for seismic response control of civil structures is presented.

Chapter 2: The formulation of the sliding mode control approach is discussed in this chapter, with an unified treatment of both active and semi-active control strategies. A systematic procedure to transform the system equations into their regular form is presented. The description of the sliding motion is investigated considering the possibility of control redundancy. Several alternative active and semi-active controller designs are presented. The controller performances are numerically evaluated using a shear building model corresponding to a realistic structure.

Chapter 3: The formulation presented in the previous chapter is extended to the case in which the sliding surface is defined using auxiliary dynamical systems. An alternative procedure is introduced to obtain the corresponding regular form of the state equations. The sliding surface design problem corresponding to this generalized definition is discussed and its frequency domain interpretation is also examined. A continuous active controller is presented and some special characteristics of the resulting closed loop system are discussed. The performance of linear and nonlinear versions of this controller are evaluated by numerical simulations

Chapter 4: The practical situation of partial state information is incorporated in the generalized sliding surface formulation developed in the previous chapter. The transformation to regular form is modified to incorporate the constraints represented by the presence of unmeasured variables in the model. The special characteristics of the corresponding sliding surface design problem are examined. This design problem can be interpreted in the context of optimal output feedback theory, and an efficient algorithm is presented to solve the resulting system of nonlinear matrix equations. This algorithm, based on a damped successive substitution scheme, is discussed in detail in Appendix A. The performance of active and semi-active controllers with an output feedback structure is evaluated by extensive numerical simulations.

Chapter 5: The main conclusions of this study are summarized in this final chapter, with some recommendations for future research on this topic.

Chapter 2

Sliding Mode Control Formulation

2.1 Introduction

This chapter deals with the formulation of sliding mode controllers for active and semi-active control of civil structures using full state feedback. The mathematical foundation of the sliding mode control is now documented in several books [33, 88, 90]. The initial mathematical complexities of this approach have, however, been somewhat responsible for cramping the adoption of this powerful concept by practice oriented groups such as the civil engineering community. It is now expected that more and more researchers will explore its application to civil structures because of its robustness and versatility of application to linear as well as nonlinear systems.

In this chapter, the general formulation of this control approach is presented with some new perspectives. The mathematical steps associated with the development are presented in such a manner that a person with some background in matrix theory can follow the formulation. As mentioned in Chapter 1, the development of a sliding mode controller consists basically of the design of a set of constraints between the state variables and the determination of appropriate control actions enforcing those constraints. To facilitate the implementation of this approach to the problem of seismic response control of civil struc-

tures, here some new analytical developments are presented. In particular, a systematic procedure is presented to transform the system equations into a special form, called as the regular form, so that the processes of defining the sliding surface and the calculation of control actions can be decoupled as two separate design steps. The formulation presented here also includes the case of control redundancy (that is, when the number of control actions exceeds the number of sliding constraints). Several new full state-feedback controllers based on an upper bound for the ground excitation are presented and the corresponding region of attractions are also investigated. A full-state semi-active controller is also developed assuming a bi-state regime for the semi-active devices. Several sets of numerical results are obtained to examine the special characteristics and to evaluate the feasibility of implementation of sliding mode controllers to civil structures subjected to earthquake-induced ground motions.

2.2 System Equations

2.2.1 Equations of Motion

The equations of motion of a linear building system with n_f degrees of freedom under seismic excitation can be written as follows:

$$\mathbf{M}\,\ddot{\mathbf{z}} + [\mathbf{C} + \mathbf{C_v}]\,\dot{\mathbf{z}} + [\mathbf{K} + \mathbf{K_v}]\,\mathbf{z} = -\mathbf{M}\,\mathbf{r}\,\ddot{x}_g + \tilde{\mathbf{D}}\,\mathbf{u_a} \tag{2.1}$$

The n_f-dimensional vector $\mathbf{z}$ represents the relative displacements of the system, i.e. the displacements with respect to a reference frame fixed to the ground. The vector $\mathbf{r}$ represents the influence of the ground excitation $\ddot{x}_g(t)$ on each degree of freedom. The $n_f \times n_f$ matrices $\mathbf{M}$, $\mathbf{C}$ and $\mathbf{K}$ represent the mass, damping and stiffness matrices, respectively. It is assumed that the mass and stiffness matrices are positive definite whereas the damping matrix is positive semi-definite.

The vector $\mathbf{u_a}$ contains the m_a active control actions whose locations are identified through the $n_f \times m_a$ location matrix $\tilde{\mathbf{D}}$. As it was mentioned in the previous chapter, active control actions are caused by external forces which are directly applied to the system, e.g. through hydraulic actuators. It is assumed that the position of these actuation devices is such that the columns of the location matrix $\tilde{\mathbf{D}}$ are linearly independent, i.e.

$$\text{rank}(\tilde{\mathbf{D}}) = m_a \tag{2.2}$$

It is also assumed that the system is equipped with m_{sa} semi-active devices. They provide the mechanism to exert control actions in the form of time-varying parametric perturbations of the damping and stiffness characteristics of the system. The semi-active devices are modelled as variable stiffness and damping mechanisms installed in parallel along diagonal braces. These braces are hinged at their ends to the main structure. The devices, therefore, induce forces only along the brace to which they are attached. The model also assumes that the semi-active devices can provide additional stiffness and/or damping working under either compression or tension. Each one of these devices can be characterized by a pair of variable damping and stiffness coefficients, c_{v_i} and k_{v_i}, respectively. The $n_f \times n_f$ matrices $\mathbf{C_v}$ and $\mathbf{K_v}$ in (2.1) are positive semi-definite matrices that represent the contribution of these m_{sa} variable damping and stiffness parameters, respectively, to the corresponding structural matrices.

It is assumed that the number of active and semi-active devices acting on the system is at most equal to the number of degrees of freedom of the model, i.e.

$$m_a \leq n_f \quad \text{and} \quad m_{sa} \leq n_f \tag{2.3}$$

In general, the matrices $\mathbf{C_v}$ and $\mathbf{K_v}$ will have a banded structure similar to that of standard damping and stiffness matrices. It will prove convenient to introduce a coordinate

transformation that reduces the variable contribution matrices $\mathbf{C_v}$ and $\mathbf{K_v}$ to a special diagonal representation.

It is assumed that there exists a nonsingular $n_f \times n_f$ matrix $\mathbf{T_d}$ such that

$$\bar{\mathbf{C}}_\mathbf{v} = \mathbf{T}_\mathbf{d}^T \mathbf{C_v} \mathbf{T_d} = \begin{bmatrix} \bar{\mathbf{C}}_\mathbf{v}^\mathbf{r} & \mathbf{0} \\ \mathbf{0} & \mathbf{0} \end{bmatrix} \text{ and } \bar{\mathbf{K}}_\mathbf{v} = \mathbf{T}_\mathbf{d}^T \mathbf{K_v} \mathbf{T_d} = \begin{bmatrix} \bar{\mathbf{K}}_\mathbf{v}^\mathbf{r} & \mathbf{0} \\ \mathbf{0} & \mathbf{0} \end{bmatrix} \tag{2.4}$$

in which both $\bar{\mathbf{C}}_\mathbf{v}^\mathbf{r}$ and $\bar{\mathbf{K}}_\mathbf{v}^\mathbf{r}$ are $m_{sa} \times m_{sa}$ diagonal matrices containing only the coefficients of the semi-active devices, i.e. $\bar{\mathbf{C}}_\mathbf{v}^\mathbf{r} = \text{diag}(c_{v_i})$ and $\bar{\mathbf{K}}_\mathbf{v}^\mathbf{r} = \text{diag}(k_{v_i})$. Using this matrix $\mathbf{T_d}$, a coordinate transformation is defined as

$$\mathbf{z} = \mathbf{T_d}\, \mathbf{d} \tag{2.5}$$

Substituting (2.5) into the equations of motion (2.1), and pre-multiplying by the transpose of the matrix $\mathbf{T_d}$, the equations of motion can be written in terms of the new coordinates $\mathbf{d}$ as follows:

$$\bar{\mathbf{M}}\, \ddot{\mathbf{d}} + \left[\bar{\mathbf{C}} + \bar{\mathbf{C}}_\mathbf{v}\right]\, \dot{\mathbf{d}} + \left[\bar{\mathbf{K}} + \bar{\mathbf{K}}_\mathbf{v}\right]\, \mathbf{d} = -\mathbf{T}_\mathbf{d}^T\, \mathbf{M}\, \mathbf{r}\, \ddot{x}_g + \mathbf{T}_\mathbf{d}^T\, \tilde{\mathbf{D}}\, \mathbf{u_a} \tag{2.6}$$

where

$$\bar{\mathbf{M}} = \mathbf{T}_\mathbf{d}^T \mathbf{M} \mathbf{T_d}\,,\ \bar{\mathbf{C}} = \mathbf{T}_\mathbf{d}^T \mathbf{C} \mathbf{T_d} \text{ and } \bar{\mathbf{K}} = \mathbf{T}_\mathbf{d}^T \mathbf{K} \mathbf{T_d} \tag{2.7}$$

A very common model used in the analysis and design of building structures is the so-called shear building or shear frame. In this model, it is assumed that the total mass of the structure is lumped at the floor levels and the floor beams are infinitely rigid as compared to the columns. The columns are assumed infinitely rigid with respect to axial deformations and the damping characteristics of the system are modelled by interstory dashpots. Under these assumptions, the deformed configuration can be described only in terms of the horizontal displacements at the floor levels. Therefore, a plane (2D) shear building model will have as many degrees of freedom as floor levels. For a plane shear

building model in which the semi-active devices are installed between adjacent stories, the diagonal representation indicated in (2.4) can be easily achieved if the coordinates $\mathbf{d}$ represent the interstory deformations.

2.2.2 State Equations

The following state vector $\boldsymbol{\eta}$ of dimension $n = 2n_f$ is defined:

$$\boldsymbol{\eta} = \left\{ \begin{array}{c} \mathbf{d} \\ \dot{\mathbf{d}} \end{array} \right\} \tag{2.8}$$

According to this definition and considering (2.5), the first n_f components of the state vector represent linear combinations of relative displacements, whereas the remaining n_f state variables denote linear combinations of velocity coordinates.

With this definition, the equations of motion (2.6) can be written in state space form as

$$\dot{\boldsymbol{\eta}} = \mathbf{A}\,\boldsymbol{\eta} + \mathbf{A_v}\,\boldsymbol{\eta} + \mathbf{B_a}\,\mathbf{u_a} + \mathbf{e}\,\ddot{x}_g \tag{2.9}$$

where the state matrix $\mathbf{A}$ and the variable state matrix $\mathbf{A_v}$ are given, respectively, by

$$\mathbf{A} = \left[\begin{array}{cc} \mathbf{0} & \mathbf{I}_{n_f} \\ -\bar{\mathbf{M}}^{-1}\bar{\mathbf{K}} & -\bar{\mathbf{M}}^{-1}\bar{\mathbf{C}} \end{array} \right] \quad \text{and} \quad \mathbf{A_v} = \left[\begin{array}{cc} \mathbf{0} & \mathbf{0} \\ -\bar{\mathbf{M}}^{-1}\bar{\mathbf{K}}_\mathbf{v} & -\bar{\mathbf{M}}^{-1}\bar{\mathbf{C}}_\mathbf{v} \end{array} \right] \tag{2.10}$$

and the active control input matrix $\mathbf{B_a}$ and disturbance input vector $\mathbf{e}$ are given, respectively, by

$$\mathbf{B_a} = \left[\begin{array}{c} \mathbf{0} \\ \bar{\mathbf{M}}^{-1}\mathbf{T}_\mathbf{d}^T\,\tilde{\mathbf{D}} \end{array} \right] \quad \text{and} \quad \mathbf{e} = \left[\begin{array}{c} \mathbf{0} \\ -\bar{\mathbf{M}}^{-1}\mathbf{T}_\mathbf{d}^T\,\mathbf{M}\,\mathbf{r} \end{array} \right] \tag{2.11}$$

Note that, since $\bar{\mathbf{M}}$ and $\mathbf{T_d}$ are nonsingular matrices, the rank of $\mathbf{B_a}$ is the same as the rank of the location matrix $\tilde{\mathbf{D}}$, that is, $\text{rank}(\mathbf{B_a}) = m_a$.

Considering the structure of the matrices $\bar{\mathbf{K}}_\mathbf{v}$ and $\bar{\mathbf{C}}_\mathbf{v}$, it can be shown that the contribution of the semi-active devices to the state equations can be written as follows:

$$\mathbf{A_v}\boldsymbol{\eta} = \mathbf{B_{sa}}\mathbf{u_{sa}} \tag{2.12}$$

where the control vector $\mathbf{u_{sa}}$ is defined as

$$\mathbf{u_{sa}} = -\left[\begin{array}{cc} \bar{\mathbf{K}}_{\mathbf{v}}^{\mathbf{r}} & \bar{\mathbf{C}}_{\mathbf{v}}^{\mathbf{r}} \end{array}\right] \left\{\begin{array}{c} \boldsymbol{\xi} \\ \dot{\boldsymbol{\xi}} \end{array}\right\} \tag{2.13}$$

in which the vector $\boldsymbol{\xi}$ denotes the m_{sa} components of the vector $\mathbf{d}$ associated with semi-active actions, given by

$$\boldsymbol{\xi} = \mathbf{L}^T \mathbf{d} \;\text{ with }\; \mathbf{L}^T = \left[\begin{array}{cc} \mathbf{I}_{m_{sa}} & \mathbf{0} \end{array}\right] \tag{2.14}$$

The $n \times m_{sa}$ input matrix $\mathbf{B_{sa}}$ is given by

$$\mathbf{B_{sa}} = \left[\begin{array}{c} \mathbf{0} \\ \bar{\mathbf{M}}^{-1}\mathbf{L} \end{array}\right] \tag{2.15}$$

Note that based on the definition of the matrix $\mathbf{L}$ and the fact that the mass matrix is nonsingular, we have that $\text{rank}(\mathbf{B_{sa}}) = m_{sa}$.

Substituting (2.12) into (2.9), the state equations can be written more compactly in the following form:

$$\dot{\boldsymbol{\eta}} = \mathbf{A}\,\boldsymbol{\eta} + \tilde{\mathbf{B}}\,\tilde{\mathbf{u}} + \mathbf{e}\,\ddot{x}_g \tag{2.16}$$

where the $n \times (m_a + m_{sa})$ input matrix $\tilde{\mathbf{B}}$ is defined as

$$\tilde{\mathbf{B}} = \left[\begin{array}{cc} \mathbf{B_a} & \mathbf{B_{sa}} \end{array}\right] = \left[\begin{array}{cc} \mathbf{0} & \mathbf{0} \\ \bar{\mathbf{M}}^{-1}\mathbf{T}_{\mathbf{d}}^T\,\tilde{\mathbf{D}} & \bar{\mathbf{M}}^{-1}\mathbf{L} \end{array}\right] \tag{2.17}$$

and the $(m_a + m_{sa})$-dimensional control vector $\tilde{\mathbf{u}}$ is given by

$$\tilde{\mathbf{u}} = \left\{\begin{array}{c} \mathbf{u_a} \\ \mathbf{u_{sa}} \end{array}\right\} \tag{2.18}$$

Here we note that the possibility of active and semi-active devices co-acting at the same location has not been ruled out, because the only assumption made about the location of the actuation devices was related to the active controllers. Therefore,

$$\text{rank}\left(\left[\begin{array}{cc} \mathbf{T}_{\mathbf{d}}^T\,\tilde{\mathbf{D}} & \mathbf{L} \end{array}\right]\right) = m_c \leq m_a + m_{sa} \tag{2.19}$$

Considering the fact that $\bar{\mathbf{M}}$ is nonsingular, it is easy to see from (2.17) that the rank of the input matrix $\tilde{\mathbf{B}}$ is also equal to m_c and therefore not necessarily equal to the number of control components. Since it is desired to express the input term of the state equations in terms of a set of independent control actions, we take into account the fact that it is always possible to construct the following factorization [81]:

$$\left[\begin{array}{cc} \mathbf{T}_{\mathbf{d}}^T \tilde{\mathbf{D}} & \mathbf{L} \end{array} \right] = \mathbf{D}\,\mathbf{Y}^T \tag{2.20}$$

where $\mathbf{D}$ and $\mathbf{Y}$ are $n_f \times m_c$ and $m_c \times (m_a + m_{sa})$ matrices whose rank is equal to m_c. Using the factorization, it is possible to define the following input matrix $\mathbf{B}$:

$$\mathbf{B} = \left[\begin{array}{c} \mathbf{0} \\ \bar{\mathbf{M}}^{-1}\,\mathbf{D} \end{array} \right] \tag{2.21}$$

and the m_c-dimensional vector $\mathbf{u}$

$$\mathbf{u} = \mathbf{Y}^T \tilde{\mathbf{u}} \tag{2.22}$$

such that the state equations can be finally written as

$$\dot{\boldsymbol{\eta}} = \mathbf{A}\,\boldsymbol{\eta} + \mathbf{B}\,\mathbf{u} + \mathbf{e}\,\ddot{x}_g \tag{2.23}$$

in which

$$\text{rank}\,(\mathbf{B}) = m_c \leq n_f \tag{2.24}$$

2.3 Sliding Surface

The main idea of the sliding mode control approach consists of enforcing a set of m_s predefined relationships or constraints between the state variables of the following form:

$$\mathbf{s}(\boldsymbol{\eta}) = \left\{ \begin{array}{c} s_1(\boldsymbol{\eta}) \\ s_2(\boldsymbol{\eta}) \\ \vdots \\ s_{m_s}(\boldsymbol{\eta}) \end{array} \right\} = \mathbf{0} \tag{2.25}$$

where it is assumed that the number of constraints does not exceed the number of independent control actions, i.e.

$$m_r = m_c - m_s \geq 0 \tag{2.26}$$

where the parameter m_r is referred to as the control redundancy index.

The set of equations (2.25) define a surface in the n-dimensional state space, referred to as the *sliding surface* [87]. If the scalar functions s_i take the form of linear algebraic relations between the state variables, then the sliding surface can be regarded as the solution subspace of a set of homogeneous linear equations and the definition (2.25) can be written as

$$\mathbf{s}(\boldsymbol{\eta}) = \mathbf{C_s}\,\boldsymbol{\eta} = \mathbf{0} \tag{2.27}$$

where $\mathbf{C_s}$ denotes a $m_s \times n$ constant matrix. It is assumed that this definition has no redundant information in the form of dependent equations, i.e.

$$\text{rank}\,(\mathbf{C_s}) = m_s \tag{2.28}$$

Since the sliding surface has now a direct interpretation as the null space of the matrix $\mathbf{C_s}$, it is easy to see that this surface defines a $(n - m_s)$-dimensional subspace of the state space.

The objective of the control system is to apply the appropriate control actions to drive the system state $\boldsymbol{\eta}$ towards the sliding surface, and keep it there. The resulting motion of the system, in which the state is forced to satisfy (2.25), is called *sliding motion* [87]. This is represented in Figure (2.1). The sliding surface design problem, which in the case of a linear definition reduces to the process of selecting an appropriate matrix $\mathbf{C_s}$, is concerned therefore with the specification of some desirable characteristics for the associated sliding motion. Obviously, a fundamental requirement for any sliding surface candidate is the stability of the corresponding sliding motion.

2.4 Sliding Motion

In this section, the equations describing the sliding motion corresponding to a linear sliding surface are obtained following the method proposed by Utkin [87]. In view of the constraints on the state vector represented by the equations (2.27), it is clear that a reduced number of variables will be needed to describe this motion. Assuming that the system reaches the sliding manifold at some time t_h and it is forced to stay there by some control action $\hat{\mathbf{u}}$, the sliding motion conditions are given by

$$\mathbf{s}(\boldsymbol{\eta}) = \mathbf{C_s}\boldsymbol{\eta} = \mathbf{0} \tag{2.29}$$

$$\dot{\mathbf{s}}(\boldsymbol{\eta}) \mid_{\mathbf{u}=\hat{\mathbf{u}}} = \mathbf{C_s}\dot{\boldsymbol{\eta}} = \mathbf{0} \tag{2.30}$$

Since the $m_s \times n$ matrix $\mathbf{C_s}$ has rank m_s, it includes at least one $m_s \times m_s$ submatrix $\mathbf{C_{s2}}$ of rank m_s [81]. This allows one to express the m_s components of the state vector associated with the columns of any of these nonsingular submatrices in terms of the remaining $n_r = n - m_s$ states. Therefore, by separating the state variables into the corresponding vectors $\boldsymbol{\eta_2}$ and $\boldsymbol{\eta_1}$ of dimensions m_s and n_r, respectively, we can write (2.29) and (2.30) as follows:

$$\boldsymbol{\eta_2} = -\mathbf{C_r}\,\boldsymbol{\eta_1} \tag{2.31}$$

$$\dot{\boldsymbol{\eta}}_{\mathbf{2}} = -\mathbf{C_r}\,\dot{\boldsymbol{\eta}}_{\mathbf{1}} \tag{2.32}$$

in which $\mathbf{C_r}$ is a $m_s \times n_r$ matrix that expresses the dependency of the variables $\boldsymbol{\eta_2}$ on the variables $\boldsymbol{\eta_1}$.

The state equations (2.23) can be written in the following partitioned form which reflects the arrangement of the state variables into the vectors $\boldsymbol{\eta_1}$ and $\boldsymbol{\eta_2}$:

$$\begin{Bmatrix} \dot{\boldsymbol{\eta}}_{\mathbf{1}} \\ \dot{\boldsymbol{\eta}}_{\mathbf{2}} \end{Bmatrix} = \begin{bmatrix} \mathbf{A_{11}} & \mathbf{A_{12}} \\ \mathbf{A_{21}} & \mathbf{A_{22}} \end{bmatrix} \begin{Bmatrix} \boldsymbol{\eta_1} \\ \boldsymbol{\eta_2} \end{Bmatrix} + \begin{bmatrix} \mathbf{B_1} \\ \mathbf{B_2} \end{bmatrix} \mathbf{u} + \begin{Bmatrix} \mathbf{e_1} \\ \mathbf{e_2} \end{Bmatrix} \ddot{x}_g \tag{2.33}$$

The two expressions (2.31) and (2.32) make it possible to eliminate the variables $\boldsymbol{\eta_2}$ from the description of the sliding motion. Under the control $\hat{\mathbf{u}}$ enforcing the dynamic condition (2.32), the evolution of the system can be described by n_r independent equations of the form

$$\dot{\boldsymbol{\eta}}_{\mathbf{1}} = \mathbf{A_{11}}\boldsymbol{\eta_1} + \mathbf{A_{12}}\boldsymbol{\eta_2} + \mathbf{B_1}\,\hat{\mathbf{u}} + \mathbf{e_1}\,\ddot{x}_g \tag{2.34}$$

and taking into account the relation (2.31), it follows that the sliding motion equations are given by

$$\dot{\boldsymbol{\eta}}_{\mathbf{1}} = [\mathbf{A_{11}} - \mathbf{A_{12}}\mathbf{C_r}]\;\boldsymbol{\eta_1} + \mathbf{B_1}\,\hat{\mathbf{u}} + \mathbf{e_1}\,\ddot{x}_g \tag{2.35}$$

The sliding surface design process therefore consists of the specification of the $m_s n_r$ coefficients of the matrix $\mathbf{C_r}$ such that the reduced order dynamics described by (2.35) shows some desirable characteristics. But this description has the disadvantage of depending explicitly on the control $\hat{\mathbf{u}}$. This control action must be obtained from the condition (2.30), and it will be also function of the matrix defining the sliding surface, thus complicating the design procedure.

It is therefore convenient to investigate under which conditions the participation of the control actions can be eliminated from the sliding motion equations (2.35). This would allow one to separate the process of defining the sliding motion from the process of choosing the control which ensures that motion. By considering (2.35), it is clear that this situation will happen if the control $\hat{\mathbf{u}}$ enforcing the sliding motion belongs to the null space of the matrix $\mathbf{B_1}$. Therefore, a necessary condition to achieve this convenient representation is the existence of such null space. In the sequel, a special coordinate transformation is introduced to guarantee this condition.

2.5 Regular Form

2.5.1 Sliding Motion Description

Through an appropriate state transformation, we will seek a representation of the system where the control action does not explicitly appear in the reduced order equations describing the sliding motion. This special representation is called the *regular form* [87]. Obviously, the transformation required to produce this decoupling depends on the control input matrix $\mathbf{B}$. A procedure to generate this transformation was proposed by Lukyanov and Utkin [49], based on the work by Brandin and Razorenov [6]. A particular form of this procedure was used by Yang and co-workers for the case of linear systems [108]. Also, Dorling and Zinober [17] proposed a different approach to generate this transformation. In this work, yet another convenient and systematic approach is proposed to construct such transformation.

Let $\mathbf{N_2}$ be a $n \times m_c$ matrix whose columns constitute an orthonormal basis for $\mathcal{R}(\mathbf{B})$, i.e. the column space of the matrix $\mathbf{B}$; and let $\mathbf{N_1}$ be a $n \times (n - m_c)$ matrix whose columns constitute an orthonormal basis for the orthogonal complement of $\mathcal{R}(\mathbf{B})$. The following state transformation is defined:

$$\boldsymbol{\eta} = \mathbf{T}\,\mathbf{y} \tag{2.36}$$

in which

$$\mathbf{T} = \begin{bmatrix} \mathbf{N_1} & \mathbf{N_2} \end{bmatrix} \tag{2.37}$$

Note that $\mathbf{T}$ is unitary by construction, and therefore

$$\mathbf{T}^{-1} = \mathbf{T}^{T} \tag{2.38}$$

Substituting (2.36) in the state equations (2.23), premultiplying by $\mathbf{T}^{-1}$ and considering (2.38), we obtain

$$\dot{\mathbf{y}} = \bar{\mathbf{A}}\,\mathbf{y} + \bar{\mathbf{B}}\,\mathbf{u} + \bar{\mathbf{e}}\,\ddot{x}_g \tag{2.39}$$

where

$$\bar{\mathbf{A}} = \mathbf{T}^T \mathbf{A}\, \mathbf{T},\ \bar{\mathbf{B}} = \mathbf{T}^T \mathbf{B} \ \text{ and } \ \bar{\mathbf{e}} = \mathbf{T}^T \mathbf{e} \tag{2.40}$$

The linear definition of the sliding surface can also be written in terms of the new state variables as follows:

$$\mathbf{s}(\mathbf{y}) = \bar{\mathbf{C}}_\mathbf{s} \mathbf{y} = \mathbf{0} \tag{2.41}$$

where

$$\bar{\mathbf{C}}_\mathbf{s} = \mathbf{C}_\mathbf{s} \mathbf{T} \tag{2.42}$$

Since the matrix $\mathbf{T}$ is nonsingular, the resulting matrix $\bar{\mathbf{C}}_\mathbf{s}$ has the same rank as $\mathbf{C}_\mathbf{s}$, i.e. $\text{rank}(\bar{\mathbf{C}}_\mathbf{s}) = m_s$. It was mentioned before that this will allow one to describe the sliding motion in terms of a reduced set of variables. In particular, and based on the definition of the transformation $\mathbf{T}$, a description of the sliding motion will be sought in terms of the first n_r components of the transformed state vector $\mathbf{y}$. Let $\mathbf{y}$ be partitioned as follows:

$$\mathbf{y} = \left\{ \begin{array}{c} \mathbf{y_1} \\ \mathbf{y_2} \end{array} \right\} \tag{2.43}$$

with the first n_r components arranged in the vector $\mathbf{y_1}$ and the remaining m_s variables collected in the vector $\mathbf{y_2}$. The matrix $\bar{\mathbf{C}}_\mathbf{s}$ is partitioned accordingly in the following form:

$$\bar{\mathbf{C}}_\mathbf{s} = \left[\begin{array}{cc} \bar{\mathbf{C}}_{\mathbf{s1}} & \bar{\mathbf{C}}_{\mathbf{s2}} \end{array} \right] \tag{2.44}$$

where the submatrices $\bar{\mathbf{C}}_{\mathbf{s1}}$ and $\bar{\mathbf{C}}_{\mathbf{s2}}$ have dimensions $m_s \times n_r$ and $m_s \times m_s$, respectively. To write the sliding equations in terms of $\mathbf{y_1}$, it is clearly necessary to assume that the sliding surface matrix will be designed such that the submatrix $\bar{\mathbf{C}}_{\mathbf{s2}}$ is nonsingular.

The state equations (2.39) can also be written in partitioned form as follows:

$$\left\{ \begin{array}{c} \dot{\mathbf{y}}_\mathbf{1} \\ \dot{\mathbf{y}}_\mathbf{2} \end{array} \right\} = \left[\begin{array}{cc} \bar{\mathbf{A}}_{11} & \bar{\mathbf{A}}_{12} \\ \bar{\mathbf{A}}_{21} & \bar{\mathbf{A}}_{22} \end{array} \right] \left\{ \begin{array}{c} \mathbf{y_1} \\ \mathbf{y_2} \end{array} \right\} + \left[\begin{array}{c} \bar{\mathbf{B}}_1 \\ \bar{\mathbf{B}}_2 \end{array} \right] \mathbf{u} + \left\{ \begin{array}{c} \bar{\mathbf{e}}_1 \\ \bar{\mathbf{e}}_2 \end{array} \right\} \ddot{x}_g \tag{2.45}$$

By considering (2.37), the transformed matrix $\bar{\mathbf{B}}$ can be written as

$$\bar{\mathbf{B}} = \begin{bmatrix} \mathbf{N_1}^T \\ \mathbf{N_2}^T \end{bmatrix} \mathbf{B} = \begin{bmatrix} \mathbf{0} \\ \hat{\mathbf{B}} \end{bmatrix} \tag{2.46}$$

in which $\hat{\mathbf{B}}$ is a $m_c \times m_c$ nonsingular matrix. Therefore, it is easy to see that the $n_r \times m_c$ submatrix $\bar{\mathbf{B}}_\mathbf{1}$ in (2.45) has the following structure:

$$\bar{\mathbf{B}}_\mathbf{1} = \begin{bmatrix} \mathbf{0} \\ \bar{\mathbf{B}}_\mathbf{1b} \end{bmatrix} \tag{2.47}$$

where the submatrix $\bar{\mathbf{B}}_\mathbf{1b}$, with dimensions $m_r \times m_c$, denotes the top m_r rows of the matrix $\hat{\mathbf{B}}$. Hence, the partition $\bar{\mathbf{B}}_\mathbf{1}$ has rank $m_r < m_c$ and it is clear that the state transformation (2.36) achieves a representation that guarantees the existence of a nontrivial null space of $\bar{\mathbf{B}}_\mathbf{1}$ by minimizing its rank. Note that in the case $m_s = m_c$, the matrix $\bar{\mathbf{B}}_\mathbf{1}$ reduces to a null matrix.

This transformation renders possible to obtain a description of the sliding motion in terms of the variables $\mathbf{y_1}$ with no participation of the control actions. The sliding motion conditions (2.29) and (2.30) can be written in terms of the transformed variables as follows:

$$\mathbf{s}(\mathbf{y}) = \bar{\mathbf{C}}_\mathbf{s}\mathbf{y} = \mathbf{0} \tag{2.48}$$

$$\dot{\mathbf{s}}(\mathbf{y}) \mid_{\mathbf{u}=\hat{\mathbf{u}}} = \bar{\mathbf{C}}_\mathbf{s}\dot{\mathbf{y}} = \mathbf{0} \tag{2.49}$$

and considering the partitioning defined in (2.45) and (2.44), it follows that the motion of the system when constrained to satisfy the condition (2.49) can be described in terms of the following n_r equations:

$$\dot{\mathbf{y}}_\mathbf{1} = \bar{\mathbf{A}}_\mathbf{11}\mathbf{y_1} + \bar{\mathbf{A}}_\mathbf{12}\mathbf{y_2} + \bar{\mathbf{B}}_\mathbf{1}\,\hat{\mathbf{u}} + \bar{\mathbf{e}}_\mathbf{1}\,\ddot{x}_g \tag{2.50}$$

The control $\hat{\mathbf{u}}$ enforcing this condition must be obtained by considering

$$\dot{\mathbf{s}}(\mathbf{y}) \mid_{\mathbf{u}=\hat{\mathbf{u}}} = \bar{\mathbf{C}}_\mathbf{s}\dot{\mathbf{y}} = \bar{\mathbf{C}}_\mathbf{s}\left[\bar{\mathbf{A}}\,\mathbf{y} + \bar{\mathbf{B}}\,\hat{\mathbf{u}} + \bar{\mathbf{e}}\,\ddot{x}_g\right] = \mathbf{0} \tag{2.51}$$

and therefore $\hat{\mathbf{u}}$ must be a solution of

$$\bar{\mathbf{C}}_{\mathbf{s}}\bar{\mathbf{B}}\,\hat{\mathbf{u}} = -\bar{\mathbf{C}}_{\mathbf{s}}\bar{\mathbf{A}}\,\mathbf{y} - \bar{\mathbf{C}}_{\mathbf{s}}\bar{\mathbf{e}}\,\ddot{x}_g \tag{2.52}$$

Note that by construction

$$\text{rank}(\bar{\mathbf{C}}_{\mathbf{s}}\bar{\mathbf{B}}) = m_s \tag{2.53}$$

Hence, since the rank of the coefficient matrix is m_s, the solution space has dimension m_r. Therefore, the solution it is not unique for the cases with redundancy of control actions, that is $m_r > 1$.

If the $m_c \times m_s$ matrix $\left[\bar{\mathbf{C}}_{\mathbf{s}}\bar{\mathbf{B}}\right]^R$ denotes a right inverse of the matrix $\bar{\mathbf{C}}_{\mathbf{s}}\bar{\mathbf{B}}$, that is

$$\bar{\mathbf{C}}_{\mathbf{s}}\bar{\mathbf{B}}\ \left[\bar{\mathbf{C}}_{\mathbf{s}}\bar{\mathbf{B}}\right]^R = \mathbf{I}_{m_s} \tag{2.54}$$

then the control actions $\hat{\mathbf{u}}$ that satisfy (2.52) can be written as

$$\hat{\mathbf{u}} = -\left[\bar{\mathbf{C}}_{\mathbf{s}}\bar{\mathbf{B}}\right]^R \left\{\bar{\mathbf{C}}_{\mathbf{s}}\bar{\mathbf{A}}\,\mathbf{y} + \bar{\mathbf{C}}_{\mathbf{s}}\bar{\mathbf{e}}\,\ddot{x}_g\right\} \tag{2.55}$$

Now, if $\hat{\mathbf{u}}$ is additionally required to be contained in the null space of $\bar{\mathbf{B}}_{\mathbf{1}}$, then the following m_r conditions must be satisfied:

$$\bar{\mathbf{B}}_{\mathbf{1b}}\,\hat{\mathbf{u}} = \mathbf{0} \tag{2.56}$$

The control actions $\hat{\mathbf{u}}$ that satisfy (2.52) and (2.56) can be obtained as a solution of

$$\begin{bmatrix} \bar{\mathbf{B}}_{\mathbf{1b}} \\ \bar{\mathbf{C}}_{\mathbf{s}}\bar{\mathbf{B}} \end{bmatrix} \hat{\mathbf{u}} = \begin{Bmatrix} \mathbf{0} \\ -\bar{\mathbf{C}}_{\mathbf{s}}\bar{\mathbf{A}}\,\mathbf{y} - \bar{\mathbf{C}}_{\mathbf{s}}\bar{\mathbf{e}}\,\ddot{x}_g \end{Bmatrix} \tag{2.57}$$

It will now be shown that the matrix on the left-hand side of (2.57) is nonsingular, thus ensuring that a unique $\hat{\mathbf{u}}$ can be found. Considering the definitions (2.45), (2.46) and (2.47), it is possible to write

$$\hat{\mathbf{B}} = \begin{bmatrix} \bar{\mathbf{B}}_{\mathbf{1b}} \\ \bar{\mathbf{B}}_{\mathbf{2}} \end{bmatrix} \tag{2.58}$$

and taking into account (2.44), the product $\bar{\mathbf{C}}_{\mathbf{s}}\bar{\mathbf{B}}$ can be written as

$$\bar{\mathbf{C}}_{\mathbf{s}}\bar{\mathbf{B}} = \begin{bmatrix} \bar{\mathbf{C}}_{\mathbf{s1b}} & \bar{\mathbf{C}}_{\mathbf{s2}} \end{bmatrix} \begin{bmatrix} \bar{\mathbf{B}}_{\mathbf{1b}} \\ \bar{\mathbf{B}}_{\mathbf{2}} \end{bmatrix} \tag{2.59}$$

in which the submatrix $\bar{\mathbf{C}}_{\mathbf{s1b}}$ indicates the last m_r columns of $\bar{\mathbf{C}}_{\mathbf{s1}}$. Therefore, the coefficient matrix of the system (2.57) can be factored as

$$\begin{bmatrix} \bar{\mathbf{B}}_{\mathbf{1b}} \\ \bar{\mathbf{C}}_{\mathbf{s}}\bar{\mathbf{B}} \end{bmatrix} = \begin{bmatrix} \mathbf{I}_{m_r} & \mathbf{0} \\ \bar{\mathbf{C}}_{\mathbf{s1b}} & \bar{\mathbf{C}}_{\mathbf{s2}} \end{bmatrix} \begin{bmatrix} \bar{\mathbf{B}}_{\mathbf{1b}} \\ \bar{\mathbf{B}}_{\mathbf{2}} \end{bmatrix} = \begin{bmatrix} \mathbf{I}_{m_r} & \mathbf{0} \\ \bar{\mathbf{C}}_{\mathbf{s1b}} & \bar{\mathbf{C}}_{\mathbf{s2}} \end{bmatrix} \hat{\mathbf{B}} \tag{2.60}$$

which clearly shows that it is nonsingular, based on the full rank of the matrices $\hat{\mathbf{B}}$ and $\bar{\mathbf{C}}_{\mathbf{s2}}$. Hence, there is a unique solution $\hat{\mathbf{u}}$ that satisfies (2.57) and it is given by

$$\hat{\mathbf{u}} = \hat{\mathbf{B}}^{-1} \begin{bmatrix} \mathbf{I}_{m_r} & \mathbf{0} \\ -\bar{\mathbf{C}}_{\mathbf{s2}}^{-1}\bar{\mathbf{C}}_{\mathbf{s1b}} & \bar{\mathbf{C}}_{\mathbf{s2}}^{-1} \end{bmatrix} \begin{Bmatrix} \mathbf{0} \\ -\bar{\mathbf{C}}_{\mathbf{s}}\bar{\mathbf{A}}\,\mathbf{y} - \bar{\mathbf{C}}_{\mathbf{s}}\bar{\mathbf{e}}\,\ddot{x}_g \end{Bmatrix} \tag{2.61}$$

This can be written more compactly as follows:

$$\hat{\mathbf{u}} = \mathbf{u}_{\mathbf{s}} + \mathbf{u}_{\mathbf{e}} \tag{2.62}$$

where the components $\mathbf{u}_{\mathbf{s}}$ and $\mathbf{u}_{\mathbf{e}}$, which depend respectively on the system states and the external excitation, are defined as

$$\mathbf{u}_{\mathbf{s}} = -\left[\bar{\mathbf{C}}_{\mathbf{s}}\bar{\mathbf{B}}\right]^{\ddagger}\bar{\mathbf{C}}_{\mathbf{s}}\bar{\mathbf{A}}\,\mathbf{y} \;\text{ and }\; \mathbf{u}_{\mathbf{e}} = -\left[\bar{\mathbf{C}}_{\mathbf{s}}\bar{\mathbf{B}}\right]^{\ddagger}\bar{\mathbf{C}}_{\mathbf{s}}\bar{\mathbf{e}}\,\ddot{x}_g \tag{2.63}$$

in which the matrix $\left[\bar{\mathbf{C}}_{\mathbf{s}}\bar{\mathbf{B}}\right]^{\ddagger}$ denotes a particular right inverse of $\left[\bar{\mathbf{C}}_{\mathbf{s}}\bar{\mathbf{B}}\right]$, given by

$$\left[\bar{\mathbf{C}}_{\mathbf{s}}\bar{\mathbf{B}}\right]^{\ddagger} = \hat{\mathbf{B}}^{-1} \begin{bmatrix} \mathbf{0} \\ \bar{\mathbf{C}}_{\mathbf{s2}}^{-1} \end{bmatrix} \tag{2.64}$$

and characterized by the fact that

$$\bar{\mathbf{B}}_{\mathbf{1b}}\left[\bar{\mathbf{C}}_{\mathbf{s}}\bar{\mathbf{B}}\right]^{\ddagger} = \mathbf{0} \tag{2.65}$$

Finally, substituting (2.62) and (2.63) into the equations (2.50) and considering (2.65), it follows that the evolution of the system subject to the dynamic condition (2.49) can be described as follows:

$$\dot{\mathbf{y}}_{\mathbf{1}} = \bar{\mathbf{A}}_{\mathbf{11}}\mathbf{y}_{\mathbf{1}} + \bar{\mathbf{A}}_{\mathbf{12}}\mathbf{y}_{\mathbf{2}} + \bar{\mathbf{e}}_{\mathbf{1}}\,\ddot{x}_g \tag{2.66}$$

Considering (2.48), the sliding motion equations are given by

$$\dot{\mathbf{y}}_1 = \left[\bar{\mathbf{A}}_{11} - \bar{\mathbf{A}}_{12}\mathbf{C}_{s2}^{-1}\mathbf{C}_{s1}\right]\mathbf{y}_1 + \bar{\mathbf{e}}_1\,\ddot{x}_g \tag{2.67}$$

Equation (2.67) offers a very convenient framework to perform the design of the sliding surface. The selection of the sliding surface must be performed by appropriately choosing a constant matrix $\bar{\mathbf{C}}_r = \mathbf{C}_{s2}^{-1}\mathbf{C}_{s1}$ such that the resulting reduced order dynamics shows some desirable characteristics.

2.5.2 Transformation Matrix

A direct procedure to generate the transformation $\mathbf{T}$ introduced in (2.36) is obtained by considering the singular value decomposition of the control input matrix $\mathbf{B}$ as follows:

$$\mathbf{B} = \mathbf{V}_1\,\mathbf{R}\,\mathbf{V}_2^T \tag{2.68}$$

in which $\mathbf{V}_1$ and $\mathbf{V}_2$ are $n \times n$ and $m_c \times m_c$ unitary matrices, respectively. The matrix $\mathbf{R}$ has the following structure:

$$\mathbf{R} = \begin{bmatrix} \mathbf{\Sigma} \\ \mathbf{0} \end{bmatrix} \tag{2.69}$$

where $\mathbf{\Sigma} = \text{diag}(\sigma_i)$ with $\sigma_i > 0$, $i = 1, 2, ..., m_c$. By construction, the first m_c columns of the matrix $\mathbf{V}_1$ constitute an orthonormal basis for the column space of $\mathbf{B}$. This factorization of $\mathbf{B}$ can be used to define a unitary transformation matrix $\mathbf{T}$ in the following form:

$$\mathbf{T} = \mathbf{V}_1\mathbf{E}_p \tag{2.70}$$

where $\mathbf{E}_p$ is a $n \times n$ permutation matrix that conveniently interchanges the columns of $\mathbf{V}_1$. This matrix can be defined, for example, as

$$\mathbf{E}_p = \begin{bmatrix} \mathbf{0} & \mathbf{I}_{m_c} \\ \mathbf{I}_{n-m_c} & \mathbf{0} \end{bmatrix} \tag{2.71}$$

Note that for this particular selection of $\mathbf{E_p}$ the transformed matrix $\bar{\mathbf{B}}$ takes the form

$$\bar{\mathbf{B}} = \mathbf{E}_\mathbf{p}^T \mathbf{V}_\mathbf{1}^T \mathbf{B} = \begin{bmatrix} \mathbf{0} \\ \mathbf{\Sigma V}_\mathbf{2}^T \end{bmatrix} \tag{2.72}$$

and therefore, by considering (2.46), the nonsingular matrix $\hat{\mathbf{B}}$ is given by

$$\hat{\mathbf{B}} = \mathbf{\Sigma V}_\mathbf{2}^T \tag{2.73}$$

This expression for $\hat{\mathbf{B}}$ provides a straightforward computation of its inverse, required in equation (2.64), and given by $\hat{\mathbf{B}}^{-1} = \mathbf{V_2 \Sigma}^{-1}$, where $\mathbf{\Sigma}^{-1} = \text{diag}(1/\sigma_i)$.

2.6 Sliding Surface Design

Several approaches have been proposed to appropriately design the sliding surface. Some of the most commonly used procedures are based on eigenstructure assignment techniques. In this case, the matrix $\mathbf{C_r} = \mathbf{C_{s2}^{-1} C_{s1}}$ is determined such that the eigenvalues of the sliding motion matrix $\bar{\mathbf{A}}_\mathbf{11} - \bar{\mathbf{A}}_\mathbf{12} \mathbf{C_r}$ are located in some predetermined locations of the complex plane [89]. It is also possible to assign, at least partially, the corresponding eigenvector structure [17].

Another classical method for sliding surface design is based on the minimization of a quadratic performance index of the form [18, 89]:

$$J = \int_{t_h}^{\infty} \mathcal{L}_1 \, dt \tag{2.74}$$

in which $\mathcal{L}_1$ represents a quadratic function of the form:

$$\mathcal{L}_1 = \mathbf{d}^T \mathbf{Q_1 d} + \dot{\mathbf{d}}^T \mathbf{Q_2} \dot{\mathbf{d}} \tag{2.75}$$

where $\mathbf{Q_1}$ and $\mathbf{Q_2}$ are $n_f \times n_f$ positive definite weighting matrices. The lower limit of the integral is explicitly denoted as t_h to indicate that this performance index is evaluated for

the system under sliding conditions. This time t_h, referred to as the *hitting time*, is the time for which the system reaches the sliding surface, which without any loss of generality can be set $t_h = 0$.

Introducing the transformation of coordinates given by (2.36), the performance index takes the following form:

$$J_1 = \int_0^\infty \left(\mathbf{y}_1^T \, \bar{\mathbf{Q}}_{11} \, \mathbf{y}_1 + 2 \, \mathbf{y}_1^T \, \bar{\mathbf{Q}}_{12} \, \mathbf{y}_2 + \mathbf{y}_2^T \, \bar{\mathbf{Q}}_{22} \, \mathbf{y}_2 \right) dt \tag{2.76}$$

where the matrices $\bar{\mathbf{Q}}_{11}$, $\bar{\mathbf{Q}}_{12}$ and $\bar{\mathbf{Q}}_{22}$ are submatrices of the transformed weighting matrix $\bar{\mathbf{Q}}$ as follows:

$$\bar{\mathbf{Q}} = \mathbf{T}^T \begin{bmatrix} \mathbf{Q}_1 & \mathbf{0} \\ \mathbf{0} & \mathbf{Q}_2 \end{bmatrix} \mathbf{T} = \begin{bmatrix} \bar{\mathbf{Q}}_{11} & \bar{\mathbf{Q}}_{12} \\ \bar{\mathbf{Q}}_{12}^T & \bar{\mathbf{Q}}_{22} \end{bmatrix} \tag{2.77}$$

Note that the resulting submatrix $\bar{\mathbf{Q}}_{22}$ is positive definite.

This cost function must be minimized subject to the constraints of the sliding motion equations. Assuming that the system is acted upon by the control $\hat{\mathbf{u}}$ defined in (2.62) and neglecting the effect of the external excitation, the resulting motion can be described by

$$\dot{\mathbf{y}}_1 = \bar{\mathbf{A}}_{11} \mathbf{y}_1 + \bar{\mathbf{A}}_{12} \mathbf{y}_2 \tag{2.78}$$

If the vector $\mathbf{y}_2$ is regarded as a control term, then the problem of minimizing (2.76) subject to (2.78) can be solved as a classical optimal control problem. This renders an optimal solution in the form of a linear relation between $\mathbf{y}_2$ and $\mathbf{y}_1$, given by

$$\mathbf{y}_2 = -\bar{\mathbf{C}}_\mathbf{r} \mathbf{y}_1 \quad \text{with} \quad \bar{\mathbf{C}}_\mathbf{r} = \bar{\mathbf{Q}}_{22}^{-1} \left[\bar{\mathbf{A}}_{12}^T \, \bar{\mathbf{P}} + \bar{\mathbf{Q}}_{12}^T \right] \tag{2.79}$$

where the matrix $\bar{\mathbf{P}}$ is the solution of the following algebraic Ricatti equation:

$$\bar{\mathbf{P}} \, \bar{\mathbf{A}}_1 + \bar{\mathbf{A}}_1^T \, \bar{\mathbf{P}} + \bar{\mathbf{P}} \, \bar{\mathbf{A}}_{12} \, \bar{\mathbf{Q}}_{22}^{-1} \, \bar{\mathbf{A}}_{12}^T \, \bar{\mathbf{P}} = -\bar{\mathbf{Q}}_1 \tag{2.80}$$

in which the matrix $\bar{\mathbf{Q}}_1$ is given by

$$\bar{\mathbf{Q}}_1 = \bar{\mathbf{Q}}_{11} - \bar{\mathbf{Q}}_{12} \bar{\mathbf{Q}}_{22}^{-1} \bar{\mathbf{Q}}_{12}^T \tag{2.81}$$

Finally, taking (2.42) into account, the sliding surface matrix can be obtained as

$$\mathbf{C_s} = \mathbf{T}^T \bar{\mathbf{Q}}_{\mathbf{22}}^{-1} \left[\begin{array}{cc} \bar{\mathbf{A}}_{\mathbf{12}}^T \bar{\mathbf{P}} + \bar{\mathbf{Q}}_{\mathbf{12}}^T & \bar{\mathbf{Q}}_{\mathbf{22}} \end{array} \right] \tag{2.82}$$

2.7 Control System Design

Having established the sliding surface, we must now define the control actions required to force the system state to reach this sliding surface from any point in the state space, and then maintain it there. In general, these control actions involve some form of discontinuity with respect to this surface, needed to alter the structure of the system each time the state $\boldsymbol{\eta}$ tends to move away from $\mathbf{s}(\boldsymbol{\eta}) = \mathbf{0}$. By these discontinuities we are trying to modify the trajectories in the phase space in such a way that they point towards the sliding surface.

A general approach based on Lyapunov's direct method will be used for the design of the controller. The idea is to guarantee that the origin is an asymptotically stable equilibrium point for the motion in the space $\{s_1, s_2, \ldots, s_{m_s}\}$, as it is represented in Figure (2.2). Let V be a Lyapunov function candidate of the form:

$$V = \frac{1}{2} \mathbf{s}^T \boldsymbol{\Pi}\, \mathbf{s} \tag{2.83}$$

in which $\boldsymbol{\Pi}$ is denotes a $m_s \times m_s$ positive definite matrix to be defined later. The function V is positive definite, that is, $V > 0$ whenever $\mathbf{s} \neq \mathbf{0}$. The time derivative of this function is given by

$$\frac{d}{dt}(V) = \mathbf{s}^T \boldsymbol{\Pi}\, \dot{\mathbf{s}} \tag{2.84}$$

Considering the state equations (2.23) and the definition of the sliding surface given by (2.27), it follows that the dynamic evolution of the quantities $s_1, s_2, ..., s_{m_s}$ is governed by

$$\dot{\mathbf{s}} = \mathbf{C_s} \left\{ \mathbf{A}\, \boldsymbol{\eta} + \mathbf{e}\, \ddot{x}_g \right\} + \mathbf{C_s B}\, \mathbf{u} \tag{2.85}$$

Substituting (2.85) into (2.84), the time derivative of V can be written as

$$\frac{d}{dt}(V) = \mathbf{s}^T \mathbf{\Pi}\, \mathbf{C_s} \{\mathbf{A}\,\boldsymbol{\eta} + \mathbf{e}\,\ddot{x}_g\} + \mathbf{s}^T \mathbf{\Pi}\, \mathbf{C_s} \mathbf{B}\,\mathbf{u} \tag{2.86}$$

In order to assure the existence of sliding motion and to guarantee that any motion is going to be attracted to the sliding surface, the purpose of the controller is to force (2.86) to be a negative definite function (with exclusion of any discontinuity points as the time derivative may not be defined there). In the following, several possible controller designs are presented for both active and semi-active control strategies.

2.7.1 Active Control

Typically, a sliding mode controller has the following structure [14]:

$$\mathbf{u} = \mathbf{u_1}(\boldsymbol{\eta}, \ddot{x}_g) + \mathbf{u_2}(\boldsymbol{\eta}) \tag{2.87}$$

where the component $\mathbf{u_1}$ involves, in general, some form of state feedback and disturbance measurements. On the other hand, the component $\mathbf{u_2}$ represents some linear or nonlinear, continuous or discontinuous form of state feedback.

The aforementioned controller structure is based on the availability of information about the external disturbance. This information is required to compensate the effect of the disturbance in the equations (2.85). However, it is desirable to design an active controller with no direct or static dependency on the external excitation. In the sequel, several alternative controllers are formulated which do not require instantaneous information of the ground motion, but only use a bounding value.

A possible family of designs with such characteristic can be generated by selecting the component $\mathbf{u_1}$ equal to the control $\mathbf{u_s}$ defined in (2.63). Considering the definitions (2.36), (2.40) and (2.42) one can write

$$\mathbf{u_1} = \mathbf{u_s} = -\left[\bar{\mathbf{C}}_\mathbf{s}\bar{\mathbf{B}}\right]^\ddagger \mathbf{C_s}\mathbf{A}\,\boldsymbol{\eta} \tag{2.88}$$

where $\left[\bar{\mathbf{C}}_\mathbf{s}\bar{\mathbf{B}}\right]^\ddagger$ was defined in (2.64). Noting that

$$\mathbf{C_s B} = \bar{\mathbf{C}}_\mathbf{s}\bar{\mathbf{B}} \tag{2.89}$$

it is immediate that this matrix is a right inverse for the product $\mathbf{C_s B}$, i.e.

$$\mathbf{C_s B}\,\left[\bar{\mathbf{C}}_\mathbf{s}\bar{\mathbf{B}}\right]^\ddagger = \mathbf{I}_{m_s} \tag{2.90}$$

Substituting into (2.86), the time derivative of V now takes the form

$$\frac{d}{dt}\,(V) = \mathbf{s}^T\mathbf{\Pi}\,\mathbf{C_s e}\,\ddot{x}_g + \mathbf{s}^T\mathbf{\Pi}\,\mathbf{C_s B}\,\mathbf{u_2} \tag{2.91}$$

and depending on the choice of the component $\mathbf{u_2}$ several possible controllers can be formulated.

Discontinuous Control

Let $\mathbf{u_2}$ be defined as follows:

$$\mathbf{u_2} = -\left[\bar{\mathbf{C}}_\mathbf{s}\bar{\mathbf{B}}\right]^\ddagger \mathbf{\Delta}\,\mathrm{sign}\,(\mathbf{C_s}\boldsymbol{\eta}) \tag{2.92}$$

in which $\mathbf{\Delta}$ is a matrix of design parameters of the form $\mathbf{\Delta} = \mathrm{diag}(\delta_i)$ with $\delta_i > 0$ for $i = 1, 2, \ldots, m_s$ and where $\left[\bar{\mathbf{C}}_\mathbf{s}\bar{\mathbf{B}}\right]^\ddagger$ has been defined in (2.64). The vector-valued function sign represents a m_s-dimensional vector whose components are given by the sign of the corresponding entries of its argument.

Substituting $\mathbf{u_2}$ into (2.91) and selecting $\mathbf{\Pi} = \mathbf{I}_{m_s}$ for the definition of the function V, it follows that

$$\frac{d}{dt}\,(V) = \mathbf{s}^T\mathbf{C_s e}\,\ddot{x}_g - \mathbf{s}^T\mathbf{\Delta}\,\mathrm{sign}\,(\mathbf{s}) \tag{2.93}$$

where the definition of the sliding surface (2.27) has been also taken into account.

To enforce the global asymptotic stability of the point $\mathbf{s} = \mathbf{0}$ and therefore to guarantee the attraction to the sliding surface, the control actions should force the time derivative of

V to be negative for any $\mathbf{s} \neq \mathbf{0}$. Therefore, it is interesting to investigate the existence of regions for which the attraction can be guaranteed.

Considering the first term of the right hand side of (2.93), one can write

$$\mathbf{s}^T \mathbf{C_s e}\, \ddot{x}_g \leq \mid \mathbf{s}^T \mathbf{C_s e} \mid\mid \ddot{x}_g \mid \tag{2.94}$$

Let $\ddot{x}_g^{\max}$ be a bounding value for the ground acceleration to which the structure is likely to be subjected. This value may be chosen as the maximum ground acceleration value that can be expected at the site. That is,

$$\mid \ddot{x}_g \mid \leq \ddot{x}_g^{\max} \tag{2.95}$$

and therefore it can be written

$$\mathbf{s}^T \mathbf{C_s e}\, \ddot{x}_g \leq \mid \mathbf{s}^T \mathbf{C_s e} \mid \ddot{x}_g^{\max} \tag{2.96}$$

Additionally, by using the Cauchy-Schwartz inequality,

$$\mid \mathbf{s}^T \mathbf{C_s e} \mid \leq \parallel \mathbf{s} \parallel_2 \parallel \mathbf{C_s e} \parallel_2 \tag{2.97}$$

and taking into account that

$$\parallel \mathbf{s} \parallel_2 \leq \parallel \mathbf{s} \parallel_1 \tag{2.98}$$

where $\parallel . \parallel_p$denotes the p-norm, one can write

$$\mathbf{s}^T \mathbf{C_s e}\, \ddot{x}_g \leq \alpha \ddot{x}_g^{\max} \parallel \mathbf{s} \parallel_1 \tag{2.99}$$

where the parameter α has been defined as $\alpha = \parallel \mathbf{C_s e} \parallel_2$.

On the other hand, considering that

$$\mathbf{s}^T \boldsymbol{\Delta}\, \mathrm{sign}\,(\mathbf{s}) \geq \delta_{\min}\, \mathbf{s}^T\, \mathrm{sign}\,(\mathbf{s}) \tag{2.100}$$

in which $\delta_{\min}$ denotes the smallest entry of the diagonal matrix $\mathbf{\Delta}$, and

$$\mathbf{s}^T \operatorname{sign}(\mathbf{s}) = \| \mathbf{s} \|_1 \tag{2.101}$$

then it follows that

$$\mathbf{s}^T \mathbf{\Delta} \operatorname{sign}(\mathbf{s}) \geq \delta_{\min} \| \mathbf{s} \|_1 \tag{2.102}$$

By considering (2.99) and (2.102), one can write

$$\frac{d}{dt}(V) \leq \left(\alpha \ddot{x}_g^{\max} - \delta_{\min}\right) \| \mathbf{s} \|_1 \tag{2.103}$$

and therefore a sufficient condition for the time derivative of V to be negative definite is given by

$$\delta_{\min} > \alpha \ddot{x}_g^{\max} \tag{2.104}$$

Continuous Control

In general, discontinuous sliding mode controllers are characterized by a remarkable robustness with respect to parameter uncertainties and external disturbances. However, the associated switching of the control actions can also lead to a phenomenon known as chattering, characterized by a high frequency control activity which is in general undesirable. To avoid this problem, one can use a continuous control law to approximate the behavior of the classical sliding mode controller. Several such controllers have been proposed by Ambrosino *et al.* [1], Burton and Zinober [9] and Slotine and Sastry [74], among others. Excellent applications of continuous sliding mode controllers to civil structures are presented by Yang *et al.* [108]. Many of the aforementioned control laws are based on the availability of information about the external disturbance. However, using the concepts from the theory of control of uncertain systems developed by Leitmann and co-workers [47, 13], it is still possible to develop controllers based only on bounds on the possible size

of the disturbance, as shown in [13, 68, 122]. In the following, several possible continuous controllers for the general case $m_c \geq m_s$ are formulated based on a bounding value for the ground acceleration.

Let $\mathbf{u_2}$ be defined as follows:

$$\mathbf{u_2} = -\left[\bar{\mathbf{C}}_\mathbf{s}\bar{\mathbf{B}}\right]^\ddagger \boldsymbol{\Delta}\mathbf{C}_\mathbf{s}\boldsymbol{\eta} \tag{2.105}$$

in which $\boldsymbol{\Delta}$ is a matrix of design parameters of the form $\boldsymbol{\Delta} = \mathrm{diag}(\delta_i)$ with $\delta_i > 0$ for $i = 1, 2, \ldots, m_s$ and where $\left[\bar{\mathbf{C}}_\mathbf{s}\bar{\mathbf{B}}\right]^\ddagger$ has been defined in (2.64). Substituting $\mathbf{u_2}$ into (2.91) and selecting again $\boldsymbol{\Pi} = \mathbf{I}_{m_s}$ for the definition of the function V, it follows that

$$\frac{d}{dt}(V) = \mathbf{s}^T\mathbf{C}_\mathbf{s}\mathbf{e}\,\ddot{x}_g - \mathbf{s}^T\boldsymbol{\Delta}\,\mathbf{s} \tag{2.106}$$

where the definition of the sliding surface (2.27) has been also taken into account.

The existence of regions of attraction is investigated next. Considering the first term of the right hand side of (2.106), one can write as before

$$\mathbf{s}^T\mathbf{C}_\mathbf{s}\mathbf{e}\,\ddot{x}_g \leq \mid \mathbf{s}^T\mathbf{C}_\mathbf{s}\mathbf{e} \mid \ddot{x}_g^{\max} \tag{2.107}$$

where $\ddot{x}_g^{\max}$ is a bounding value for the ground acceleration as defined in (2.95).

Next, by considering the Cauchy-Schwartz inequality (2.97) and the fact that

$$\|\mathbf{s}\|_2\|\mathbf{C}_\mathbf{s}\mathbf{e}\|_2 \leq \frac{1}{2}\left(\|\mathbf{s}\|_2^2 + \|\mathbf{C}_\mathbf{s}\mathbf{e}\|_2^2\right) \tag{2.108}$$

it follows

$$\mathbf{s}^T\mathbf{C}_\mathbf{s}\mathbf{e}\,\ddot{x}_g \leq \frac{\ddot{x}_g^{\max}}{2}\left(\|\mathbf{s}\|_2^2 + \alpha^2\right) \tag{2.109}$$

where again the parameter α has been defined as $\alpha = \| \mathbf{C}_\mathbf{s}\mathbf{e} \|_2$.

On the other hand, it can be shown that

$$\mathbf{s}^T\boldsymbol{\Delta}\,\mathbf{s} \geq \delta_{\min}\|\mathbf{s}\|_2^2 \tag{2.110}$$

in which $\delta_{\min}$ denotes as before the smallest entry of the diagonal matrix $\mathbf{\Delta}$.

Finally, by taking (2.109) and (2.110) into account, the time derivative of the Lyapunov function can now be shown to satisfy to following inequality:

$$\frac{d}{dt}(V) \leq \frac{1}{2}\left(\ddot{x}_g^{\max} - 2\delta_{\min}\right)\|\mathbf{s}\|_2^2 + \frac{\ddot{x}_g^{\max}}{2}\alpha^2 \tag{2.111}$$

Therefore, it is possible to establish a region in the $(s_1, s_2, \ldots s_{m_s})$ space defined by the following scalar function

$$g_1(s) = -a_1\, s^2 + b_1 \; < 0 \tag{2.112}$$

where $s = \|\mathbf{s}\|_2$ and

$$a_1 = 2\delta_{\min} - \ddot{x}_g^{\max} \tag{2.113}$$

$$b_1 = \ddot{x}_g^{\max}\alpha^2 \tag{2.114}$$

for which, provided that $a_1 > 0$, the attraction to the sliding surface is guaranteed. Note that now the control cannot guarantee the global asymptotic stability of the point $\mathbf{s} = \mathbf{0}$ but instead it assures that all trajectories will ultimately lie within a bounded neighborhood of that point. Notice also that this is a conservative bound and in practice the system will stay in a region closer to the origin $\mathbf{s} = \mathbf{0}$ than the lower bound defined by (2.112).

It is important to remark that the continuous control law defined by (2.88) and (2.105) can not guarantee the existence of the ideal sliding conditions (2.29) and (2.30). Outside the region defined by (2.112), the control actions are directing the system state toward the sliding surface. But in general, this continuous controller will lack the authority to generate a permanent sliding regime and therefore, the behavior of the controlled system will not be described by the sliding motion equations. In this context, the sliding surface and the associated sliding conditions can be regarded as auxiliary design tools.

Another continuous controller can be constructed by considering the singular value decomposition of the product matrix $\mathbf{C_s B}$ as follows:

$$\mathbf{C_s B} = \mathbf{U_1 G\, U_2^T} \tag{2.115}$$

where $\mathbf{U_1}$ and $\mathbf{U_2}$ are unitary matrices with dimensions $m_s \times m_s$ and $m_c \times m_c$, respectively. Considering that $m_s \leq m_c$, the matrix $\mathbf{G}$ has the following structure:

$$\mathbf{G} = \left[\begin{array}{cc} \mathbf{\Gamma} & \mathbf{0} \end{array} \right] \tag{2.116}$$

with $\mathbf{\Gamma} = \text{diag}(\gamma_i)$. Due to the fact that $\text{rank}(\mathbf{C_s B}) = m_s$, the diagonal entries of $\mathbf{\Gamma}$ are strictly positive, i.e. $\gamma_i > 0$, $i = 1, 2, ..., m_s$.

Using the factorization (2.115), the component $\mathbf{u_2}$ is defined as follows:

$$\mathbf{u_2} = -\mathbf{U_r\, \Delta U_1^T C_s \eta} \tag{2.117}$$

in which the $m_c \times m_s$ matrix $\mathbf{U_r}$ is constructed by considering the first m_s columns of the matrix $\mathbf{U_2}$. Therefore, the columns of $\mathbf{U_r}$ define an orthonormal basis for the row space of the product matrix $\mathbf{C_s B}$. The matrix $\mathbf{\Delta}$ has the same meaning as before, i.e. $\mathbf{\Delta} = \text{diag}(\delta_i)$ with $\delta_i > 0$ for $i = 1, 2, \ldots, m_s$.

The region of attraction is investigated by substituting the proposed $\mathbf{u_2}$ into (2.91) as follows:

$$\frac{d}{dt}(V) = \mathbf{s}^T \mathbf{\Pi}\, \mathbf{C_s e}\, \ddot{x}_g - \mathbf{s}^T \mathbf{\Pi}\, \mathbf{U_1 \Gamma\, \Delta\, U_1^T s} \tag{2.118}$$

in which the definition of the sliding surface (2.27) was considered and the following result was used:

$$\mathbf{C_s B\, U_r} = \mathbf{U_1 G\, U_2^T\, U_r} = \mathbf{U_1} \left[\begin{array}{cc} \mathbf{\Gamma} & \mathbf{0} \end{array} \right] \left[\begin{array}{c} \mathbf{I}_{m_s} \\ \mathbf{0} \end{array} \right] = \mathbf{U_1 \Gamma} \tag{2.119}$$

Selecting $\mathbf{\Pi} = \mathbf{I}_{m_s}$ for the definition of the function V, the time derivative of V can be written as

$$\frac{d}{dt}(V) = \mathbf{s}^T \mathbf{C_s e}\, \ddot{x}_g - \mathbf{s}^T \mathbf{\Theta}\, \mathbf{s} \tag{2.120}$$

in which $\mathbf{\Theta}$ denotes a $m_s \times m_s$ positive definite matrix defined as

$$\mathbf{\Theta} = \mathbf{U_1 \Gamma \Delta U_1^T} \tag{2.121}$$

Akin to the previous case, if $\ddot{x}_g^{\max}$ is a bounding value for the ground acceleration as defined in (2.95), then one can obtain

$$\mathbf{s}^T \mathbf{C_s e}\, \ddot{x}_g \leq \frac{\ddot{x}_g^{\max}}{2} \left(\|\mathbf{s}\|_2^2 + \alpha^2 \right) \tag{2.122}$$

where the parameter α has been defined before.

On the other hand, it can be shown that

$$\mathbf{s}^T \mathbf{\Theta}\, \mathbf{s} \geq \lambda_{\min} \|\mathbf{s}\|_2^2 \tag{2.123}$$

in which $\lambda_{\min}$ denotes the smallest eigenvalue of the matrix $\mathbf{\Theta}$.

Finally, by taking (2.122) and (2.123) into account, the time derivative of the Lyapunov function can now be shown to satisfy to following inequality:

$$\frac{d}{dt}(V) \leq \frac{1}{2} \left(\ddot{x}_g^{\max} - 2\lambda_{\min} \right) \|\mathbf{s}\|_2^2 + \frac{\ddot{x}_g^{\max}}{2} \alpha^2 \tag{2.124}$$

Therefore, depending upon the choice of the design parameters in the matrix $\mathbf{\Delta}$ and provided that $2\lambda_{\min} > \ddot{x}_g^{\max}$, there exists a region in the $(s_1, s_2, \ldots s_{m_s})$ space defined by the following scalar function

$$g_2(s) = -a_2\, s^2 + b_1 \; < 0 \tag{2.125}$$

in which

$$a_2 = 2\lambda_{\min} - \ddot{x}_g^{\max} \tag{2.126}$$

where the attraction to the sliding surface, represented by the point $\mathbf{s} = \mathbf{0}$, is guaranteed.

Finally, it is noted that for the case $m_c = m_s$, $\mathbf{C_s B}$ is a nonsingular matrix for which one could avoid using its singular value decomposition and propose a controller of the following form

$$\mathbf{u_2} = -\boldsymbol{\Delta}\ [\mathbf{C_s}\,\mathbf{B}]^T \mathbf{C_s}\boldsymbol{\eta} \tag{2.127}$$

in which $\boldsymbol{\Delta}$ has the same meaning as before. The region of attraction in this case is also defined by (2.125), but now $\lambda_{\min}$ denotes the smallest eigenvalue of the positive definite matrix $\boldsymbol{\Theta}$ redefined as follows:

$$\boldsymbol{\Theta} = \mathbf{C_s B}\,\boldsymbol{\Delta}\ [\mathbf{C_s}\,\mathbf{B}]^T \tag{2.128}$$

2.7.2 Semi-Active Control

In the case of semi-active control, the control actions $\mathbf{u_{sa}}$ cannot achieve any arbitrary value. They are constrained by the fact that the semi-active devices can only provide nonnegative stiffness and damping values k_{v_i} and c_{v_i}. Therefore, although these control actions may succeed in bringing the system state towards the sliding surface, they may not be able to force the system to stay there.

Ideally it is desired to force the system to stay on the sliding surface $\mathbf{s} = \mathbf{0}$. However, because of the limited control action available in the semi-active case, $\mathbf{s}$ may not be identically equal to zero. The magnitude of the nonzero entries of the vector $\mathbf{s}$ represents the extent of separation of the system from the desired sliding surface. A nonnegative measure of this separation can be represented by the following function

$$V = \frac{1}{2}\mathbf{s}^T\mathbf{s} \tag{2.129}$$

The objective of the semi-active control is to minimize the value of this function, in order to reduce any tendency of the system state moving away from $\mathbf{s} = \mathbf{0}$. That is, the control

actions should be such that they make the time rate of change of the function (2.129) as small as possible, preferably less than zero.

The time derivative of this function is given by

$$\frac{d}{dt}(V) = \mathbf{s}^T \mathbf{C_s} \{\mathbf{A}\,\boldsymbol{\eta} + \mathbf{e}\,\ddot{x}_g\} + \mathbf{s}^T \mathbf{C_s} \mathbf{B_{sa}}\,\mathbf{u_{sa}} \tag{2.130}$$

The last term on the right hand of this equation can be expressed as

$$\mathbf{s}^T \mathbf{C_s} \mathbf{B_{sa}} \mathbf{u_{sa}} = \mathbf{v}^T \mathbf{u_{sa}} \tag{2.131}$$

where the m_{sa}-dimensional vector $\mathbf{v}$ is defined as

$$\mathbf{v} = \mathbf{B}_{\mathbf{sa}}^T \mathbf{C}_{\mathbf{s}}^T \mathbf{C_s} \boldsymbol{\eta} \tag{2.132}$$

and considering the definition of the semi-active control actions $\mathbf{u_{sa}}$ given in (2.13), it follows that

$$\mathbf{v}^T \mathbf{u_{sa}} = -\sum_{i=1}^{m_{sa}} v_i \left(\xi_i\, k_{v_i} + \dot{\xi}_i\, c_{v_i}\right) \tag{2.133}$$

From this equation, it is immediately apparent that whenever the factors $v_i \xi_i$ and $v_i \dot{\xi}_i$ are negative, the smallest values should be adopted for the corresponding coefficients k_{v_i} and c_{v_i}; and whenever these terms are positive, the largest values of the coefficients should be selected.

This can be achieved by the following control law, assuming that the each semi-active device can only provide two different values of stiffness ($k_{v_i}^{\min}$ and $k_{v_i}^{\max}$) and damping ($c_{v_i}^{\min}$ and $c_{v_i}^{\max}$):

$$k_{v_i}(\boldsymbol{\eta}) = \frac{1}{2}\left(k_{v_i}^{\max}\,(1 + \operatorname{sign}(v_i \xi_i)) + k_{v_i}^{\min}\,(1 - \operatorname{sign}(v_i \xi_i))\right) \tag{2.134}$$

$$c_{v_i}(\boldsymbol{\eta}) = \frac{1}{2}\left(c_{v_i}^{\max}\left(1 + \operatorname{sign}(v_i \dot{\xi}_i)\right) + c_{v_i}^{\min}\left(1 - \operatorname{sign}(v_i \dot{\xi}_i)\right)\right) \tag{2.135}$$

An obvious alternative to increase the efficiency of the proposed control action is to design the semi-active device such that $k_{v_i}^{\min}$ and $c_{v_i}^{\min}$ are zero. In this case,

$$\mathbf{v}^T \mathbf{u_{sa}} \leq 0 \tag{2.136}$$

and the control law reduces to

$$k_{v_i}(\boldsymbol{\eta}) = \frac{k_{v_i}^{\max}}{2}\left(1 + \text{sign}(v_i \xi_i)\right) \tag{2.137}$$

$$c_{v_i}(\boldsymbol{\eta}) = \frac{c_{v_i}^{\max}}{2}\left(1 + \text{sign}(v_i \dot{\xi}_i)\right) \tag{2.138}$$

This behavior can be achieved by simply disconnecting the corresponding devices which for this case will act according to a on/off regime. It is important to mention that in a vibrating structure, attaching and detaching a device by opening and closing of fluid passages is perhaps one of the easiest practical approaches.

2.8 Numerical Results

The applicability of the full state feedback control algorithms developed in this chapter is examined in this section. Since the primary focus of this work is on the control of (usually massive) civil structures subjected to seismic motions, a 10-story shear building model subjected to recorded earthquake induced ground motions, is considered as an example problem. For the chosen building model to be a realistic representation of a typical civil structure, the mass and frequency characteristics are chosen similar to those likely to be encountered in a typical medium sized multi-story building, the floor weights of which correspond to about 400 square meter of floor area on each floor. Each story has the same mass, stiffness and damping parameters. These properties are indicated in Figure (2.3), in which the natural frequencies of this example structure are also shown. The resulting

proportional damping matrix for the structure provided a modal damping ratio of 3% of the critical in the fundamental mode. The proposed full state feedback active and semi-active controllers are examined in the following.

2.8.1 Active Control

To evaluate the performance of active control schemes and their effectiveness in reducing structural responses, two different methods of force application were considered: Force applied through (1) a system of active tendons (ATS) and (2) a tuned mass damper (TMD). These two arrangements are indicated in Figure (2.3). Intuitively, it is perhaps most effective to apply the controlling force on the top of the building. For this reason, the tuned mass damper was situated on the building roof or the top floor. Depending on the aspect ratio of the building, the application of the tendon force on the top may, however, be associated with large vertical forces. To avoid this, therefore, the tendon force was applied only at the level of the first floor, even though it is realized that the force at a lower level may not be as effective as on the top.

The numerical results have also been obtained for different seismic events, to evaluate the effectiveness of the control method for different disturbances. In particular, the ground acceleration records obtained in (1) El Centro, 1941, (2) San Fernando, 1971, (3) Loma Prieta, 1989, and (4) Kern County, 1952 (recorded at the Hollywood basement site), earthquake events have been considered. The first three acceleration records were normalized to a maximum ground acceleration level of $0.3g$, whereas the Hollywood record was normalized to a peak acceleration value of $0.2g$. The ground acceleration response spectra for three percent damping ratio are shown in Figure (2.4) for the four inputs. Also shown, along the frequency axis are the locations of the natural frequencies of the structure by small circles. It is noted that the response spectra for the four motions have different frequency

characteristic. This will have some bearing on the controlled and uncontrolled response obtained for the structure.

In the case of the controlled force applied through a tuned mass damper, the TMD was nearly tuned to the first modal frequency with a frequency ratio of 0.91. The mass of the damper was about 30% of the top floor mass and about 3% of the total building mass. The damping ratio of the TMD was chosen to be about 11% of the critical value. The control force was provided between the damper mass and the reaction wall (or support) on the top floor.

For the numerical applications involving active control presented here, the number of sliding constraints is equal to the number of control actions and therefore $m_r = 0$. The design of the corresponding sliding surface was based on the minimization of a quadratic criterion of the form indicated in (2.75). Two different sets of weighting matrices $\mathbf{Q_1}$ and $\mathbf{Q_2}$ were used to achieve comparable results in terms of response reductions. For the case of active tuned mass damper control, these matrices were selected as

$$\mathbf{Q_1} = 10^5 \, \mathrm{diag}(1, 1, 1, 1, 1, 1, 1, 1, 1, 1.50, 0.05) \tag{2.139}$$

$$\mathbf{Q_2} = \mathrm{diag}(1, 1, 1, 1, 1, 1, 1, 1, 1, 1.50, 0.10) \tag{2.140}$$

whereas for the case of active tendon control they were chosen as

$$\mathbf{Q_1} = 10^3 \, \mathrm{diag}(150, 1, 1, 1, 1, 1, 1, 1, 1, 1) \tag{2.141}$$

$$\mathbf{Q_2} = \mathrm{diag}(60, 1, 1, 1, 1, 1, 1, 60, 300, 300) \tag{2.142}$$

A continuous controller was used in the numerical simulations for both the active tuned mass damper and the active tendon cases. The controller was selected to be of the form indicated in equation (2.87), defined as the sum of two components $\mathbf{u_1}$ and $\mathbf{u_2}$ given by

(2.88) and (2.127), respectively. Since $m_s = 1$, the matrix $\mathbf{\Delta}$ appearing in the expression for $\mathbf{u_2}$ reduces in this case to a single scalar parameter which is defined as $\delta = \bar{\delta}/\|\hat{\mathbf{B}}\|_2^2$. The value of the normalized parameter $\bar{\delta}$ was selected as $\bar{\delta} = 7.84$ and $\bar{\delta} = 78.10$ for the cases of active tuned mass damper and active tendon, respectively. To provide a basis for comparison between the two systems of force application, the parameters defining the control system (given by the matrices $\mathbf{Q_1}$ and $\mathbf{Q_2}$ and the parameter $\bar{\delta}$) were selected in such a way the peak displacement of the top floor is equal to 40% of the corresponding uncontrolled case, when the building is subjected to El Centro excitation.

Figure (2.5) shows the time histories of the top floor displacements for the controlled and uncontrolled cases for both the active tendon and active tuned mass damper cases. Similar results are shown in Figure (2.6) for the shear force in the first story. These results are obtained for the El Centro ground motion. It is observed that the control actions do modify the response and reduce the peak values.

Figure (2.7) shows the floor acceleration response spectra for the top floor for the two cases, again compared with the response spectra for uncontrolled cases. It is noted that active control does reduce the maximum floor acceleration (as represented by the response spectrum value at the high frequencies) as well as the peak floor response spectrum value.

From a practical stand point, it is desirable to know what one can expect in terms of the required actuator force and power and their maximum values to achieve such a response control. The time histories of the actuator control forces for the tuned mass damper and active tendon systems are shown in Figure (2.8). The magnitude of the actuator force required in tendon control is much larger than the force required with the tuned mass damper. The time histories of the corresponding mechanical power are shown in Figure (2.9). The instantaneous power is determined as the product of control force and the

velocity of the actuator in the direction of the force. The control force is assumed to be positive when it opposes the velocity of the corresponding degree of freedom. That is, in the case of the active tuned mass damper, the control force is assumed positive when it opposes the drift velocity between the top floor and the moving mass. In the active tendon case, the control force is assumed positive when it opposes the relative velocity of the first floor mass. According to this sign convention, a positive value for the power indicates that the actuation system is absorbing mechanical energy from the building system. As it can be observed from the figure, the mechanical power fluctuates on the positive and negative sides. By comparing the power for the two cases, it is observed that active tuned mass damper actuation is characterized by higher rates of mechanical energy transfer with respect to active tendon actuation.

In the previous set of results only the response of a single floor or a single story, obtained only for a single seismic input were compared. In the following paragraphs, the controlled response of all building floors is examined comparatively for different seismic inputs.

Table (2.1) shows the uncontrolled and controlled displacement response results for the tuned mass damper and active tendon systems for each of the four seismic inputs. For each seismic input, the results in the first column (that is, columns (2), (7), (13) and (18)) are the uncontrolled response values of different floors with no control devices installed. The results in the next three columns correspond to the tuned mass damper, whereas those in the last column under each earthquake are for the active tendon system. The results are presented normalized in the form of response reduction factors. The response reduction factor is defined as the ratio between the controlled and uncontrolled maximum values of a given response quantity. A response reduction factor value less than 1.0 indicates that the control scheme is effective in reducing the response; the smaller the value, the more effective

the control scheme. For the tuned mass damper, the results in columns (3), (8), (14) and (19) are for only the tuned mass damper without any active control force. They indicate the effectiveness of the TMD as a passive device. This effectiveness varies with the seismic input. The tuned mass damper as a passive device, is seen to be most effective with El Centro motion and the least the Loma Prieta motion. The results in the next column sets (that is, columns (4), (9), (15), and (20) are for the active TMD (that is, with active control force). These results, therefore, indicate the combined effect of active and passive control. The ratio of the values in these columns to the ones in the preceding columns are shown in the next set of columns (columns (5), (10), (16) and (21)). These values indicate that application of control force through a tuned mass damper can be effectively used to control the response. This effectiveness, is, however, seen to depend on the seismic input. For the example problem considered, the device is most effective on the El Centro earthquake and least effective on the Loma Prieta earthquake with regard to the response of the upper floors and also in the San Fernando earthquake with regard to the displacement responses of the lower floors. The results in the last column set (that is, columns (6), (11), (17), and (22)) are for the active tendon system. It is noted that active tendon systems can also be used for controlling the response.

The results presented in Table (2.2) are parallel to those in Table (2.1), but for the acceleration response of various floors. It is noted that the control is not as effective in reducing the acceleration response as it is in reducing the displacement response. In fact, in some instances, especially with active tendon system, there is some increase in the accelerations of especially the lower floors.

From the perspective of the practical implementation of any active structural control scheme, the maximum values of the required control force and associated mechanical power

are important operational parameters. These maximum values, in general, depend upon several factors. Intuitively it seems reasonable to think that in a well designed control algorithm, the control requirements are directly related to the reduction in the response achieved. If a larger reduction is desired then a correspondingly larger level of control force may be required. Unfortunately, in the sliding mode control approach this relationship between the magnitude of control actions and the level of control achieved is not easy to establish a priori. That is, it is not straightforward to regulate the amount of response reduction to a desired predefined level. For a given controller design, the level of control achieved and the corresponding control requirements are determined, to a large extent, by the sliding surface used.

For example, if the sliding surface matrix is selected by the minimization of a quadratic functional, then the choice of the corresponding weighting matrices determines the sliding surface. A change in any element of these matrices will result into a different sliding surface. For a given controller and for a given input ground motion, once a sliding surface is fixed, it determines the time history of the required control force. Considering the quadratic criterion defined before, the matrix $\mathbf{Q_1}$ contains the weights associated with displacement states and the matrix $\mathbf{Q_2}$ contains the weights associated with velocity states. These two matrices were selected to have a diagonal form, but it is not quite clear which elements of $\mathbf{Q_1}$ and $\mathbf{Q_2}$ will predominantly govern the relationship between the level of control action and the magnitude of reduction in the response.

For force actuation through a tuned mass damper, the weighting element affecting the damper's velocity intuitively appears to be the relevant parameter. The following numerical results seem to justify this assumption. For these results, the weighting matrix

$\mathbf{Q_2}$ is redefined as follows:

$$\mathbf{Q_2} = \text{diag}(1, 1, 1, 1, 1, 1, 1, 1, 1, 1.50, 0.01\rho_1) \tag{2.143}$$

in which ρ_1 denotes a parameter penalizing the TMD velocity. Figure (2.10) shows the numerical results obtained for different sliding surfaces generated by changing the values of the velocity weight parameter, for the El Centro earthquake. In this figure, the response reduction factors for the top floor displacement, top floor acceleration and 1st story shear, are represented versus the parameter ρ_1. The figure also shows the corresponding values of the normalized maximum control force (normalized by a floor weight) and associated mechanical power, again versus the parameter ρ_1. It is noted that as the parameter ρ_1 is increased, a smaller reduction in the response, and a correspondingly smaller control requirements are obtained. It is relevant to mention that it was not possible to obtain such relationship between the response reduction and control requirements by arbitrarily changing other parameters of the weighting matrices.

Results similar to those presented in Figure (2.10) are presented in Figure (2.11) for the control force applied through the active tendon system, also for the El Centro earthquake. Here the parameter which produced desirable monotonic relationships between the response reduction and control requirements was the weighting element associated with the relative displacement of the mass where the tendon forces are applied. Therefore, the weighting matrix $\mathbf{Q_1}$for this case is written as follows:

$$\mathbf{Q_1} = 10^3\,\text{diag}(\rho_2, 1, 1, 1, 1, 1, 1, 1, 1, 1) \tag{2.144}$$

in which ρ_2 indicates a parameter penalizing the displacement of the first floor. The relationship between the control actions and response factors here is similar to that in Figure (2.10), except for the response quantity of 1st story shear which is seen to decrease

with decreasing power levels and with decreasing control force. It is so because of the fact that this particular response quantity is directly affected by the applied control force and corresponding first floor displacement. A reduced control force applied to the first floor also translates into a reduced shear force value. Figure (2.11) also shows the results for the shear in the second story, which is clearly seen to follow the same trend as the top floor accelerations and displacement.

Table (2.3) compares the maximum values of the control force for both methods of force application and for different earthquakes. The first part of the table is for the tuned mass damper and the second part for the active tendon system. For both actuation systems, case (a) pertains to a lower reduction in the response and case (b) for a higher reduction in the response. For tuned mass damper control, these cases correspond to the values of $\rho_1 = 70$ and $\rho_1 = 10$, respectively. For active tendon control, these cases were obtained with $\rho_2 = 2150$ and $\rho_2 = 150$, respectively. The response quantity considered to quantify the reduction in the response is the displacement of the top floor. The corresponding response reduction factors are shown in columns (1) and (5) for case (a) and in columns (3) and (7) for case (b), for both actuation systems. The maximum values of the control force required to produce those response reductions are given in columns (2) and (6) for case (a) and in columns (4) and (8) for case (b). These values are presented as the ratio of the control force to the floor weight. It is observed that control force values are the smallest for the tuned mass damper system and the highest for the active tendon system. The force required in the active tendon system, being large, may not be practically feasible. It is also noticed that different seismic inputs demand different levels of control force.

For design purposes, it is desirable to have information such as that shown in Figures (2.10) and (2.11) and Table (2.3) whereby one can assess the magnitude of the control

requirements that may be necessary to achieve a particular reduction in the response. It is mentioned that these results were developed based on rather intuitive arguments and they may not correspond with the most optimum choice of the sliding surface. That is, it may be quite possible to obtain better response reduction than shown in these figures for a given level of control effort or obtain a smaller level of control effort for a given reduction in the response.

2.8.2 Semi-Active Control

The results presented in the previous section indicate that active control can, indeed, reduce a structure's response, but the magnitude of the control force and maximum instantaneous power demand can be quite high. As such, alternative methods of controlling structures are being sought. One promising approach which has attracted attention of researchers is the semi-active control approach. In this approach no external energy is input in to the structure, as opposed to the case of the active control scheme. One appropriately regulates the stiffness, damping and, if possible, mass characteristics of the structure to achieve desirable results such as a reduction of dynamic response. Such parametric regulation can be performed for example by controlling valve opening and closing for stiffness and damping change or by changing the viscosity of a damper fluid for damping coefficient change. Such operations may require only a nominal amount of external power. This has led to research on the application of electrorheological and magnetorheological dampers for seismic response control. These devices can even change the damping and stiffness properties on a continuous basis.

A somewhat idealized situation is considered to numerically examine the effectiveness of semi-active control schemes. It is assumed that the damping and stiffness matrices of the structure can be independently changed by turning on or off the stiffness and damp-

ing elements provided in diagonal bracings as indicated in Figure (2.12). Therefore, the regulation of the semi-active devices is done according to algorithm defined in (2.137) and (2.138).

For the numerical applications involving semi-active control, the number of sliding constraints was selected as $m_s = 1$. The design of the sliding surface was performed by assignment of the sliding motion eigenvalues. Let $\{\lambda_1, \lambda_2, \ldots \lambda_n\}$ denote the set of eigenvalues corresponding to the uncontrolled system, given by the eigenvalues of the matrix $\mathbf{A}$ in the state equations (2.23). The sliding motion eigenvalues $\{\hat{\lambda}_1, \hat{\lambda}_2, \ldots \hat{\lambda}_{n_r}\}$were assigned as follows:

$$\hat{\lambda}_i = \lambda_i \text{ for } i = 1, 2, \ldots n_r - 3 \tag{2.145}$$

$$\hat{\lambda}_{n_r-2} = -0.50\omega_2(1-j),\ \hat{\lambda}_{n_r-1} = -0.50\omega_2(1+j) \text{ and } \hat{\lambda}_{n_r} = -0.70\omega_2 \tag{2.146}$$

where $j = \sqrt{-1}$ and ω_2 denotes the second fundamental frequency of the uncontrolled system. Several sets of numerical results corresponding to semi-active damping and stiffness control are presented in the following.

Semi-Active Damping Control

For this set of results, supplementary on-off viscous dampers are installed in the first nine stories (i.e., $m_{sa} = 9$). The maximum damping coefficient for the devices in the first seven stories is $1.75\, c_{ref}$, where c_{ref} is a reference value selected as $c_{ref} = 6.15$[MNs/m]. The damping coefficients for the devices in the $8th$ and $9th$ stories are $1.05\, c_{ref}$ and $0.70\, c_{ref}$, respectively. This distribution of damping in different stories has been arbitrarily selected. If these additional dampers are left on all the time, the first mode damping ratio is increased from a value of 3% to about 5.2% of the critical.

The responses of the controlled and uncontrolled systems are compared in Figure (2.13),

which shows the time histories of the top floor displacement and the 1st story shear force for El Centro ground motion. It is noted that the supplementary damping devices are effective in reducing both responses.

The introduction of any additional damping in a structure, whether it is changed or not, will lead to some dissipation of vibration energy and thus a reduction in the dynamic response. The question then is, does the regulation of the dampers, according to (2.138), improve the performance of the system when compared to the case in which the dampers operate in a fully passive mode? To investigate this, the numerical results presented in Figure (2.14) were obtained. In this figure, various floor and story responses are compared for the two cases of passive and semi-active dampers. The response reduction factors for relative displacement, acceleration and shear force responses corresponding to the fully passive case are less that 1.0 and they indicate the increased ability of the system to dissipate energy. However, the response reduction factors associated with switching of the damping devices show that semi-active control did not reduce the response any further in this particular case.

The effect of the magnitude of the supplementary damper coefficient on the semi-active performance was numerically investigated and several sets of results were obtained. Even when damper coefficients as large as to generate a maximum damping force equal to 75% of the floor weight were used, the semi-active operation did not produce any significantly smaller responses than those obtained when the dampers were left on all the time. It must be remarked that these conclusions have been established by comparing passive dampers with damping coefficient $c_{v_i}^{\max}$ and semi-active dampers with two-state damping coefficients $(0, c_{v_i}^{\max})$. That is, the passive case is defined by dampers with a constant damping coefficient equal to the upper limit for the coefficient in the semi-active case.

Since the results obtained here depend upon the choice of a sliding surface used, theoretically it may still be possible to get better results with switchable damping perhaps with another more optimum sliding surface, specifically adapted to the characteristics of the semi-active damping control operation. However, the results presented here indicate that linear viscous dampers are quite effective as passive devices, but their active regulation may not be significantly beneficial for this type of structural systems. Nonetheless, semi-active control systems based on damping regulation may be quite effective for other structural systems. A typical example is found in vehicle suspension systems. In this case, high values of damping may adversely affect the performance of the isolation system and the determination of the optimal amount of damping is a crucial problem. For these systems, semi-active dampers may provide an effective way to improve the isolation characteristics [38]. Another example is found in bridge structures, for which hybrid vibration isolation systems consisting of rubber bearings and variable dampers have been proposed as an effective way to reduce seismic responses [115].

Semi-Active Stiffness Control

The numerical results for semi-active stiffness control are presented in this section. The structure is provided with switchable bracings, which can be attached and detached according to the control algorithm. Two different cases were considered to investigate the effect of the number and position of the semi-active devices on the performance of the controlled system. In the first model, it is assumed that there are active bracings installed in the first four floors of the structure (i.e., $m_{sa} = 4$). The first two stories have devices with a parameters $\{0.3k_{ref}, 0.25c_{ref}\}$. The third and fourth stories have devices with parameters equal to $\{0.2k_{ref}, 0.15c_{ref}\}$ and $\{0.1k_{ref}, 0.1c_{ref}\}$, respectively. In the second model, we assume that there are active bracings installed in all floors but the top one

(i.e., $m_{sa} = 9$). The values of the stiffness and damping parameters for the first seven stories are $\{0.3k_{ref}, 0.25c_{ref}\}$. The devices in the eighth and ninth stories are characterized by $\{0.2k_{ref}, 0.15c_{ref}\}$ and $\{0.1k_{ref}, 0.1c_{ref}\}$, respectively. For both models considered, the reference value k_{ref} is equal to the story stiffness, that is $k_{ref} = 654.98$ [MN/m], and the damping reference value c_{ref} is given by $c_{ref} = 6.15$ [MN.sec/m].

First, the results corresponding to the case $m_{sa} = 9$ are presented. Figure (2.15) shows the uncontrolled and semi-active controlled response time histories of the top floor displacement and 1st story shear force for the El Centro ground motion. The effectiveness of the semi-active control is clearly seen from these plots. The maximum displacement of the top floor is reduced to 63% of the peak uncontrolled displacement, whereas the maximum shear force in the 1st story shows a reduction of 54% with respect to the corresponding maximum uncontrolled value.

Figure (2.16) shows the control effectiveness in terms of the reduction it brings about in various floor and story responses. It is noticed that a mere addition of stiffness passively can increase some response quantities; it depends on where the structure's dominant frequencies are situated with respect to the input motion response spectrum. In the case of this particular building, the addition of stiffness puts the structure in the higher acceleration response spectrum range. As a result, the acceleration response of the higher floors are increased. Also increased are the shear forces in the higher stories. On the other hand, the semi-active operation of the supplemental stiffness clearly reduces most of the response quantities. It is noticed that the displacement and interstory shear responses are significantly reduced for all floors. However, the reduction in the acceleration response is not as significant; in fact, for the first floor the acceleration response is slightly increased.

Figure (2.17) shows the time history for the control force generated by the semi-active

device installed in the first story. To show the dissipation of energy caused by active regulation of the stiffness, this figure also shows, for the same device, the control force versus the corresponding story drift. The formation of hysteresis loops due to semi-active stiffness control is clearly seen from this figure.

The results of Tables (2.4) and (2.5) allows to compare the effectiveness of semi-active control for different seismic inputs. The results in Table (2.4) are for relative displacement responses. For each earthquake input, the results in the first set of columns (nos. 2, 7, 12, and 17) are the uncontrolled response values, whereas the values in columns (3), (8), (13) and (18) represent the response reduction factors when the structure is passively stiffened. It can be seen that a passive stiffening induces, in general, a reduction in the displacement response for most floors, but this depends on the seismic input. In the case of the Loma Prieta ground motion, the responses are slightly increased. The results in the next column sets (nos. 4, 9, 14, and 19) are for only the supplementary damping elements acting passively. In this case, of course, all floor displacement values are decreased. When both the stiffness and damping elements are installed and act passively the damping elements tend to compensate any increase caused by the passive stiffening. These results are shown in columns (5), (10), (15) and (20). The next set of columns show the results when stiffness elements are actively regulated. The final reduction in the response caused by active regulations is quite evident. The approach seems to be most effective on the El Centro motion and least on the Loma Prieta motion. This suggests that perhaps an adaptive sliding mode control approach, which adapts itself to special characteristics of the input motion is likely to perform better.

The effectiveness of semi-active stiffness control in reducing the acceleration response of various floor is indicated by the results presented in Table (2.5). It is observed that the

acceleration control is not as good as the displacement control. In some cases, especially for the Loma Prieta earthquake there is some increase in the floor accelerations. This small increase in the acceleration response can be reduced by increasing the level of passive damping associated with the device. This also suggest a need to further improve the performance of the sliding mode control algorithm by incorporation of acceleration weighting in the selection of the sliding surface parameters.

The effect of the device stiffness on the performance of the controlled structure is shown in Figure (2.18). This figure shows the reduction factors for the absolute acceleration of the sixth floor and the top floor displacement as a function of the normalized stiffness, when the structure is subjected to El Centro excitation. The reduction factors corresponding to the passively stiffened structure are also shown in these figures. Note that for zero device stiffness the reduction in the response is caused by the additional damping introduced by the devices. Increasing the active stiffness has the effect of improving the performance of the controlled structure. From the responses corresponding to the passive stiffness case, we clearly observe that additional stiffness may or may not increase some response quantities. This effect depends on the relative position of the resulting fundamental frequencies with respect to the input motion response spectrum.

Figure (2.19) shows the performance of the control system for the case $m_{sa} = 4$, when the structure is subjected to El Centro excitation. This figure is similar to Figure (2.16) and it shows the response reduction factors for various floor and story responses. It is noticed again in this case that the passive stiffening can increase some response quantities, in particular the interstory shear forces and the floor accelerations corresponding to the higher stories. By comparing Figures (2.16) and (2.19), it can be seen that the performance of the controlled system is affected by the reduced number of semi-active devices. In this

case, the maximum displacement of the top floor is reduced to 85% of the peak uncontrolled displacement, whereas the maximum shear force in the 1st story shows a reduction of 62% with respect to the corresponding maximum uncontrolled value.

2.9 Conclusions

The analytical formulation of the sliding mode control approach, applied to active and semi-active control of civil structures, has been presented. A systematic and convenient methodology was introduced to transform the equations of motion into a form suitable for the development of the control algorithm. The possibility of control redundancy was also considered in the formulation. Several active and semi-active controllers were presented, and their performances were numerically evaluated using a shear building model corresponding to a realistic structure.

The numerical results for active control indicate that, if the required control force can be provided, active control schemes can be quite effective in reducing the seismically induced responses. This effectiveness was observed to vary with the seismic input considered. With respect to the control requirements, it was observed that the peak control force in the active tendon system was much larger than that required in the tuned mass damper system. The force required in the tuned mass damper system seems to be reasonable but it is associated with high velocities of the auxiliary mass.

In the application of semi-active control schemes, it was observed that the passive installation of supplementary linear viscous damping devices reduced the structural response by merely cyclic dissipation of energy, but their active regulation did not produce any larger reductions, at least for the structural applications considered in this study. On the other hand, the switching on and off of the supplementary stiffness elements was found to be

useful in reducing the structural response. Depending upon the frequency characteristics of the structure vis-à-vis the frequency content of the seismic input a passive stiffening of a structure may reduce or increase certain response quantities, but a proper active switching of the supplementary stiffness can reduce the response of a passively stiffened structure.

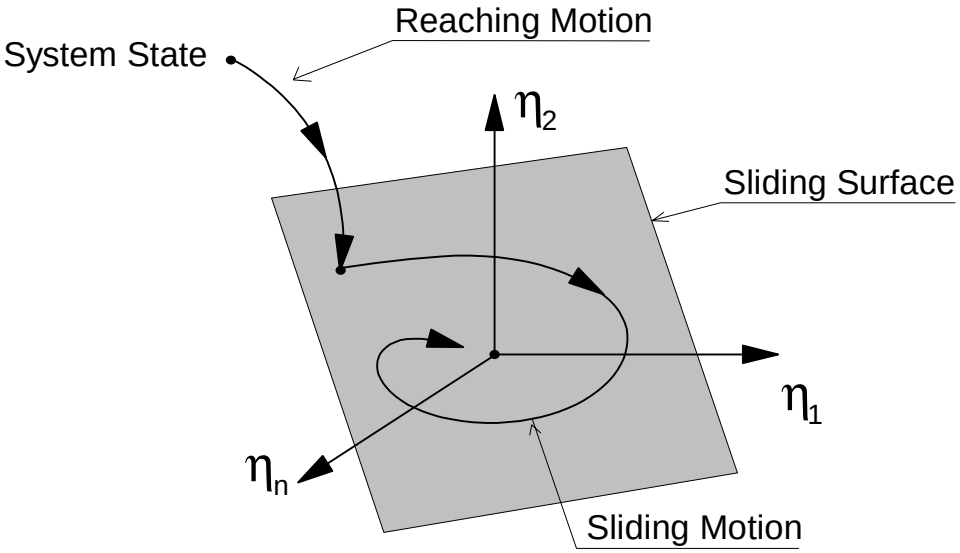

Figure 2.1: Representation of the sliding surface in the state space and the corresponding reaching and sliding phases of the motion.

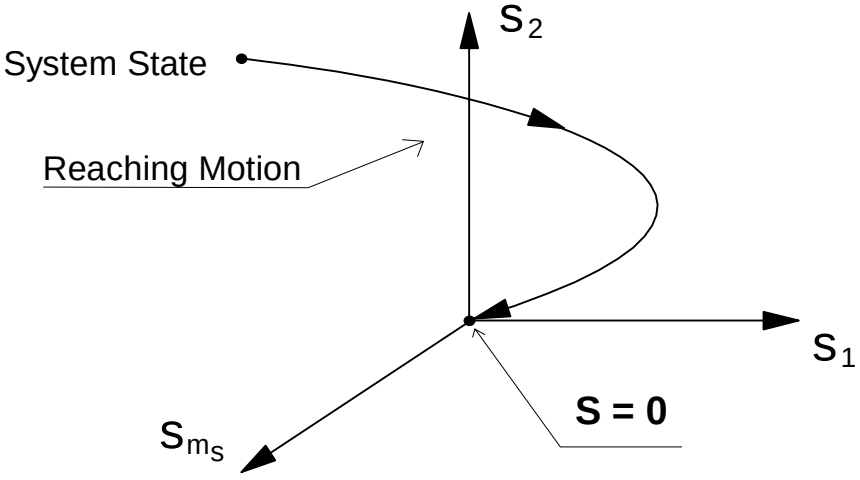

Figure 2.2: Representation of the sliding surface as an asymptotically stable equilibrium point.

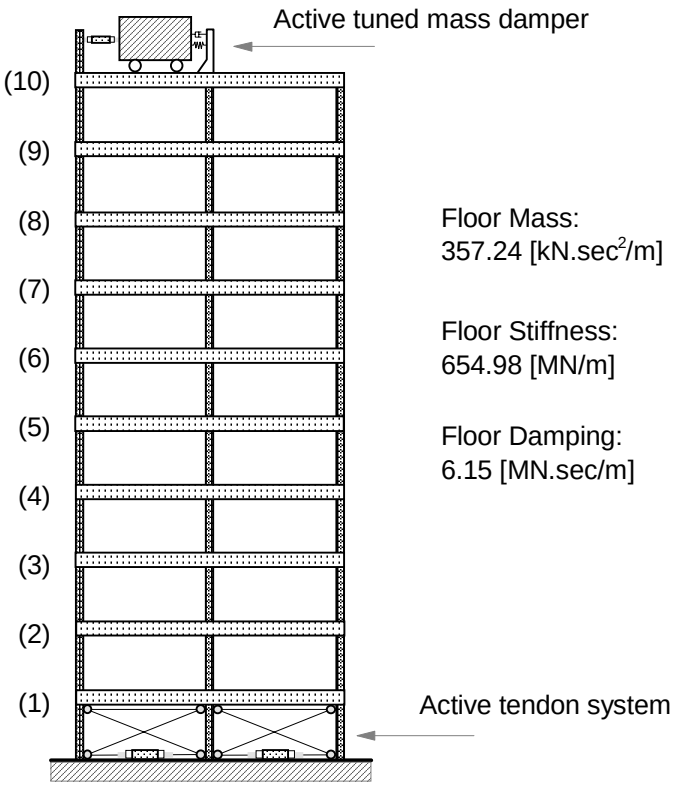

	Natural Freqs. [rad/sec]
1	6.40
2	19.06
3	31.29
4	42.82
5	53.39
6	62.78
7	70.76
8	77.16
9	81.83
10	84.68

Figure 2.3: 10-story building model with active tuned mass damper and active tendon system.

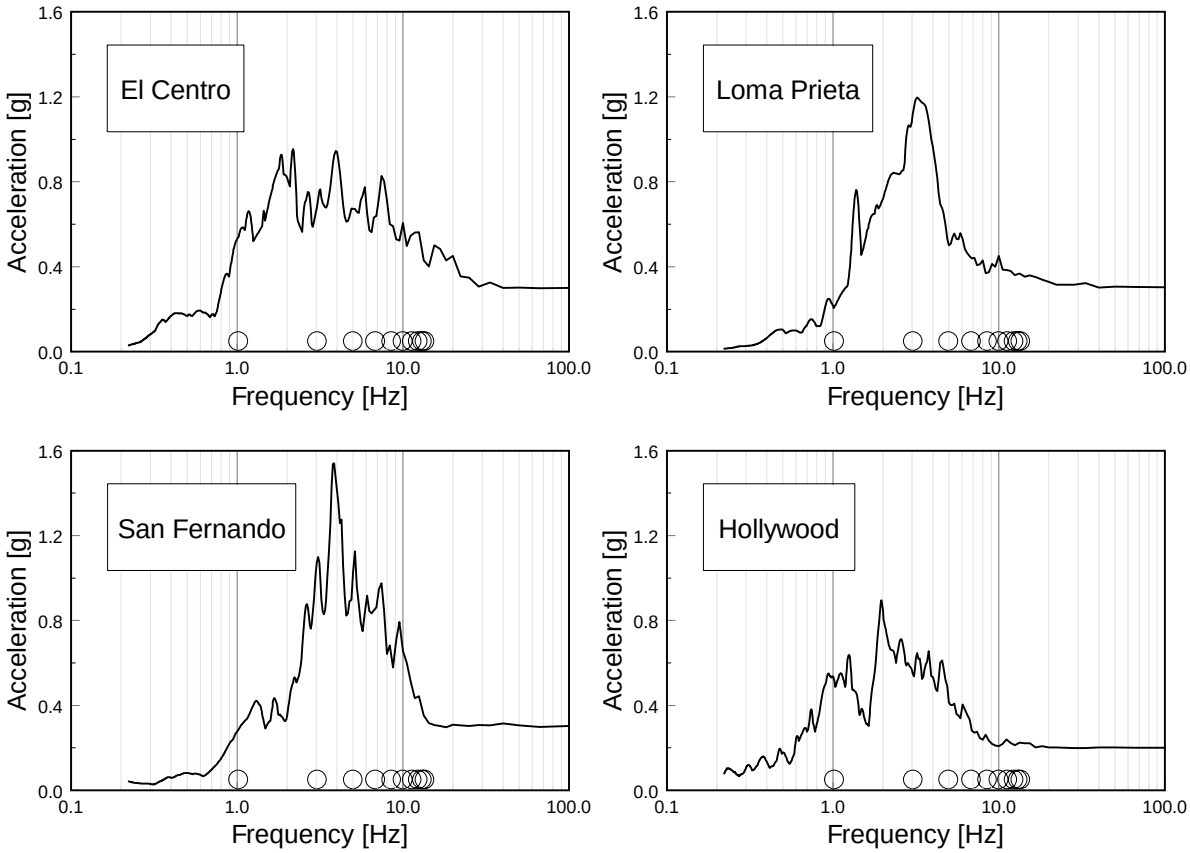

Figure 2.4: Acceleration response spectra for the ground acceleration records used in the numerical simulations.

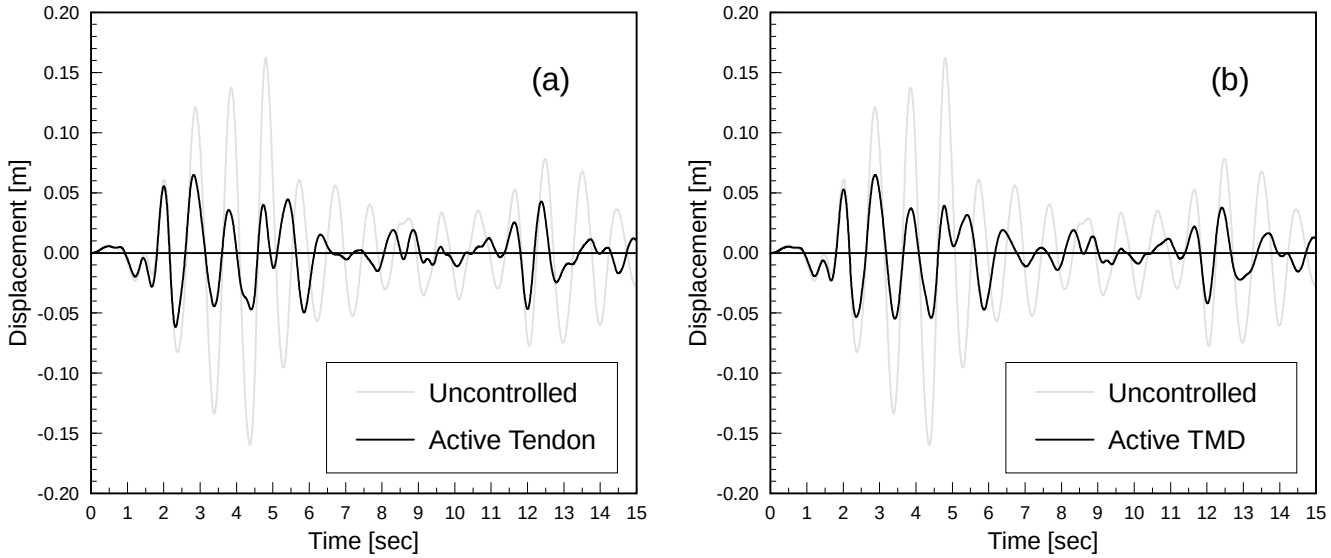

Figure 2.5: Comparison of uncontrolled and controlled top floor displacement using active tendon control and active tuned mass damper control.

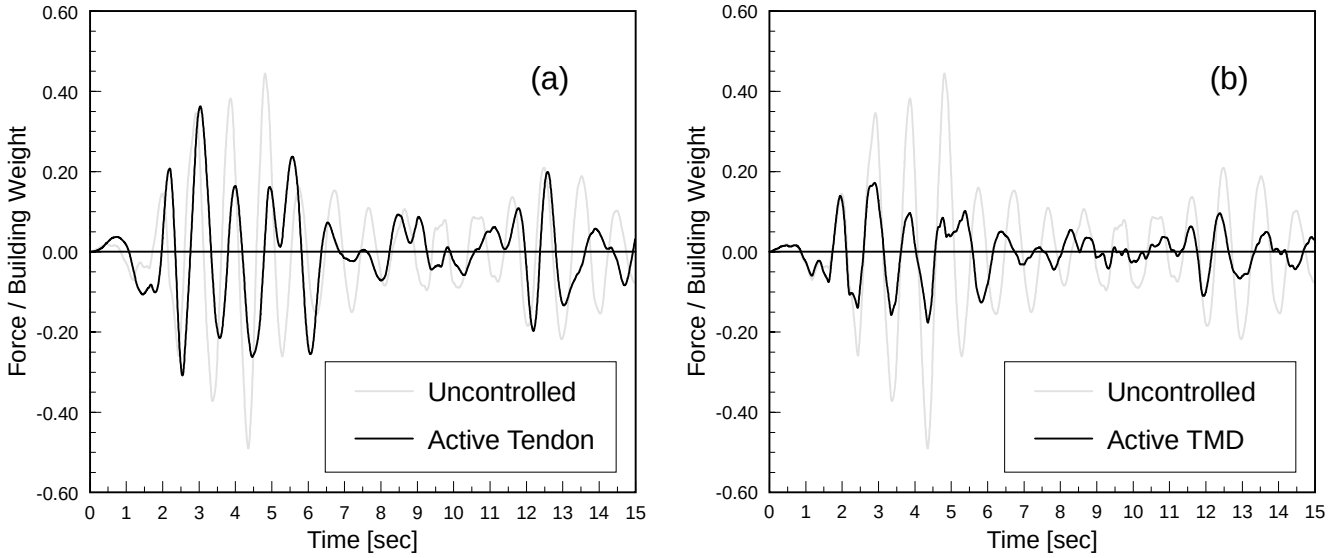

Figure 2.6: Comparison of uncontrolled and controlled 1st story shear force using active tendon control and active tuned mass damper control.

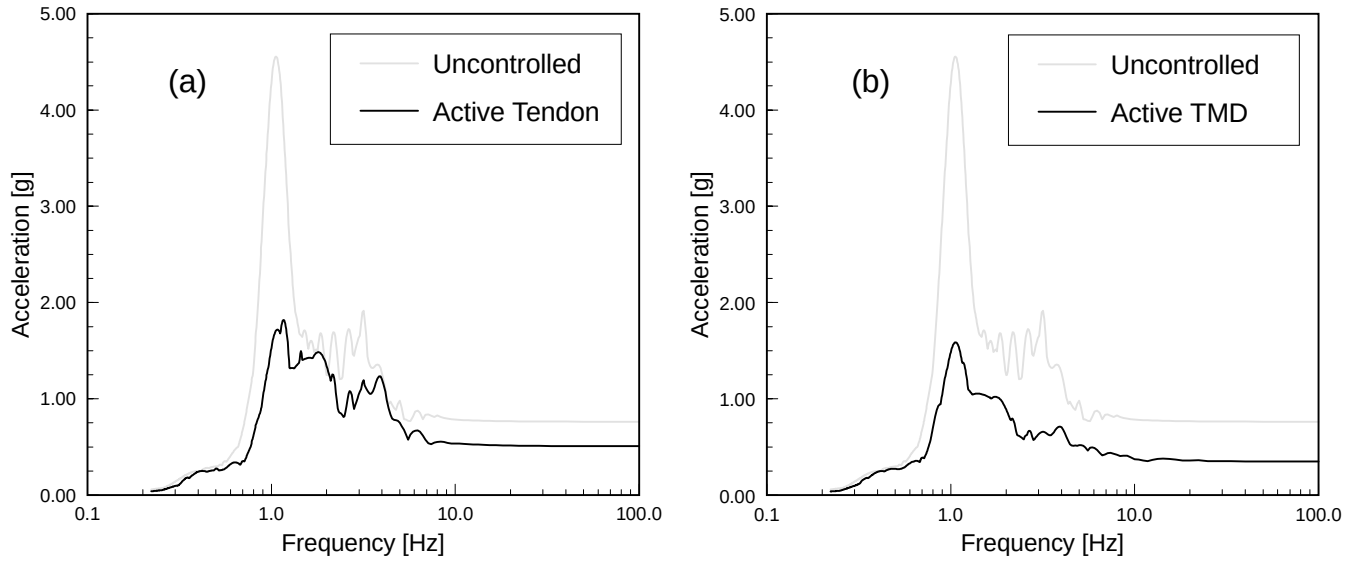

Figure 2.7: Comparison of uncontrolled and controlled floor response spectra for top floor using active tendon control and active tuned mass damper control.

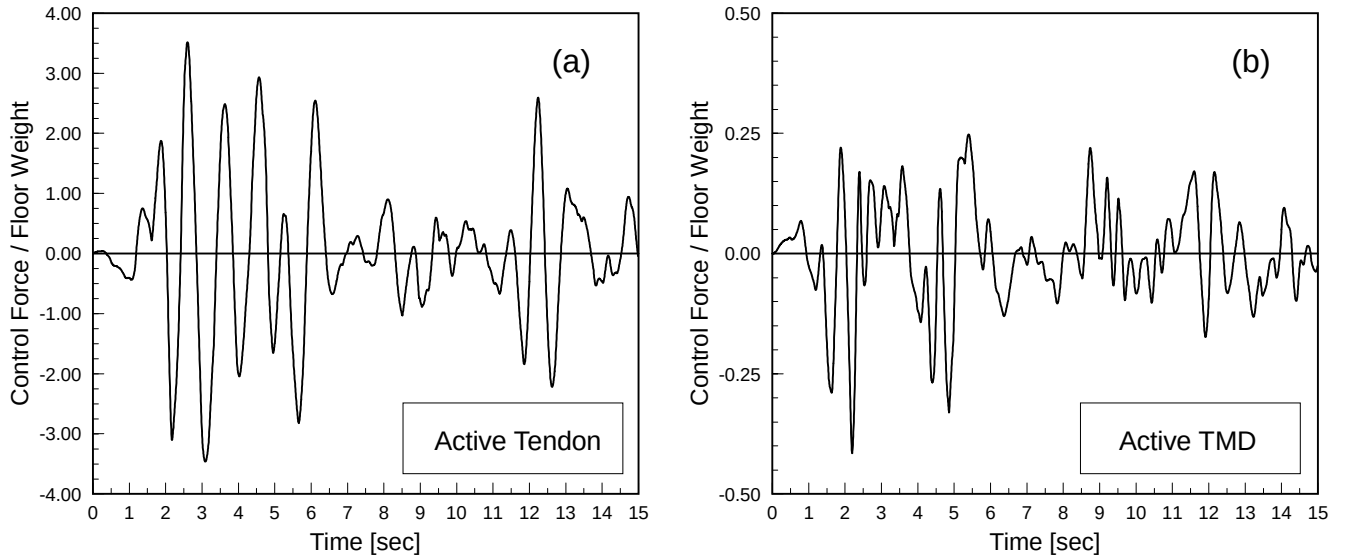

Figure 2.8: Control force for active tendon control and active tuned mass damper control.

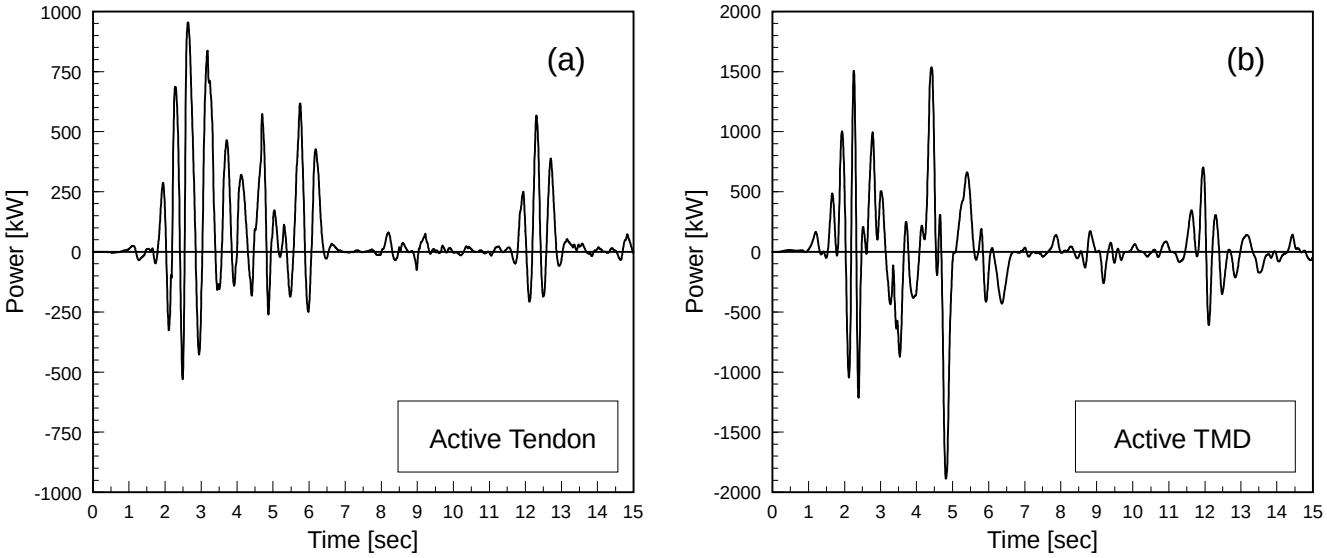

Figure 2.9: Mechanical power for active tendon control and active tuned mass damper control.

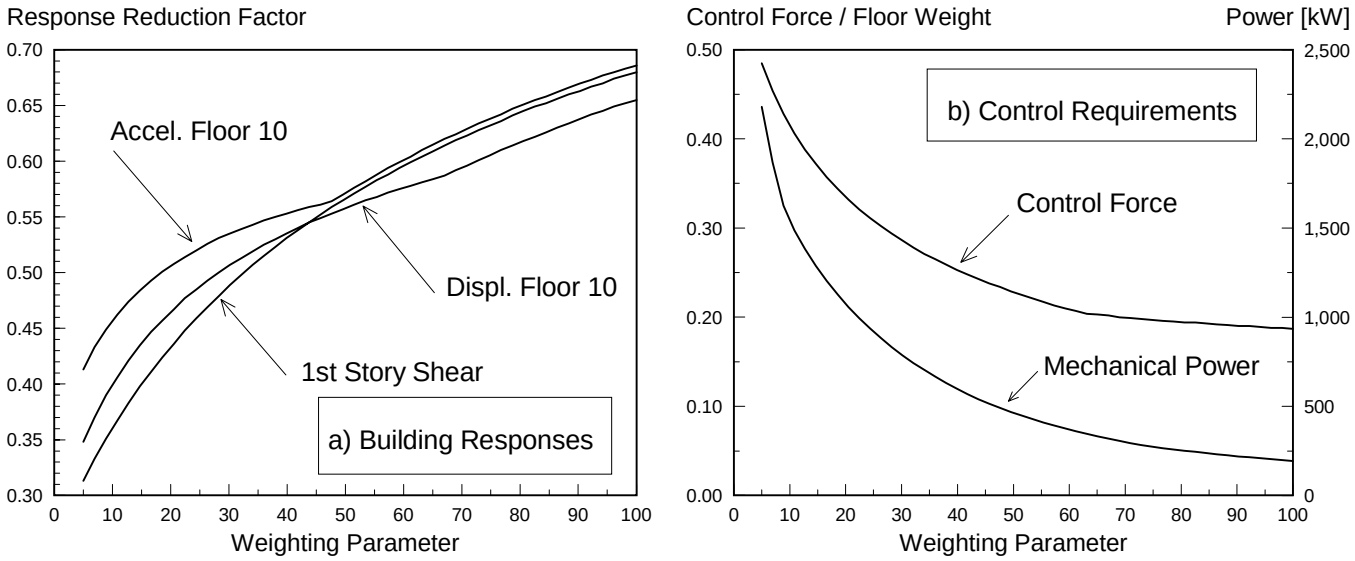

Figure 2.10: Building responses and control requirements as a function of the parameter defining the sliding surface for active tuned mass damper control.

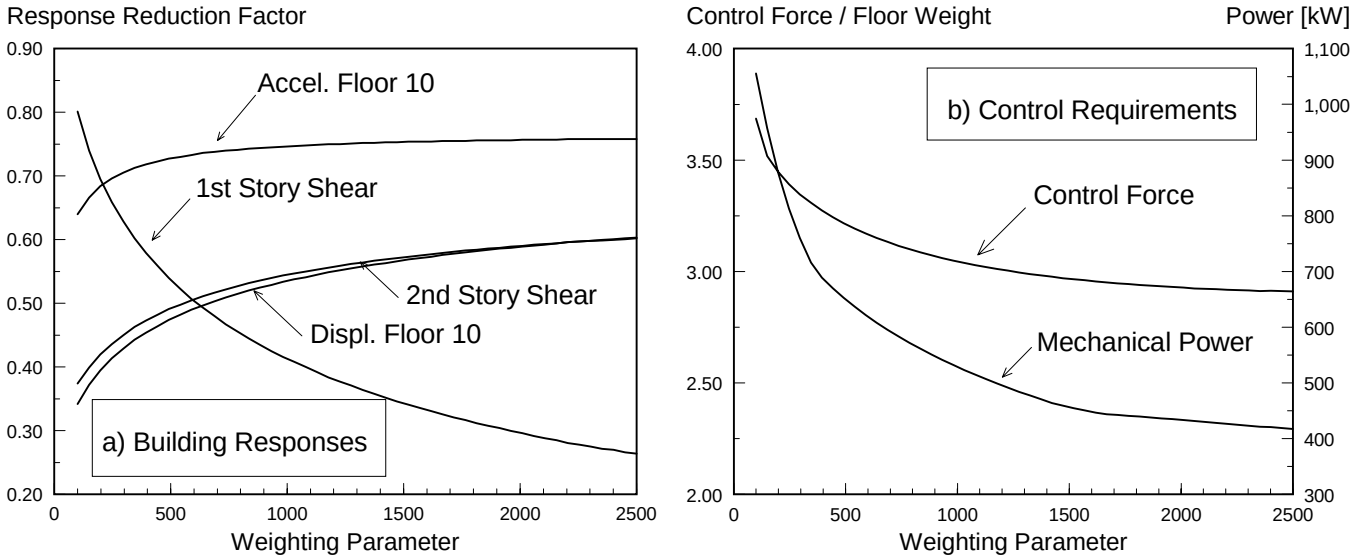

Figure 2.11: Building responses and control requirements as a function of the parameter defining the sliding surface for active tendon control.

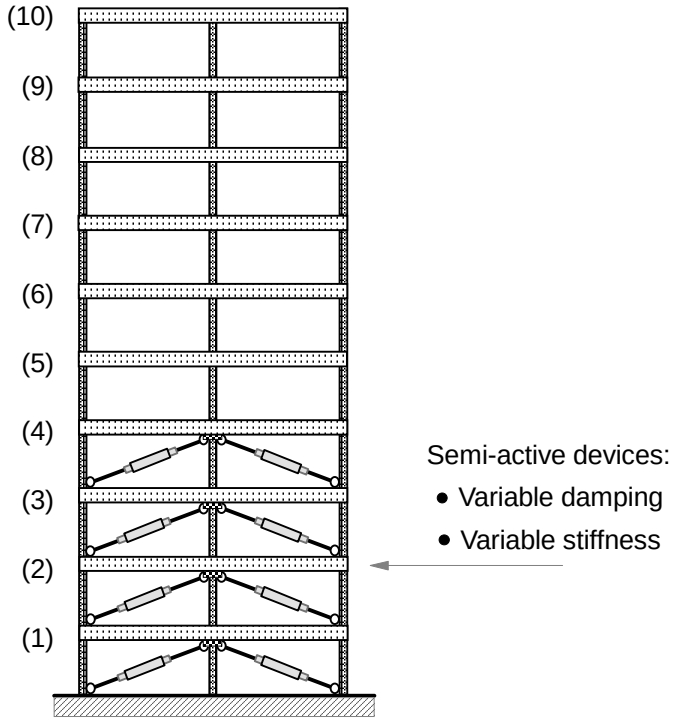

Figure 2.12: 10-story building model equipped with semi-active devices.

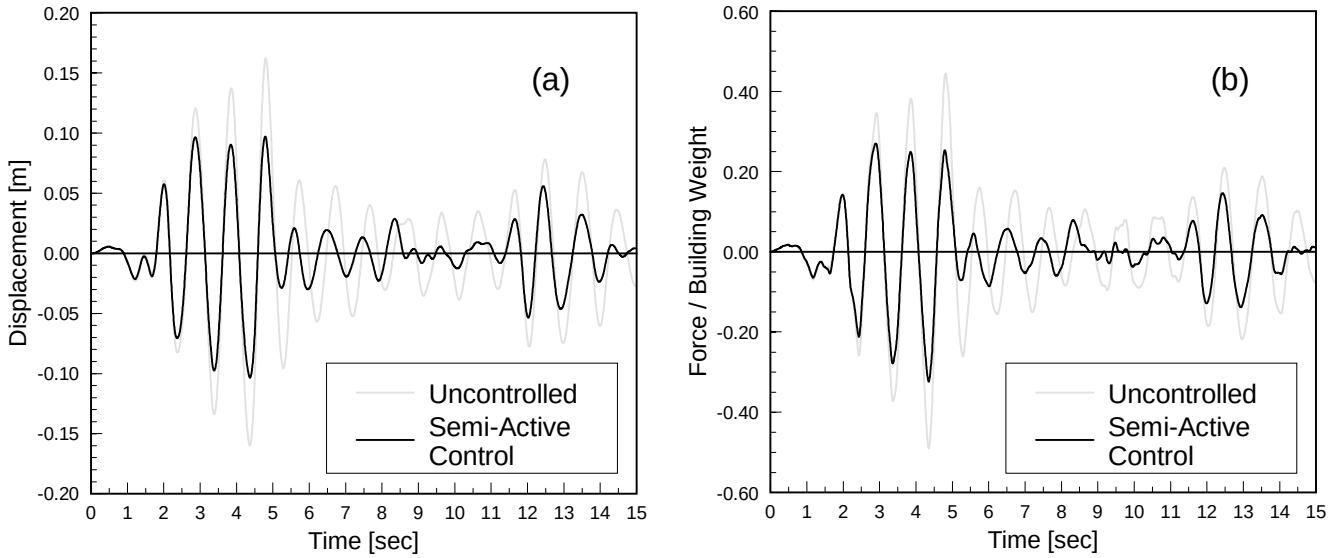

Figure 2.13: Comparison of uncontrolled and controlled top floor displacement and 1st story shear force using semi-active damping control.

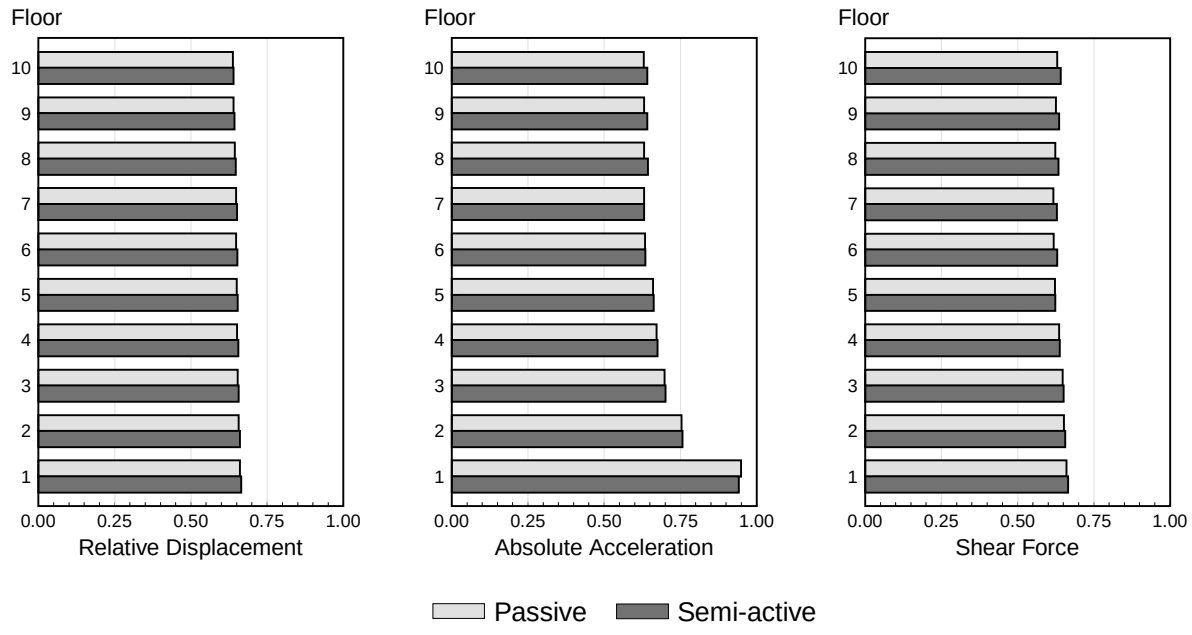

Figure 2.14: Comparison of response reduction factors for passive and semi-active damping control.

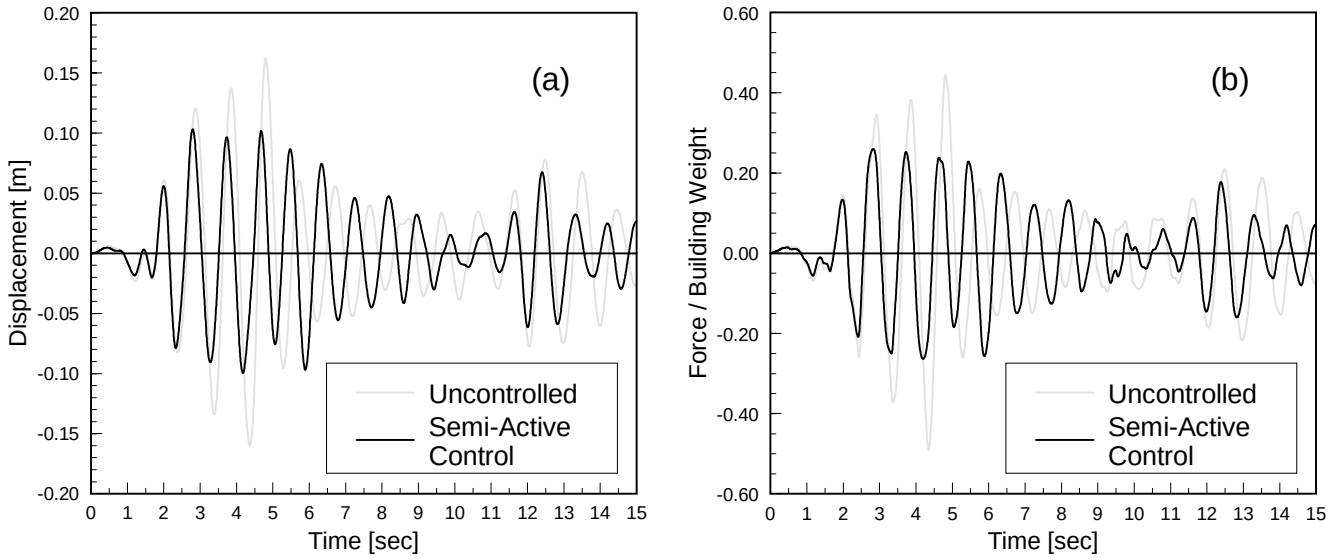

Figure 2.15: Comparison of uncontrolled and controlled top floor displacement and 1st story shear force using semi-active stiffness control.

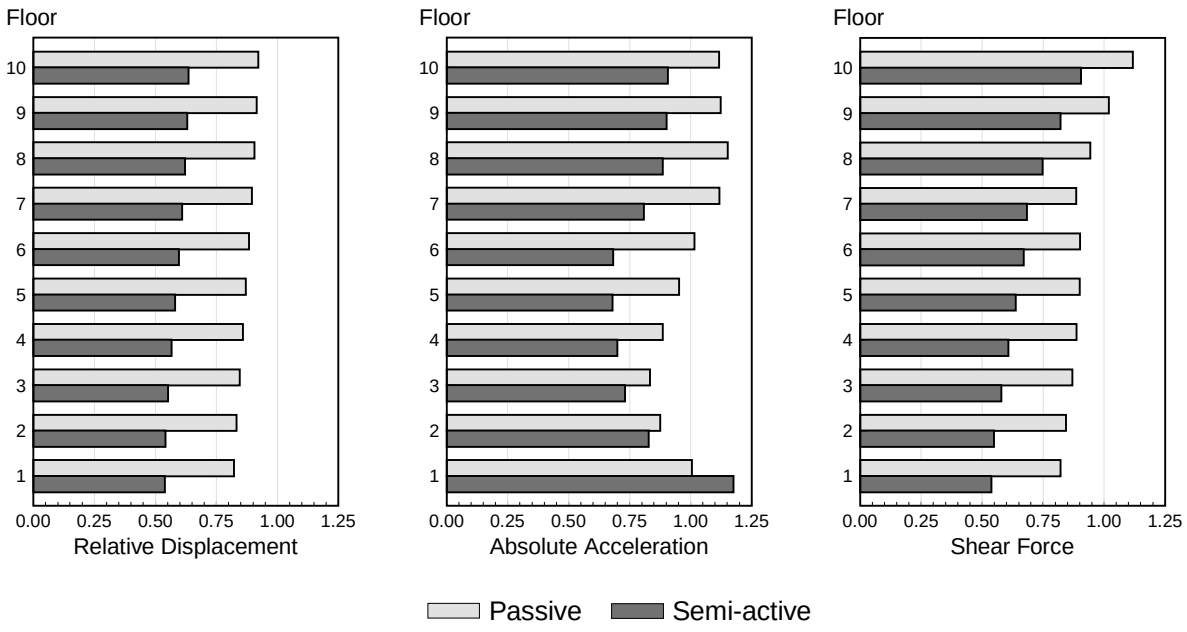

Figure 2.16: Comparison of response reduction factors for passive and semi-active stiffness control.

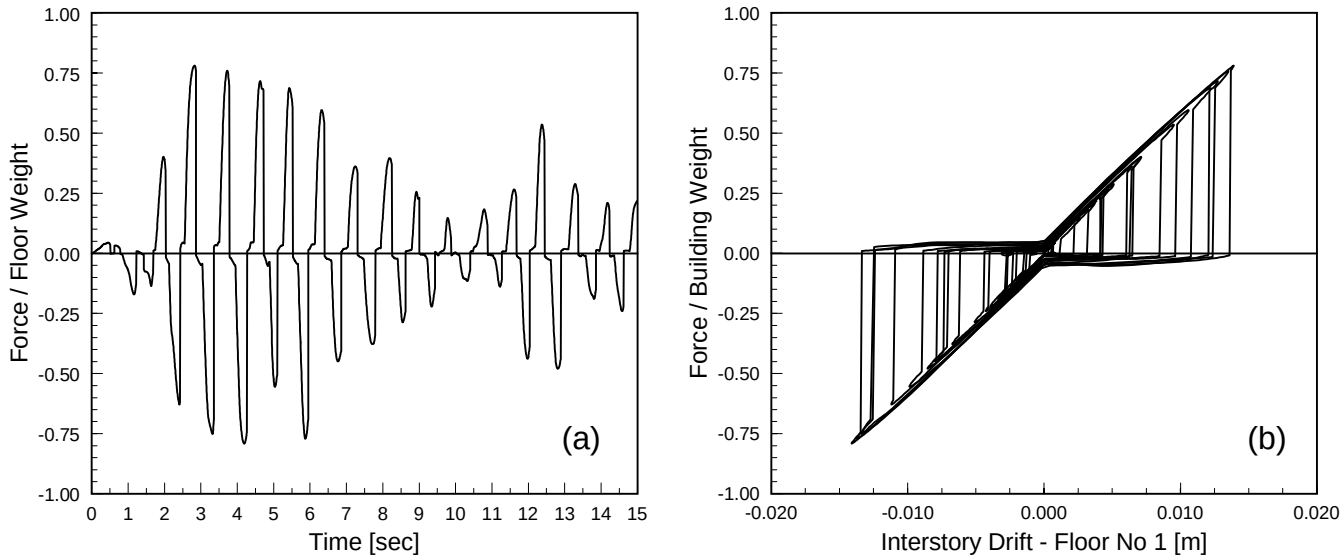

Figure 2.17: Control force time-history and force-displacement relation for the device installed at 1st story level for semi-active stiffness control.

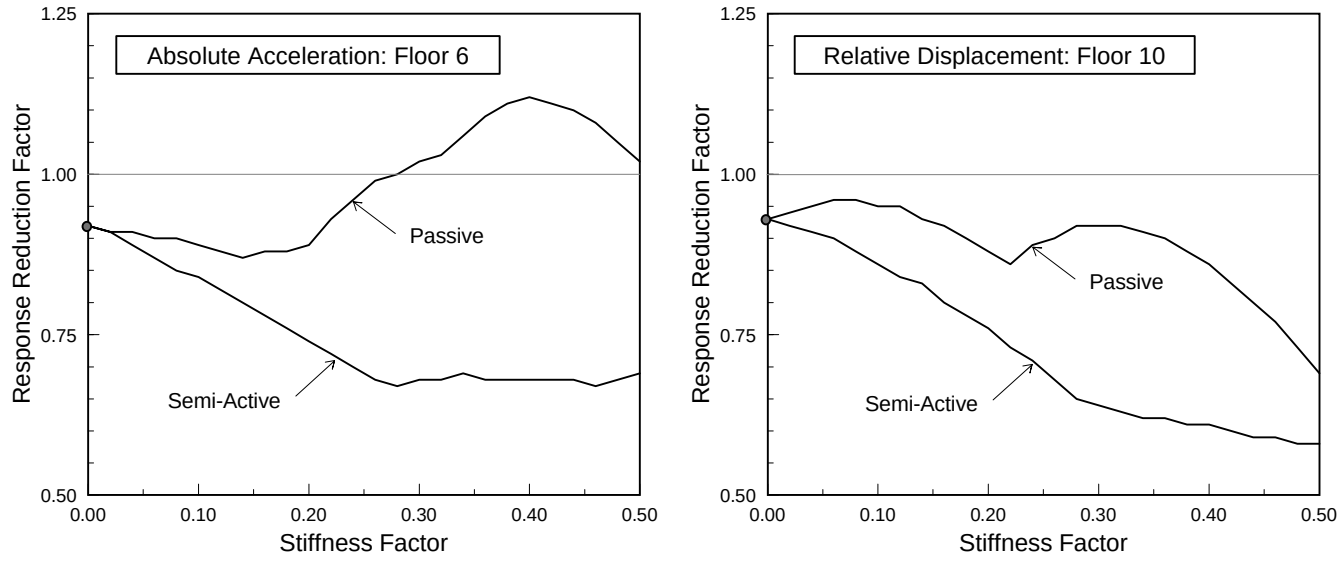

Figure 2.18: Effect of passive and semi-active additional stiffness.

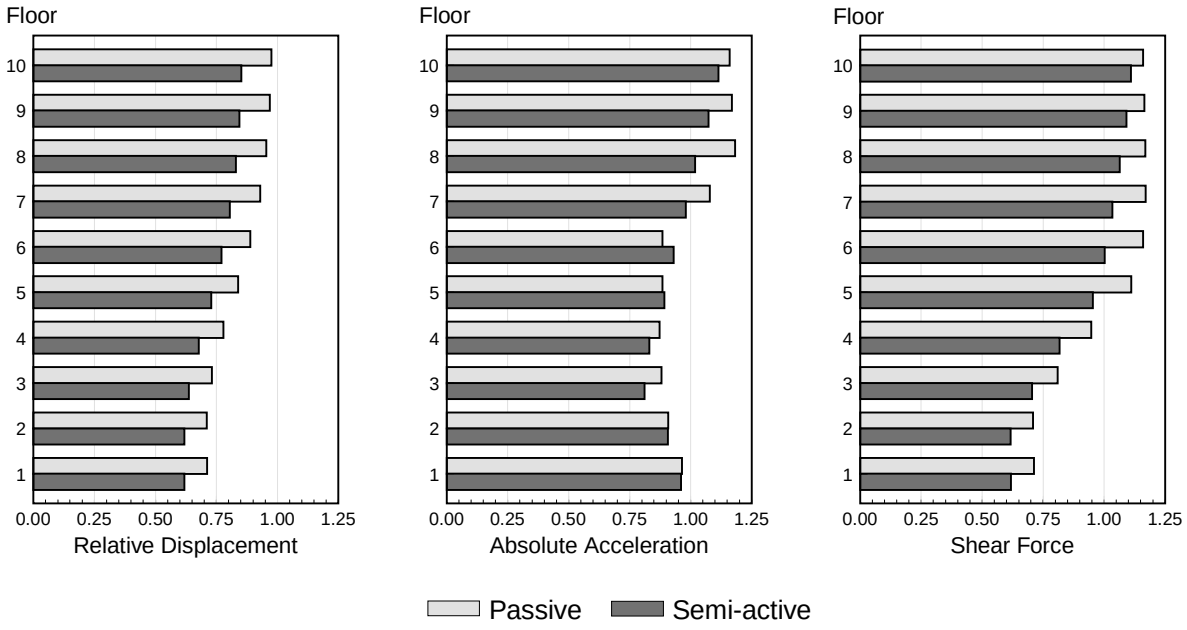

Figure 2.19: Comparison of response reduction factors for passive and semi-active stiffness control.

Floor	El Centro					San Fernando				
	Response	Response Reduction Factor				Response	Response Reduction Factor			
		TMD			ATS		TMD			ATS
	[cm]	Passive	Active	[4]/[3]	Active	[cm]	Passive	Active	[9]/[8]	Active
[1]	[2]	[3]	[4]	[5]	[6]	[7]	[8]	[9]	[10]	[11]
10	**16.25**	0.64	0.40	0.63	0.40	**8.92**	0.73	0.51	0.70	0.51
9	**15.87**	0.63	0.39	0.62	0.40	**8.68**	0.72	0.53	0.73	0.51
8	**15.14**	0.63	0.39	0.62	0.40	**8.21**	0.73	0.55	0.76	0.51
7	**14.13**	0.63	0.39	0.62	0.39	**7.53**	0.73	0.58	0.79	0.51
6	**12.90**	0.62	0.38	0.61	0.38	**6.69**	0.75	0.60	0.81	0.51
5	**11.36**	0.61	0.37	0.60	0.38	**5.71**	0.77	0.63	0.82	0.51
4	**9.54**	0.61	0.36	0.59	0.38	**4.70**	0.79	0.65	0.82	0.50
3	**7.45**	0.61	0.35	0.58	0.41	**3.68**	0.79	0.65	0.82	0.45
2	**5.13**	0.61	0.36	0.59	0.46	**2.56**	0.79	0.64	0.81	0.46
1	**2.63**	0.61	0.36	0.59	0.74	**1.32**	0.79	0.63	0.80	0.78

Floor	Loma Prieta					Hollywood				
	Response	Response Reduction Factor				Response	Response Reduction Factor			
		TMD			ATS		TMD			ATS
	[cm]	Passive	Active	[15]/[14]	Active	[cm]	Passive	Active	[20]/[19]	Active
[12]	[13]	[14]	[15]	[16]	[17]	[18]	[19]	[20]	[21]	[22]
10	**6.17**	0.98	0.78	0.80	0.90	**15.94**	0.76	0.46	0.60	0.41
9	**5.96**	0.98	0.80	0.82	0.90	**15.58**	0.76	0.46	0.60	0.41
8	**5.74**	0.95	0.81	0.84	0.87	**14.87**	0.76	0.45	0.60	0.40
7	**5.53**	0.93	0.79	0.85	0.80	**13.81**	0.75	0.46	0.60	0.40
6	**5.23**	0.94	0.76	0.81	0.72	**12.44**	0.75	0.46	0.61	0.40
5	**4.78**	0.94	0.73	0.77	0.65	**10.78**	0.75	0.46	0.61	0.40
4	**4.14**	0.95	0.70	0.74	0.62	**8.88**	0.75	0.46	0.62	0.40
3	**3.29**	0.95	0.68	0.72	0.57	**6.78**	0.75	0.46	0.62	0.40
2	**2.27**	0.96	0.67	0.70	0.57	**4.56**	0.75	0.47	0.63	0.47
1	**1.15**	0.96	0.67	0.70	0.98	**2.28**	0.75	0.48	0.63	0.79

Table 2.1: Maximum relative displacements using active tuned mass damper and active tendon control.

Floor	El Centro					San Fernando				
	Response	Response Reduction Factor				Response	Response Reduction Factor			
		TMD			ATS		TMD			ATS
	[g]	Passive	Active	[4]/[3]	Active	[g]	Passive	Active	[9]/[8]	Active
[1]	[2]	[3]	[4]	[5]	[6]	[7]	[8]	[9]	[10]	[11]
10	**0.76**	0.67	0.46	0.68	0.67	**0.48**	0.97	0.57	0.59	0.82
9	**0.72**	0.68	0.46	0.68	0.64	**0.44**	0.95	0.56	0.59	0.79
8	**0.64**	0.70	0.48	0.69	0.61	**0.39**	0.86	0.70	0.81	0.67
7	**0.60**	0.66	0.54	0.82	0.53	**0.35**	0.80	0.85	1.07	0.67
6	**0.58**	0.57	0.53	0.93	0.45	**0.35**	0.83	0.88	1.07	0.75
5	**0.54**	0.66	0.52	0.78	0.53	**0.41**	0.87	0.72	0.83	0.69
4	**0.50**	0.69	0.51	0.74	0.58	**0.43**	0.90	0.66	0.73	0.71
3	**0.44**	0.70	0.56	0.80	0.59	**0.37**	0.91	0.72	0.79	0.70
2	**0.35**	0.75	0.70	0.93	0.78	**0.33**	0.96	0.82	0.85	0.82
1	**0.26**	0.91	1.03	1.13	1.41	**0.31**	0.98	0.90	0.92	1.14

Floor	Loma Prieta					Hollywood				
	Response	Response Reduction Factor				Response	Response Reduction Factor			
		TMD			ATS		TMD			ATS
	[g]	Passive	Active	[15]/[14]	Active	[g]	Passive	Active	[20]/[19]	Active
[12]	[13]	[14]	[15]	[16]	[17]	[18]	[19]	[20]	[21]	[22]
10	**0.49**	0.92	0.53	0.57	0.81	**0.69**	0.78	0.45	0.58	0.59
9	**0.42**	0.92	0.64	0.70	0.87	**0.67**	0.76	0.46	0.61	0.56
8	**0.33**	0.98	0.83	0.85	0.95	**0.64**	0.75	0.47	0.63	0.50
7	**0.28**	0.95	0.96	1.01	0.86	**0.60**	0.73	0.49	0.67	0.44
6	**0.36**	0.97	0.71	0.73	0.85	**0.55**	0.71	0.51	0.72	0.43
5	**0.42**	0.98	0.60	0.61	0.85	**0.48**	0.67	0.53	0.79	0.44
4	**0.43**	0.98	0.54	0.55	0.81	**0.42**	0.69	0.55	0.81	0.45
3	**0.37**	0.99	0.61	0.61	0.75	**0.36**	0.73	0.60	0.83	0.53
2	**0.28**	1.00	0.89	0.89	1.09	**0.29**	0.80	0.69	0.87	0.59
1	**0.29**	1.00	0.94	0.95	1.28	**0.21**	0.95	0.85	0.89	0.86

Table 2.2: Maximum absolute accelerations using active tuned mass damper and active tendon control.

	Active tuned mass damper			
	Case (a)		Case (b)	
	Response reduction factor	Maximum control force [Floor weight]	Response reduction factor	Maximum control force [Floor weight]
	[1]	[2]	[3]	[4]
El Centro	0.60	0.20	0.40	0.42
San Fernando	0.70	0.13	0.51	0.28
Loma Prieta	0.92	0.15	0.78	0.40
Hollywood	0.71	0.13	0.46	0.26

	Active tendon system			
	Case (a)		Case (b)	
	Response reduction factor	Maximum control force [Floor weight]	Response reduction factor	Maximum control force [Floor weight]
	[5]	[6]	[7]	[8]
El Centro	0.60	2.92	0.40	3.52
San Fernando	0.77	2.38	0.51	2.39
Loma Prieta	0.96	2.49	0.90	2.65
Hollywood	0.61	3.24	0.41	3.57

Table 2.3: Maximum control force requirements using active tuned mass damper and active tendon control.

Floor	El Centro					San Fernando				
	Response	Response Reduction Factor				Response	Response Reduction Factor			
		Passive			Semi-Active		Passive			Semi-Active
	Building weight	Stiffness	Damping	Stiffness Damping		Building weight	Stiffness	Damping	Stiffness Damping	
[1]	[2]	[3]	[4]	[5]	[6]	[7]	[8]	[9]	[10]	[11]
10	**0.08**	1.22	0.93	1.12	0.90	**0.05**	1.20	0.97	1.15	0.96
9	**0.15**	1.11	0.93	1.02	0.82	**0.09**	1.09	0.98	1.04	0.91
8	**0.21**	1.03	0.93	0.94	0.75	**0.13**	0.97	0.98	0.94	0.85
7	**0.27**	0.97	0.93	0.88	0.68	**0.16**	0.87	0.98	0.85	0.79
6	**0.31**	0.99	0.93	0.90	0.67	**0.18**	0.86	0.97	0.85	0.78
5	**0.36**	0.98	0.93	0.90	0.64	**0.20**	0.89	0.96	0.87	0.80
4	**0.40**	0.97	0.92	0.89	0.61	**0.22**	0.95	0.96	0.92	0.84
3	**0.44**	0.95	0.93	0.87	0.58	**0.22**	1.02	0.95	0.99	0.88
2	**0.47**	0.92	0.94	0.84	0.55	**0.23**	1.01	0.94	0.97	0.86
1	**0.49**	0.90	0.94	0.82	0.54	**0.25**	0.94	0.93	0.91	0.79

Floor	Loma Prieta					Hollywood				
	Response	Response Reduction Factor				Response	Response Reduction Factor			
		Passive			Semi-Active		Passive			Semi-Active
	Building weight	Stiffness	Damping	Stiffness Damping		Building weight	Stiffness	Damping	Stiffness Damping	
[12]	[13]	[14]	[15]	[16]	[17]	[18]	[19]	[20]	[21]	[22]
10	**0.05**	1.18	0.91	1.09	0.99	**0.07**	1.10	0.91	1.04	0.93
9	**0.09**	1.05	0.91	0.97	0.93	**0.14**	0.99	0.91	0.94	0.83
8	**0.12**	0.96	0.92	0.90	0.90	**0.20**	0.90	0.91	0.85	0.75
7	**0.14**	0.90	0.97	0.87	0.89	**0.26**	0.81	0.90	0.77	0.68
6	**0.15**	0.91	0.97	0.89	0.89	**0.31**	0.80	0.90	0.76	0.66
5	**0.16**	0.95	0.98	0.93	0.90	**0.36**	0.79	0.90	0.75	0.65
4	**0.17**	1.03	0.97	1.00	0.93	**0.39**	0.78	0.89	0.75	0.64
3	**0.19**	1.02	0.97	0.99	0.92	**0.42**	0.78	0.89	0.75	0.64
2	**0.21**	1.04	0.96	1.01	0.93	**0.43**	0.79	0.90	0.75	0.64
1	**0.21**	1.08	0.96	1.04	0.95	**0.43**	0.80	0.93	0.76	0.65

Table 2.4: Maximum interstory shear forces using passive and semi-active control.

Floor	El Centro					San Fernando				
	Response	Response Reduction Factor				Response	Response Reduction Factor			
		Passive			Semi-Active		Passive			Semi-Active
	[g]	Stiffness	Damping	Stiffness Damping		[g]	Stiffness	Damping	Stiffness Damping	
[1]	[2]	[3]	[4]	[5]	[6]	[7]	[8]	[9]	[10]	[11]
10	**0.76**	1.22	0.93	1.12	0.91	**0.48**	1.20	0.97	1.15	0.97
9	**0.72**	1.23	0.93	1.12	0.90	**0.44**	1.17	0.98	1.13	0.98
8	**0.64**	1.26	0.93	1.15	0.89	**0.39**	1.12	0.97	1.09	1.02
7	**0.60**	1.22	0.92	1.12	0.81	**0.35**	1.20	0.96	1.17	1.09
6	**0.58**	1.11	0.91	1.02	0.68	**0.35**	1.32	0.94	1.25	1.11
5	**0.54**	1.05	0.94	0.95	0.68	**0.41**	1.13	0.91	1.05	0.95
4	**0.50**	0.97	0.94	0.88	0.70	**0.43**	1.01	0.90	0.95	0.95
3	**0.44**	0.91	0.94	0.83	0.73	**0.37**	1.10	0.90	1.03	0.99
2	**0.35**	0.91	0.95	0.87	0.83	**0.33**	0.99	0.96	0.94	0.88
1	**0.26**	1.04	0.98	1.00	1.17	**0.31**	0.93	0.98	0.92	0.94

Floor	Loma Prieta					Hollywood				
	Response	Response Reduction Factor				Response	Response Reduction Factor			
		Passive			Semi-Active		Passive			Semi-Active
	[g]	Stiffness	Damping	Stiffness Damping		[g]	Stiffness	Damping	Stiffness Damping	
[12]	[13]	[14]	[15]	[16]	[17]	[18]	[19]	[20]	[21]	[22]
10	**0.49**	1.18	0.91	1.09	0.99	**0.69**	1.10	0.91	1.04	0.93
9	**0.42**	1.14	0.92	1.06	1.05	**0.67**	1.08	0.91	1.02	0.90
8	**0.33**	1.16	0.97	1.13	1.11	**0.64**	1.04	0.90	0.99	0.86
7	**0.28**	1.28	0.97	1.24	1.25	**0.60**	0.99	0.90	0.95	0.80
6	**0.36**	1.17	0.94	1.12	1.16	**0.55**	1.01	0.89	0.94	0.75
5	**0.42**	1.12	0.93	1.06	1.08	**0.48**	1.03	0.92	0.97	0.76
4	**0.43**	1.12	0.93	1.06	1.04	**0.42**	1.01	0.92	0.95	0.78
3	**0.37**	1.16	0.93	1.11	1.06	**0.36**	0.95	0.89	0.89	0.77
2	**0.28**	1.24	0.95	1.19	1.16	**0.29**	0.89	0.90	0.88	0.84
1	**0.29**	0.94	0.99	0.93	0.94	**0.21**	0.99	0.96	0.99	1.06

Table 2.5: Maximum absolute accelerations using passive and semi-active control.

Chapter 3

Generalized Sliding Surface

3.1 Introduction

Based on the numerical results presented in the previous chapter, it can be stated that the selection of the sliding surface is a critical step in the development of an effective sliding mode control system. In the classical sliding mode control formulation, as discussed in Chapter 2, the sliding surface is defined in static form as a set of linear equations in terms of the state variables. As mentioned in the discussion of the numerical results presented in Chapter 2, the design framework based on the classical static definition of the sliding surface was found not very flexible. Sometimes, in spite of the fact that the design is done based on an optimality criterion, it may lead to inappropriate sliding constraints. In this cases, the resulting control design is characterized by the fact that increased control actions do not necessarily translate into a better control of the response. Therefore, the selection of a "proper" sliding surface is quite important for achieving a control design not only efficient but also flexible. This design flexibility becomes important if the active control system is part of an integrated protection system in which the response reduction responsibilities are apportioned among structural members, passive devices and active systems.

This chapter will explore the use of more general definitions for the sliding surface using

auxiliary dynamical systems. This type of dynamic sliding surface has been proposed to eliminate chattering in sliding mode controllers for robot manipulators [121]. In the context of control of civil structures, the frequency domain interpretation that can be associated with a generalized definition of this type will add flexibility to the sliding surface design process. A particular case of this approach was explored by Yang and co-workers [112], in which the sliding surface and the associated sliding motion are defined in the reduced space corresponding only to the auxiliary states. This chapter explores the definition of the sliding surface in an augmented state space as a function not only of the original variables but also of the auxiliary states corresponding to the added systems. Additionally, an active controller is formulated utilizing only bounding information regarding the intensity of the ground motion.

3.2 System Equations

The state equations for a linear building system with n_f degrees of freedom under seismic excitation are given by equation (2.23), which is repeated here

$$\dot{\boldsymbol{\eta}} = \mathbf{A}\,\boldsymbol{\eta} + \mathbf{B}\,\mathbf{u} + \mathbf{e}\,\ddot{x}_g \tag{3.1}$$

in which the $n \times m_c$ matrix $\mathbf{B}$, defined before by equation (2.21), is given by

$$\mathbf{B} = \begin{bmatrix} \mathbf{0} \\ \bar{\mathbf{M}}^{-1}\,\mathbf{D} \end{bmatrix} \tag{3.2}$$

with $\text{rank}(\mathbf{B}) = m_c$, and where the m_c-dimensional control vector $\mathbf{u}$ contains the contributions of any active and semi-active devices installed in the structure.

As discussed in Chapter 2, the aim of the sliding mode control approach is to design the appropriate control actions to force the system to identically satisfy a pre-specified set of m_s constraints between the state variables. Since the control actions are only applied

to impose the sliding constraints, and with the purpose of facilitating the design process, it is convenient to uncouple the equations describing the sliding motion from the control actions. As mentioned before, it is advantageous to obtain a system representation, known as the regular form, for which the sliding motion can be described without explicit control action terms. A convenient procedure, based on the singular value decomposition of the input matrix $\mathbf{B}$, was proposed in Chapter 2 to achieve this representation. In the following, a new formulation is presented to achieve such a regular form systematically.

3.3 Regular Form

Since the control terms in the state equations are associated with the input matrix $\mathbf{B}$ defined in equation (3.2), the transformation to regular form will depend on the structure of this matrix, and in particular, on the nonzero block represented by the product $\bar{\mathbf{M}}^{-1}\mathbf{D}$.

Let $\mathbf{U_2}$ be an $n_f \times m_c$ matrix whose columns constitute an orthonormal basis for $\mathcal{R}(\bar{\mathbf{M}}^{-1}\mathbf{D})$, that is, the range (or column space) of the matrix $\bar{\mathbf{M}}^{-1}\mathbf{D}$. Also, let the columns of an $n_f \times (n_f - m_c)$ matrix $\mathbf{U_1}$ constitute an orthonormal basis for $\left\{\mathcal{R}(\bar{\mathbf{M}}^{-1}\mathbf{D})\right\}^{\perp}$, i.e., the orthogonal complement of $\mathcal{R}(\bar{\mathbf{M}}^{-1}\mathbf{D})$. These two matrices can be obtained by applying the Gram-Schmidt process to the columns of the matrix $\bar{\mathbf{M}}^{-1}\mathbf{D}$.

In terms of the matrices $\mathbf{U_1}$ and $\mathbf{U_2}$, the following $n \times n$ matrix $\mathbf{T}$ is defined as:

$$\mathbf{T} = \begin{bmatrix} \mathbf{I}_{n_f} & \mathbf{0} & \mathbf{0} \\ \mathbf{0} & \mathbf{U_1} & \mathbf{U_2} \end{bmatrix} \tag{3.3}$$

Note that by construction

$$\mathbf{U_1}^T\mathbf{U_1} = \mathbf{I}_{n-m_c}, \;\; \mathbf{U_2}^T\mathbf{U_2} = \mathbf{I}_{m_c} \;\; \text{and} \;\; \mathbf{U_1}^T\mathbf{U_2} = \mathbf{0}_{(n-m_c)\times m_c} \tag{3.4}$$

and therefore the matrix $\mathbf{T}$ is unitary, that is

$$\mathbf{T}^{-1} = \mathbf{T}^T \tag{3.5}$$

This matrix $\mathbf{T}$ is used to define a state transformation as follows:

$$\boldsymbol{\eta} = \mathbf{T}\,\mathbf{y} \tag{3.6}$$

After substituting (3.6) into the equations (3.1) and premultiplying by $\mathbf{T}^T$, the transformed state equations are given by

$$\dot{\mathbf{y}} = \bar{\mathbf{A}}\,\mathbf{y} + \bar{\mathbf{B}}\,\mathbf{u} + \bar{\mathbf{e}}\,\ddot{x}_g \tag{3.7}$$

where

$$\bar{\mathbf{A}} = \mathbf{T}^T\mathbf{A}\,\mathbf{T},\ \ \bar{\mathbf{B}} = \mathbf{T}^T\mathbf{B}\ \text{ and }\ \bar{\mathbf{e}} = \mathbf{T}^T\mathbf{e} \tag{3.8}$$

By considering the definition (3.3), it is immediately clear that the transformed matrix $\bar{\mathbf{B}}$ takes the following form:

$$\bar{\mathbf{B}} = \begin{bmatrix} \mathbf{0} \\ \hat{\mathbf{B}} \end{bmatrix} \tag{3.9}$$

in which $\hat{\mathbf{B}}$ is a $m_c \times m_c$ nonsingular matrix given by

$$\hat{\mathbf{B}} = \mathbf{U}_\mathbf{2}^T\bar{\mathbf{M}}^{-\mathbf{1}}\,\mathbf{D} \tag{3.10}$$

With this structure for the input matrix $\bar{\mathbf{B}}$, the first $n - m_c$ equations of (3.7) do not contain any control terms now.

As mentioned in Chapter 2, it is assumed that the number of constraints does not exceed the number of independent control actions. That is, the control redundancy index, defined in Equation (2.26), satisfies $m_r \geq 0$. For the case $m_r = 0$, that is, when the number of control actions is equal to the number of sliding constraints, the transformation (3.6) automatically leads to a set of sliding motion equations, given by the upper $n - m_c$ equations of (3.7), without explicit control terms. Thus, in this case equations (3.7) represent the regular form of the state equations. As indicated in Chapter 2, for the case $m_r \geq 1$, additional constraints will have to be imposed on the admissible control actions

to obtain sliding motion equations uncoupled from the control terms. This is discussed in the following sections.

3.4 Sliding Surface

As mentioned before, the sliding surface represents m_s constraints. Let the transformed state vector $\mathbf{y}$ be accordingly partitioned as follows:

$$\mathbf{y} = \left\{ \begin{array}{c} \mathbf{y_1} \\ \mathbf{y_2} \end{array} \right\} \tag{3.11}$$

with the first $n_r = n - m_s$ components arranged in the vector $\mathbf{y_1}$ and the remaining m_s variables collected in the vector $\mathbf{y_2}$.

Normally, the sliding surface is defined as a set of linear constraints on the state vector $\mathbf{y}$. However, to add flexibility in the choice of desirable sliding motions, here the sliding constraints are defined in terms of two m_s-dimensional vectors $\tilde{\mathbf{y}}_\mathbf{1}$ and $\tilde{\mathbf{y}}_\mathbf{2}$ as follows:

$$\mathbf{s} = \tilde{\mathbf{y}}_\mathbf{1} + \tilde{\mathbf{y}}_\mathbf{2} = \mathbf{0} \tag{3.12}$$

The vectors $\tilde{\mathbf{y}}_\mathbf{1}$ and $\tilde{\mathbf{y}}_\mathbf{2}$ are the outputs of two auxiliary dynamical systems with the following state-space realizations of order n_{s_1} and n_{s_2}, respectively:

$$\left\{ \begin{array}{l} \dot{\boldsymbol{\varphi}}_\mathbf{1} = \bar{\mathbf{F}}_\mathbf{1}\, \boldsymbol{\varphi}_\mathbf{1} + \bar{\mathbf{G}}_\mathbf{1}\mathbf{y}_\mathbf{1} \\ \tilde{\mathbf{y}}_1 = \bar{\mathbf{H}}_\mathbf{1}\, \boldsymbol{\varphi}_\mathbf{1} + \bar{\mathbf{C}}_{\mathbf{s1}}\mathbf{y}_\mathbf{1} \end{array} \right. \quad \text{and} \quad \left\{ \begin{array}{l} \dot{\boldsymbol{\varphi}}_\mathbf{2} = \bar{\mathbf{F}}_\mathbf{2}\, \boldsymbol{\varphi}_\mathbf{2} + \bar{\mathbf{G}}_\mathbf{2}\mathbf{y}_\mathbf{2} \\ \tilde{\mathbf{y}}_2 = \bar{\mathbf{H}}_\mathbf{2}\, \boldsymbol{\varphi}_\mathbf{2} + \bar{\mathbf{C}}_{\mathbf{s2}}\mathbf{y}_\mathbf{2} \end{array} \right. \tag{3.13}$$

in which it is assumed that the $m_s \times m_s$ matrix $\bar{\mathbf{C}}_{\mathbf{s2}}$ is nonsingular, i.e. $\text{rank}(\bar{\mathbf{C}}_{\mathbf{s2}}) = m_s$. The matrices $\bar{\mathbf{F}}_\mathbf{1}$, $\bar{\mathbf{G}}_\mathbf{1}$, $\bar{\mathbf{F}}_\mathbf{2}$ and $\bar{\mathbf{G}}_\mathbf{2}$ are preselected to define the dynamic systems. The output matrices $\bar{\mathbf{H}}_\mathbf{1}$, $\bar{\mathbf{C}}_{\mathbf{s1}}$, $\bar{\mathbf{H}}_\mathbf{2}$ and $\bar{\mathbf{C}}_{\mathbf{s2}}$ will be determined based on some optimality condition imposed on the sliding motion. These supplementary parameters will be shown to provide additional flexibility to the design process, making easier the tuning of the resulting design to meet different performance specifications.

The auxiliary systems (3.13) used to define the sliding surface can be incorporated into the state equations to define an augmented system of order $n_e = n_{s_1} + n_{s_2} + n$ as follows:

$$\dot{\mathbf{y}}_\mathbf{e} = \bar{\mathbf{A}}_\mathbf{e}\mathbf{y}_\mathbf{e} + \bar{\mathbf{B}}_\mathbf{e}\mathbf{u} + \bar{\mathbf{e}}_\mathbf{e}\ddot{x}_g \tag{3.14}$$

in which

$$\bar{\mathbf{A}}_\mathbf{e} = \begin{bmatrix} \bar{\mathbf{F}}_\mathbf{1} & \mathbf{0} & \bar{\mathbf{G}}_\mathbf{1} & \mathbf{0} \\ \mathbf{0} & \bar{\mathbf{F}}_\mathbf{2} & \mathbf{0} & \bar{\mathbf{G}}_\mathbf{2} \\ \mathbf{0} & \mathbf{0} & \bar{\mathbf{A}}_{\mathbf{11}} & \bar{\mathbf{A}}_{\mathbf{12}} \\ \mathbf{0} & \mathbf{0} & \bar{\mathbf{A}}_{\mathbf{21}} & \bar{\mathbf{A}}_{\mathbf{22}} \end{bmatrix}, \bar{\mathbf{B}}_\mathbf{e} = \begin{bmatrix} \mathbf{0} \\ \mathbf{0} \\ \bar{\mathbf{B}}_\mathbf{1} \\ \bar{\mathbf{B}}_\mathbf{2} \end{bmatrix}, \mathbf{y}_\mathbf{e} = \begin{Bmatrix} \boldsymbol{\varphi}_\mathbf{1} \\ \boldsymbol{\varphi}_\mathbf{2} \\ \mathbf{y}_\mathbf{1} \\ \mathbf{y}_\mathbf{2} \end{Bmatrix} \text{ and } \bar{\mathbf{e}}_\mathbf{e} = \begin{Bmatrix} \mathbf{0} \\ \mathbf{0} \\ \bar{\mathbf{e}}_\mathbf{1} \\ \bar{\mathbf{e}}_\mathbf{2} \end{Bmatrix} \tag{3.15}$$

where $\bar{\mathbf{A}}$, $\bar{\mathbf{B}}$ and $\bar{\mathbf{e}}$ have been conveniently partitioned. The sliding surface can also be written more compactly in terms of the augmented state vector $\mathbf{y}_\mathbf{e}$ as follows:

$$\mathbf{s} = \bar{\mathbf{C}}_\mathbf{e}\,\mathbf{y}_\mathbf{e} = \mathbf{0} \tag{3.16}$$

where the matrix $\bar{\mathbf{C}}_\mathbf{e}$ is defined as

$$\bar{\mathbf{C}}_\mathbf{e} = \begin{bmatrix} \bar{\mathbf{H}}_\mathbf{1} & \bar{\mathbf{H}}_\mathbf{2} & \bar{\mathbf{C}}_{\mathbf{s1}} & \bar{\mathbf{C}}_{\mathbf{s2}} \end{bmatrix} \tag{3.17}$$

3.5 Sliding Motion Description

Assuming that the system reaches the sliding surface at some time t_h (hitting time) and it is forced to stay there by some control action $\hat{\mathbf{u}}$, the sliding motion conditions are given by

$$\mathbf{s} = \bar{\mathbf{C}}_\mathbf{e}\,\mathbf{y}_\mathbf{e} = \mathbf{0} \tag{3.18}$$

$$\dot{\mathbf{s}}\,|_{\mathbf{u}=\hat{\mathbf{u}}} = \bar{\mathbf{C}}_\mathbf{e}\,\dot{\mathbf{y}}_\mathbf{e} = \mathbf{0} \tag{3.19}$$

By utilizing the state equations (3.14) in equation (3.19), it follows that $\hat{\mathbf{u}}$ must be obtained as a solution of the following system of m_c equations:

$$\bar{\mathbf{C}}_\mathbf{e}\bar{\mathbf{B}}_\mathbf{e}\hat{\mathbf{u}} = -\bar{\mathbf{C}}_\mathbf{e}\bar{\mathbf{A}}_\mathbf{e}\,\mathbf{y}_\mathbf{e} - \bar{\mathbf{C}}_\mathbf{e}\bar{\mathbf{e}}_\mathbf{e}\,\ddot{x}_g \tag{3.20}$$

Based on the definitions of the matrices $\bar{\mathbf{C}}_\mathbf{e}$ and $\bar{\mathbf{B}}_\mathbf{e}$, it is easy to show that

$$\bar{\mathbf{C}}_\mathbf{e}\bar{\mathbf{B}}_\mathbf{e} = \bar{\mathbf{C}}_\mathbf{s}\bar{\mathbf{B}} \tag{3.21}$$

in which $\bar{\mathbf{B}}$ is defined in (3.8) and $\bar{\mathbf{C}}_\mathbf{s}$ is given by

$$\bar{\mathbf{C}}_\mathbf{s} = \begin{bmatrix} \bar{\mathbf{C}}_{\mathbf{s1}} & \bar{\mathbf{C}}_{\mathbf{s2}} \end{bmatrix} \tag{3.22}$$

Therefore, considering (2.53) and (3.21), it follows that the rank of the coefficient matrix $\bar{\mathbf{C}}_\mathbf{e}\bar{\mathbf{B}}_\mathbf{e}$ in (3.20) is equal to m_s. When $m_c = m_s$, the coefficient matrix is nonsingular and the equations (3.20) will provide a unique solution for the control $\hat{\mathbf{u}}$. However, when $m_c > m_s$ there is redundancy of control actions and the multiple solutions $\hat{\mathbf{u}}$ have the general form:

$$\hat{\mathbf{u}} = -\left[\bar{\mathbf{C}}_\mathbf{s}\bar{\mathbf{B}}\right]^R \left\{\bar{\mathbf{C}}_\mathbf{e}\bar{\mathbf{A}}_\mathbf{e}\,\mathbf{y}_\mathbf{e} + \bar{\mathbf{C}}_\mathbf{e}\bar{\mathbf{e}}_\mathbf{e}\,\ddot{x}_g\right\} \tag{3.23}$$

in which $\left[\bar{\mathbf{C}}_\mathbf{s}\bar{\mathbf{B}}\right]^R$ denotes a right inverse of the product $\bar{\mathbf{C}}_\mathbf{s}\bar{\mathbf{B}}$, as indicated in (2.54).

To determine a unique solution, further restrictions needs to be imposed on the admissible controls. If the admissible $\hat{\mathbf{u}}$ is required to satisfy $\hat{\mathbf{u}} \in \mathcal{N}(\bar{\mathbf{B}}_\mathbf{1})$, that is, $\hat{\mathbf{u}}$ belongs to the null space of $\bar{\mathbf{B}}_\mathbf{1}$, then following a similar derivation as in (2.57)-(2.63) a unique solution can be obtained for (3.20) of the form:

$$\hat{\mathbf{u}} = -\left[\bar{\mathbf{C}}_\mathbf{s}\bar{\mathbf{B}}\right]^\ddagger \bar{\mathbf{C}}_\mathbf{e}\left\{\bar{\mathbf{A}}_\mathbf{e}\,\mathbf{y}_\mathbf{e} + \bar{\mathbf{e}}_\mathbf{e}\,\ddot{x}_g\right\} \tag{3.24}$$

in which the matrix $\left[\bar{\mathbf{C}}_\mathbf{s}\bar{\mathbf{B}}\right]^\ddagger$ is a special right inverse of $\left[\bar{\mathbf{C}}_\mathbf{s}\bar{\mathbf{B}}\right]$ defined by equation (2.64), which is repeated here

$$\left[\bar{\mathbf{C}}_\mathbf{s}\bar{\mathbf{B}}\right]^\ddagger = \hat{\mathbf{B}}^{-1}\begin{bmatrix} \mathbf{0} \\ \bar{\mathbf{C}}_{\mathbf{s2}}^{-1} \end{bmatrix} \tag{3.25}$$

By substituting (3.24) into (3.14), it can be shown that the behavior of the system subjected to the control $\hat{\mathbf{u}}$ can be described by the following system of order $n_c = n_{s_1} + n_{s_2} + n_r$:

$$\dot{\mathbf{y}}_\mathbf{c} = \bar{\mathbf{A}}_\mathbf{c}\,\mathbf{y}_\mathbf{c} + \bar{\mathbf{B}}_\mathbf{c}\,\mathbf{y}_\mathbf{2} + \bar{\mathbf{e}}_\mathbf{c}\,\ddot{x}_g \tag{3.26}$$

where

$$\bar{\mathbf{A}}_\mathbf{c} = \begin{bmatrix} \bar{\mathbf{F}}_1 & \mathbf{0} & \bar{\mathbf{G}}_1 \\ \mathbf{0} & \bar{\mathbf{F}}_2 & \mathbf{0} \\ \mathbf{0} & \mathbf{0} & \bar{\mathbf{A}}_{11} \end{bmatrix}, \bar{\mathbf{B}}_\mathbf{c} = \begin{bmatrix} \mathbf{0} \\ \bar{\mathbf{G}}_2 \\ \bar{\mathbf{A}}_{12} \end{bmatrix}, \mathbf{y_c} = \begin{Bmatrix} \boldsymbol{\varphi}_1 \\ \boldsymbol{\varphi}_2 \\ \mathbf{y}_1 \end{Bmatrix} \text{ and } \bar{\mathbf{e}}_\mathbf{c} = \begin{Bmatrix} \mathbf{0} \\ \mathbf{0} \\ \bar{\mathbf{e}}_1 \end{Bmatrix} \tag{3.27}$$

Therefore, with the imposition of the additional constraints on the admissible control actions, the behavior of the system subjected to the constraint (3.19) is described by a system of equations which do not have any control term appearing explicitly. Note also that in the case $m_c = m_s$, the partition matrix $\bar{\mathbf{B}}_\mathbf{1}$ reduces to a null matrix and the control $\hat{\mathbf{u}}$ automatically satisfies the condition $\hat{\mathbf{u}} \in \mathcal{N}(\bar{\mathbf{B}}_\mathbf{1})$.

Finally, to obtain the sliding motion equations the static constraint $\mathbf{s} = \mathbf{0}$ must be incorporated into (3.26). Considering (3.16) and (3.17), and taking into account that $\bar{\mathbf{C}}_{\mathbf{s2}}$ is nonsingular, the sliding surface constraint equation can be solved for $\mathbf{y_2}$ as

$$\mathbf{y_2} = \bar{\mathbf{K}}_\mathbf{c}\, \mathbf{y_c} \tag{3.28}$$

in which

$$\bar{\mathbf{K}}_\mathbf{c} = -\bar{\mathbf{C}}_{\mathbf{s2}}^{-1} \begin{bmatrix} \bar{\mathbf{H}}_1 & \bar{\mathbf{H}}_2 & \bar{\mathbf{C}}_{\mathbf{s1}} \end{bmatrix} \tag{3.29}$$

Substituting equation (3.29) into equation (3.26), one can write

$$\dot{\mathbf{y}}_\mathbf{c} = \left[\bar{\mathbf{A}}_\mathbf{c} + \bar{\mathbf{B}}_\mathbf{c}\bar{\mathbf{K}}_\mathbf{c}\right] \mathbf{y_c} + \bar{\mathbf{e}}_\mathbf{e}\ddot{x}_g \tag{3.30}$$

This reduced system of equations describes the behavior of the system under ideal sliding motion conditions. The matrices $\bar{\mathbf{A}}_\mathbf{c}$, $\bar{\mathbf{B}}_\mathbf{c}$ and $\bar{\mathbf{K}}_\mathbf{c}$, and therefore the characteristics of this constrained motion, depend on the two sets of matrices ($\bar{\mathbf{F}}_\mathbf{1}$,$\bar{\mathbf{G}}_\mathbf{1}$,$\bar{\mathbf{H}}_\mathbf{1}$,$\bar{\mathbf{C}}_{\mathbf{s1}}$) and ($\bar{\mathbf{F}}_\mathbf{2}$,$\bar{\mathbf{G}}_\mathbf{2}$,$\bar{\mathbf{H}}_\mathbf{2}$,$\bar{\mathbf{C}}_{\mathbf{s2}}$) defining the sliding surface.

3.6 Sliding Surface Design

The sliding surface design problem involves the calculation of matrices $\bar{\mathbf{H}}_\mathbf{1}$,$\bar{\mathbf{C}}_{\mathbf{s1}}$,$\bar{\mathbf{H}}_\mathbf{2}$ and $\bar{\mathbf{C}}_{\mathbf{s2}}$. For this, it is common to use the minimization of a performance index or cost function

which is quadratic in the state vector components $\mathbf{y_1}$ and $\mathbf{y_2}$. In the following, however, a performance index is defined in terms of two sets of output variables related to the auxiliary systems (3.13) instead of $\mathbf{y_1}$ and $\mathbf{y_2}$.

The performance index to be minimized is of the following form:

$$J = \int_{t_h}^{\infty} \left(\mathbf{q}_1^T \, \mathbf{Q_1} \mathbf{q_1} + \mathbf{q}_2^T \mathbf{Q_2} \mathbf{q_2} \right) dt \tag{3.31}$$

where $\mathbf{Q_1}$ and $\mathbf{Q_2}$ are $n_q \times n_q$ and $m_s \times m_s$ positive semi-definite and positive definite weighting matrices, respectively. The variables $\mathbf{q_1}$ and $\mathbf{q_2}$ are defined by the following output equations:

$$\mathbf{q_1} = \bar{\mathbf{D}}_1 \boldsymbol{\varphi}_1 + \bar{\mathbf{E}}_1 \mathbf{y_1} \;\text{ and }\; \mathbf{q_2} = \bar{\mathbf{D}}_2 \boldsymbol{\varphi}_2 + \bar{\mathbf{E}}_2 \mathbf{y_2} \tag{3.32}$$

in which it is required that the $m_s \times m_s$ matrix $\bar{\mathbf{E}}_2$ be nonsingular. The variables $\boldsymbol{\varphi_1}$ and $\boldsymbol{\varphi_2}$ are the state variables corresponding to the realizations indicated in equations (3.13). The introduction of the matrices $\bar{\mathbf{D}}_1$, $\bar{\mathbf{E}}_1$, $\bar{\mathbf{D}}_2$ and $\bar{\mathbf{E}}_2$ in the definition of the outputs $\mathbf{q_1}$ and $\mathbf{q_2}$ is intended to facilitate the design process, offering additional flexibility for the determination of the sliding surface. The lower limit of the integral in equation (3.31) is explicitly denoted as t_h to indicate that this performance index is evaluated for the system under sliding conditions. As mentioned before, this time t_h is the time for which the system reaches the sliding surface, and without any loss of generality can be set $t_h = 0$.

Substituting $\mathbf{q_1}$ and $\mathbf{q_2}$ from equations (3.32) into equation (3.31), the performance index can be expressed as

$$J = \int_0^{\infty} \left(\mathbf{y_c}^T \, \bar{\mathbf{W}}_{11} \, \mathbf{y_c} + 2 \mathbf{y_c}^T \, \bar{\mathbf{W}}_{12} \, \mathbf{y_2} + \mathbf{y_2}^T \, \bar{\mathbf{W}}_{22} \, \mathbf{y_2} \right) \, dt \tag{3.33}$$

where $\mathbf{y_c}$ was defined in equation (3.27) and the weighting matrices are given by

$$\bar{\mathbf{W}}_{11} = \begin{bmatrix} \bar{\mathbf{D}}_1^T \mathbf{Q_1} \bar{\mathbf{D}}_1 & \mathbf{0} & \bar{\mathbf{D}}_1^T \mathbf{Q_1} \bar{\mathbf{E}}_1 \\ \mathbf{0} & \bar{\mathbf{D}}_2^T \mathbf{Q_2} \bar{\mathbf{D}}_2 & \mathbf{0} \\ \left[\bar{\mathbf{D}}_1^T \mathbf{Q_1} \bar{\mathbf{E}}_1 \right]^T & \mathbf{0} & \bar{\mathbf{E}}_1^T \mathbf{Q_1} \bar{\mathbf{E}}_1 \end{bmatrix}, \tag{3.34}$$

$$\bar{\mathbf{W}}_{\mathbf{12}} = \begin{bmatrix} \mathbf{0} \\ \bar{\mathbf{D}}_{\mathbf{2}}^T \mathbf{Q_2} \bar{\mathbf{E}}_{\mathbf{2}} \\ \mathbf{0} \end{bmatrix} \quad \text{and} \quad \bar{\mathbf{W}}_{\mathbf{22}} = \left[\bar{\mathbf{E}}_{\mathbf{2}}^T \mathbf{Q_2} \bar{\mathbf{E}}_{\mathbf{2}} \right] \tag{3.35}$$

It is desired to minimize this cost function under the condition that the system is forced to satisfy $\dot{\mathbf{s}} \,|_{\mathbf{u}=\hat{\mathbf{u}}} = \mathbf{0}$. The corresponding state equations are given by (3.26), and if the external excitation is omitted, they take the following form:

$$\dot{\mathbf{y}}_{\mathbf{c}} = \bar{\mathbf{A}}_{\mathbf{c}} \, \mathbf{y}_{\mathbf{c}} + \bar{\mathbf{B}}_{\mathbf{c}} \, \mathbf{y_2} \tag{3.36}$$

The problem of minimizing (3.33) subject to (3.36) can be solved as a classical optimal control problem with cross-terms in the cost function. In view of the definition of $\bar{\mathbf{W}}_{\mathbf{12}}$ in equation (3.35), it is noted that the cross terms in equation (3.33) depend only on $\boldsymbol{\varphi}_{\mathbf{2}}$ and $\mathbf{y_2}$. Therefore, they depend entirely on the definition of the second output variable in (3.32). In case of a static definition of the form $\mathbf{q_2} = \bar{\mathbf{E}}_{\mathbf{2}} \mathbf{y_2}$, it is seen that the cross terms vanish from the expression of the performance index.

The optimal $\mathbf{y_2}$ can be determined as follows [2]:

$$\mathbf{y_2} = -\bar{\mathbf{W}}_{\mathbf{22}}^{-1} \left[\hat{\mathbf{B}}_{\mathbf{c}}^T \, \mathbf{P} - \bar{\mathbf{W}}_{\mathbf{12}}^T \right] \, \mathbf{y_c} \tag{3.37}$$

in which the $n_c \times n_c$ matrix $\mathbf{P}$ is the solution of the following Riccati equation:

$$\mathbf{P} \, \bar{\mathbf{A}}_{\mathbf{c}} + \bar{\mathbf{A}}_{\mathbf{c}}^T \, \mathbf{P} - \mathbf{P} \, \bar{\mathbf{B}}_{\mathbf{c}} \, \bar{\mathbf{W}}_{\mathbf{22}}^{-1} \, \bar{\mathbf{B}}_{\mathbf{c}}^T \, \mathbf{P} = -\hat{\mathbf{W}}_{\mathbf{11}} \tag{3.38}$$

where the matrix $\hat{\mathbf{W}}_{\mathbf{11}}$ is given by

$$\hat{\mathbf{W}}_{\mathbf{11}} = \bar{\mathbf{W}}_{\mathbf{11}} - \bar{\mathbf{W}}_{\mathbf{12}} \bar{\mathbf{W}}_{\mathbf{22}}^{-1} \bar{\mathbf{W}}_{\mathbf{12}}^T \tag{3.39}$$

Equation (3.37) indicates the linear relation that must be satisfied by the state variables under optimal sliding conditions. Comparing equations (3.28) and (3.37), it follows that

$$\bar{\mathbf{K}}_{\mathbf{c}} = -\bar{\mathbf{W}}_{\mathbf{22}}^{-1} \left[\bar{\mathbf{B}}_{\mathbf{c}}^T \, \mathbf{P} - \bar{\mathbf{W}}_{\mathbf{12}}^T \right] \tag{3.40}$$

By selecting $\bar{\mathbf{C}}_{\mathbf{s2}} = \bar{\mathbf{E}}_{\mathbf{2}}^T \mathbf{Q_2} \bar{\mathbf{E}}_{\mathbf{2}}$, the matrices $\bar{\mathbf{H}}_{\mathbf{1}}$, $\bar{\mathbf{H}}_{\mathbf{2}}$ and $\bar{\mathbf{C}}_{\mathbf{s1}}$ defining the sliding surface in (3.17) can be obtained by an appropriate partition of $\bar{\mathbf{B}}_{\mathbf{c}}^T \mathbf{P} - \bar{\mathbf{W}}_{\mathbf{12}}^T$ of the form:

$$\bar{\mathbf{B}}_{\mathbf{c}}^T \mathbf{P} - \bar{\mathbf{W}}_{\mathbf{12}}^T = \left[\begin{array}{ccc} \bar{\mathbf{H}}_{\mathbf{1}} & \bar{\mathbf{H}}_{\mathbf{2}} & \bar{\mathbf{C}}_{\mathbf{s1}} \end{array} \right] \tag{3.41}$$

Finally, the sliding surface can be written in terms of the original state variables as follows:

$$\mathbf{s} = \mathbf{C}_{\mathbf{e}} \boldsymbol{\eta}_{\mathbf{e}} = \mathbf{0} \tag{3.42}$$

where

$$\mathbf{C}_{\mathbf{e}} = \left[\begin{array}{ccc} \bar{\mathbf{H}}_{\mathbf{1}} & \bar{\mathbf{H}}_{\mathbf{2}} & \bar{\mathbf{C}}_{\mathbf{s1}} \mathbf{P_1} + \bar{\mathbf{C}}_{\mathbf{s2}} \mathbf{P_2} \end{array} \right] \text{ and } \boldsymbol{\eta}_{\mathbf{e}} = \left\{ \begin{array}{c} \boldsymbol{\varphi}_{\mathbf{1}} \\ \boldsymbol{\varphi}_{\mathbf{2}} \\ \boldsymbol{\eta} \end{array} \right\} \tag{3.43}$$

and in which $\mathbf{P_1}$ and $\mathbf{P_2}$ have dimensions $n_r \times n$ and $m_s \times n$, respectively, and they denote partitions of the matrix $\mathbf{T}^T$ of the form:

$$\mathbf{T}^T = \left[\begin{array}{c} \mathbf{P_1} \\ \mathbf{P_2} \end{array} \right] \tag{3.44}$$

Since there were no restrictions imposed on the structure of the matrix defining the sliding surface, the resulting control system will have, in general, full-state feedback characteristics. That is, the computation of $\mathbf{s}$ using (3.42) will require information about all displacement and velocity variables in the model.

Frequency-Dependent Weighting Interpretation

As indicated by Gupta [28], the performance index defined in (3.31) is equivalent to a frequency-dependent weighting of the participation of the variables $\mathbf{y_1}$ and $\mathbf{y_2}$ in the resulting performance index. This provides a convenient option to selectively penalize some frequencies more that others to achieve some desirable characteristics.

The variables $\mathbf{q_1}$ and $\mathbf{q_2}$ are defined by the following realizations:

$$\left\{ \begin{array}{l} \dot{\boldsymbol{\varphi}}_{\mathbf{1}} = \bar{\mathbf{F}}_{\mathbf{1}} \boldsymbol{\varphi}_{\mathbf{1}} + \bar{\mathbf{G}}_{\mathbf{1}} \mathbf{y}_{\mathbf{1}} \\ \mathbf{q_1} = \bar{\mathbf{D}}_{\mathbf{1}} \boldsymbol{\varphi}_{\mathbf{1}} + \bar{\mathbf{E}}_{\mathbf{1}} \mathbf{y}_{\mathbf{1}} \end{array} \right. \text{ and } \left\{ \begin{array}{l} \dot{\boldsymbol{\varphi}}_{\mathbf{2}} = \bar{\mathbf{F}}_{\mathbf{2}} \boldsymbol{\varphi}_{\mathbf{2}} + \bar{\mathbf{G}}_{\mathbf{2}} \mathbf{y}_{\mathbf{2}} \\ \mathbf{q_2} = \bar{\mathbf{D}}_{\mathbf{2}} \boldsymbol{\varphi}_{\mathbf{2}} + \bar{\mathbf{E}}_{\mathbf{2}} \mathbf{y}_{\mathbf{2}} \end{array} \right. \tag{3.45}$$

and this can be written in the Laplace domain as follows:

$$\mathbf{q_1}(\mathrm{s}) = \mathbf{H_1}(\mathrm{s})\,\mathbf{y_1}(\mathrm{s}) \;\text{ and }\; \mathbf{q_2}(\mathrm{s}) = \mathbf{H_2}(\mathrm{s})\,\mathbf{y_2}(\mathrm{s}) \tag{3.46}$$

where $\mathbf{H_1}(\mathrm{s})$ and $\mathbf{H_2}(\mathrm{s})$ denote the corresponding transfer function matrices defined, respectively, by

$$\mathbf{H_1}(\mathrm{s}) = \bar{\mathbf{D}}_\mathbf{1}\left[\bar{\mathbf{F}}_\mathbf{1} - \mathrm{s}\mathbf{I}_{n_{s_1}}\right]^{-1}\bar{\mathbf{G}}_\mathbf{1} + \bar{\mathbf{E}}_\mathbf{1} \tag{3.47}$$

$$\mathbf{H_2}(\mathrm{s}) = \bar{\mathbf{D}}_\mathbf{2}\left[\bar{\mathbf{F}}_\mathbf{2} - \mathrm{s}\mathbf{I}_{n_{s_2}}\right]^{-1}\bar{\mathbf{G}}_\mathbf{2} + \bar{\mathbf{E}}_\mathbf{2} \tag{3.48}$$

On the other hand, by considering Parseval's theorem, the performance index (3.31) can be evaluated in the frequency domain as

$$J = \int_{-\infty}^{\infty} \left(\mathbf{q}_1^*(i\omega)\,\mathbf{Q_1}\mathbf{q_1}(i\omega) + \mathbf{q}_2^*(i\omega)\mathbf{Q_2}\mathbf{q_2}(i\omega)\right) d\omega \tag{3.49}$$

where $(.)^*$ denotes complex conjugate transpose. Therefore, using (3.46), J can be written in the following form:

$$J = \int_{-\infty}^{\infty} \left(\mathbf{y}_1^*(i\omega)\,\hat{\mathbf{Q}}_\mathbf{1}(i\omega)\mathbf{y_1}(i\omega) + \mathbf{y}_2^*(i\omega)\hat{\mathbf{Q}}_\mathbf{2}(i\omega)\mathbf{y_2}(i\omega)\right) d\omega \tag{3.50}$$

where the weighting matrices $\hat{\mathbf{Q}}_\mathbf{1}(i\omega) = \mathbf{H}_1^*(i\omega)\,\mathbf{Q_1}\mathbf{H_1}(i\omega)$ and $\hat{\mathbf{Q}}_\mathbf{2}(i\omega) = \mathbf{H}_2^*(i\omega)\,\mathbf{Q_2}\mathbf{H_2}(i\omega)$ are functions of frequency. This expression puts in evidence the selective penalization of the contribution of the variables $\mathbf{y_1}$ and $\mathbf{y_2}$ to the performance index. This type of generalized performance index was used by Young and Ozguner [121] in the design of sliding mode controllers for robot manipulators. In this case, the frequency-dependent weighting characteristics of the cost function were used to eliminate high frequency components in the control signal.

3.7 Controller Design

The controller must attract the system state toward the sliding surface $\mathbf{s} = \mathbf{0}$ and must keep it there. As it was done before in Chapter 2, a general approach based on Lyapunov's

direct method is used to design such a controller. Let V be a Lyapunov function candidate of the form

$$V = \frac{1}{2}\mathbf{s}^T\mathbf{\Pi}\,\mathbf{s} \tag{3.51}$$

in which $\mathbf{\Pi}$ is denotes a $m_s \times m_s$ positive definite matrix to be defined later. The time derivative of this function is given by

$$\frac{d}{dt}(V) = \mathbf{s}^T\mathbf{\Pi}\,\dot{\mathbf{s}} \tag{3.52}$$

In order to assure the existence of sliding motion and to guarantee that any motion is going to be attracted to the sliding surface, the purpose of the controller is to force (3.52) to be a negative definite function. Considering the augmented state equations (3.14) and the definition of the sliding surface given by (3.16), it follows that

$$\dot{\mathbf{s}} = \bar{\mathbf{C}}_\mathbf{e}\left\{\bar{\mathbf{A}}_\mathbf{e}\,\mathbf{y_e} + \bar{\mathbf{e}}_\mathbf{e}\,\ddot{x}_g\right\} + \bar{\mathbf{C}}_\mathbf{e}\bar{\mathbf{B}}_\mathbf{e}\mathbf{u} \tag{3.53}$$

Substituting (3.53) into (3.52), the time derivative of V takes the form

$$\frac{d}{dt}(V) = \mathbf{s}^T\mathbf{\Pi}\,\bar{\mathbf{C}}_\mathbf{e}\left\{\bar{\mathbf{A}}_\mathbf{e}\,\mathbf{y_e} + \bar{\mathbf{e}}_\mathbf{e}\,\ddot{x}_g\right\} + \mathbf{s}^T\mathbf{\Pi}\,\bar{\mathbf{C}}_\mathbf{e}\bar{\mathbf{B}}_\mathbf{e}\mathbf{u} \tag{3.54}$$

In the following, an active nonlinear controller is proposed and the corresponding region of attraction is investigated. Some interesting characteristics of the resulting closed-loop system under the linear version of this controller are also discussed in a later section.

3.7.1 Active Control

Taking into account the definitions of the augmented state matrix and the sliding surface matrix, given by equations (3.15) and (3.17), respectively, one can write

$$\bar{\mathbf{C}}_\mathbf{e}\bar{\mathbf{A}}_\mathbf{e} = \left[\begin{array}{cccc} \mathbf{K_1} & \mathbf{K_2} & \mathbf{Q_1} & \mathbf{Q_2} \end{array}\right] \tag{3.55}$$

where following notation was introduced:

$$\mathbf{K_1} = \bar{\mathbf{H}}_1\bar{\mathbf{F}}_1,\ \mathbf{Q_1} = \bar{\mathbf{H}}_1\bar{\mathbf{G}}_1 + \bar{\mathbf{C}}_{s1}\bar{\mathbf{A}}_{11} + \bar{\mathbf{C}}_{s2}\bar{\mathbf{A}}_{21},$$

$$\mathbf{K_2} = \bar{\mathbf{H}}_2\bar{\mathbf{F}}_2 \text{ and } \mathbf{Q_2} = \bar{\mathbf{H}}_1\bar{\mathbf{G}}_2 + \bar{\mathbf{C}}_{s1}\bar{\mathbf{A}}_{12} + \bar{\mathbf{C}}_{s2}\bar{\mathbf{A}}_{22} \tag{3.56}$$

and substituting (3.55) into equation (3.54), it follows that

$$\frac{d}{dt}(V) = \mathbf{s}^T\mathbf{\Pi}\{\mathbf{K}_1\boldsymbol{\varphi}_1 + \mathbf{K}_2\boldsymbol{\varphi}_2 + \mathbf{Q}_1\mathbf{y}_1 + \mathbf{Q}_2\mathbf{y}_2\} + \mathbf{s}^T\mathbf{\Pi}\,\bar{\mathbf{C}}_e\,\bar{\mathbf{e}}_e\,\ddot{x}_g + \mathbf{s}^T\mathbf{\Pi}\,\bar{\mathbf{C}}_e\bar{\mathbf{B}}_e\mathbf{u_a} \tag{3.57}$$

Next, by considering the relation between the state variables $\mathbf{y}$ and $\boldsymbol{\eta}$, the time derivative of V can be expressed as

$$\frac{d}{dt}(V) = \mathbf{s}^T\mathbf{\Pi}\{\mathbf{K}_1\boldsymbol{\varphi}_1 + \mathbf{K}_2\boldsymbol{\varphi}_2 + \mathbf{Q_a}\boldsymbol{\eta}\} + \mathbf{s}^T\mathbf{\Pi}\,\bar{\mathbf{C}}_e\bar{\mathbf{e}}_e\,\ddot{x}_g + \mathbf{s}^T\mathbf{\Pi}\,\bar{\mathbf{C}}_e\bar{\mathbf{B}}_e\mathbf{u_a} \tag{3.58}$$

where the matrix $\mathbf{Q_a}$ is defined as

$$\mathbf{Q_a} = \mathbf{Q_1}\mathbf{P_1} + \mathbf{Q_2}\mathbf{P_2} \tag{3.59}$$

in which $\mathbf{P_1}$ and $\mathbf{P_2}$ denote the partitions of the matrix $\mathbf{T}^T$ defined according to (3.44).

The active controller $\mathbf{u_a}$ is designed according to the general structure indicated in equation (2.87), that is

$$\mathbf{u_a} = \mathbf{u_1} + \mathbf{u_2} \tag{3.60}$$

in which the component $\mathbf{u_1}$ is appropriately selected so that it compensates the effects of the system's response on the time derivative of V. This control term is defined as

$$\mathbf{u_1} = -\left[\bar{\mathbf{C}}_s\bar{\mathbf{B}}\right]^{\ddagger}\mathbf{K}_s\,\boldsymbol{\eta}_e \tag{3.61}$$

where $\left[\bar{\mathbf{C}}_s\bar{\mathbf{B}}\right]^{\ddagger}$ and $\boldsymbol{\eta}_e$are given by (3.25) and (3.43), respectively. The $m_s \times n_e$ matrix $\mathbf{K_s}$ is given by

$$\mathbf{K_s} = \begin{bmatrix} \mathbf{K_1} & \mathbf{K_2} & \mathbf{Q_a} \end{bmatrix} \tag{3.62}$$

Substituting (3.60) and (3.61) into (3.58) and selecting $\mathbf{\Pi} = \mathbf{I}_{m_s}$, it follows that the time derivative of V now takes the form

$$\frac{d}{dt}(V) = \mathbf{s}^T \bar{\mathbf{C}}_\mathbf{e} \bar{\mathbf{e}}_\mathbf{e} \, \ddot{x}_g + \mathbf{s}^T \bar{\mathbf{C}}_\mathbf{e} \bar{\mathbf{B}}_\mathbf{e} \mathbf{u_2} \tag{3.63}$$

The objective of the second term $\mathbf{u_2}$ in the controller definition is to compensate the effects of any unmeasured disturbances on the time derivative of V so that this function is negative, at least for some region in the $(s_1, s_2, \ldots s_{m_s})$ space. Depending on the choice of the component $\mathbf{u_2}$ several possible designs can be formulated. Here, the component $\mathbf{u_2}$ will be selected as some linear or nonlinear form of state feedback, and a general expression is proposed in the form

$$\mathbf{u_2} = -\left[\bar{\mathbf{C}}_\mathbf{s} \bar{\mathbf{B}}\right]^\ddagger \left[\mathbf{\Delta} + \mathbf{E} \left\|\mathbf{s}\right\|_2^2\right] \mathbf{C}_\mathbf{e} \boldsymbol{\eta}_\mathbf{e} \tag{3.64}$$

in which $\mathbf{\Delta} = \text{diag}(\delta_i)$ and $\mathbf{E} = \text{diag}(\varepsilon_i)$ are positive definite and semi-definite matrices of design parameters. That is, $\delta_i > 0$ and $\varepsilon_i \geq 0$ for $i = 1, 2, \ldots, m_s$. It is noted that the contribution of the matrix $\mathbf{E}$ in the definition of the controller is weighted by the square of the distance to the sliding surface. The resulting contribution to the control action therefore is a cubic function of this distance.

After substituting (3.64) into (3.63) and noting that

$$\bar{\mathbf{C}}_\mathbf{e} \bar{\mathbf{e}}_\mathbf{e} = \mathbf{C}_\mathbf{e} \mathbf{e}_\mathbf{e} \tag{3.65}$$

where $\mathbf{C}_\mathbf{e}$ is given in (3.43) and the augmented vector $\mathbf{e}_\mathbf{e}$ is defined as

$$\mathbf{e}_\mathbf{e} = \left\{ \begin{array}{c} \mathbf{0} \\ \mathbf{0} \\ \mathbf{e} \end{array} \right\} \tag{3.66}$$

the time derivative of V can be written as

$$\frac{d}{dt}(V) = \mathbf{s}^T \mathbf{C}_\mathbf{e} \mathbf{e}_\mathbf{e} \, \ddot{x}_g + \mathbf{s}^T \left[\mathbf{\Delta} + \mathbf{E} \left\|\mathbf{s}\right\|_2^2\right] \mathbf{s} \tag{3.67}$$

in which the external excitation $\ddot{x}_g$ appears as an unmeasured disturbance.

Considering the first term of the right hand side of (3.67), one can write

$$\mathbf{s}^T\mathbf{C_e}\mathbf{e_e}\,\ddot{x}_g \leq \mid \mathbf{s}^T\mathbf{C_e}\mathbf{e_e} \mid \ddot{x}_g^{\max} \tag{3.68}$$

where $\ddot{x}_g^{\max}$ is an estimate for the maximum ground acceleration value that can be expected at the site. Additionally, by using the Cauchy-Schwartz inequality

$$\mid \mathbf{s}^T\mathbf{C_e}\mathbf{e_e} \mid \leq \|\mathbf{s}\|_2\|\mathbf{C_e}\mathbf{e_e}\|_2 \tag{3.69}$$

and the fact that

$$\|\mathbf{s}\|_2\|\mathbf{C_e}\mathbf{e_e}\|_2 \leq \frac{1}{2}\left(\|\mathbf{s}\|_2^2 + \|\mathbf{C_e}\mathbf{e_e}\|_2^2\right) \tag{3.70}$$

it follows that

$$\mathbf{s}^T\mathbf{C_e}\mathbf{e_e}\,\ddot{x}_g \leq \frac{\ddot{x}_g^{\max}}{2}\left(\|\mathbf{s}\|_2^2 + \alpha_e^2\right) \tag{3.71}$$

where the parameter α_e has been defined as $\alpha_e = \| \mathbf{C_e}\mathbf{e_e} \|_2$.

Therefore, by considering (3.71) and the fact that

$$\mathbf{s}^T\mathbf{\Delta}\mathbf{s} \geq \delta_{\min}\|\mathbf{s}\|_2^2 \;\text{ and }\; \mathbf{s}^T\mathbf{E}\mathbf{s} \geq \varepsilon_{\min}\|\mathbf{s}\|_2^2 \tag{3.72}$$

where $\delta_{\min}$ and $\varepsilon_{\min}$ denote the smallest diagonal entries of $\mathbf{\Delta}$ and $\mathbf{E}$, respectively, it can be shown that the time derivative of the Lyapunov function satisfies the following inequality:

$$\frac{d}{dt}(V) \leq \frac{1}{2}\left(\ddot{x}_g^{\max} - 2\left(\delta_{\min} + \varepsilon_{\min}\|\mathbf{s}\|_2^2\right)\right)\|\mathbf{s}\|_2^2 + \frac{1}{2}\ddot{x}_g^{\max}\alpha_e^2 \tag{3.73}$$

If the following scalar function is defined

$$g_3(s) = -\varepsilon_{\min}\,s^4 - a_3\,s^2 + b_3 \tag{3.74}$$

in which $s = \|\mathbf{s}\|_2$ and

$$a_3 = 2\delta_{\min} - \ddot{x}_g^{\max} \tag{3.75}$$

$$b_3 = \ddot{x}_g^{\max} \alpha_e^2 \tag{3.76}$$

then it is possible to determine a region in the $(s_1, s_2, \ldots s_{m_s})$ space defined by the following condition:

$$g_3(s) < 0 \tag{3.77}$$

for which the attraction to the sliding surface, represented by the point $\mathbf{s} = \mathbf{0}$, is guaranteed.

A conservative estimate of the region of attraction can be obtained by considering $\mathbf{E} = \mathbf{0}$. In this case $\varepsilon_{\min} = 0$ and, provided that $\delta_{\min}$ is selected such that $a_3 > 0$, the attraction to the sliding surface is guaranteed for those points $\mathbf{s}$ in the $(s_1, s_2, \ldots s_{m_s})$ space that satisfy

$$s^2 = \|\mathbf{s}\|_2^2 > \frac{b_3}{a_3} \tag{3.78}$$

In the general case, the presence of a nonzero matrix $\mathbf{E}$ will cause the system to stay closer to the sliding surface.

3.7.2 Closed-Loop Characteristics

Using a controller with the structure defined in equation (3.60), the behavior of the corresponding unforced system is described by

$$\dot{\boldsymbol{\eta}}_\mathbf{e} = \mathbf{A_e}\boldsymbol{\eta}_\mathbf{e} + \mathbf{B_e}\left\{\mathbf{u_1} + \mathbf{u_2}\right\} \tag{3.79}$$

in which the augmented matrices $\mathbf{A_e}$ and $\mathbf{B_e}$ are given, respectively, by

$$\mathbf{A_e} = \begin{bmatrix} \bar{\mathbf{F}}_\mathbf{1} & \mathbf{0} & \mathbf{G_1 P_1} \\ \mathbf{0} & \bar{\mathbf{F}}_\mathbf{2} & \mathbf{G_2 P_2} \\ \mathbf{0} & \mathbf{0} & \mathbf{A} \end{bmatrix} \text{ and } \mathbf{B_e} = \begin{bmatrix} \mathbf{0} \\ \mathbf{0} \\ \mathbf{B} \end{bmatrix} \tag{3.80}$$

Note that the eigenvalues of the matrix $\mathbf{A_e}$ are given by the union of the eigenvalues of the matrices $\bar{\mathbf{F}}_\mathbf{1}$ and $\bar{\mathbf{F}}_\mathbf{2}$ (which are selected asymptotically stable) and the original system matrix $\mathbf{A}$ (which is asymptotically stable by definition of the problem).

Substituting the definition for the component $\mathbf{u_1}$, given by (3.61), one obtains

$$\dot{\boldsymbol{\eta}}_{\mathbf{e}} = \mathbf{A}_{\mathbf{e}}\boldsymbol{\eta}_{\mathbf{e}} - \mathbf{B}_{\mathbf{e}}\left[\mathbf{C}_{\mathbf{s}}\mathbf{B}\right]^{\ddagger}\mathbf{K}_{\mathbf{s}}\,\boldsymbol{\eta}_{\mathbf{e}} + \mathbf{B}_{\mathbf{e}}\mathbf{u_2} \tag{3.81}$$

By considering the definitions of the matrices $\mathbf{C}_{\mathbf{e}}$ and $\mathbf{A}_{\mathbf{e}}$, given by (3.43) and (3.80), respectively, it is easy to show that

$$\mathbf{K}_{\mathbf{s}} = \mathbf{C}_{\mathbf{e}}\mathbf{A}_{\mathbf{e}} \tag{3.82}$$

and after some rearrangement, equations (3.81) can be written as

$$\dot{\boldsymbol{\eta}}_{\mathbf{e}} = \mathbf{A}_{\mathbf{s}}\boldsymbol{\eta}_{\mathbf{e}} + \mathbf{B}_{\mathbf{e}}\mathbf{u_2} \tag{3.83}$$

in which the matrix $\mathbf{A}_{\mathbf{s}}$ is given by

$$\mathbf{A}_{\mathbf{s}} = \left[\mathbf{I}_{n_e} - \mathbf{P}_{\mathbf{s}}\right]\mathbf{A}_{\mathbf{e}} \tag{3.84}$$

where the matrix $\mathbf{P}_{\mathbf{s}}$ is defined as

$$\mathbf{P}_{\mathbf{s}} = \mathbf{B}_{\mathbf{e}}\left[\mathbf{C}_{\mathbf{s}}\mathbf{B}\right]^{\ddagger}\mathbf{C}_{\mathbf{e}} \tag{3.85}$$

Since $\mathbf{P}_{\mathbf{s}}\mathbf{P}_{\mathbf{s}} = \mathbf{P}_{\mathbf{s}}$, this matrix is a projection matrix. In particular, it represents a projection onto $\mathcal{R}(\mathbf{B}_{\mathbf{e}}\left[\mathbf{C}_{\mathbf{s}}\mathbf{B}\right]^{\ddagger})$ (range of $\mathbf{B}_{\mathbf{e}}\left[\mathbf{C}_{\mathbf{s}}\mathbf{B}\right]^{\ddagger}$) parallel to $\mathcal{N}(\mathbf{C}_{\mathbf{e}})$ (null space of $\mathbf{C}_{\mathbf{e}}$). The matrix $\mathbf{I}_{n_e} - \mathbf{P}_{\mathbf{s}}$ represents the complementary projection and it is easy to see that

$$\mathbf{C}_{\mathbf{e}}\left[\mathbf{I}_{n_e} - \mathbf{P}_{\mathbf{s}}\right] = \mathbf{0} \tag{3.86}$$

and therefore

$$\mathbf{C}_{\mathbf{e}}\mathbf{A}_{\mathbf{s}} = \mathbf{0} \tag{3.87}$$

Some characteristics of the eigenstructure of the matrix $\mathbf{A}_{\mathbf{s}}$ are investigated in the following. The corresponding eigenvalue problem is written as

$$\mathbf{A}_{\mathbf{s}}\boldsymbol{\Phi}_{\mathbf{s}} = \boldsymbol{\Lambda}_{\mathbf{s}}\boldsymbol{\Phi}_{\mathbf{s}} \tag{3.88}$$

and after premultiplying by $\mathbf{C_e}$ and considering (3.87), it follows that the eigenstructure of $\mathbf{A_s}$ satisfies

$$\mathbf{C_e \Lambda_s \Phi_s = 0} \tag{3.89}$$

Since $\text{rank}(\mathbf{C_e}) = m_s$, equation (3.87) indicates that the matrix $\mathbf{A_s}$ has m_s zero eigenvalues. For these eigenvalues, the condition (3.89) is automatically satisfied. For the remaining $n_e - m_s$ nonzero eigenvalues, condition (3.89) indicates that the corresponding eigenvectors are orthogonal to the sliding surface matrix $\mathbf{C_e}$.

Now, substituting the definition for $\mathbf{u_2}$, given by (3.64), and assuming $\mathbf{E = 0}$ it follows that (3.83) reduces to

$$\dot{\boldsymbol{\eta}}_\mathbf{e} = \mathbf{A_{cl}} \boldsymbol{\eta}_\mathbf{e} \tag{3.90}$$

in which the closed-loop matrix $\mathbf{A_{cl}}$ is defined as

$$\mathbf{A_{cl}} = \mathbf{A_s} - \mathbf{B_e} \left[\mathbf{C_s B}\right]^\ddagger \boldsymbol{\Delta} \mathbf{C_e} \tag{3.91}$$

Note that

$$\mathbf{C_e A_{cl}} = -\boldsymbol{\Delta} \mathbf{C_e} \tag{3.92}$$

Some characteristics of the eigenstructure of the matrix $\mathbf{A_{cl}}$ are investigated in the following. The corresponding eigenvalue problem is written as

$$\mathbf{A_{cl} \Phi_{cl} = \Lambda_{cl} \Phi_{cl}} \tag{3.93}$$

and after premultiplying by $\mathbf{C_e}$ and considering (3.92), it follows that the eigenstructure of $\mathbf{A_{cl}}$ satisfies

$$\mathbf{C_e \Lambda_{cl} \Phi_{cl} = -\boldsymbol{\Delta} C_e \Phi_{cl}} \tag{3.94}$$

In particular, if the matrix $\boldsymbol{\Delta}$ is selected as $\boldsymbol{\Delta} = \delta\, \mathbf{I}_{m_s}$, the above condition takes the form

$$\mathbf{C_e \Lambda_{cl} \Phi_{cl} = -\delta C_e \Phi_{cl}} \tag{3.95}$$

which indicates that $\lambda = -\delta$ is an eigenvalue with at least multiplicity m_s. Also, from condition (3.95) it follows that any closed-loop eigenvectors corresponding to eigenvalues $\lambda \neq -\delta$ are orthogonal to the sliding surface matrix $\mathbf{C_e}$.

It is interesting to look at the equations (3.53) governing the dynamic behavior of the sliding surface variables. For the unforced case, they can be written as

$$\dot{\mathbf{s}} = \mathbf{C_e}\dot{\boldsymbol{\eta}}_\mathbf{e} = \mathbf{C_e}\mathbf{A_{cl}}\boldsymbol{\eta}_\mathbf{e} = -\boldsymbol{\Delta}\,\mathbf{s} \tag{3.96}$$

and considering the previous conclusions, it follows that the evolution of the sliding surface variables depends only on the eigenvalue $\lambda = -\delta$ and the corresponding eigenvector subspace.

3.8 Numerical Results

The applicability of sliding mode control algorithms based on a generalized or dynamic definition of the sliding surface is examined in this section by numerical simulations. The proposed active controller is numerically studied using the 10-story shear building model selected as the example case and analyzed previously in Chapter 2. The effect of the number and location of the actuation devices is investigated and to show the flexibility offered by the formulation, several designs are considered and their performance evaluated for different seismic inputs.

The active control system considered here consists of two sets of active tendons or bracings installed in the first two stories which can operate independently. As indicated in Figure (3.1), they are assumed to act between the foundation and the first two floor masses. Again, the effect of the frequency content of the external disturbance is numerically evaluated by considering the same ground excitations as in Chapter 2. That is, the ground acceleration time histories of (1) El Centro, 1941, (2) San Fernando, 1971, (3) Loma Prieta,

1989, and (4) Kern County (Hollywood site), 1952 are considered, with the first three records normalized to a maximum ground acceleration level of $0.3g$, and the Hollywood record normalized to a maximum level of $0.2g$. The corresponding acceleration response spectra were shown before in Figure (2.4).

To compare the performance and influence of the number of control devices used, the numerical results have been obtained for two different actuation cases. In the first case two actuators applying forces independently at the first and second floor levels are used. In the second case, only one actuator applying force at the first floor level is used. For both cases, the sliding surface is designed using the static relation $\mathbf{q_1} = \mathbf{y_1}$ in place of the first auxiliary system defined in equations (3.13) and (3.32). This implies that the matrices in equation (3.13) and (3.32) associated with this auxiliary system are simply:

$$\bar{\mathbf{F}}_\mathbf{1} = \mathbf{0}, \bar{\mathbf{G}}_\mathbf{1} = \mathbf{0}, \bar{\mathbf{D}}_\mathbf{1} = \mathbf{0} \text{ and } \bar{\mathbf{E}}_\mathbf{1} = \mathbf{I}_{n_r} \tag{3.97}$$

To specify the second auxiliary system, penalizing the participation of the variables $\mathbf{y_2}$ in the performance index, the following matrices were chosen:

$$\hat{\mathbf{F}}_\mathbf{2} = \begin{bmatrix} 0 & 1 \\ -\omega_o^2 & -2\zeta_o\omega_o \end{bmatrix}, \hat{\mathbf{G}}_\mathbf{2} = \begin{bmatrix} 0 \\ 1 \end{bmatrix}, \hat{\mathbf{D}}_\mathbf{2} = \begin{bmatrix} 0 & \beta_o \end{bmatrix} \text{ and } \hat{\mathbf{E}}_\mathbf{2} = [1] \tag{3.98}$$

in which ω_o, ζ_o and β_o are some design parameters. As will be shown later, the parameters ω_o, ζ_o and β_o provide flexibility in adjusting the control efforts conveniently to achieve a desired response reduction. These matrices are used to define the auxiliary system matrices for the two actuation cases mentioned above. For the case of only one actuator on the first floor ($m_c = 1$), the number of sliding constraints is $m_s = 1$ and the matrices associated with the second auxiliary system in equations (3.13) and (3.32) are defined as:

$$\bar{\mathbf{F}}_\mathbf{2} = \hat{\mathbf{F}}_\mathbf{2}, \bar{\mathbf{G}}_\mathbf{2} = \hat{\mathbf{G}}_\mathbf{2}, \bar{\mathbf{D}}_\mathbf{2} = \hat{\mathbf{D}}_\mathbf{2} \text{ and } \bar{\mathbf{E}}_\mathbf{2} = \hat{\mathbf{E}}_\mathbf{2} \tag{3.99}$$

For the case with two actuation devices ($m_c = 2$), here the number of sliding constraints is selected as $m_s = 2$. One could also choose $m_s = 1$, a case with control redundancy. For $m_s = 2$, the matrices associated with the second auxiliary system in equations (3.13) and (3.32) are defined as:

$$\bar{\mathbf{F}}_\mathbf{2} = \begin{bmatrix} \hat{\mathbf{F}}_\mathbf{2} & \mathbf{0} \\ \mathbf{0} & \hat{\mathbf{F}}_\mathbf{2} \end{bmatrix}, \bar{\mathbf{G}}_\mathbf{2} = \begin{bmatrix} \hat{\mathbf{G}}_\mathbf{2} & \mathbf{0} \\ \mathbf{0} & \hat{\mathbf{G}}_\mathbf{2} \end{bmatrix}, \bar{\mathbf{D}}_\mathbf{2} = \begin{bmatrix} \hat{\mathbf{D}}_\mathbf{2} & \mathbf{0} \\ \mathbf{0} & \hat{\mathbf{D}}_\mathbf{2} \end{bmatrix} \text{ and } \bar{\mathbf{E}}_\mathbf{2} = \begin{bmatrix} \hat{\mathbf{E}}_\mathbf{2} & \mathbf{0} \\ \mathbf{0} & \hat{\mathbf{E}}_\mathbf{2} \end{bmatrix} \quad (3.100)$$

For both actuation cases, the weighting matrices $\mathbf{Q_1}$ and $\mathbf{Q_2}$ in the definition of the performance index (3.31) are chosen as identity matrices of appropriate dimensions.

Figure (3.2) shows the time histories of the controlled and uncontrolled top floor displacement and first story shear force for the case $m_c = 2$, when the structure is subjected to El Centro ground acceleration record. The sliding surface design parameters are selected as $\omega_o = 8.00$, $\zeta_o = 0.70$ and $\beta_o = 85.00$. The control actions are governed by (3.60) with the matrix $\mathbf{\Delta}$ selected as $\mathbf{\Delta} = \delta\, \mathbf{I}_{m_s}$, in which $\delta = 30.00$, and the matrix $\mathbf{E}$ is chosen as $\mathbf{E} = \mathbf{0}$. In particular, the maximum displacement is reduced to 66% of its maximum uncontrolled value. The effectiveness of the control system in reducing the absolute floor acceleration response and corresponding floor response spectra is shown in Figure (3.3); Figure (3.3a) shows the time histories of the top floor acceleration responses and Figure (3.3b) shows the corresponding response spectra (3% damping), both for the controlled and uncontrolled responses. Both the maximum floor acceleration and the peak floor response spectrum values are reduced to about 64% of their uncontrolled response values. The controlled floor response spectrum curve also shows the effectiveness of the control system in reducing the response in the whole frequency range.

The time histories of the control forces required at the two floor levels to achieve the results presented in the previous paragraph are shown in Figure (3.4). It is seen that the proposed design for the control system naturally allocates more relevance to the actua-

tion device acting on the second floor level. This location is obviously more effective for the control force application to modify the dynamic behavior of a building system whose response is dominated by the first vibration mode. The maximum values of the control forces required at the first and second floor levels are, respectively, 0.45 and 0.98 times the respective floor weights. Figure (3.5) shows the time histories of the mechanical power corresponding to both actuation devices. It is observed that the power oscillates on the negative and positive sides for the first story device, whereas the values of power corresponding to the second story device are mostly positive and much higher than the previous ones. It is noted that, according to the sign convention assumed here, a positive value of mechanical power means that the control action is opposing the corresponding velocity. Again, the results shown in Figure (3.5) emphasize the higher level of participation of the second story actuation in the resulting control system.

For design purposes, it is desirable to assess the maximum control requirements that may be necessary to achieve a pre-set level of reduction in the response. Here this can be conveniently done by changing the parameter ω_o used for defining the sliding surface. Figure (3.6a) shows the levels of response reduction obtained as a function of the parameter ω_o in terms of response reduction factors. The response reduction factor is defined as the ratio of the controlled to the uncontrolled peak values for a given response quantity. The corresponding levels of the maximum control forces required at the two floor levels, as a function of the parameter ω_o, are shown in Figure (3.6b). These results correspond to the El Centro ground excitation. The response reductions curves are monotonic, except for the shear forces in the first two stories. Since the shear forces in these two stories are directly affected by the applied control forces, they increase when the control forces are increased beyond a certain level. It is noted that the parameter ω_o can be used to obtain a family of

controller designs for which a decrease in the response is associated with an increase in the control force. That is, the introduction of auxiliary systems in the definition of the sliding surface has made it possible to obtain a "proper" sliding surface conveniently such that an increase in the control effort translates into an increased reduction in the response. In a traditional sliding mode control approach without these compensators or auxiliary systems, obtaining a proper sliding surface is not so straightforward as some choices of parameters could lead to a situation where an increased control effort may not result into an increased reduction in the response.

Figure (3.7) is similar to the previous figure, and it shows the levels of response reduction and corresponding control requirements now as a function of the parameter β_o used to define the sliding surface. Again, the results are obtained for El Centro ground motion. In this case, smaller reductions of response and control demands are associated with increasing values of the parameter β_o. The first story shear is also shown in the figure and it follows a different behavior, as it was mentioned previously. Figure (3.8) show the variation of two closed-loop natural frequencies and damping ratios as a function of the parameter used to define the sliding surface. The frequencies ω_1 and ω_2 represented in the figure correspond approximately to the first two fundamental frequencies of the uncontrolled system, whereas ζ_1 and ζ_2 denote the associated damping ratios. Figure (3.8a) shows the variation of these frequencies and damping ratios that results from an increase in the value of the parameter ω_0. It is observed that the damping ratio corresponding to the first natural frequency increases drastically as soon as the value of the design parameter ω_0 is higher than the first natural frequency of the uncontrolled system. The other damping ratio and the two frequencies are practically indifferent to variations of ω_0. The effect on the first modal damping ratio explains the higher response reductions achieved with higher values of this

design parameter. Similarly, Figure (3.8b) shows the variations in the modal characteristics produced by an increase of the parameter β_o. In this case, the value of this parameter affects both damping ratios in the same direction, and increasing values of β_o are associated with smaller values of ζ_1 and ζ_2. This explains the smaller response reductions and control demands that correspond to higher values of the parameter β_o.

Next, the design based only on one actuator applying forces at the first floor level is investigated. The sliding surface design parameters for this case are selected as $\omega_o = 8.00$, $\zeta_o = 0.75$ and $\beta_o = 42.00$. The control actions are again governed by (3.60) with a diagonal matrix $\mathbf{\Delta}$ defined in terms of a control parameter δ, chosen as $\delta = 80.00$, and the matrix $\mathbf{E}$ chosen as $\mathbf{E} = \mathbf{0}$. Figure (3.9) shows the time histories of the controlled and uncontrolled top floor displacement and first story shear force for the case $m_c = 1$, when the structure is subjected to San Fernando ground acceleration record. The maximum controlled displacement and first story shear are reduced to 73% and 83%, respectively, of the corresponding peak uncontrolled values. Figure (3.10) investigates the reduction achieve in acceleration responses. Figure (3.10a) shows the time histories of the top floor absolute acceleration for the controlled and uncontrolled cases, whereas Figure (3.10b) shows the corresponding floor response spectra. The reduction induced by the control system for both types of responses can be easily appreciated from these figures. The corresponding control requirements are presented in Figure (3.11). The control force, normalized with respect to the floor weight and shown in Figure (3.11a), achieves a maximum value of 1.33. The time history of the corresponding mechanical power is shown in Figure (3.11b), and it reveals higher levels of actuation demand than those required in the previous case with two independent actuators.

In the following, both designs ($m_c = 2$ and $m_c = 1$) are compared by investigating the

response reductions at various levels when the building is subjected to different earthquakes. For a meaningful comparison, the two control systems were designed such that they produce the same level of reduction for the top floor displacement when the structure is subjected to El Centro ground motion. This response reduction was arbitrarily chosen equal to 0.66 in terms of the corresponding response reduction factor. The two sets of parameters given before for each case ($m_c = 2$ and $m_c = 1$) were purposely selected to satisfy this condition, and therefore they are used for the results presented in Tables (3.1)-(3.3).

Table (3.1) shows, for each earthquake, the relative displacement response reduction factors of all floor levels. It is noted that the control system with two active devices performs in general better than the system with only one actuation device as the controlled responses are noted to be somewhat smaller for lower stories in the former case. Also, from the results in the table for different excitations it is observed that the effectiveness of the control systems does depend on the ground excitation. Both control designs are observed to be the most effective with El Centro excitation and the least with the Loma Prieta case. The same observation was done in Chapter 2, when investigating the performance of controller designs based on a static sliding surface. Table (3.2) shows the results corresponding to floor acceleration responses. In general, the control design based on two actuators performs slightly better in reducing accelerations of higher floors. It is interesting to note that lower floor accelerations do not show the distinctive increase that was associated with the active tendon control system based on a static sliding surface numerically investigated in Chapter 2. The maximum control force values required to achieve the response reductions reported in Tables (3.1) and (3.2) are shown in Table (3.3). For all cases of ground excitation, it is noted that the control system based on a single device acting on the first story level demands a much higher control actions to produce a comparable level response reductions.

It is interesting to investigate the effect of a failure in one of the components of the control system and its consequences on the resulting performance. For the case $m_c = 2$ and for El Centro ground excitation, a failure will be simulated by assuming that the second story actuator goes off-line at time $t = 2.12$ [sec]. This time corresponds to the time in which the peak acceleration of the ground motion occurs. Figure (3.12) shows the resulting control requirements for the first story device. It is observed that both the control force and the associated mechanical power, shown in Figures (3.12a) and (3.12b), respectively, are increased with respect to the corresponding normal operation condition values, which were shown before in Figures (3.4) and (3.5). From Figure (3.12) it can be seen how the control system demands a greater participation of the only operating actuator to compensate for the second story device. The effect on the resulting performance of the controlled system is shown in Figure (3.13). This figure shows the response reduction factors for different floors and for different response quantities for both cases of normal operation and failure of second story actuator. It is observed that the failure of one actuator obviously degrades the resulting performance of the control system. However, the controlled system not only remains stable but also shows response reductions factors averaging 0.85 for most of the responses shown in Figure (3.13).

Next, the effect of the nonlinear term in the definition of the component $\mathbf{u_2}$, given by equation (3.64), is investigated. Using the same parameters to define the sliding surface for the case $m_c = 2$ considered before, another controller is now designed by selecting the matrix $\mathbf{\Delta}$ as $\mathbf{\Delta} = \delta\,\mathbf{I}_{m_s}$, with $\delta = 20.00$, and the matrix $\mathbf{E}$ as $\mathbf{E} = \varepsilon\,\mathbf{I}_{m_s}$ where ε is defined in terms of a normalized parameter as $\varepsilon = \bar{\varepsilon}\|\mathbf{C_e}\|_2^2$. The value of $\bar{\varepsilon}$ is chosen as $\bar{\varepsilon} = 15.00$. The performance of this control system is compared with the previous design, which was based on the linear version of the component $\mathbf{u_2}$. Figure (5.14) shows the function $g_3(s)$

which determines the regions of attraction for both cases. To compute $g_3(s)$, as defined in (3.74), the parameter $\ddot{x}_g^{\max}$ is selected as $\ddot{x}_g^{\max} = 0.3g$ whereas the parameter α_e, which depends on the sliding surface design, is given by $\alpha_e = 0.92$. It is observed how the incorporation of the nonlinear term results in a more authoritative bound for the value of s. Also shown in this figure is the maximum value of the variable s, for the uncontrolled system under the El Centro excitation. This value is given by $s_{\max} = 0.36$. It is observed that despite the fact of being conservative, the bounds on the region of attraction given by the function $g_3(s)$ are smaller than this maximum uncontrolled value and therefore they have practical significance. The effectiveness of the control system for the linear and nonlinear cases is compared in Figure (3.15). This figure shows the response reduction factors for different floors and for different response quantities. It is observed that the incorporation of the nonlinear term in the definition of the control does not modify significantly the resulting performance. The effect of the nonlinear term can nevertheless be appreciated by considering the evolution of the sliding surface variables. Figure (3.16) shows the variables s_1 and s_2 for both linear and nonlinear control cases. Also indicated in the figure are the maximum values of the control forces. It is observed that the nonlinear term imposes a more severe restriction on the sliding surface variables, which are constrained in this case to a smaller neighborhood of $\mathbf{s} = \mathbf{0}$.

3.9 Conclusions

This chapter presented the development of full state feedback sliding mode control algorithms based on a generalized definition of the sliding surface. To gain additional flexibility in the design of a better sliding surface, two auxiliary dynamical systems were introduced. The sliding surface is then defined in terms of the outputs of these auxiliary systems.

These auxiliary systems implicitly introduce a frequency weighting in the cost function used for calculating the sliding constraints. Also, another systematic approach is presented to achieve the regular form of the equation of motion to affect a uncoupling of sliding motion and control actions. The approach is general enough such that it can be applied to cases where a simple re-ordering of equations of motion will not achieve these uncoupling objectives. A nonlinear continuous active controller is formulated and the corresponding region of attraction is investigated.

The numerical results indicate the advantage of using a generalized definition of the sliding surface for the design of the control system. It was observed that this type of formulation introduces more flexibility and allows more easily to tune the parameters of the control system to achieve different performance specifications. This task is not straightforward when using a static definition of the sliding surface, as it was mentioned previously. The effect of the number and locations of actuations devices was investigated. By comparing the results obtained for different design alternatives, it is concluded that the design process naturally identifies the location of an actuator acting on the second story level as more efficient for control purposes. Also, the maximum control requirements were found smaller than those corresponding to the single actuation case with static sliding surface studied in Chapter 2. Additionally, the robustness of the control system to endure the failure of an actuation component was investigated, and the effect of nonlinear terms in the controller definitions was also evaluated.

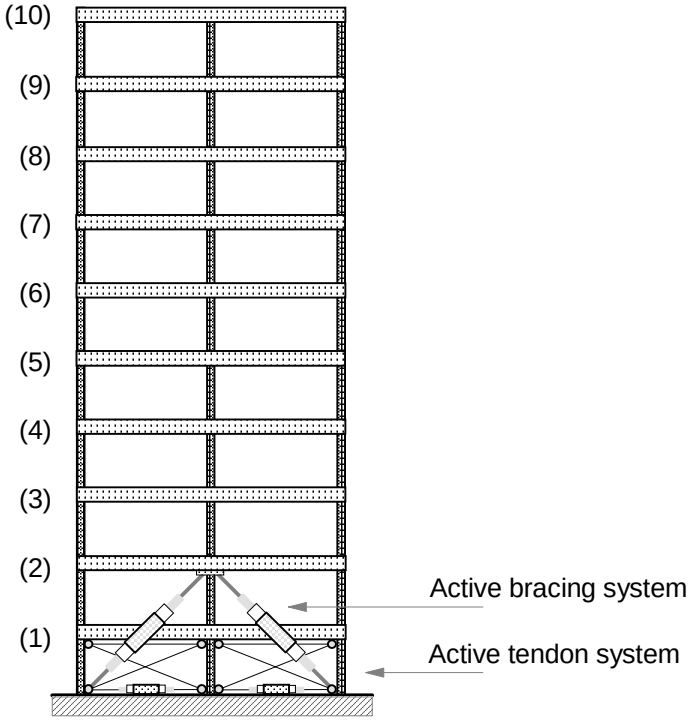

Figure 3.1: 10-story building model with active bracing and active tendon systems.

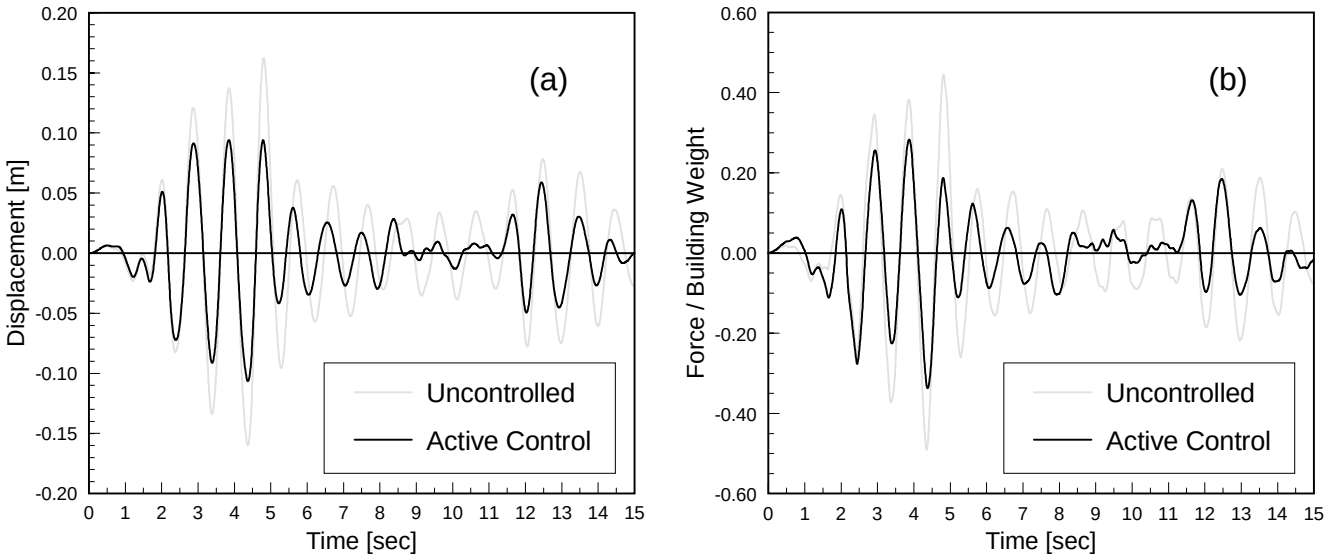

Figure 3.2: Comparison of uncontrolled and controlled top floor displacement and 1st story shear force for El Centro ground acceleration record (number of active devices: 2).

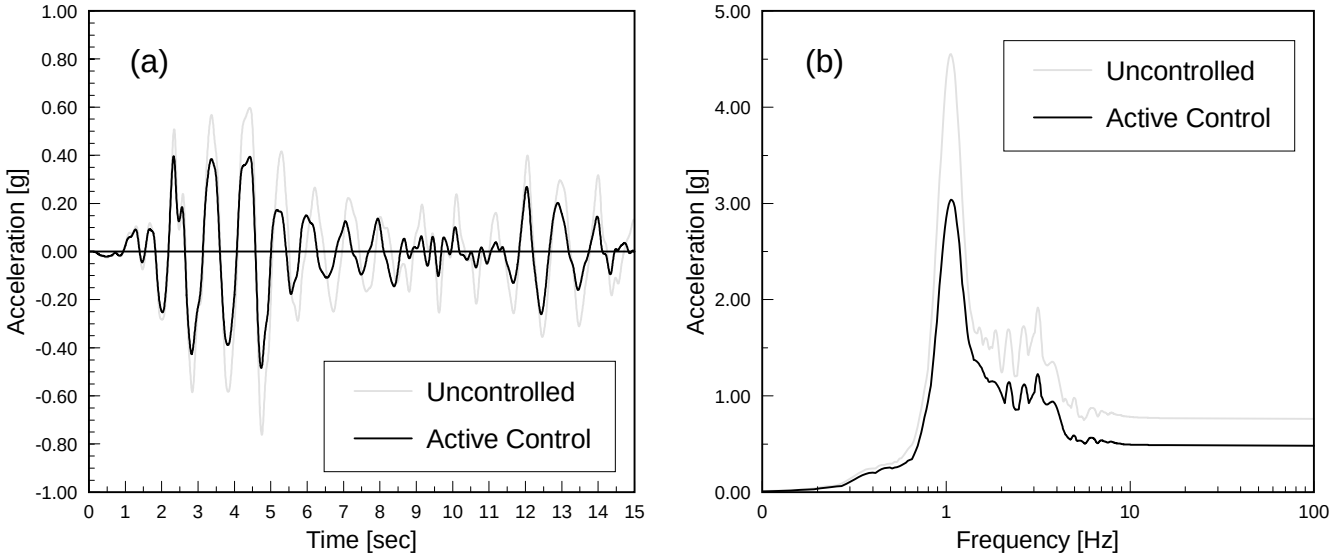

Figure 3.3: Comparison of uncontrolled and controlled top floor acceleration and top floor response spectra for El Centro ground acceleration record (number of active devices: 2).

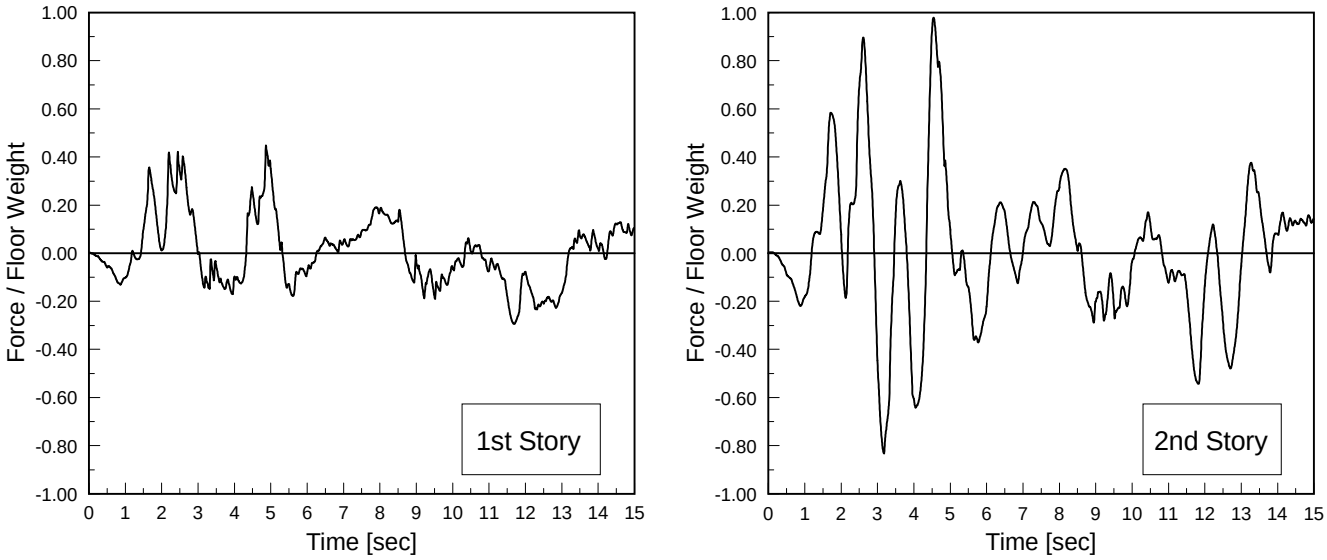

Figure 3.4: Control forces for El Centro ground acceleration record (number of active devices: 2).

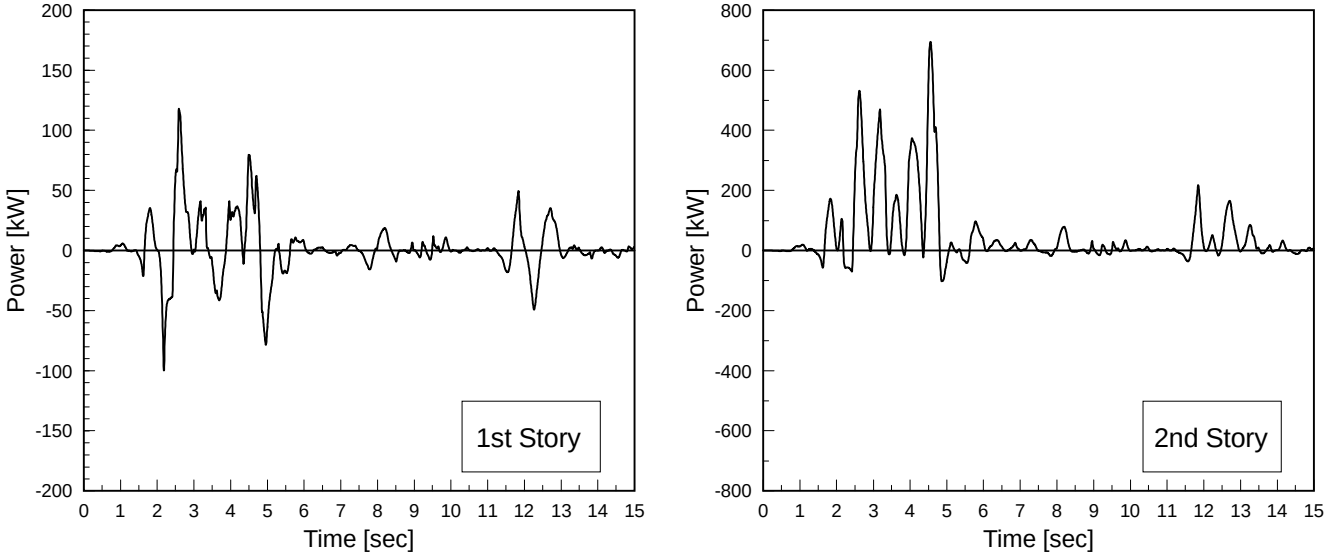

Figure 3.5: Mechanical power for El Centro ground acceleration record (number of active devices: 2).

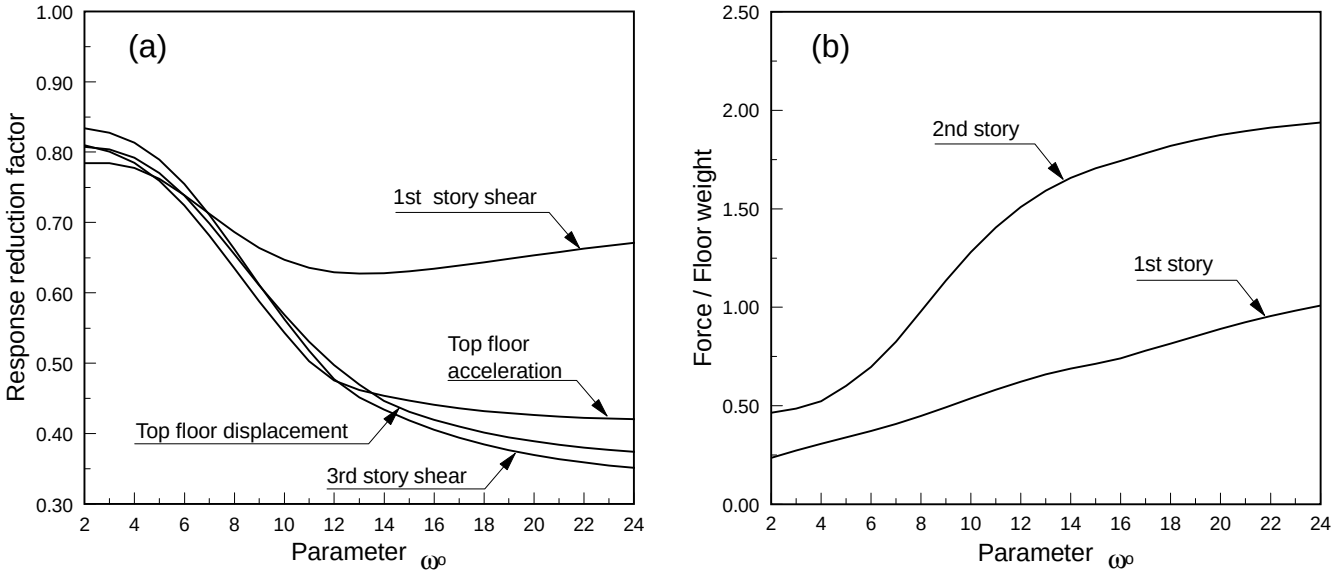

Figure 3.6: Maximum building responses and control requirements as a function of the parameter ω_o for El Centro ground acceleration record (number of active devices: 2).

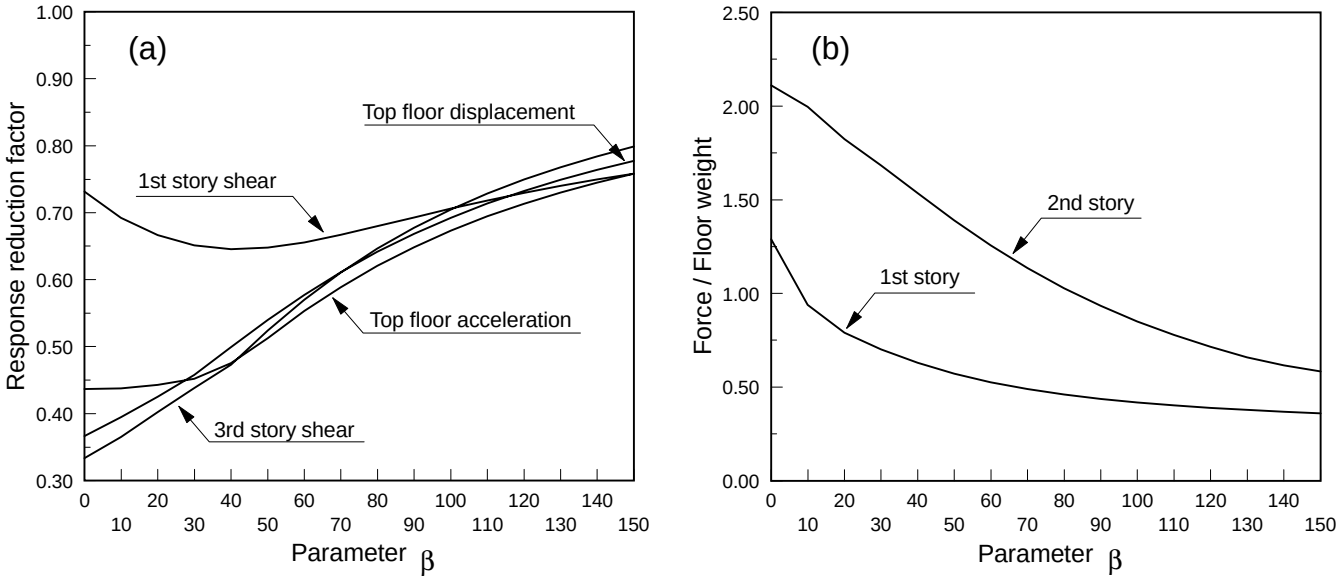

Figure 3.7: Maximum building responses and control requirements as a function of the parameter β for El Centro ground acceleration record (number of active devices: 2).

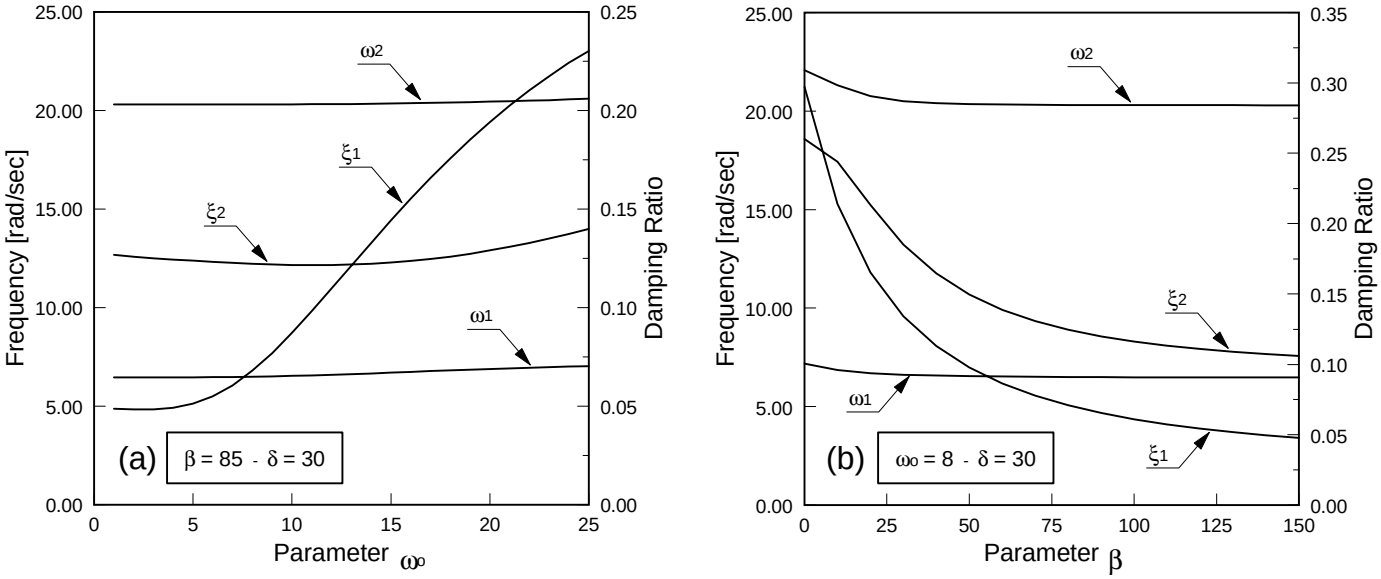

Figure 3.8: Natural frequencies and modal damping ratios as a function of the parameters defining the sliding surface (number of active devices: 2).

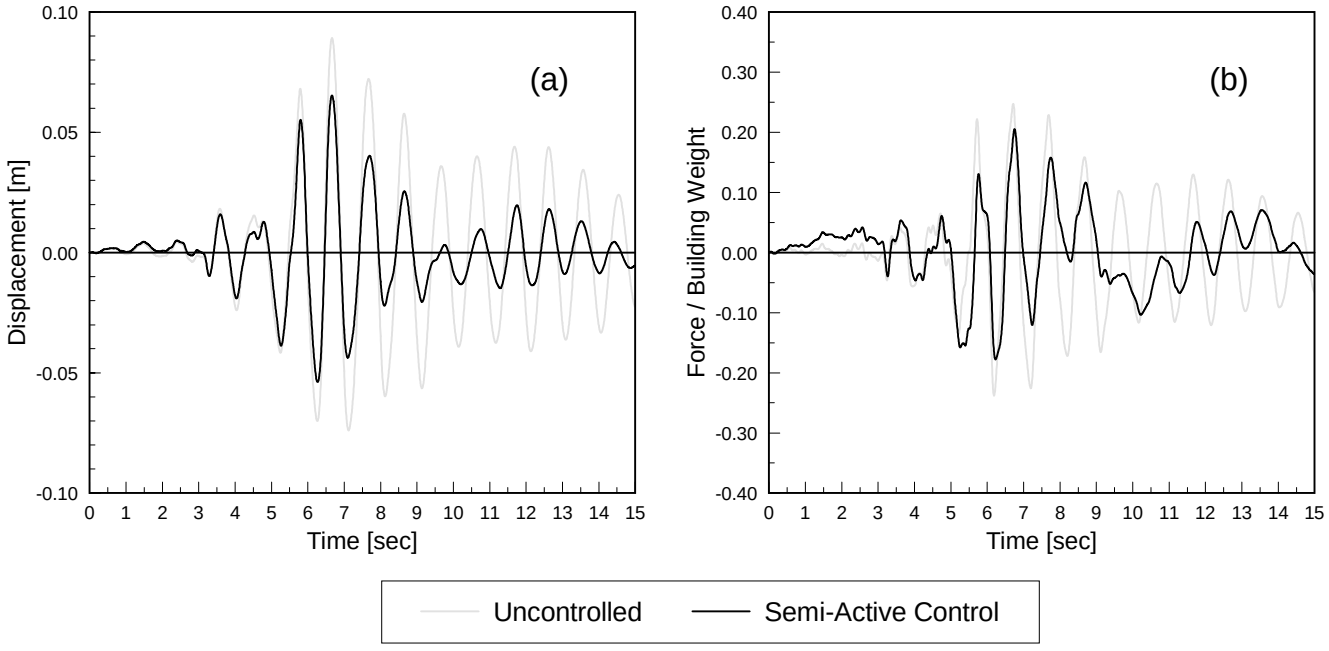

Figure 3.9: Comparison of uncontrolled and controlled top floor displacement and 1st story shear force for San Fernando ground acceleration record (number of active devices: 1).

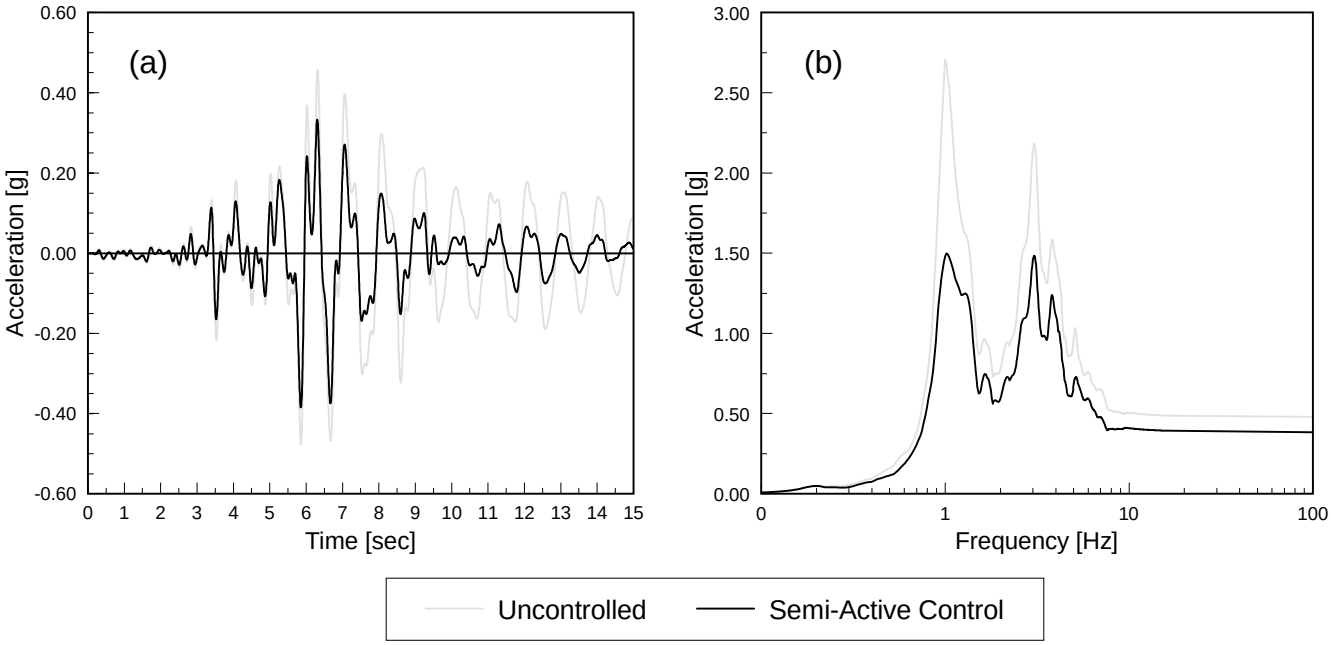

Figure 3.10: Comparison of uncontrolled and controlled top floor acceleration and top floor response spectra for San Fernando ground acceleration record (number of active devices: 1).

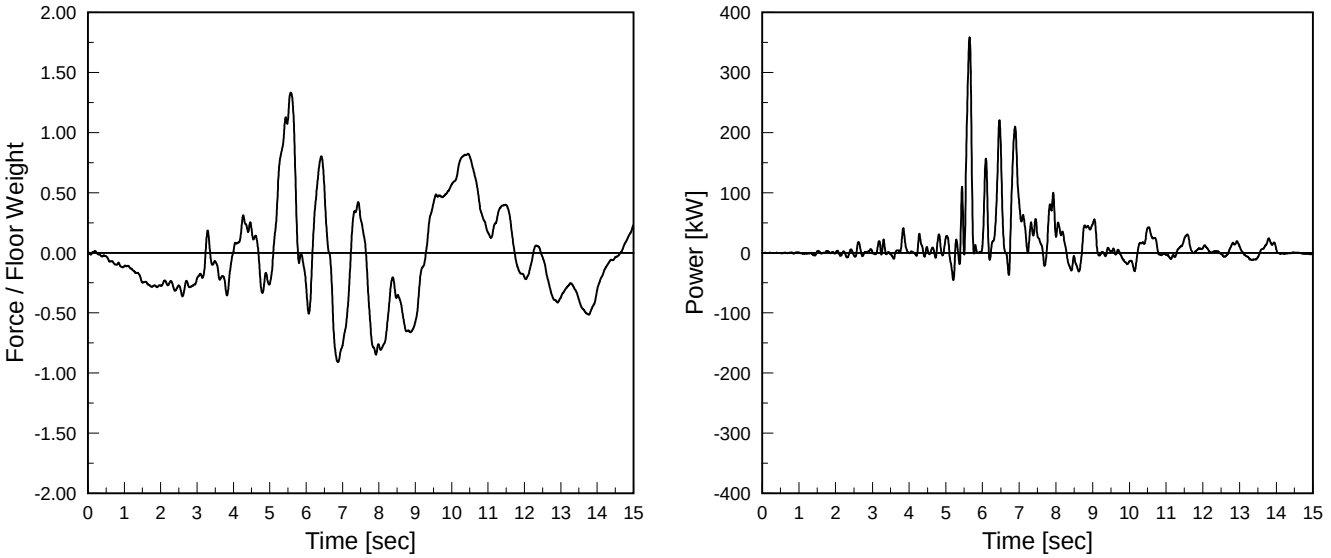

Figure 3.11: Control force and mechanical power for San Fernando ground acceleration record (number of active devices: 1).

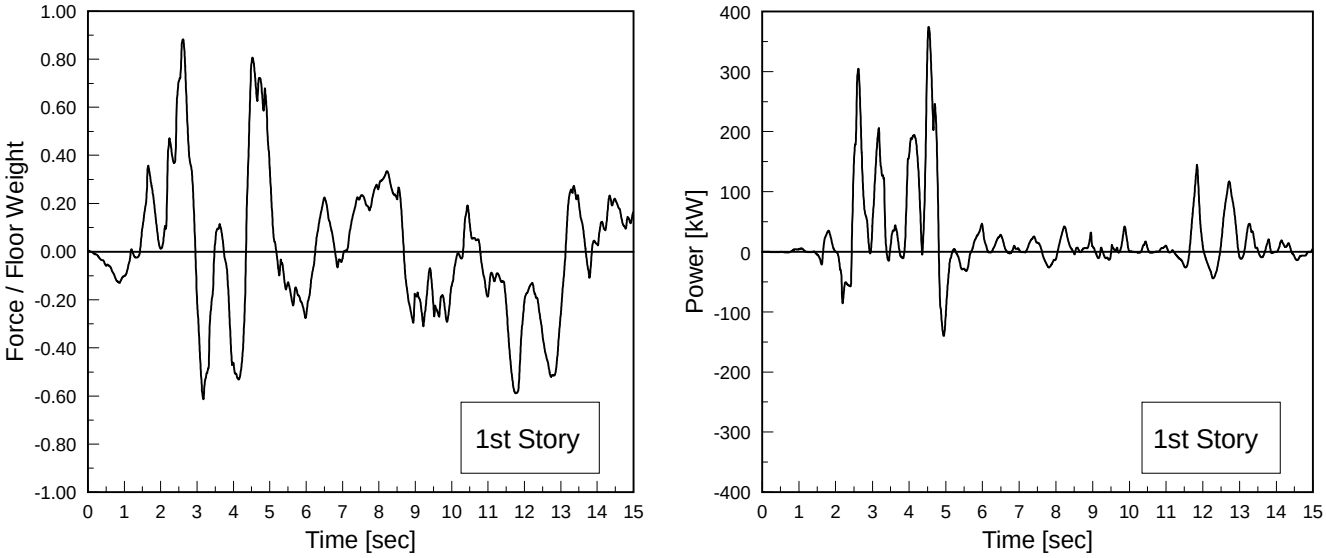

Figure 3.12: Control force and power for El Centro ground acceleration record in the event of failure of 2nd story actuation device (number of active devices: 2).

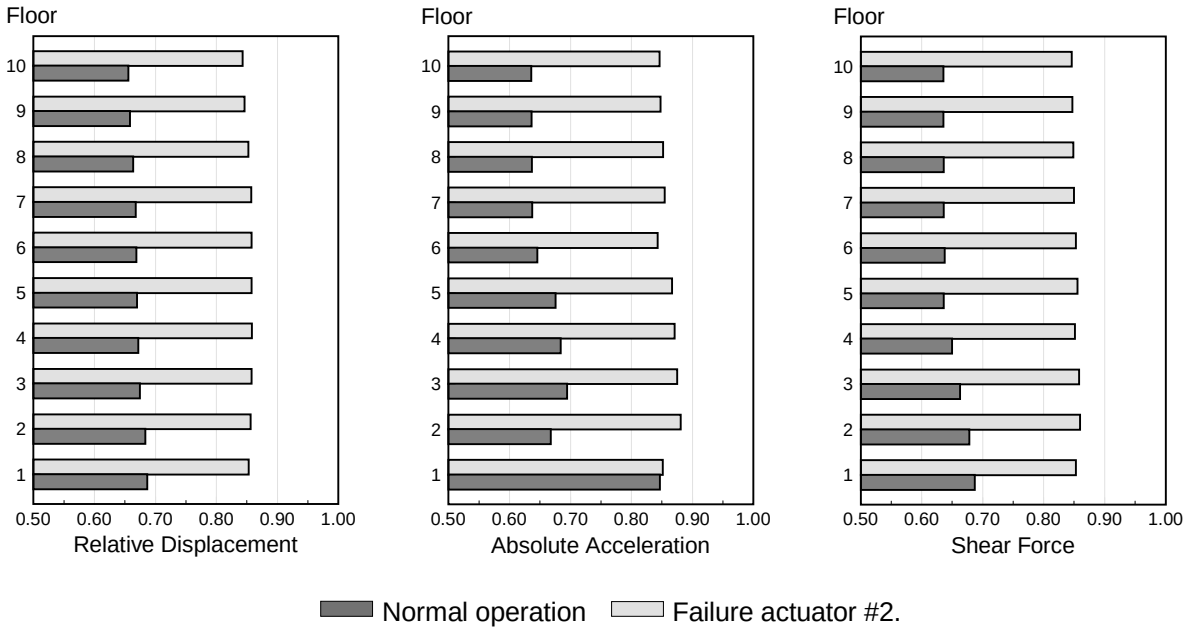

Figure 3.13: Comparison of response reduction factors during normal operation and the event of actuator failure (number of active devices: 2).

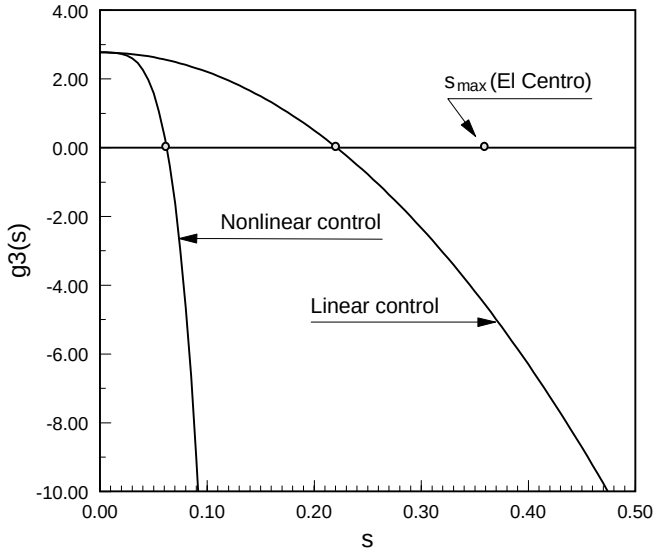

Figure 3.14: Comparison of the function $g_3(s)$ defining the region of attraction for the linear and nonlinear control cases.

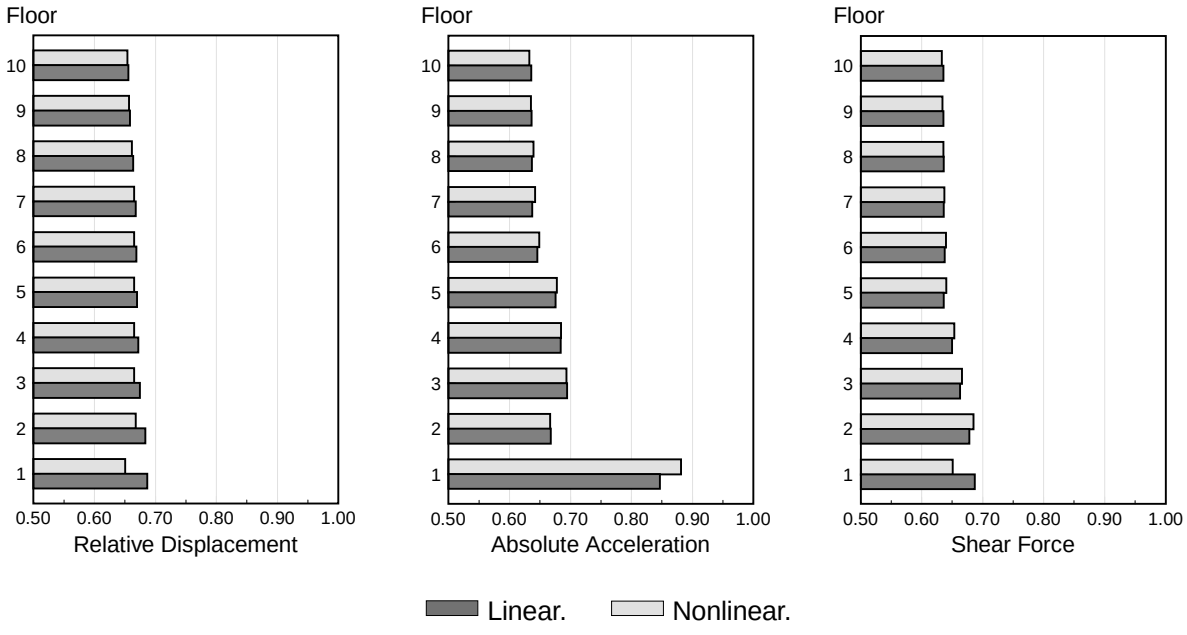

Figure 3.15: Comparison of response reduction factors using linear and nonlinear control for El Centro ground acceleration record (number of active devices: 2).

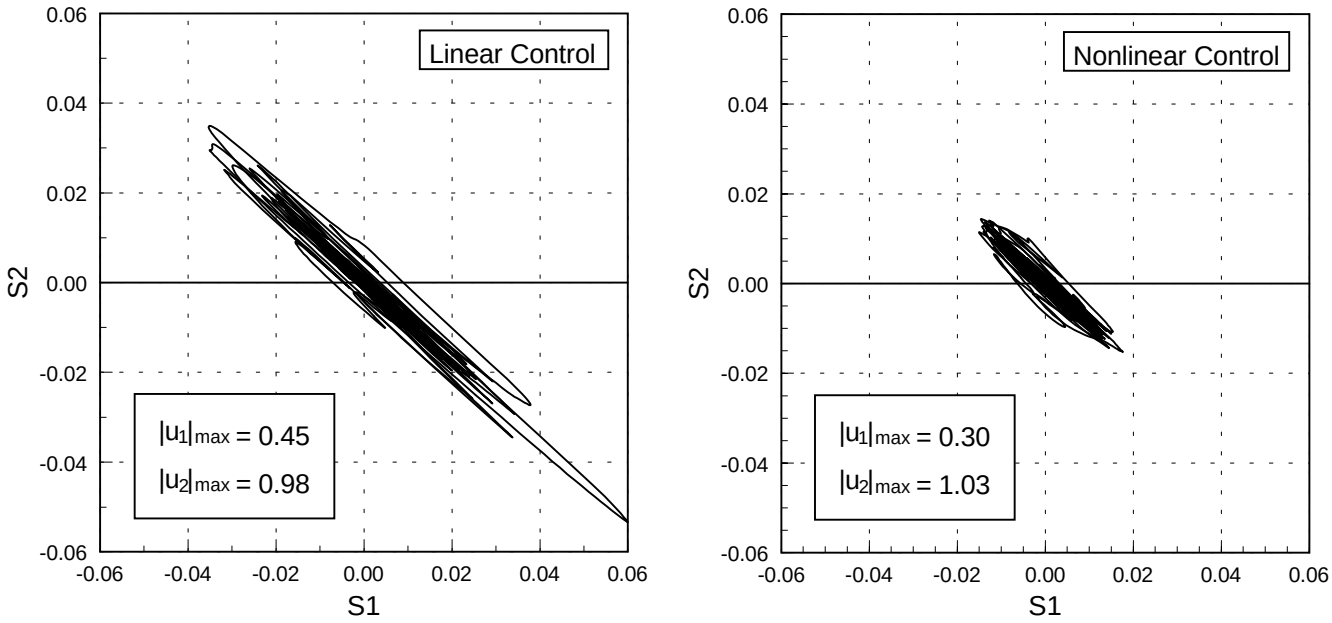

Figure 3.16: Comparison of sliding surface variables using linear and nonlinear control for El Centro ground acceleration record (number of active devices: 2).

Floor	El Centro			San Fernando		
	Response	Response Reduction Factor		Response	Response Reduction Factor	
	[cm]	$m_c = 1$	$m_c = 2$	[cm]	$m_c = 1$	$m_c = 2$
[1]	[2]	[3]	[4]	[5]	[6]	[7]
10	**16.25**	0.66	0.66	**8.92**	0.73	0.73
9	**15.87**	0.66	0.66	**8.68**	0.73	0.72
8	**15.14**	0.67	0.66	**8.21**	0.73	0.72
7	**14.13**	0.67	0.67	**7.53**	0.72	0.72
6	**12.90**	0.68	0.67	**6.69**	0.72	0.71
5	**11.36**	0.68	0.67	**5.71**	0.71	0.71
4	**9.54**	0.69	0.67	**4.70**	0.73	0.70
3	**7.45**	0.70	0.67	**3.68**	0.74	0.70
2	**5.13**	0.72	0.68	**2.56**	0.76	0.70
1	**2.63**	0.82	0.69	**1.32**	0.83	0.69

Floor	Loma Prieta			Hollywood		
	Response	Response Reduction Factor		Response	Response Reduction Factor	
	[cm]	$m_c = 1$	$m_c = 2$	[cm]	$m_c = 1$	$m_c = 2$
[8]	[9]	[10]	[11]	[12]	[13]	[14]
10	**6.17**	0.92	0.89	**15.94**	0.69	0.66
9	**5.96**	0.93	0.90	**15.58**	0.69	0.66
8	**5.74**	0.90	0.88	**14.87**	0.68	0.66
7	**5.53**	0.86	0.83	**13.81**	0.68	0.66
6	**5.23**	0.80	0.77	**12.44**	0.68	0.66
5	**4.78**	0.79	0.75	**10.78**	0.68	0.66
4	**4.14**	0.78	0.73	**8.88**	0.68	0.65
3	**3.29**	0.76	0.69	**6.78**	0.68	0.65
2	**2.27**	0.72	0.66	**4.56**	0.68	0.64
1	**1.15**	0.77	0.68	**2.28**	0.81	0.67

Table 3.1: Maximum relative displacements using active control (generalized sliding surface / full state feedback).

Floor	El Centro			San Fernando		
	Response	Response Reduction Factor		Response	Response Reduction Factor	
	[g]	$m_c = 1$	$m_c = 2$	[g]	$m_c = 1$	$m_c = 2$
[1]	[2]	[3]	[4]	[5]	[6]	[7]
10	**0.76**	0.65	0.64	**0.48**	0.81	0.78
9	**0.72**	0.65	0.64	**0.44**	0.79	0.78
8	**0.64**	0.64	0.64	**0.39**	0.76	0.75
7	**0.60**	0.62	0.64	**0.35**	0.74	0.72
6	**0.58**	0.64	0.65	**0.35**	0.73	0.71
5	**0.54**	0.68	0.68	**0.41**	0.71	0.66
4	**0.50**	0.69	0.68	**0.43**	0.69	0.63
3	**0.44**	0.71	0.69	**0.37**	0.70	0.62
2	**0.35**	0.74	0.67	**0.33**	0.78	0.67
1	**0.26**	0.78	0.85	**0.31**	0.73	0.80

Floor	Loma Prieta			Hollywood		
	Response	Response Reduction Factor		Response	Response Reduction Factor	
	[g]	$m_c = 1$	$m_c = 2$	[g]	$m_c = 1$	$m_c = 2$
[8]	[9]	[10]	[11]	[12]	[13]	[14]
10	**0.49**	0.74	0.71	**0.69**	0.69	0.67
9	**0.42**	0.78	0.73	**0.67**	0.69	0.67
8	**0.33**	0.85	0.79	**0.64**	0.69	0.67
7	**0.28**	0.81	0.80	**0.60**	0.67	0.66
6	**0.36**	0.79	0.73	**0.55**	0.66	0.66
5	**0.42**	0.77	0.69	**0.48**	0.64	0.65
4	**0.43**	0.75	0.67	**0.42**	0.66	0.65
3	**0.37**	0.73	0.64	**0.36**	0.68	0.65
2	**0.28**	0.76	0.65	**0.29**	0.67	0.58
1	**0.29**	0.81	0.80	**0.21**	0.64	0.74

Table 3.2: Maximum absolute accelerations using active control (generalized sliding surface / full state feedback).

	Active tendon or bracing system				
	$m_c = 1$		$m_c = 2$		
	Response reduction factor	Maximum control force [Floor weight]	Response reduction factor	Maximum control force 1st Story [Floor weight]	Maximum control force 2nd Story [Floor weight]
	[1]	[2]	[3]	[4]	[5]
El Centro	0.66	2.15	0.66	0.45	0.98
San Fernando	0.73	1.33	0.73	0.33	0.66
Loma Prieta	0.92	0.97	0.89	0.28	0.49
Hollywood	0.69	2.14	0.66	0.39	0.99

Table 3.3: Maximum control force requirements (generalized sliding surface / full state feedback).

Chapter 4

Output Feedback Formulation

4.1 Introduction

The developments in Chapters 2 and 3 were based on the assumption that all system states can be measured and are available for feedback. However, in practice it may not be feasible to measure all the states. Usually, information on only a limited number of states may be available. In such cases, one may choose to use an observer to estimate the other states. This can, however, introduce some undesirable time delays due to on-line computations. Observers can also degrade the performance of a control system significantly. To avoid these problems, here a general output feedback procedure is formulated so that different combinations of unavailable system states do not participate in the design of sliding surface or the controller. This necessitates the modification of the procedure to obtain the regular form. Special attention must also be paid in constructing the sliding surface and defining the sliding motion to eliminate the effect of unmeasured states. The special requirements imposed on the system states to eliminate the effect of unmeasured states lead to a constrained optimality criterion for the design of sliding surface. An active controller is formulated which utilizes only the upper bound information on the intensity of ground motion and also on the unmeasured states. A bi-state semi-active

controller based only on the measured variables is also developed. Several sets of numerical results are obtained to validate the formulation. The output feedback numerical results are compared with those obtained for the full-state feedback case to ascertain the effect of using limited information on the control. Since the numerical results presented in Chapter 3 demonstrated the advantages of introducing auxiliary systems or compensators in the definition of the sliding surface, the output feedback formulation will be developed based on this generalized sliding surface definition. This general formulation includes the static sliding surface as a particular case.

4.2 System Equations

The state equations for a linear building system with n_f degrees of freedom under seismic excitation, given by equation (2.23), are repeated here

$$\dot{\boldsymbol{\eta}} = \mathbf{A}\,\boldsymbol{\eta} + \mathbf{B}\,\mathbf{u} + \mathbf{e}\,\ddot{x}_g \tag{4.1}$$

in which the $n \times m_c$ matrix $\mathbf{B}$, defined before by equation (2.21), is given by

$$\mathbf{B} = \begin{bmatrix} \mathbf{0} \\ \bar{\mathbf{M}}^{-1}\,\mathbf{D} \end{bmatrix} \tag{4.2}$$

with $\text{rank}(\mathbf{B}) = m_c$. The m_c-dimensional control vector $\mathbf{u}$ contains the contributions of any active and semi-active devices installed in the structure.

It will be assumed that only a subset of the physical variables can be directly measured by an appropriate array of sensors distributed along the building. Let the n_a-dimensional vector $\boldsymbol{\eta}_\mathbf{a}$ indicate those state variables that can be directly measured. By using an $n \times n$ permutation matrix $\mathbf{S}$, it is possible to define

$$\bar{\boldsymbol{\eta}} = \begin{Bmatrix} \boldsymbol{\eta}_\mathbf{u} \\ \boldsymbol{\eta}_\mathbf{a} \end{Bmatrix} = \mathbf{S}\,\boldsymbol{\eta} \tag{4.3}$$

where the last n_a components of the vector $\bar{\boldsymbol{\eta}}$ correspond to the available variables $\boldsymbol{\eta}_\mathbf{a}$, and the remaining $n_u = n - n_a$ unmeasured or unavailable variables are collected in the vector $\boldsymbol{\eta}_\mathbf{u}$. Equation (4.3) can be written in partitioned form as follows:

$$\left\{ \begin{array}{c} \boldsymbol{\eta}_\mathbf{u} \\ \boldsymbol{\eta}_\mathbf{a} \end{array} \right\} = \left[\begin{array}{cc} \mathbf{S_{11}} & \mathbf{S_{12}} \\ \mathbf{S_{21}} & \mathbf{S_{22}} \end{array} \right] \left\{ \begin{array}{c} \mathbf{d} \\ \dot{\mathbf{d}} \end{array} \right\} \tag{4.4}$$

where now the partitions of the matrix $\mathbf{S}$ have appropriate dimensions and directly identify the participations of the coordinates $\mathbf{d}$ and $\dot{\mathbf{d}}$ in the definitions of $\boldsymbol{\eta}_\mathbf{a}$ and $\boldsymbol{\eta}_\mathbf{u}$. It is noted that in the full information case, in which all state variables are available for control purposes, the submatrices $\mathbf{S_{11}}$ and $\mathbf{S_{12}}$ vanish and the block $\left[\begin{array}{cc} \mathbf{S_{21}} & \mathbf{S_{22}} \end{array} \right]$ becomes an identity matrix.

In the following, a formulation is presented to eliminate the effect of the unmeasured states $\boldsymbol{\eta}_\mathbf{u}$ in the definition of the sliding surface and the design of an appropriate controller. In general, the same basic steps employed in the previous chapter are followed, with some modifications to account for the partial availability of state information. First, the regular form is obtained with the objective of uncoupling the sliding motion description from the corresponding control actions. Such uncoupled sliding motion equations will then be used to obtain the sliding constraints through some optimality criterion. At this stage it will be observed that, due to the imposition of an output feedback structure, the solution of this problem presents some special characteristics. Having defined the sliding surface, the controller design problem will be formulated. These development are described in the following sections.

4.3 Regular Form

The process of getting the regular form of the state equations is similar to the one presented in Chapter 3, except that it has to be modified to account for the unmeasured states. Let $\mathbf{V}$ be an $n_f \times m_c$ matrix whose columns constitute an orthonormal basis for $\mathcal{R}(\bar{\mathbf{M}}^{-1}\mathbf{D})$,

that is, the range (or column space) of the matrix $\bar{\mathbf{M}}^{-1}\mathbf{D}$. Also, let the columns of an $n_f \times (n_f - m_c)$ matrix $\mathbf{U_1}$ constitute an orthonormal basis for $\left\{\mathcal{R}(\bar{\mathbf{M}}^{-1}\mathbf{D})\right\}^{\perp}$, i.e., the orthogonal complement of $\mathcal{R}(\bar{\mathbf{M}}^{-1}\mathbf{D})$. These two matrices can be obtained by applying the Gram-Schmidt process to the columns of $\bar{\mathbf{M}}^{-1}\mathbf{D}$. Furthermore, let an $n_f \times m_c$ matrix $\mathbf{U_2}$ be defined as

$$\mathbf{U_2} = \mathbf{VQ} \tag{4.5}$$

where $\mathbf{Q}$ is an $m_c \times m_c$ unitary matrix obtained from the QR decomposition of the product $[\mathbf{S_{12}V}]^T$ as follows:

$$[\mathbf{S_{12}V}]^T = \mathbf{QR} \tag{4.6}$$

where $\mathbf{S_{12}}$, defined in (4.4), is the matrix identifying the unmeasured velocity coordinates. The matrix $\mathbf{R}$ has dimensions $m_c \times n_u$ with an upper triangular structure which depends on the rank of the product $[\mathbf{S_{12}V}]^T$. Therefore, the matrices $\mathbf{Q}$ and $\mathbf{R}$ depend upon the availability of information about the state variables. For the velocity feedback case, in which all velocities $\dot{\mathbf{d}}$ are available from direct measurements, $\mathbf{S_{12}}$ becomes a matrix with no rows and $\mathbf{R}$ becomes a matrix with no columns. Therefore, for this case, $\mathbf{Q}$ can be selected arbitrarily and so is assigned as the identity matrix, i.e. $\mathbf{Q} = \mathbf{I}_{m_c}$.

In terms of the matrices $\mathbf{U_1}$ and $\mathbf{U_2}$, the following $n \times n$ matrix $\mathbf{T}$ is defined as:

$$\mathbf{T} = \begin{bmatrix} \mathbf{I}_{n_f} & \mathbf{0} & \mathbf{0} \\ \mathbf{0} & \mathbf{U_1} & \mathbf{U_2} \end{bmatrix} \tag{4.7}$$

Note that by construction

$$\mathbf{U_1^T U_1} = \mathbf{I}_{n-m_c}, \;\; \mathbf{U_2^T U_2} = \mathbf{Q^T V^T VQ} = \mathbf{I}_{m_c}$$

$$\text{and} \;\; \mathbf{U_1^T U_2} = \mathbf{U_1^T VQ} = \mathbf{0}_{(n-m_c)\times m_c} \tag{4.8}$$

and therefore the matrix $\mathbf{T}$ is unitary, that is

$$\mathbf{T}^{-1} = \mathbf{T}^T \tag{4.9}$$

This matrix $\mathbf{T}$ is used to define a state transformation as follows:

$$\boldsymbol{\eta} = \mathbf{T}\,\mathbf{y} \tag{4.10}$$

After substituting (4.10) into the equations (4.1) and premultiplying by $\mathbf{T}^T$, the transformed state equations are given by

$$\dot{\mathbf{y}} = \bar{\mathbf{A}}\,\mathbf{y} + \bar{\mathbf{B}}\,\mathbf{u} + \bar{\mathbf{e}}\,\ddot{x}_g \tag{4.11}$$

where

$$\bar{\mathbf{A}} = \mathbf{T}^T\mathbf{A}\,\mathbf{T},\ \ \bar{\mathbf{B}} = \mathbf{T}^T\mathbf{B}\ \text{ and }\ \bar{\mathbf{e}} = \mathbf{T}^T\mathbf{e} \tag{4.12}$$

By considering the definition (4.7), it is easy to see that the transformed matrix $\bar{\mathbf{B}}$ takes the following form:

$$\bar{\mathbf{B}} = \begin{bmatrix} \mathbf{0} \\ \hat{\mathbf{B}} \end{bmatrix} \tag{4.13}$$

in which $\hat{\mathbf{B}}$ is a $m_c \times m_c$ nonsingular matrix given by

$$\hat{\mathbf{B}} = \mathbf{Q}^T\mathbf{V}^T\bar{\mathbf{M}}^{-1}\mathbf{D} \tag{4.14}$$

With this structure for the input matrix $\bar{\mathbf{B}}$, the first $n - m_c$ equations of (4.11) do not contain any control terms. Thus, for the case $m_r = 0$ this representation leads to a set of sliding motion equations without explicit control terms. As indicated in previous chapters, additional constraints will have to be imposed on the admissible control actions to obtain sliding motion equations uncoupled from the control terms for the case $m_r \geq 1$.

4.4 Sliding Surface

The generalized definition for the sliding surface previously considered in Chapter 3 will be adopted here. This equation is repeated here as,

$$\mathbf{s} = \tilde{\mathbf{y}}_1 + \tilde{\mathbf{y}}_2 = \mathbf{0} \tag{4.15}$$

As mentioned earlier, $\tilde{\mathbf{y}}_1$ and $\tilde{\mathbf{y}}_2$ are the outputs of two auxiliary systems defined by equations (3.13) with vectors $\mathbf{y_1}$ and $\mathbf{y_2}$ as the inputs. In Chapter 3, $\mathbf{y_1}$ and $\mathbf{y_2}$ depended on all the physical state variables of the model and the resulting definition of the sliding surface corresponded to a full state feedback formulation. In this chapter, a definition of the sliding surface is sought which depends only on the available information, represented by the variables $\boldsymbol{\eta}_\mathbf{a}$. That is, the contribution of the unmeasured states $\boldsymbol{\eta}_\mathbf{u}$ is to be eliminated from the equations describing the sliding surface. The conditions that allow such definition are investigated in the following.

Using equations (4.3) and (4.10), the state vector $\mathbf{y}$ can be expressed in terms of the re-arranged measured and unmeasured quantities as follows:

$$\mathbf{y} = [\mathbf{ST}]^T \bar{\boldsymbol{\eta}} \tag{4.16}$$

This equation can be written in a partitioned form as

$$\left\{ \begin{array}{c} \mathbf{y_1} \\ \mathbf{y_2} \end{array} \right\} = \left[\begin{array}{cc} \mathbf{P_{11}} & \mathbf{P_{12}} \\ \mathbf{P_{21}} & \mathbf{P_{22}} \end{array} \right] \left\{ \begin{array}{c} \boldsymbol{\eta}_\mathbf{u} \\ \boldsymbol{\eta}_\mathbf{a} \end{array} \right\} \tag{4.17}$$

where the blocks $\mathbf{P_{ij}}$ indicate submatrices of $[\mathbf{ST}]^T$ with the appropriate dimensions. On the other hand, considering (4.4) and (4.7), the product matrix $[\mathbf{ST}]^T$ in equation (4.16) can be written in partitioned form as follows:

$$[\mathbf{ST}]^T = \left[\begin{array}{cc} \mathbf{S_{11}^T} & \mathbf{S_{21}^T} \\ [\mathbf{S_{12}U_1}]^T & [\mathbf{S_{22}U_1}]^T \\ [\mathbf{S_{12}U_2}]^T & [\mathbf{S_{22}U_2}]^T \end{array} \right] \tag{4.18}$$

In view of the definition of $\mathbf{U_2}$ in (4.5), the $m_c \times n_u$ matrix $[\mathbf{S_{12}U_2}]^T$ can be written as

$$[\mathbf{S_{12}U_2}]^T = \mathbf{Q}^T [\mathbf{S_{12}V}]^T \tag{4.19}$$

which, taking into account (4.6), can also be written as follows:

$$[\mathbf{S_{12}U_2}]^T = \mathbf{R} \tag{4.20}$$

Considering the upper triangular structure of the matrix $\mathbf{R}$ and the fact that by construction the rank of this matrix is equal to the rank of $[\mathbf{S_{12}V}]$, it follows that if the following condition is satisfied:

$$\text{rank}(\mathbf{S_{12}V}) \leq m_r \tag{4.21}$$

then the $m_s \times n_u$ matrix $\mathbf{P_{21}}$ in (4.17) will have zero entries. Thus, from (4.17), the component $\mathbf{y_2}$ of the transformed state vector can be written as

$$\mathbf{y_2} = \mathbf{P_{22}}\boldsymbol{\eta}_\mathbf{a} \tag{4.22}$$

Therefore, if the condition (4.21) holds, the component $\mathbf{y_2}$ of the transformed state vector will not be affected by the unmeasured quantities, and the unmeasured variables will not participate in the definition of the second auxiliary system in (3.13). Note that this condition imposes a constraint on the design of the control system. Since the matrix $\mathbf{S_{12}}$ is associated with the velocity coordinates, it will be necessary to measure at least some velocities to limit the rank of the product $\mathbf{S_{12}V}$ as indicated in (4.21). It is noted that if all velocities $\dot{\mathbf{d}}$ are measured, then $\mathbf{S_{12}}$ becomes a null matrix and the condition (4.21) is automatically satisfied.

To eliminate the contribution of the unmeasured states from the vector $\mathbf{y_1}$, consider a matrix $\bar{\mathbf{M}}_\mathbf{1}$, defined such that its row space is contained in $\mathcal{N}(\mathbf{P}_{\mathbf{11}}^T)$, i.e., the left null space of the matrix $\mathbf{P_{11}}$. That is, a matrix $\bar{\mathbf{M}}_\mathbf{1}$ is constructed such that

$$\bar{\mathbf{M}}_\mathbf{1}\mathbf{P_{11}} = \mathbf{0} \tag{4.23}$$

The number of columns of $\bar{\mathbf{M}}_\mathbf{1}$ depends on the row dimension of $\mathbf{P_{11}}$ and it is equal to n_r. On the other hand, the number of rows of the matrix $\bar{\mathbf{M}}_\mathbf{1}$ is a design parameter and it will be determined later. If one assumes that the number of available states is at least equal to

the number of sliding constraints, i.e. $n_a \geq m_s$, then the maximum number of independent rows for such a matrix $\bar{\mathbf{M}}_\mathbf{1}$ is equal to $n_r - n_u$.

Premultiplying the first n_r rows of equation (4.17) by $\bar{\mathbf{M}}_\mathbf{1}$ and considering (4.23), one can write

$$\bar{\mathbf{M}}_\mathbf{1}\mathbf{y}_\mathbf{1} = \bar{\mathbf{M}}_\mathbf{1}\mathbf{P}_{\mathbf{12}}\boldsymbol{\eta}_\mathbf{a} \tag{4.24}$$

Hence, the unmeasured variables $\boldsymbol{\eta}_\mathbf{u}$ can be eliminated from the definition of the first auxiliary system in (3.13) if the matrices $\bar{\mathbf{G}}_\mathbf{1}$ and $\bar{\mathbf{C}}_{\mathbf{s1}}$ are defined as follows:

$$\bar{\mathbf{G}}_\mathbf{1} = \hat{\mathbf{G}}_\mathbf{1}\bar{\mathbf{M}}_\mathbf{1} \;\text{ and }\; \bar{\mathbf{C}}_{\mathbf{s1}} = \hat{\mathbf{C}}_{\mathbf{s1}}\bar{\mathbf{M}}_\mathbf{1} \tag{4.25}$$

where $\hat{\mathbf{G}}_\mathbf{1}$ and $\hat{\mathbf{C}}_{\mathbf{s1}}$ have appropriate dimensions.

To incorporate the constraints (4.25) in the sliding surface design procedure, an n_ζ-dimensional vector $\boldsymbol{\zeta}_\mathbf{1}$ is defined as follows:

$$\boldsymbol{\zeta}_\mathbf{1} = \bar{\mathbf{M}}_\mathbf{1}\mathbf{y}_\mathbf{1} \tag{4.26}$$

in which the $n_\zeta \times n_r$ matrix $\bar{\mathbf{M}}_\mathbf{1}$ is not only selected such that it satisfies the condition (4.23), but also such that its row space is contained in $\mathcal{R}(\mathbf{P}_{\mathbf{12}})$. In particular, the rows of $\bar{\mathbf{M}}_\mathbf{1}$ are chosen such that they constitute an orthonormal basis for the subspace $\mathcal{N}(\mathbf{P}_{\mathbf{11}}^T) \cap \mathcal{R}(\mathbf{P}_{\mathbf{12}})$. The dimension n_ζ of the vector $\boldsymbol{\zeta}_\mathbf{1}$ is therefore is equal to the dimension of this intersection subspace. For the numerical applications presented later, a basis for the intersection subspace is computed using the algorithm based on the singular value decomposition described by Golub and Van Loan [27].

Therefore, if the condition (4.21) is satisfied and the matrix $\bar{\mathbf{M}}_\mathbf{1}$ is constructed to satisfy the aforementioned requirements, the sliding surface can defined in terms of the measured variables according to (4.15), with the vectors $\tilde{\mathbf{y}}_\mathbf{1}$ and $\tilde{\mathbf{y}}_\mathbf{2}$ as the outputs of two

auxiliary dynamical systems with the following state-space realizations of order n_{s_1} and n_{s_2}, respectively:

$$\left\{ \begin{array}{l} \dot{\boldsymbol{\varphi}}_1 = \bar{\mathbf{F}}_1 \boldsymbol{\varphi}_1 + \hat{\mathbf{G}}_1 \boldsymbol{\zeta}_1 \\ \tilde{\mathbf{y}}_1 = \bar{\mathbf{H}}_1 \boldsymbol{\varphi}_1 + \hat{\mathbf{C}}_{\mathbf{s1}} \boldsymbol{\zeta}_1 \end{array} \right. \quad \text{and} \quad \left\{ \begin{array}{l} \dot{\boldsymbol{\varphi}}_2 = \bar{\mathbf{F}}_2 \boldsymbol{\varphi}_2 + \bar{\mathbf{G}}_2 \mathbf{y}_2 \\ \tilde{\mathbf{y}}_2 = \bar{\mathbf{H}}_2 \boldsymbol{\varphi}_2 + \bar{\mathbf{C}}_{\mathbf{s2}} \mathbf{y}_2 \end{array} \right. \tag{4.27}$$

in which it is assumed that the $m_s \times m_s$ matrix $\bar{\mathbf{C}}_{\mathbf{s2}}$ is nonsingular, i.e. $\text{rank}(\bar{\mathbf{C}}_{\mathbf{s2}}) = m_s$. The matrices $\bar{\mathbf{F}}_{\mathbf{1}}$, $\hat{\mathbf{G}}_{\mathbf{1}}$, $\bar{\mathbf{F}}_{\mathbf{2}}$ and $\bar{\mathbf{G}}_{\mathbf{2}}$ are preselected, whereas the matrices $\bar{\mathbf{H}}_{\mathbf{1}}$, $\hat{\mathbf{C}}_{\mathbf{s1}}$, $\bar{\mathbf{H}}_{\mathbf{2}}$ and $\bar{\mathbf{C}}_{\mathbf{s2}}$ will be determined based on some optimality condition imposed on the sliding motion.

The auxiliary systems (4.27) in conjunction with the state equations (4.11) can be used to define an augmented system of order $n_e = n_{s_1} + n_{s_2} + n$ as follows:

$$\dot{\mathbf{y}}_{\mathbf{e}} = \bar{\mathbf{A}}_{\mathbf{e}} \mathbf{y}_{\mathbf{e}} + \bar{\mathbf{B}}_{\mathbf{e}} \mathbf{u} + \bar{\mathbf{e}}_{\mathbf{e}} \ddot{x}_g \tag{4.28}$$

in which the matrix $\bar{\mathbf{B}}_{\mathbf{e}}$ and the vectors $\mathbf{y}_{\mathbf{e}}$ and $\bar{\mathbf{e}}_{\mathbf{e}}$ were defined in (3.15), and the matrix $\bar{\mathbf{A}}_{\mathbf{e}}$ is now given by

$$\bar{\mathbf{A}}_{\mathbf{e}} = \begin{bmatrix} \bar{\mathbf{F}}_{\mathbf{1}} & \mathbf{0} & \hat{\mathbf{G}}_{\mathbf{1}} \bar{\mathbf{M}}_{\mathbf{1}} & \mathbf{0} \\ \mathbf{0} & \bar{\mathbf{F}}_{\mathbf{2}} & \mathbf{0} & \bar{\mathbf{G}}_{\mathbf{2}} \\ \mathbf{0} & \mathbf{0} & \bar{\mathbf{A}}_{\mathbf{11}} & \bar{\mathbf{A}}_{\mathbf{12}} \\ \mathbf{0} & \mathbf{0} & \bar{\mathbf{A}}_{\mathbf{21}} & \bar{\mathbf{A}}_{\mathbf{22}} \end{bmatrix} \tag{4.29}$$

The sliding surface can also be written more compactly in terms of the augmented state vector $\mathbf{y}_{\mathbf{e}}$ as follows:

$$\mathbf{s} = \bar{\mathbf{C}}_{\mathbf{e}} \, \mathbf{y}_{\mathbf{e}} = \mathbf{0} \tag{4.30}$$

where the matrix $\bar{\mathbf{C}}_{\mathbf{e}}$ is defined as

$$\bar{\mathbf{C}}_{\mathbf{e}} = \begin{bmatrix} \bar{\mathbf{H}}_{\mathbf{1}} & \bar{\mathbf{H}}_{\mathbf{2}} & \hat{\mathbf{C}}_{\mathbf{s1}} \bar{\mathbf{M}}_{\mathbf{1}} & \bar{\mathbf{C}}_{\mathbf{s2}} \end{bmatrix} \tag{4.31}$$

4.5 Sliding Motion

The equations describing the behavior of the system constrained to the sliding surface and the stability characteristics of the resulting motion are discussed in the following.

4.5.1 Sliding Motion Description

Assuming that the system reaches the sliding surface at some time t_h (hitting time) and it is forced to stay there by some control action $\hat{\mathbf{u}}$, the corresponding sliding motion conditions are given by

$$\mathbf{s} = \bar{\mathbf{C}}_{\mathbf{e}}\,\mathbf{y}_{\mathbf{e}} = \mathbf{0} \tag{4.32}$$

$$\dot{\mathbf{s}}\,|_{\mathbf{u}=\hat{\mathbf{u}}} = \bar{\mathbf{C}}_{\mathbf{e}}\,\dot{\mathbf{y}}_{\mathbf{e}} = \mathbf{0} \tag{4.33}$$

It was shown in Chapter 3 that if the admissible control actions are forced to satisfy the following condition:

$$\bar{\mathbf{B}}_{\mathbf{1}}\,\hat{\mathbf{u}} = \mathbf{0} \tag{4.34}$$

then the control $\hat{\mathbf{u}}$ enforcing the sliding condition (4.33) can be uniquely determined as

$$\hat{\mathbf{u}} = -\left[\bar{\mathbf{C}}_{\mathbf{s}}\bar{\mathbf{B}}\right]^{\ddagger}\bar{\mathbf{C}}_{\mathbf{e}}\left\{\bar{\mathbf{A}}_{\mathbf{e}}\,\mathbf{y}_{\mathbf{e}} + \bar{\mathbf{e}}_{\mathbf{e}}\,\ddot{x}_g\right\} \tag{4.35}$$

in which the matrix $\left[\bar{\mathbf{C}}_{\mathbf{s}}\bar{\mathbf{B}}\right]^{\ddagger}$ was defined in (3.25). The behavior of the system subjected to the control $\hat{\mathbf{u}}$ is described by the following system of order $n_c = n_{s_1} + n_{s_2} + n_r$:

$$\dot{\mathbf{y}}_{\mathbf{c}} = \bar{\mathbf{A}}_{\mathbf{c}}\,\mathbf{y}_{\mathbf{c}} + \bar{\mathbf{B}}_{\mathbf{c}}\,\mathbf{y}_{\mathbf{2}} + \bar{\mathbf{e}}_{\mathbf{c}}\,\ddot{x}_g \tag{4.36}$$

in which the matrix $\bar{\mathbf{B}}_{\mathbf{c}}$ and the vectors $\mathbf{y}_{\mathbf{c}}$ and $\bar{\mathbf{e}}_{\mathbf{c}}$ were defined in (3.27). The matrix $\bar{\mathbf{A}}_{\mathbf{c}}$ is redefined as

$$\bar{\mathbf{A}}_{\mathbf{c}} = \begin{bmatrix} \bar{\mathbf{F}}_{\mathbf{1}} & \mathbf{0} & \hat{\mathbf{G}}_{\mathbf{1}}\bar{\mathbf{M}}_{\mathbf{1}} \\ \mathbf{0} & \bar{\mathbf{F}}_{\mathbf{2}} & \mathbf{0} \\ \mathbf{0} & \mathbf{0} & \bar{\mathbf{A}}_{\mathbf{11}} \end{bmatrix} \tag{4.37}$$

The equations describing the behavior of the system under sliding motion are obtained by incorporating the static constraint $\mathbf{s} = \mathbf{0}$ in (4.36). Considering (4.30) and (4.31), and taking into account that $\bar{\mathbf{C}}_{\mathbf{s2}}$ is nonsingular, the sliding surface constraint equation can be solved for $\mathbf{y}_{\mathbf{2}}$ as

$$\mathbf{y}_{\mathbf{2}} = \hat{\mathbf{K}}_{\mathbf{c}}\,\mathbf{y}_{\mathbf{c}} \tag{4.38}$$

in which the matrix $\hat{\mathbf{K}}_\mathbf{c}$ is given by

$$\hat{\mathbf{K}}_\mathbf{c} = -\bar{\mathbf{C}}_{\mathbf{s2}}^{-1} \left[\begin{array}{ccc} \bar{\mathbf{H}}_\mathbf{1} & \bar{\mathbf{H}}_\mathbf{2} & \hat{\mathbf{C}}_{\mathbf{s1}}\bar{\mathbf{M}}_\mathbf{1} \end{array} \right] \tag{4.39}$$

Substituting equation (4.38) into equation (4.36), the sliding motion behavior of the system is described by the following system of equations of order n_c:

$$\dot{\mathbf{y}}_\mathbf{c} = \left[\bar{\mathbf{A}}_\mathbf{c} + \bar{\mathbf{B}}_\mathbf{c}\hat{\mathbf{K}}_\mathbf{c} \right] \mathbf{y}_\mathbf{c} + \bar{\mathbf{e}}_\mathbf{e}\ddot{x}_g \tag{4.40}$$

Considering the definitions of $\bar{\mathbf{A}}_\mathbf{c}$, $\bar{\mathbf{B}}_\mathbf{c}$ and $\hat{\mathbf{K}}_\mathbf{c}$, it is easy to see that for a given matrix $\bar{\mathbf{M}}_\mathbf{1}$ the characteristics of the sliding motion depend on the two sets of matrices ($\bar{\mathbf{F}}_\mathbf{1}$,$\bar{\mathbf{G}}_\mathbf{1}$,$\bar{\mathbf{H}}_\mathbf{1}$,$\hat{\mathbf{C}}_{\mathbf{s1}}$) and ($\bar{\mathbf{F}}_\mathbf{2}$,$\bar{\mathbf{G}}_\mathbf{2}$,$\bar{\mathbf{H}}_\mathbf{2}$,$\bar{\mathbf{C}}_{\mathbf{s2}}$) defining the sliding surface.

4.5.2 Stability Characteristics of $\bar{\mathbf{A}}_\mathbf{c}$

A crucial requirement for selecting a sliding surface is that the corresponding sliding motion is stable. The matrix $\bar{\mathbf{A}}_\mathbf{c} + \bar{\mathbf{B}}_\mathbf{c}\hat{\mathbf{K}}_\mathbf{c}$ characterizes the dynamics of the system (4.36) under the closed-loop condition $\mathbf{y_2} = \hat{\mathbf{K}}_\mathbf{c}\,\mathbf{y_c}$. Therefore, the matrix $\hat{\mathbf{K}}_\mathbf{c}$ must assure that the eigenvalues of the matrix $\bar{\mathbf{A}}_\mathbf{c} + \bar{\mathbf{B}}_\mathbf{c}\hat{\mathbf{K}}_\mathbf{c}$ have negative real parts. Before proceeding with the details of the design of the sliding surface, it is interesting to investigate the stability characteristics of equations (4.36).

The characteristic equation corresponding to the matrix $\bar{\mathbf{A}}_\mathbf{c}$ is given by

$$\det(\bar{\mathbf{A}}_\mathbf{c} - \lambda\mathbf{I}_{n_c}) = 0 \tag{4.41}$$

which can be written as

$$\det(\bar{\mathbf{F}}_\mathbf{1} - \lambda\mathbf{I}_{n_{s1}}) \det(\bar{\mathbf{F}}_\mathbf{2} - \lambda\mathbf{I}_{n_{s2}}) \det(\bar{\mathbf{A}}_{\mathbf{11}} - \lambda\mathbf{I}_{n_r}) = 0 \tag{4.42}$$

Therefore, because of the triangular structure of $\bar{\mathbf{A}}_\mathbf{c}$, its eigenvalues are given by the union of the eigenvalues of the matrices $\bar{\mathbf{F}}_\mathbf{1}$, $\bar{\mathbf{F}}_\mathbf{2}$ and $\bar{\mathbf{A}}_{\mathbf{11}}$. The first two matrices are the design

parameters of the auxiliary systems. They must, therefore, be selected such that they have asymptotically stable eigenvalues. Hence, the stability of the matrix $\bar{\mathbf{A}}_\mathbf{c}$ is dictated by the eigenvalues of the partition $\bar{\mathbf{A}}_{\mathbf{11}}$. If the eigenvalues of this submatrix do not have strictly negative real parts, then the sliding surface design process must force the system (4.40) to become stable through an appropriate selection of $\hat{\mathbf{K}}_\mathbf{c}$.

To investigate the stability characteristics of $\bar{\mathbf{A}}_{\mathbf{11}}$, the lower right bock of the transformation matrix $\mathbf{T}$ defined in (4.7) is partitioned as follows:

$$\left[\begin{array}{cc} \mathbf{U_1} & \mathbf{U_2} \end{array} \right] = \left[\begin{array}{cc} \mathbf{V_1} & \mathbf{V_2} \end{array} \right] \tag{4.43}$$

where $\mathbf{V_1}$ and $\mathbf{V_2}$ have dimensions $n_f \times (n_f - m_s)$ and $n_f \times m_s$, respectively. Using this notation and considering the structure of the state matrix $\mathbf{A}$ given by equation (2.10), the matrix $\bar{\mathbf{A}}_{\mathbf{11}}$ can be written as

$$\bar{\mathbf{A}}_{\mathbf{11}} = \left[\begin{array}{cc} \mathbf{0} & \mathbf{V_1} \\ -\mathbf{V_1}^T\bar{\mathbf{M}}^{-\mathbf{1}}\bar{\mathbf{K}} & -\mathbf{V_1}^T\bar{\mathbf{M}}^{-\mathbf{1}}\bar{\mathbf{C}}\,\mathbf{V_1} \end{array} \right] \tag{4.44}$$

The characteristic equation corresponding to the matrix $\bar{\mathbf{A}}_{\mathbf{11}}$ is given by

$$\det(\bar{\mathbf{A}}_{\mathbf{11}} - \lambda\mathbf{I}_{n_r}) = \det\left(\left[\begin{array}{cc} -\lambda\mathbf{I}_{n_f} & \mathbf{V_1} \\ -\mathbf{V_1}^T\bar{\mathbf{M}}^{-\mathbf{1}}\bar{\mathbf{K}} & -\mathbf{V_1}^T\bar{\mathbf{M}}^{-\mathbf{1}}\bar{\mathbf{C}}\,\mathbf{V_1} - \lambda\mathbf{I}_{(n_f-m_s)} \end{array} \right] \right) = 0 \tag{4.45}$$

The matrix $\bar{\mathbf{A}}_{\mathbf{11}} - \lambda\mathbf{I}_{n_r}$ can be factored as

$$\left[\begin{array}{cc} -\lambda\mathbf{I}_{n_f} & \mathbf{V_1} \\ -\mathbf{V_1}^T\bar{\mathbf{M}}^{-\mathbf{1}}\bar{\mathbf{K}} & -\mathbf{V_1}^T\bar{\mathbf{M}}^{-\mathbf{1}}\bar{\mathbf{C}}\,\mathbf{V_1} - \lambda\mathbf{I}_{(n_f-m_s)} \end{array} \right] =$$

$$= \left[\begin{array}{cc} \mathbf{I}_{n_f} & \mathbf{0} \\ \frac{1}{\lambda}\mathbf{V_1}^T\bar{\mathbf{M}}^{-\mathbf{1}}\bar{\mathbf{K}} & \mathbf{I}_{(n_f-m_s)} \end{array} \right] \left[\begin{array}{cc} -\lambda\mathbf{I}_{n_f} & \mathbf{V_1} \\ \mathbf{0} & -\mathbf{V_1}^T\bar{\mathbf{M}}^{-\mathbf{1}}\left[\frac{1}{\lambda}\bar{\mathbf{K}} + \bar{\mathbf{C}}\right]\mathbf{V_1} - \lambda\mathbf{I}_{(n_f-m_s)} \end{array} \right] \tag{4.46}$$

Noting that the determinant of the first factor is equal to 1, the characteristic equation of the matrix $\bar{\mathbf{A}}_{\mathbf{11}}$ is given by

$$\det(\bar{\mathbf{A}}_{\mathbf{11}} - \lambda\mathbf{I}_{n_r}) = (-\lambda)^{n_f} \det\left(-\mathbf{V_1}^T\bar{\mathbf{M}}^{-\mathbf{1}}\left[\frac{1}{\lambda}\bar{\mathbf{K}} + \bar{\mathbf{C}}\right]\mathbf{V_1} - \lambda\mathbf{I}_{(n_f-m_s)} \right) = 0 \tag{4.47}$$

This can be finally written as

$$\det(\bar{\mathbf{A}}_{\mathbf{11}} - \lambda \mathbf{I}_{n_r}) = (-\lambda)^{m_s} \det(\lambda^2 \mathbf{I}_{(n_f - m_s)} + \lambda \mathbf{V}_\mathbf{1}^T \bar{\mathbf{M}}^{-\mathbf{1}} \bar{\mathbf{C}} \mathbf{V}_\mathbf{1} + \mathbf{V}_\mathbf{1}^T \bar{\mathbf{M}}^{-\mathbf{1}} \bar{\mathbf{K}} \mathbf{V}_\mathbf{1}) = 0 \quad (4.48)$$

Therefore the matrix $\bar{\mathbf{A}}_{\mathbf{11}}$, and consequently the matrix $\bar{\mathbf{A}}_\mathbf{c}$, has at least m_s zero eigenvalues. Hence, the system (4.36) is either marginally stable ($m_s = 1$) or unstable ($m_s > 1$). Therefore, it is necessary for the sliding surface design process to provide a stabilizing matrix $\hat{\mathbf{K}}_\mathbf{c}$.

4.6 Sliding Surface Design

The sliding surface design problem involves the determination of matrices $\bar{\mathbf{H}}_\mathbf{1}$,$\hat{\mathbf{C}}_{\mathbf{s1}}$,$\bar{\mathbf{H}}_\mathbf{2}$ and $\bar{\mathbf{C}}_{\mathbf{s2}}$. For this, a performance index is defined in terms of two sets of output variables related to the auxiliary systems (4.27). The minimization of this performance index under sliding conditions renders an optimal linear relation between the augmented states. This relation is adopted as the sliding surface.

The performance index to be minimized has the same form as in Chapter 3,

$$J = \int_{t_h}^{\infty} \left(\mathbf{q}_\mathbf{1}^T \mathbf{Q}_\mathbf{1} \mathbf{q}_\mathbf{1} + \mathbf{q}_\mathbf{2}^T \mathbf{Q}_\mathbf{2} \mathbf{q}_\mathbf{2} \right) dt \quad (4.49)$$

where $\mathbf{Q}_\mathbf{1}$ and $\mathbf{Q}_\mathbf{2}$ are $n_q \times n_q$ and $m_s \times m_s$ positive semi-definite and positive definite weighting matrices, respectively. The variables $\mathbf{q}_\mathbf{1}$ and $\mathbf{q}_\mathbf{2}$ are now defined by the following output equations:

$$\mathbf{q}_\mathbf{1} = \bar{\mathbf{D}}_\mathbf{1} \boldsymbol{\varphi}_\mathbf{1} + \hat{\mathbf{E}}_\mathbf{1} \boldsymbol{\zeta}_\mathbf{1} \quad \text{and} \quad \mathbf{q}_\mathbf{2} = \bar{\mathbf{D}}_\mathbf{2} \boldsymbol{\varphi}_\mathbf{2} + \bar{\mathbf{E}}_\mathbf{2} \mathbf{y}_\mathbf{2} \quad (4.50)$$

in which it is required that the $m_s \times m_s$ matrix $\bar{\mathbf{E}}_\mathbf{2}$ be nonsingular. The variables $\boldsymbol{\varphi}_\mathbf{1}$ and $\boldsymbol{\varphi}_\mathbf{2}$ are the state variables corresponding to the realizations indicated in equations (4.27). The lower limit of the integral in equation (4.49) is the hitting time t_h, and without any loss of generality is set $t_h = 0$.

Using $\mathbf{q_1}$ and $\mathbf{q_2}$ defined by (4.50) in the performance index definition (4.49), the cost function can be expressed as before in the following form:

$$J = \int_0^\infty \left(\mathbf{y_c}^T \, \bar{\mathbf{W}}_{\mathbf{11}} \, \mathbf{y_c} + 2\mathbf{y_c}^T \, \bar{\mathbf{W}}_{\mathbf{12}} \, \mathbf{y_2} + \mathbf{y_2}^T \, \bar{\mathbf{W}}_{\mathbf{22}} \, \mathbf{y_2} \right) dt \tag{4.51}$$

in which the vector $\mathbf{y_c}$ and the matrices $\bar{\mathbf{W}}_{\mathbf{12}}$ and $\bar{\mathbf{W}}_{\mathbf{22}}$ were defined earlier in equations (3.27) and (3.35), respectively, and where the matrix $\bar{\mathbf{W}}_{\mathbf{11}}$ is redefined as follows:

$$\bar{\mathbf{W}}_{\mathbf{11}} = \begin{bmatrix} \bar{\mathbf{D}}_1^T \mathbf{Q_1} \bar{\mathbf{D}}_1 & \mathbf{0} & \bar{\mathbf{D}}_1^T \mathbf{Q_1} \hat{\mathbf{E}}_1 \bar{\mathbf{M}}_1 \\ \mathbf{0} & \bar{\mathbf{D}}_2^T \mathbf{Q_2} \bar{\mathbf{D}}_2 & \mathbf{0} \\ \left[\bar{\mathbf{D}}_1^T \mathbf{Q_1} \hat{\mathbf{E}}_1 \bar{\mathbf{M}}_1 \right]^T & \mathbf{0} & \bar{\mathbf{M}}_1^T \hat{\mathbf{E}}_1^T \mathbf{Q_1} \hat{\mathbf{E}}_1 \bar{\mathbf{M}}_1 \end{bmatrix} \tag{4.52}$$

As seen in Chapter 3, the minimization of (4.51) subject to the corresponding unforced sliding equations

$$\dot{\mathbf{y}}_\mathbf{c} = \bar{\mathbf{A}}_\mathbf{c} \, \mathbf{y_c} + \bar{\mathbf{B}}_\mathbf{c} \, \mathbf{y_2} \tag{4.53}$$

will provide, in general, an optimal solution of the form $\mathbf{y_2} = \bar{\mathbf{K}}_\mathbf{c} \, \mathbf{y_c}$ where $\mathbf{y_2}$ depends not only on the states $\boldsymbol{\varphi_1}$ and $\boldsymbol{\varphi_2}$ but also, in general, on all the components of the vector $\mathbf{y_1}$.

To eliminate the effect of the unmeasured states from the definition of the sliding surface, it is desired to obtain an optimal solution, that depends only on $\boldsymbol{\varphi_1}$, $\boldsymbol{\varphi_2}$ and $\boldsymbol{\zeta_1}$, of the following form:

$$\mathbf{y_2} = \mathbf{N_c} \begin{Bmatrix} \boldsymbol{\varphi_1} \\ \boldsymbol{\varphi_2} \\ \boldsymbol{\zeta_1} \end{Bmatrix} \tag{4.54}$$

where $\mathbf{N_c}$, yet to be determined, is a matrix with appropriate dimensions. Equation (4.54) can be written as

$$\mathbf{y_2} = \mathbf{N_c} \mathbf{C_c} \, \mathbf{y_c} \tag{4.55}$$

in which

$$\mathbf{C_c} = \begin{bmatrix} \mathbf{I}_{n_{s1}} & \mathbf{0} & \mathbf{0} \\ \mathbf{0} & \mathbf{I}_{n_{s2}} & \mathbf{0} \\ \mathbf{0} & \mathbf{0} & \bar{\mathbf{M}}_\mathbf{1} \end{bmatrix} \tag{4.56}$$

The sliding surface design process can be cast now as an optimal output feedback problem, where the matrix $\mathbf{C_c}$ plays the role of an output matrix and $\mathbf{N_c}$ is the output feedback matrix to be determined by minimizing the cost function (4.51) subject to (4.53).

To eliminate the presence of cross terms in the cost function the standard procedure can be used by defining [2]

$$\mathbf{y_2} = \hat{\mathbf{y}}_\mathbf{2} - \bar{\mathbf{W}}_\mathbf{22}^{-1}\bar{\mathbf{W}}_\mathbf{12}^{T}\mathbf{y_c} \tag{4.57}$$

With this substitution, the cost function takes the form

$$J = \int_0^\infty \left(\mathbf{y_c}^T\, \hat{\mathbf{W}}_\mathbf{11}\ \mathbf{y_c} + \hat{\mathbf{y}}_\mathbf{2}^T\, \bar{\mathbf{W}}_\mathbf{22}\, \hat{\mathbf{y}}_\mathbf{2}\right) dt \tag{4.58}$$

where the matrix $\hat{\mathbf{W}}_\mathbf{11}$ has the same definition as in the full-state feedback case, given by (3.39), but with the matrix $\bar{\mathbf{W}}_\mathbf{11}$ redefined in (4.52). The corresponding state equations, under the condition $\dot{\mathbf{s}}\ |_{\mathbf{u}=\hat{\mathbf{u}}} = \mathbf{0}$ and neglecting the external excitation, are obtained by considering (4.53) and (4.57) as follows:

$$\dot{\mathbf{y}}_\mathbf{c} = \left[\bar{\mathbf{A}}_\mathbf{c}\ - \bar{\mathbf{B}}_\mathbf{c}\bar{\mathbf{W}}_\mathbf{22}^{-1}\bar{\mathbf{W}}_\mathbf{12}^{T}\right]\ \mathbf{y_c} + \bar{\mathbf{B}}_\mathbf{c}\hat{\mathbf{y}}_\mathbf{2} \tag{4.59}$$

The idea is to minimize (4.58) subject to (4.59) with a solution of the form

$$\hat{\mathbf{y}}_\mathbf{2} = \hat{\mathbf{N}}_\mathbf{c}\mathbf{C_c}\,\mathbf{y_c} \tag{4.60}$$

where $\hat{\mathbf{N}}_\mathbf{c}$ is a matrix still to be determined.

It is important to mention that in a general case, the transformation (4.57) cannot be employed to generate an output feedback solution for $\mathbf{y_2}$, because it will require complete knowledge of $\mathbf{y_c}$ which is not available. However, for this particular case, this term is given by

$$\bar{\mathbf{W}}_\mathbf{22}^{-1}\bar{\mathbf{W}}_\mathbf{12}^{T}\mathbf{y_c} = \bar{\mathbf{E}}_\mathbf{2}^{-1}\bar{\mathbf{D}}_\mathbf{2}\boldsymbol{\varphi}_\mathbf{2} \tag{4.61}$$

which depends entirely on accessible states $\boldsymbol{\varphi_2}$. This allows the use of (4.57) to determine the solution $\hat{\mathbf{N}}_\mathbf{c}$. In the sequel, necessary conditions for an optimal matrix $\hat{\mathbf{N}}_\mathbf{c}$ are derived following the derivation proposed by Mendel [56]. These necessary conditions are well-known in the context of optimal output feedback control theory. While the derivation here is not meant to be an original contribution of this work, it is presented here, in the context of sliding mode control, for the sake of completeness and continuity of the presentation.

The closed-loop dynamics under sliding motion can be obtained by substituting $\hat{\mathbf{y}}_\mathbf{2}$, with the structure indicated by equation (4.60), into equation (4.59) as follows:

$$\dot{\mathbf{y}}_\mathbf{c} = \left[\hat{\mathbf{A}}_\mathbf{c} + \bar{\mathbf{B}}_\mathbf{c}\hat{\mathbf{N}}_\mathbf{c}\mathbf{C}_\mathbf{c}\right] \mathbf{y}_\mathbf{c} \tag{4.62}$$

where

$$\hat{\mathbf{A}}_\mathbf{c} = \bar{\mathbf{A}}_\mathbf{c} - \bar{\mathbf{B}}_\mathbf{c}\bar{\mathbf{W}}_{\mathbf{22}}^{-1}\bar{\mathbf{W}}_{\mathbf{12}}^{T} \tag{4.63}$$

These equations describe the behavior of the system from the hitting time t_h, i.e., the instant in which the system initiates the sliding motion. The initial condition is given by the state of the system when hitting occurs, denoted by $\mathbf{y}_\mathbf{c}(t_h) = \mathbf{y}_\mathbf{h}$.

If the resulting closed-loop matrix $\hat{\mathbf{A}}_\mathbf{c} + \bar{\mathbf{B}}_\mathbf{c}\hat{\mathbf{N}}_\mathbf{c}\mathbf{C}_\mathbf{c}$ is asymptotically stable, then it can be shown that the performance index can be evaluated in terms of the initial conditions as follows [45]:

$$J = \mathbf{y}_\mathbf{h}^T \mathbf{M}_\mathbf{c}\mathbf{y}_\mathbf{h} \tag{4.64}$$

where the $n_c \times n_c$ matrix $\mathbf{M}_\mathbf{c}$ satisfies the following condition:

$$\mathcal{G}(\hat{\mathbf{N}}_\mathbf{c}, \mathbf{M}_\mathbf{c}) = \mathbf{0} \tag{4.65}$$

in which

$$\mathcal{G}(\hat{\mathbf{N}}_\mathbf{c}, \mathbf{M}_\mathbf{c}) = \left[\hat{\mathbf{A}}_\mathbf{c} + \bar{\mathbf{B}}_\mathbf{c}\hat{\mathbf{N}}_\mathbf{c}\mathbf{C}_\mathbf{c}\right]^T \mathbf{M}_\mathbf{c} + \mathbf{M}_\mathbf{c}\left[\hat{\mathbf{A}}_\mathbf{c} + \bar{\mathbf{B}}_\mathbf{c}\hat{\mathbf{N}}_\mathbf{c}\mathbf{C}_\mathbf{c}\right] + \hat{\mathbf{W}}_{\mathbf{11}} + \mathbf{C}_\mathbf{c}^T\hat{\mathbf{N}}_\mathbf{c}^T\bar{\mathbf{W}}_{\mathbf{22}}\hat{\mathbf{N}}_\mathbf{c}\mathbf{C}_\mathbf{c} \tag{4.66}$$

This allows the problem to be cast in the form of a static-constrained optimization problem. This optimization depends on the hitting conditions represented by the state $\mathbf{y_h}$. To remove the dependence on a specific hitting state, it is usually assumed that this initial state is a random variable with zero-mean and covariance matrix $\mathbf{Y_h} = E\left\{\mathbf{y_h}\mathbf{y_h}^T\right\}$. For an asymptotically stable closed-loop matrix $\hat{\mathbf{A}}_\mathbf{c} + \bar{\mathbf{B}}_\mathbf{c}\hat{\mathbf{N}}_\mathbf{c}\mathbf{C_c}$, the average performance index considering all possible hitting conditions can be redefined as follows:

$$\bar{J} = \mathrm{E}\left\{J\right\} = \mathrm{tr}\left\{\mathbf{M_c}\mathbf{Y_h}\right\} \tag{4.67}$$

To solve the problem of minimizing (4.67) subject to the constraints (4.65), the augmented cost $\bar{J}_a$ is defined as

$$\bar{J}_a(\hat{\mathbf{N}}_\mathbf{c}, \mathbf{M_c}, \mathbf{\Lambda_c}) = \mathrm{tr}\left\{\mathbf{M_c}\mathbf{Y_h} + \mathbf{\Lambda_c}\mathcal{G}(\hat{\mathbf{N}}_\mathbf{c}, \mathbf{M_c}\right\} \tag{4.68}$$

in which the constraint equations have been incorporated through a Lagrange multiplier matrix $\mathbf{\Lambda_c}$. The necessary conditions for an optimal solution are obtained by setting the partial derivatives of $\bar{J}_a$ with respect to $\hat{\mathbf{N}}_\mathbf{c}$, $\mathbf{M_c}$ and $\mathbf{\Lambda_c}$ equal to zero. This leads to the following system of coupled nonlinear matrix equations:

$$\bar{\mathbf{B}}_\mathbf{c}^T\mathbf{M_c}\mathbf{\Lambda_c}\mathbf{C}_\mathbf{c}^T + \bar{\mathbf{W}}_{\mathbf{22}}\hat{\mathbf{N}}_\mathbf{c}\mathbf{C_c}\mathbf{\Lambda_c}\mathbf{C}_\mathbf{c}^T = \mathbf{0} \tag{4.69}$$

$$\left[\hat{\mathbf{A}}_\mathbf{c} + \bar{\mathbf{B}}_\mathbf{c}\hat{\mathbf{N}}_\mathbf{c}\mathbf{C_c}\right]\mathbf{\Lambda_c} + \mathbf{\Lambda_c}\left[\hat{\mathbf{A}}_\mathbf{c} + \bar{\mathbf{B}}_\mathbf{c}\hat{\mathbf{N}}_\mathbf{c}\mathbf{C_c}\right]^T = -\mathbf{Y_h} \tag{4.70}$$

$$\left[\hat{\mathbf{A}}_\mathbf{c} + \bar{\mathbf{B}}_\mathbf{c}\hat{\mathbf{N}}_\mathbf{c}\mathbf{C_c}\right]^T\mathbf{M_c} + \mathbf{M_c}\left[\hat{\mathbf{A}}_\mathbf{c} + \bar{\mathbf{B}}_\mathbf{c}\hat{\mathbf{N}}_\mathbf{c}\mathbf{C_c}\right] + \mathbf{C}_\mathbf{c}^T\hat{\mathbf{N}}_\mathbf{c}^T\bar{\mathbf{W}}_{\mathbf{22}}\hat{\mathbf{N}}_\mathbf{c}\mathbf{C_c} = -\hat{\mathbf{W}}_{\mathbf{11}} \tag{4.71}$$

These conditions were first derived by Levine and Athans [48], but not in the context of sliding mode control. Several different algorithms have been proposed to solve these equations using gradient techniques, successive substitution procedures and homotopy methods. A modified successive substitution algorithm, used in the numerical examples presented in this chapter, is described later in Appendix A.

Once an optimal solution $\hat{\mathbf{N}}_\mathbf{c}$ is obtained and by selecting $\bar{\mathbf{C}}_{\mathbf{s2}} = \mathbf{I}_{m_s}$, the remaining matrices defining the sliding surface can be determined as follows:

$$\bar{\mathbf{H}}_\mathbf{1} = -\hat{\mathbf{N}}_\mathbf{1},\ \bar{\mathbf{H}}_\mathbf{2} = -\hat{\mathbf{N}}_\mathbf{2} - \bar{\mathbf{E}}_\mathbf{2}^{-1}\bar{\mathbf{D}}_\mathbf{2} \text{ and } \bar{\mathbf{C}}_{\mathbf{s1}} = -\hat{\mathbf{N}}_\mathbf{3} \tag{4.72}$$

where $\hat{\mathbf{N}}_\mathbf{1}$, $\hat{\mathbf{N}}_\mathbf{2}$ and $\hat{\mathbf{N}}_\mathbf{3}$ are appropriate partitions of the matrix $\hat{\mathbf{N}}_\mathbf{c}$ of the form

$$\hat{\mathbf{N}}_\mathbf{c} = \begin{bmatrix} \hat{\mathbf{N}}_\mathbf{1} & \hat{\mathbf{N}}_\mathbf{2} & \hat{\mathbf{N}}_\mathbf{3} \end{bmatrix} \tag{4.73}$$

Finally, the sliding surface can be written in terms of the available states in a form similar to (3.42)

$$\mathbf{s} = \mathbf{C}_\mathbf{e}\boldsymbol{\eta}_\mathbf{e} = \mathbf{0} \tag{4.74}$$

where the matrix $\mathbf{C}_\mathbf{e}$ and the vector $\boldsymbol{\eta}_\mathbf{e}$ are redefined as follows:

$$\mathbf{C}_\mathbf{e} = \begin{bmatrix} \bar{\mathbf{H}}_\mathbf{1} & \bar{\mathbf{H}}_\mathbf{2} & \hat{\mathbf{C}}_{\mathbf{s1}}\bar{\mathbf{M}}_\mathbf{1}\mathbf{P}_\mathbf{12} + \bar{\mathbf{C}}_{\mathbf{s2}}\mathbf{P}_\mathbf{22} \end{bmatrix} \text{ and } \boldsymbol{\eta}_\mathbf{e} = \begin{Bmatrix} \boldsymbol{\varphi}_\mathbf{1} \\ \boldsymbol{\varphi}_\mathbf{2} \\ \boldsymbol{\eta}_\mathbf{a} \end{Bmatrix} \tag{4.75}$$

Note that this definition for the sliding surface holds also for the full-state feedback case, i.e. $\boldsymbol{\eta}_\mathbf{a} = \boldsymbol{\eta}$. For this case, the matrix $\mathbf{S}$ in (4.16) becomes an identity matrix and the partitions $\mathbf{P}_\mathbf{11}$ and $\mathbf{P}_\mathbf{21}$ disappear from (4.17) because $n_u = 0$.

4.7 Controller Design

The controller must attract the system state toward the sliding surface $\mathbf{s} = \mathbf{0}$ and must keep it there. As before, a Lyapunov approach will be used for the design of the controller. Let V be a Lyapunov function candidate of the form

$$V = \frac{1}{2}\mathbf{s}^T\boldsymbol{\Pi}\,\mathbf{s} \tag{4.76}$$

in which $\boldsymbol{\Pi}$ denotes a $m_s \times m_s$ positive definite matrix to be defined later. The time derivative of this function is given by

$$\frac{d}{dt}(V) = \mathbf{s}^T\boldsymbol{\Pi}\,\dot{\mathbf{s}} \tag{4.77}$$

In order to assure the existence of sliding motion and to guarantee that any motion is going to be attracted to the sliding surface, the purpose of the controller is to force (4.77) to be a negative definite function. Considering the augmented state equations (4.28) and the definition of the sliding surface given by (4.30), it follows that

$$\dot{\mathbf{s}} = \bar{\mathbf{C}}_\mathbf{e} \left\{ \bar{\mathbf{A}}_\mathbf{e}\, \mathbf{y_e} + \bar{\mathbf{e}}_\mathbf{e}\, \ddot{x}_g \right\} + \bar{\mathbf{C}}_\mathbf{e} \bar{\mathbf{B}}_\mathbf{e} \mathbf{u} \tag{4.78}$$

Substituting (4.78) into (4.77), the time derivative of V takes the form

$$\frac{d}{dt}(V) = \mathbf{s}^T \mathbf{\Pi}\, \bar{\mathbf{C}}_\mathbf{e} \left\{ \bar{\mathbf{A}}_\mathbf{e}\, \mathbf{y_e} + \bar{\mathbf{e}}_\mathbf{e}\, \ddot{x}_g \right\} + \mathbf{s}^T \mathbf{\Pi}\, \bar{\mathbf{C}}_\mathbf{e} \bar{\mathbf{B}}_\mathbf{e} \mathbf{u} \tag{4.79}$$

In the following sections, the controllers for the active and semi-active cases are developed. The approach is quite similar to the one presented previously, except for the differences necessarily introduced by the unmeasured states.

4.7.1 Active Control

The case with only active control actions is characterized by $\mathbf{u} = \mathbf{u_a}$ and $\mathbf{u_{sa}} = \mathbf{0}$. Taking into account the definitions of the augmented state matrix and the sliding surface matrix, given by equations (4.29) and (4.31), respectively, and after some arrangement, equation (4.79) can be written as

$$\frac{d}{dt}(V) = \mathbf{s}^T \mathbf{\Pi} \left\{ \mathbf{K_1} \boldsymbol{\varphi_1} + \mathbf{K_2} \boldsymbol{\varphi_2} + \mathbf{Q_1} \mathbf{y_1} + \mathbf{Q_2} \mathbf{y_2} \right\} + \mathbf{s}^T \mathbf{\Pi}\, \bar{\mathbf{C}}_\mathbf{e}\, \bar{\mathbf{e}}_\mathbf{e}\, \ddot{x}_g + \mathbf{s}^T \mathbf{\Pi}\, \bar{\mathbf{C}}_\mathbf{e} \bar{\mathbf{B}}_\mathbf{e} \mathbf{u_a} \tag{4.80}$$

where $\mathbf{K_1}$ and $\mathbf{K_2}$ were defined in (3.56), and the matrices $\mathbf{Q_1}$ and $\mathbf{Q_2}$ are given, respectively, by

$$\mathbf{Q_1} = \bar{\mathbf{H}}_\mathbf{1} \bar{\mathbf{G}}_\mathbf{1} + \hat{\mathbf{C}}_{\mathbf{s1}} \bar{\mathbf{M}}_\mathbf{1} \bar{\mathbf{A}}_{\mathbf{11}} + \bar{\mathbf{C}}_{\mathbf{s2}} \bar{\mathbf{A}}_{\mathbf{21}} \text{ and}$$

$$\mathbf{Q_2} = \bar{\mathbf{H}}_\mathbf{1} \bar{\mathbf{G}}_\mathbf{2} + \hat{\mathbf{C}}_{\mathbf{s1}} \bar{\mathbf{M}}_\mathbf{1} \bar{\mathbf{A}}_{\mathbf{12}} + \bar{\mathbf{C}}_{\mathbf{s2}} \bar{\mathbf{A}}_{\mathbf{22}} \tag{4.81}$$

Considering the relation (4.17) between the transformed state variables $\mathbf{y}$ and the vectors $\boldsymbol{\eta}_{\mathbf{a}}$ and $\boldsymbol{\eta}_{\mathbf{u}}$, the time derivative of V can be expressed as

$$\frac{d}{dt}(V) = \mathbf{s}^T\boldsymbol{\Pi}\left\{\mathbf{K_1}\boldsymbol{\varphi}_{\mathbf{1}} + \mathbf{K_2}\boldsymbol{\varphi}_{\mathbf{2}} + \mathbf{Q_a}\boldsymbol{\eta}_{\mathbf{a}} + \mathbf{Q_u}\boldsymbol{\eta}_{\mathbf{u}}\right\} + \mathbf{s}^T\boldsymbol{\Pi}\,\bar{\mathbf{C}}_{\mathbf{e}}\bar{\mathbf{e}}_{\mathbf{e}}\,\ddot{x}_g + \mathbf{s}^T\boldsymbol{\Pi}\,\bar{\mathbf{C}}_{\mathbf{e}}\bar{\mathbf{B}}_{\mathbf{e}}\mathbf{u_a} \quad (4.82)$$

where the matrices $\mathbf{Q_a}$ and $\mathbf{Q_u}$ are given, respectively, by

$$\mathbf{Q_a} = \mathbf{Q_1}\mathbf{P_{12}} + \mathbf{Q_2}\mathbf{P_{22}} \quad \text{and} \quad \mathbf{Q_u} = \mathbf{Q_1}\mathbf{P_{11}} \quad (4.83)$$

The active controller $\mathbf{u_a}$ is designed according to the general structure indicated in equation (2.87), that is

$$\mathbf{u_a} = \mathbf{u_1} + \mathbf{u_2} \quad (4.84)$$

in which the component $\mathbf{u_1}$ is selected as

$$\mathbf{u_1} = -\left[\bar{\mathbf{C}}_{\mathbf{s}}\bar{\mathbf{B}}\right]^{\ddagger}\mathbf{K_s}\,\boldsymbol{\eta}_{\mathbf{e}} \quad (4.85)$$

where the matrix $\left[\bar{\mathbf{C}}_{\mathbf{s}}\bar{\mathbf{B}}\right]^{\ddagger}$ was defined previously in (3.25), whereas the matrix $\mathbf{C_e}$ and the vector $\boldsymbol{\eta}_{\mathbf{e}}$ are given by (4.75). The $m_s \times n_e$ matrix $\mathbf{K_s}$ is given by

$$\mathbf{K_s} = \left[\begin{array}{ccc} \mathbf{K_1} & \mathbf{K_2} & \mathbf{Q_a} \end{array}\right] \quad (4.86)$$

Substituting (4.84) and (4.85) into (4.82) and selecting $\boldsymbol{\Pi} = \mathbf{I}_{m_s}$, it follows that the time derivative of V now takes the form

$$\frac{d}{dt}(V) = \mathbf{s}^T\mathbf{Q_u}\boldsymbol{\eta}_{\mathbf{u}} + \mathbf{s}^T\bar{\mathbf{C}}_{\mathbf{e}}\bar{\mathbf{e}}_{\mathbf{e}}\,\ddot{x}_g + \mathbf{s}^T\bar{\mathbf{C}}_{\mathbf{e}}\bar{\mathbf{B}}_{\mathbf{e}}\mathbf{u_2} \quad (4.87)$$

The component $\mathbf{u_2}$ represents some linear or nonlinear form of state feedback and depending on the choice of $\mathbf{u_2}$ several possible designs can be formulated. A general expression for $\mathbf{u_2}$ is proposed in the following form:

$$\mathbf{u_2} = -\left[\bar{\mathbf{C}}_{\mathbf{s}}\bar{\mathbf{B}}\right]^{\ddagger}\left[\boldsymbol{\Delta} + \mathbf{E}\,\|\mathbf{s}\|_2^2\right]\mathbf{C_e}\boldsymbol{\eta}_{\mathbf{e}} \quad (4.88)$$

in which $\mathbf{\Delta} = \text{diag}(\delta_i)$ and $\mathbf{E} = \text{diag}(\varepsilon_i)$ are matrices of design parameters, with $\delta_i > 0$ and $\varepsilon_i \geq 0$ for $i = 1, 2, \ldots, m_s$. It is noted that the contribution of the matrix $\mathbf{E}$ in the definition of the controller is weighted by the square of the distance to the sliding surface. After substituting (4.88) into (4.87) and considering (3.65), it follows that the time derivative of V can be written as

$$\frac{d}{dt}(V) = \mathbf{s}^T \mathbf{C_e} \mathbf{e_e} \ddot{x}_g + \mathbf{s}^T \mathbf{Q_u} \boldsymbol{\eta}_\mathbf{u} + \mathbf{s}^T \left[\mathbf{\Delta} + \mathbf{E} \|\mathbf{s}\|_2^2 \right] \mathbf{s} \tag{4.89}$$

and this expression shows not only the external excitation $\ddot{x}_g$ but also the variables $\boldsymbol{\eta}_\mathbf{u}$ acting as unmeasured disturbances.

Considering the term involving the unmeasured variables in (4.89), one can write

$$\mathbf{s}^T \mathbf{Q_u} \boldsymbol{\eta}_\mathbf{u} \leq \mid \mathbf{s}^T \mathbf{Q_u} \boldsymbol{\eta}_\mathbf{u} \mid \tag{4.90}$$

By using the Cauchy-Schwartz inequality

$$\mid \mathbf{s}^T \mathbf{Q_u} \boldsymbol{\eta}_\mathbf{u} \mid \leq \|\mathbf{s}\|_2 \|\mathbf{Q_u} \boldsymbol{\eta}_\mathbf{u}\|_2 \tag{4.91}$$

and the fact that

$$\|\mathbf{s}\|_2 \|\mathbf{Q_u} \boldsymbol{\eta}_\mathbf{u}\|_2 \leq \frac{1}{2} \left(\|\mathbf{s}\|_2^2 + \|\mathbf{Q_u} \boldsymbol{\eta}_\mathbf{u}\|_2^2 \right) \tag{4.92}$$

it follows from (4.90), (4.91) and (4.92) that

$$\mathbf{s}^T \mathbf{Q_u} \boldsymbol{\eta}_\mathbf{u} \leq \frac{1}{2} \left(\|\mathbf{s}\|_2^2 + \|\mathbf{Q_u} \boldsymbol{\eta}_\mathbf{u}\|_2^2 \right) \tag{4.93}$$

Now, by compatibility of the matrix and vector 2-norms, one can write

$$\|\mathbf{Q_u} \boldsymbol{\eta}_\mathbf{u}\|_2 \leq \beta \|\boldsymbol{\eta}_\mathbf{u}\|_2 \tag{4.94}$$

in which the parameter β is defined as $\beta = \| \mathbf{Q_u} \|_2$. Let $\eta_{\max}$ be an upper bound for the infinity-norm of the vector $\boldsymbol{\eta}_\mathbf{u}$, that is,

$$\|\boldsymbol{\eta}_\mathbf{u}\|_\infty \leq \eta_{\max} \tag{4.95}$$

therefore, using standard vector norm properties, one can write

$$\|\boldsymbol{\eta}_{\mathbf{u}}\|_2 \leq \sqrt{n_u}\eta_{\max} \tag{4.96}$$

and considering (4.93), (4.94) and (4.96) that

$$\mathbf{s}^T\mathbf{Q}_{\mathbf{u}}\boldsymbol{\eta}_{\mathbf{u}} \leq \frac{1}{2}\left(\|\mathbf{s}\|_2^2 + n_u\eta_{\max}^2\beta^2\right) \tag{4.97}$$

The parameter $\eta_{\max}$ is a bounding value for each one of the unmeasured variables. For example, in the case of a 2D shear building with a velocity feedback scheme, the vector $\boldsymbol{\eta}_{\mathbf{u}}$ is composed of interstory drifts, and a practical limiting value can be easily assumed. A better estimate for $\eta_{\max}$ can also be obtained by a simple response spectrum analysis for a set of design ground response spectra for a given maximum ground acceleration level.

As it was done in Chapter 3, the first term on the right hand side of (3.67) can be shown to satisfy the following inequality:

$$\mathbf{s}^T\mathbf{C}_{\mathbf{e}}\mathbf{e}_{\mathbf{e}}\,\ddot{x}_g \leq \frac{\ddot{x}_g^{\max}}{2}\left(\|\mathbf{s}\|_2^2 + \alpha_e^2\right) \tag{4.98}$$

where $\alpha_e = \| \mathbf{C}_{\mathbf{e}}\mathbf{e}_{\mathbf{e}} \|_2$ and $\ddot{x}_g^{\max}$ is an estimate of the maximum ground acceleration level that can be expected at the site.

Finally, by considering (3.72), (4.97) and (4.98), it follows that the time derivative of the Lyapunov function satisfies the following inequality:

$$\frac{d}{dt}(V) \leq \frac{1}{2}\left(\ddot{x}_g^{\max} + n_u\eta_{\max}^2 - 2\left(\delta_{\min} + \varepsilon_{\min}\|\mathbf{s}\|_2^2\right)\right)\|\mathbf{s}\|_2^2 + \frac{1}{2}\left(\ddot{x}_g^{\max}\alpha_e^2 + n_u\eta_{\max}^2\beta^2\right) \tag{4.99}$$

Therefore, there exists a region in the $(s_1, s_2, \ldots s_{m_s})$ space defined by the following scalar function

$$g_4(s) = -\varepsilon_{\min}\, s^4 - a_4\, s^2 + b_4 \;< 0 \tag{4.100}$$

in which $s = \|\mathbf{s}\|_2$ and

$$a_4 = 2\delta_{\min} - \ddot{x}_g^{\max} - n_u\eta_{\max}^2 \tag{4.101}$$

$$b_4 = \ddot{x}_g^{\max} \alpha_e^2 + n_u \eta_{\max}^2 \beta^2 \tag{4.102}$$

for which the attraction to the sliding surface, represented by the point $\mathbf{s} = \mathbf{0}$, is guaranteed.

4.7.2 Semi-Active Control

The case with only semi-active control actions is characterized by $\mathbf{u} = \mathbf{u_{sa}}$ and $\mathbf{u_a} = \mathbf{0}$. As mentioned before, the control actions $\mathbf{u_{sa}}$ cannot achieve any arbitrary value, since they are constrained by the fact that the m_{sa} semi-active devices can only provide non-negative stiffness and damping values k_{v_i} and c_{v_i}. Therefore, although these control actions may succeed in bringing the system state towards the sliding surface, they may lack the control authority to enforce true sliding conditions.

The design of the semi-active controller will be done proceeding along the same lines as in Chapter 2, but using the system matrices corresponding to the augmented system. The objective of the semi-active control is to minimize the value of the function (4.76), in order to reduce any tendency of the system state moving away from $\mathbf{s} = \mathbf{0}$. The time derivative of V, given by equation (4.79), now takes the form

$$\frac{d}{dt}(V) = \mathbf{s}^T \mathbf{\Pi}\, \bar{\mathbf{C}}_\mathbf{e} \left\{ \bar{\mathbf{A}}_\mathbf{e}\, \mathbf{y_e} + \bar{\mathbf{e}}_\mathbf{e}\, \ddot{x}_g \right\} + \mathbf{s}^T \mathbf{\Pi}\, \bar{\mathbf{C}}_\mathbf{e} \bar{\mathbf{B}}_\mathbf{e} \mathbf{u_{sa}} \tag{4.103}$$

The control actions should be such that they make this rate of change as small as possible, preferably less than zero. Noting that

$$\bar{\mathbf{C}}_\mathbf{e} \bar{\mathbf{B}}_\mathbf{e} = \mathbf{C_e} \mathbf{B_e} \tag{4.104}$$

the last term of equation of the right hand side can be expressed as

$$\mathbf{s}^T \mathbf{C_e} \mathbf{B_e} \mathbf{u_{sa}} = \mathbf{v_e}^T \mathbf{u_{sa}} \tag{4.105}$$

where the m_{sa}-dimensional vector $\mathbf{v_e}$ is defined as

$$\mathbf{v_e} = \mathbf{B_e}^T \mathbf{C_e}^T \mathbf{C_e} \boldsymbol{\eta_e} \tag{4.106}$$

and considering the definition of the semi-active control actions as indicated in Chapter 2, it follows that

$$\mathbf{v_e}^T\mathbf{u_{sa}} = -\sum_{i=1}^{m_{sa}} v_{e_i}\left(\xi_i\, k_{v_i} + \dot{\xi}_i\, c_{v_i}\right) \tag{4.107}$$

Assuming that the each variable stiffness or damping device can operate according to a bi-state regime of the form ($k_{v_i}^{\min} = 0$ and $k_{v_i}^{\max}$) or ($c_{v_i}^{\min} = 0$ and $c_{v_i}^{\max}$), the semi-active control actions will be defined such that they enforce the condition

$$\mathbf{v_e}^T\mathbf{u_{sa}} \leq 0 \tag{4.108}$$

and therefore, considering equation (4.107), the corresponding controller is given by

$$k_{v_i}(\boldsymbol{\eta}_\mathbf{e}) = \frac{k_{v_i}^{\max}}{2}\left(1 + \text{sign}(v_{e_i}\xi_i)\right) \tag{4.109}$$

$$c_{v_i}(\boldsymbol{\eta}_\mathbf{e}) = \frac{c_{v_i}^{\max}}{2}\left(1 + \text{sign}(v_{e_i}\dot{\xi}_i)\right) \tag{4.110}$$

which is similar to the controller defined in equations (2.137) and (2.138).

4.8 Numerical Results

To investigate the performance of the proposed control strategies, numerical simulations are carried out using the 10-story shear building model considered before as the example problem. Both active and semi-active control strategies are evaluated considering various different output feedback structures. To demonstrate the generality of the formulation, the output feedback controllers presented here are designed based on a dynamic definition of the sliding surface. The effectiveness of the control system is evaluated using the same ground acceleration records considered before in Chapters 2 and 3.

4.8.1 Active Control

As for the example problem of Chapter 3, the active control system consists of two sets of active tendons or bracings installed in the first two stories (that is, $m_c = 2$). These devices can operate independently, acting between the foundation and the first two floor masses, as it was indicated before in Figure (3.1). Two separate cases, utilizing different output information and different auxiliary systems to define their sliding surfaces are considered to demonstrate the generality of the proposed formulation. In one of the two cases, the effect of control redundancy (i.e., $m_r > 0$) is also taken into account.

In the first case, it is assumed that the set of measured quantities consists of the interstory drifts corresponding to the first two stories where the actuation occurs, and the interstory drift velocities for the 1st, 2nd, 3rd, 6th, 8th and 10th stories ($n_a = 8$). The number of sliding constraints for this case is selected as $m_s = 2$; therefore, $m_r = 0$ and there is no control redundancy. The sliding surface is designed using the static relation $\mathbf{q_1} = \mathbf{y_1}$ in place of the first auxiliary system defined in equations (4.27) and (4.50). Therefore, $n_{s1} = 0$ and the matrices associated with this auxiliary system reduce to

$$\bar{\mathbf{F}}_\mathbf{1} = \mathbf{0},\ \bar{\mathbf{G}}_\mathbf{1} = \mathbf{0},\ \bar{\mathbf{D}}_\mathbf{1} = \mathbf{0} \text{ and } \bar{\mathbf{E}}_\mathbf{1} = \mathbf{I}_{n_r} \tag{4.111}$$

To specify the second auxiliary system, penalizing the participation of the variables $\mathbf{y_2}$ in the performance index, the following matrices were chosen:

$$\hat{\mathbf{F}}_\mathbf{2} = \begin{bmatrix} 0 & 1 \\ -\omega_o^2 & -2\zeta_o\omega_o \end{bmatrix},\ \hat{\mathbf{G}}_\mathbf{2} = \begin{bmatrix} 0 \\ 1 \end{bmatrix},\ \hat{\mathbf{D}}_\mathbf{2} = \begin{bmatrix} 0 & \beta_o \end{bmatrix} \text{ and } \hat{\mathbf{E}}_\mathbf{2} = [1] \tag{4.112}$$

in which ω_o, ζ_o and β_o are some design parameters which provide flexibility in adjusting the control efforts to achieve a desired response reduction. The second auxiliary system is then defined as follows:

$$\bar{\mathbf{F}}_\mathbf{2} = \begin{bmatrix} \hat{F}_2 & 0 \\ 0 & \hat{F}_2 \end{bmatrix},\ \bar{\mathbf{G}}_\mathbf{2} = \begin{bmatrix} \hat{G}_2 & 0 \\ 0 & \hat{G}_2 \end{bmatrix},\ \bar{\mathbf{D}}_\mathbf{2} = \begin{bmatrix} \hat{D}_2 & 0 \\ 0 & \hat{D}_2 \end{bmatrix} \text{ and } \bar{\mathbf{E}}_\mathbf{2} = \begin{bmatrix} \hat{E}_2 & 0 \\ 0 & \hat{E}_2 \end{bmatrix} \tag{4.113}$$

The sliding surface parameters for this case are chosen to be $\omega_o = 8.00$, $\zeta_o = 0.70$, $\beta_o = 158.50$. For this case, the weighting matrices in (4.49) are chosen as identity matrices of appropriate dimensions and the control parameter is selected as $\delta = 150.00$. As it is explained later, the values of these parameter were conveniently selected to facilitate the comparison between the different design alternatives.

Figure (4.1) shows the time histories of the controlled and uncontrolled top floor displacement and first story shear force, when the structure is subjected to San Fernando ground acceleration record. The figure shows the effectiveness of the control system in reducing not only the peak values for both responses (with response reduction factors of 0.73 and 0.65, respectively), but also the mean square values of both response quantities. The next figure shows the effect of the control system in acceleration-related responses. Figure (4.2*a*) shows the controlled and uncontrolled time histories of the top floor acceleration and Figure (4.2*b*) depicts the corresponding floor response spectra (3% damping). In this case, the maximum value of the floor acceleration corresponds to a response reduction factor of 0.79, which shows that, for this earthquake, the control system is less effective in reducing peak acceleration values than displacement-related responses. However, the comparison of the controlled and uncontrolled floor response spectra in Figure (4.2*b*) demonstrates an important attenuation of the spectral ordinates for a broad frequency range.

The time histories of the control forces corresponding to the previous results are shown in Figure (4.3). As it was also noticed in the discussion of the numerical results presented in Chapter 3, the design demands higher participation from the device acting at the second floor level. The maximum values of the control forces required at the first and second floor levels are, respectively, 0.39 and 0.84 times the respective floor weights. Figure (4.4) displays the time histories of the corresponding mechanical power. Again, the second story

device is associated with much higher rates of energy transfer than the first story actuator.

Next, the results corresponding to the second output feedback case are presented. In this case, it is assumed that the measured quantities are the 1st and 2nd interstory drifts and all drift velocities ($n_a = 12$). Therefore, more velocity measurements are available for this case than the first case. The number of sliding constraints is selected as $m_s = 1$, and the system is characterized by a nonzero control redundancy index ($m_r = 1$). Another difference in this case is that a compensator is now used only with the variables $\mathbf{y_1}$. That is, the second auxiliary system is a static one with $\mathbf{q_2} = \mathbf{y_2}$ (i.e., $n_{s_2} = 0$) and therefore

$$\bar{\mathbf{F}}_\mathbf{2} = \mathbf{0}, \bar{\mathbf{G}}_\mathbf{2} = \mathbf{0}, \bar{\mathbf{D}}_\mathbf{2} = \mathbf{0} \text{ and } \bar{\mathbf{E}}_\mathbf{2} = \mathbf{I}_{m_s} \tag{4.114}$$

To penalize the participation of the variables $\mathbf{y_1}$ in the performance index, the following matrices are used:

$$\bar{\mathbf{F}}_\mathbf{1} = \begin{bmatrix} 0 & 1 \\ -\omega_o^2 & -2\zeta_o\omega_o \end{bmatrix}, \ \hat{\mathbf{G}}_\mathbf{1} = \begin{bmatrix} 0 & 0 & 0 & 0 & 0 & 0 & 0 & 0 & 0 & 0 & 0 \\ 24 & 0 & 0 & 5 & 0 & 0 & 0 & 0 & 0 & 0 & 12 \end{bmatrix}, \tag{4.115}$$

$$\bar{\mathbf{D}}_\mathbf{1} = \begin{bmatrix} 0 & 1 \end{bmatrix} \text{ and } \hat{\mathbf{E}}_\mathbf{1} = \begin{bmatrix} 0 & 0 & 0 & 0 & 0 & 0 & 0 & 0 & 0 & 0 & 1 \end{bmatrix} \tag{4.116}$$

For this case, the weighting matrices in (4.49) are chosen as $\mathbf{Q_1} = q$, where q is a scalar parameter, and $\mathbf{Q_2} = \mathbf{I}_{m_s}$. For the numerical simulations presented in the following, the sliding surface parameters are selected as $\omega_o = 6.00$, $\zeta_o = 0.50$ and $q = 10.50$, whereas the control parameter is chosen as $\delta = 150.00$.

Figure (4.5) shows the time histories of the controlled and uncontrolled top floor displacement and first story shear force, when the structure is subjected to El Centro ground acceleration record. The controlled responses are characterized by reduction factors of 0.66 and 0.69, corresponding to the top displacement and the base shear, respectively. Figure (4.6) shows the controlled and uncontrolled cases for the top floor acceleration and the

corresponding floor response spectra (3% damping). The top floor acceleration responses are effectively reduced, with a peak acceleration reduction of 0.64.

Figure (4.7) displays the time histories of the control actions corresponding to this output feedback scheme. The participation of the first story actuation device is seen to be more important than in the previous case, and the corresponding maximum values of the control forces are 0.56 and 1.12 for the first and second story devices, respectively. The mechanical power time histories are shown in Figure (4.8) and it is observed now that the instantaneous values of power are mostly positive for both actuation locations.

To show that the proposed output feedback scheme with generalized sliding surface is a convenient design tool to achieve a proper sliding surface, the results in Figure (4.9) are reported. These results were obtained for El Centro ground excitation with the second design described before, that is, they correspond to output feedback with $\mathbf{y}_1$-weighting. The maximum responses are shown in Figure (4.9*a*) as a function of one of the parameters defining the design, namely the parameter q. The corresponding maximum control requirements are shown in Figure (4.9*b*). It is observed that the monotonic increase in reduction factors achieved in various responses, such as story shears and top floor displacement and acceleration, is consistent with the monotonic decrease in the control forces at the first and second floor levels. The first story shear reduction is not seen to follow the same behavior because this response quantity is directly affected by the control forces.

The variation of response reductions with the parameter q can be explained by investigating the corresponding changes of the closed-loop eigenvalues. Figure (4.10) shows the frequencies ω_1 and ω_2 as a function of the parameter q. These two natural frequencies correspond approximately to the first two fundamental frequencies of the uncontrolled system. The associated damping ratios ζ_1 and ζ_2 are also shown in the figure. It is observed

that the first modal damping ratio decreases continuously as a function of the design parameter q, and this induces smaller response reductions in the controlled system, with the corresponding decrease in the control requirements.

To investigate the failure of one of the components of the control system and its consequences on the resulting performance, the results in Figures (4.11) and (4.12) are presented. For the output feedback case with $\mathbf{y}_1$-weighting and for El Centro excitation, a failure will be simulated by assuming that the second story actuator goes off-line at the time $t = 2.12$ [sec]. As indicated in Chapter 3, this time corresponds to the occurrence of the maximum acceleration level of the ground motion. Figure (4.11) shows the resulting control requirements for the first story device. Both control force and mechanical power are significantly increased with respect to the normal operation values, with the force reaching a maximum value of almost 1.20 times the floor weight. The effect on the resulting performance of the controlled system is shown in Figure (4.12). This figure shows the response reduction factors for different floors and for different response quantities for both cases of normal operation and failure of second story actuator. It is observed that although the actuator failure degrades the resulting performance, the controlled system remains stable. In general all response quantities are still reduced, with the exception of those corresponding to the first story, which show the effect of increased control actions.

The next set of tables compare, for four different earthquake inputs, the output feedback results with the full state feedback results obtained in Chapter 3. For a meaningful comparison of the results obtained with different controllers, all design parameters were appropriately selected such that the maximum top floor displacement under El Centro excitation is reduced by a factor of 0.66. These appropriate parameter values were obtained by numerical simulations, tuning the design until the desired response reduction was obtained.

This was facilitated by the design flexibility provided by the generalized sliding surface. The first output feedback design described in this chapter ($\mathbf{y}_2$-weighting and $n_a = 8$) is denoted as case 'a', whereas the second design ($\mathbf{y}_1$-weighting and $n_a = 12$) is referred to as case 'b'.

Table (4.1) shows the relative displacement response reduction factors, whereas Table (4.2) shows the floor acceleration response reduction factors. Since the sliding surface and control parameters for each case were adjusted to obtain the same level of top floor displacement reduction, response reduction factors in Table (4.1) for different control schemes are in about the same range with some variations. The effectiveness of the control schemes in reducing their peak displacement response, however, can vary with the input. It is observed that both output feedback cases perform very well in reducing the top floor displacement, with some slightly better performance of the output feedback case 'b'. In the case of the first story displacement, which is proportional to the corresponding shear force, the output feedback case 'a' performs better with the exception of the Loma Prieta case. For the results presented in Table (4.1), all control schemes in general seem to be less effective for the Loma Prieta earthquake motion. On the other hand, it is observed that this ground motion is associated with the smallest uncontrolled displacement responses. Acceleration results in Table (4.2) are qualitatively similar to those in the previous table. For the acceleration responses, the output feedback case 'b' seems to be somewhat better than others, especially for the Loma Prieta input.

Table (4.3) compares the level of control effort required in the three different control schemes to achieve the response reduction depicted in Tables (4.1) and (4.2). It is seen from the values in the table that to achieve about the same level of reduction, the full state feedback requires the lowest amount of the control force. Also the output feedback

case 'a' where the number of available states is $n_a = 8$, in general, is seen to require larger maximum forces compared to the case 'b' where the number of available states is $n_a = 12$. Thus, the lesser the number of states available for feedback, the larger the level of control effort required to achieve a given level of reduction in the response. The sliding mode control formulation developed here confirms this naturally expected conclusion.

4.8.2 Semi-Active Control

The output feedback formulation presented in the previous chapter is used to investigate the effectiveness of semi-active stiffness control in this section. The structure is provided with semi-active devices in the form of switchable bracings installed in the first four stories, and therefore, $m_{sa} = 4$. The first two stories have devices with a parameters $\{0.3k_{ref}, 0.25c_{ref}\}$. The third and fourth stories have devices with parameters equal to $\{0.2k_{ref}, 0.15c_{ref}\}$ and $\{0.1k_{ref}, 0.1c_{ref}\}$, respectively. The reference value k_{ref} is equal to the story stiffness, that is $k_{ref} = 654.98$ [MN/m], and the damping reference value c_{ref} is given by $c_{ref} = 6.15$ [MN.sec/m]. It is assumed that the devices are able to operate in a bi-state stiffness regime with $k_{v_i}^{\min} = 0$, according to (4.109).

It is assumed that the set of measured quantities consists of the interstory drifts corresponding to the first four stories where the actuation occurs, and the interstory drift velocities for the first five stories ($n_a = 9$). The number of sliding constraints for this case is selected as $m_s = 1$. The sliding surface is designed using the static relation $\mathbf{q_1} = \mathbf{y_1}$ in place of the first auxiliary system defined in equations (4.27) and (4.50). Therefore, $n_{s1} = 0$ and the matrices associated with this auxiliary system are indicated in (4.111). The second auxiliary system, penalizing the participation of the variables $\mathbf{y_2}$ in the performance index,

is defined as follows:

$$\bar{\mathbf{F}}_{\mathbf{2}} = \hat{\mathbf{F}}_{\mathbf{2}},\ \bar{\mathbf{G}}_{\mathbf{2}} = \hat{\mathbf{G}}_{\mathbf{2}},\ \bar{\mathbf{D}}_{\mathbf{2}} = \hat{\mathbf{D}}_{\mathbf{2}} \text{ and } \bar{\mathbf{E}}_{\mathbf{2}} = \hat{\mathbf{E}}_{\mathbf{2}} \tag{4.117}$$

where the matrices $\hat{\mathbf{F}}_{\mathbf{2}}$, $\hat{\mathbf{G}}_{\mathbf{2}}$, $\hat{\mathbf{D}}_{\mathbf{2}}$ and $\hat{\mathbf{E}}_{\mathbf{2}}$ were defined before in (4.112). The sliding surface parameters are selected as $\omega_o = 6.50$, $\zeta_o = 0.04$, $\beta_o = 85.00$ and the weighting matrices in (4.49) are chosen as identity matrices of appropriate dimensions.

Figure (4.13) shows the time histories of the controlled and uncontrolled top floor displacement and first story shear force, when the structure is subjected to San Fernando ground acceleration record. The controlled responses are characterized by reduction factors of 0.91 and 0.76, corresponding to the top displacement and the base shear, respectively. It is observed that although the reduction in the peak value of the top floor response is not very significative, the mean square values of both top displacement and base shear are effectively reduced. Figure (4.14) shows the controlled and uncontrolled cases for the top floor acceleration and the corresponding floor response spectra (3% damping). The peak value of the top floor acceleration shows an increase of 15% with respect to the uncontrolled maximum value, but the spectral ordinates are effectively reduced in the frequencies corresponding to the first two natural frequencies of the uncontrolled system (approximately 1 and 3 [Hz]). Figure (4.15) shows the controlled and uncontrolled floor response spectra corresponding to the fourth and sixth floors. It can be observed also in this case a reduction of the spectral ordinates corresponding to the first two fundamental modes.

The time histories of the control actions corresponding to the devices installed in the second and fourth stories are shown in Figures (4.16a) and (4.17a), respectively. For each device, the semi-active control forces reach maximum values, normalized with respect to the floor weight, of 0.54 and 0.20, respectively. In Figures (4.16b) and (4.17b) the control forces are represented plotted against the corresponding displacement. The dissipative nature of

the semi-active control action can be appreciated from the triangular shaped loops shown in these figures. It is observed also that the control actions are characterized by some periods of high frequency activity, in which the stiffness of the semi-active devices switches very rapidly between $k_{v_i}^{\min} = 0$ and $k_{v_i}^{\max}$. This effect can also be observed in Figure (4.18), which shows the time histories of the variable stiffness parameters k_{v_2} and k_{v_4}, corresponding to the devices in the second and fourth stories.

In a practical situation, the stiffness of the semi-active device can not change instantaneously. Therefore, it is interesting to investigate the effect of a semi-active device with dynamic characteristics. Here, a very simple model is introduced to model the behavior of the device. It is assumed that under the bi-state control command ($k_{v_i} = k_{v_i}^{\min}$ or $k_{v_i} = k_{v_i}^{\max}$), the resulting stiffness, denoted as $\bar{k}_{v_i}$, is obtained as the output of the following system:

$$\left\{ \begin{array}{c} \dot{\vartheta}_1 \\ \dot{\vartheta}_2 \end{array} \right\} = \left[\begin{array}{cc} -84.85 & 60 \\ 60 & 0 \end{array} \right] \left\{ \begin{array}{c} \vartheta_1 \\ \vartheta_2 \end{array} \right\} + \left[\begin{array}{c} 60 \\ 0 \end{array} \right] k_{v_i} \tag{4.118}$$

$$\bar{k}_{v_i} = \left[\begin{array}{cc} 0 & 1 \end{array} \right] \left\{ \begin{array}{c} \vartheta_1 \\ \vartheta_2 \end{array} \right\} \quad \text{with} \quad k_{v_i}^{\min} \leq \bar{k}_{v_i} \leq k_{v_i}^{\max} \tag{4.119}$$

which corresponds to a low-pass filter with cut-off frequency $\omega_n = 60$ [rad/sec]. The cut-off frequency was arbitrarily selected with a value between the $5th$ and $6th$ natural frequencies of the building model.

Figure (4.19) shows the time histories of the controlled and uncontrolled top floor displacement and first story shear force, when the structure is subjected to El Centro ground acceleration record. The response reduction factors are 0.87 and 0.65 for the top displacement and the first story shear, respectively. The corresponding control actions are shown in Figures (4.20) and (4.21). These figures show the time histories and the force-displacement relations for the devices installed in the second and fourth stories. By comparing these results with those in Figures (4.16) and (4.17), the effect of the additional dynamics on the

shape of the force-displacement loops is evident. The time histories of the corresponding stiffness parameters $\bar{k}_{v_2}$ and $\bar{k}_{v_4}$ are shown in Figure (4.22). It is observed that the stiffness values do not switch infinitely fast between the two limiting values as in the previous case, and a finite time is required now to change from $k_{v_i}^{\min} = 0$ to $k_{v_i}^{\max}$ or vice versa.

The next set of tables compare, for different ground excitations, the semi-active output feedback results with the corresponding full state feedback and passive control results obtained in Chapter 2. For a meaningful comparison, the parameters defining the sliding surface in the output feedback case were selected such that the maximum top floor displacement under El Centro excitation is reduced by a factor of 0.85, which is the same reduction obtained in the full state feedback case with a static sliding surface. The output feedback semi-active controller with ideal switching characteristics is denoted as case 'a', whereas the same controller design with added device dynamics as defined in (4.118) and (4.119) is referred to as case 'b'.

Table (4.4) shows the relative displacement response reduction factors for four different earthquakes. The results in columns (3), (8), (14) and (19) correspond to the passive control case, in which the stiffness parameters of the added devices are set equal to their maximum values. This stiffening of the system, in general, will induce a reduction of displacement responses, but this effect is observed to depend on the frequency characteristics of the ground motion. The results in the next set of columns for each earthquake correspond to the full state feedback case with static sliding surface. This design was described in Chapter 2, and it is observed that the semi-active controller induces additional response reductions for most of the cases. The results in columns (5), (10), (16) and (21) correspond to case 'a', characterized by partial measurements ($n_a = 9$) and generalized sliding surface as described in this chapter, and the assumption that the semi-active devices can switch

infinitely fast between the limiting values of stiffness. Finally, the results in the last column for each earthquake correspond to the output feedback case 'b', with consideration of the device dynamics. The simulation results indicate that the response reductions for the output feedback cases are similar to those for the full state feedback controller. Table (4.5) shows the results for acceleration responses. It is observed that the stiffening of the structure increases the accelerations in most of the cases, and the semi-active control may or may not counteract these response increases, depending on the seismic input. To obtain significative acceleration reductions, the amount of additional damping introduced by the semi-active devices should be increased.

4.9 Conclusions

The practical situation of partial state information is incorporated in the generalized sliding surface formulation developed in the previous chapter. The transformation to regular form is modified to incorporate the constraint represented by the presence of unmeasured variables in the model. In this case, the sliding surface design problem involves the solution of a system of nonlinear matrix equations. An efficient algorithm is proposed for this purpose; it is discussed in detail in Appendix A.

Numerical results were presented to show the applicability of the formulation and effectiveness of active control in reducing the deformation and acceleration responses. The structure considered was the same building model used in previous chapters. Two independent actuators are used to apply control force through tendons at the first and second floor level. With this actuation arrangements and the level of response reduction achieved, the control force requirements are reasonable. The effectiveness of the output feedback control scheme is demonstrated. There is only slight degradation in the performance of the control

because of unavailability of all the system states, but system stability is maintained. Additionally, the robustness of the control system is examined in the event of actuator failure. Numerical simulations are also presented to examine the performance of semi-active controllers based on partial information. The response reduction produced by bi-state stiffness switching is investigated. To consider a practical situation in which the stiffness values can not change infinitely fast, a simplified model is introduced to account for the semi-active device dynamics. The results show that the performance of the resulting control system is comparable to that of the full state feedback case with ideal switching.

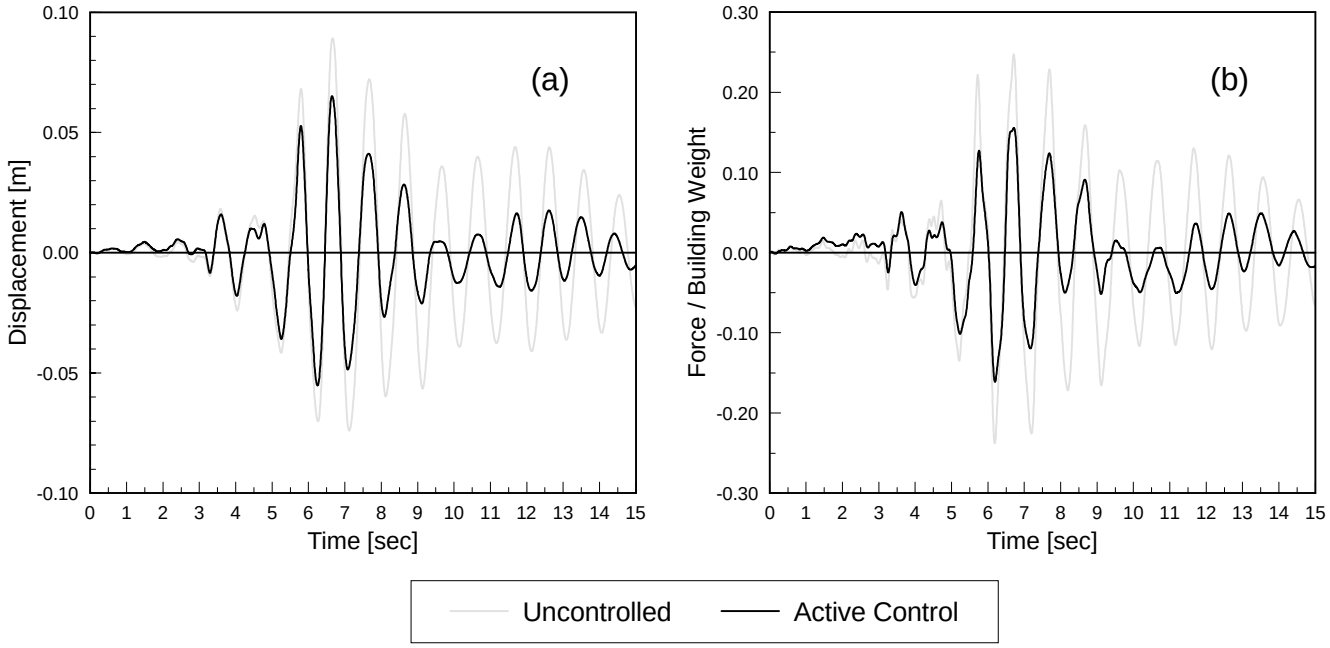

Figure 4.1: Comparison of uncontrolled and controlled top floor displacement and first story shear force for San Fernando ground acceleration record (y2 weighting - number of measurements: 8).

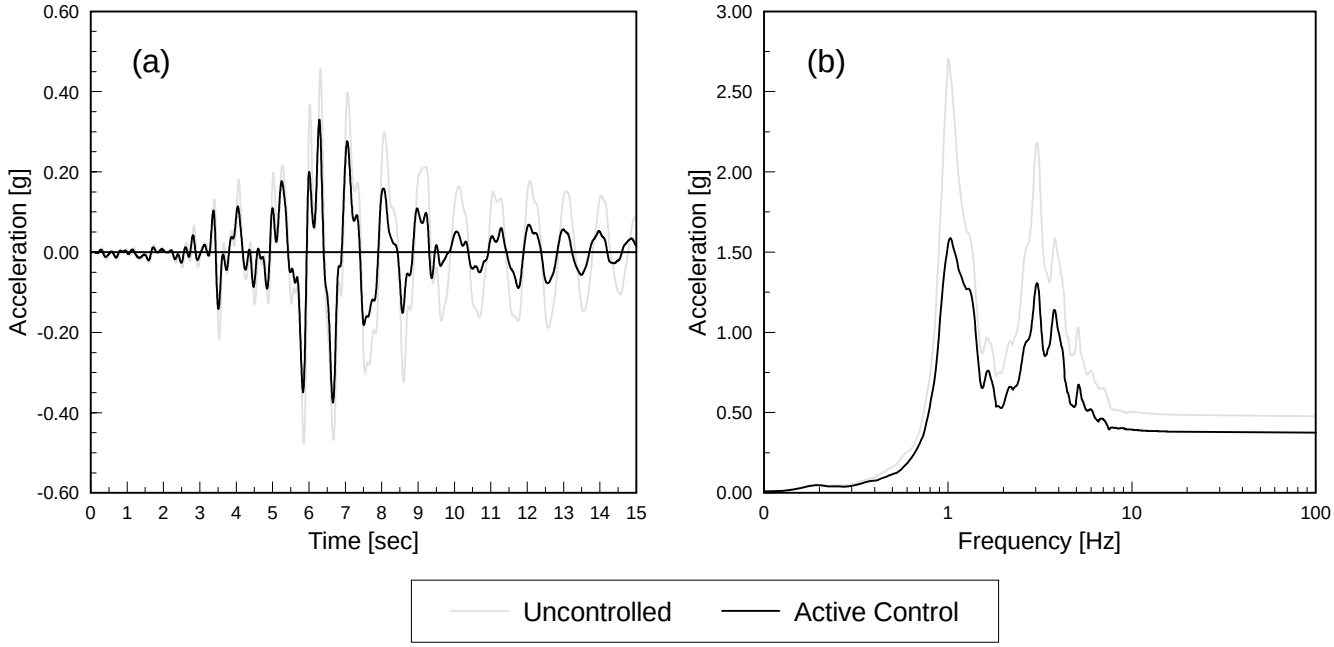

Figure 4.2: Comparison of uncontrolled and controlled top floor acceleration and top floor response spectra for San Fernando ground acceleration record (y2 weighting - number of measurements: 8).

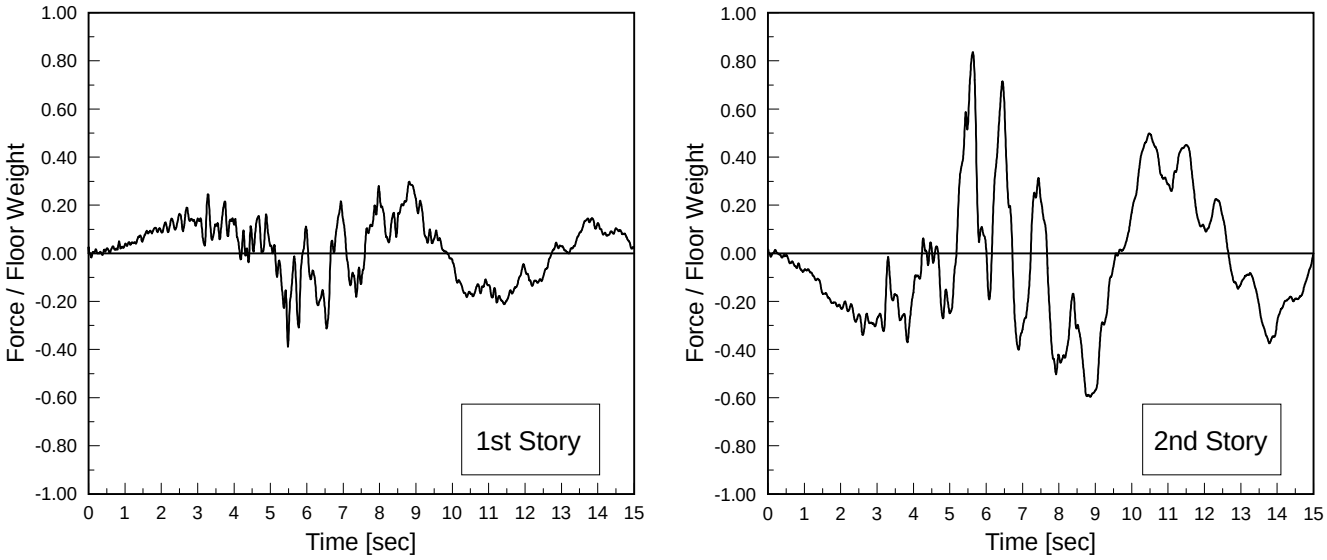

Figure 4.3: Control forces for San Fernando ground acceleration record (y2 weighting - number of measurements: 8).

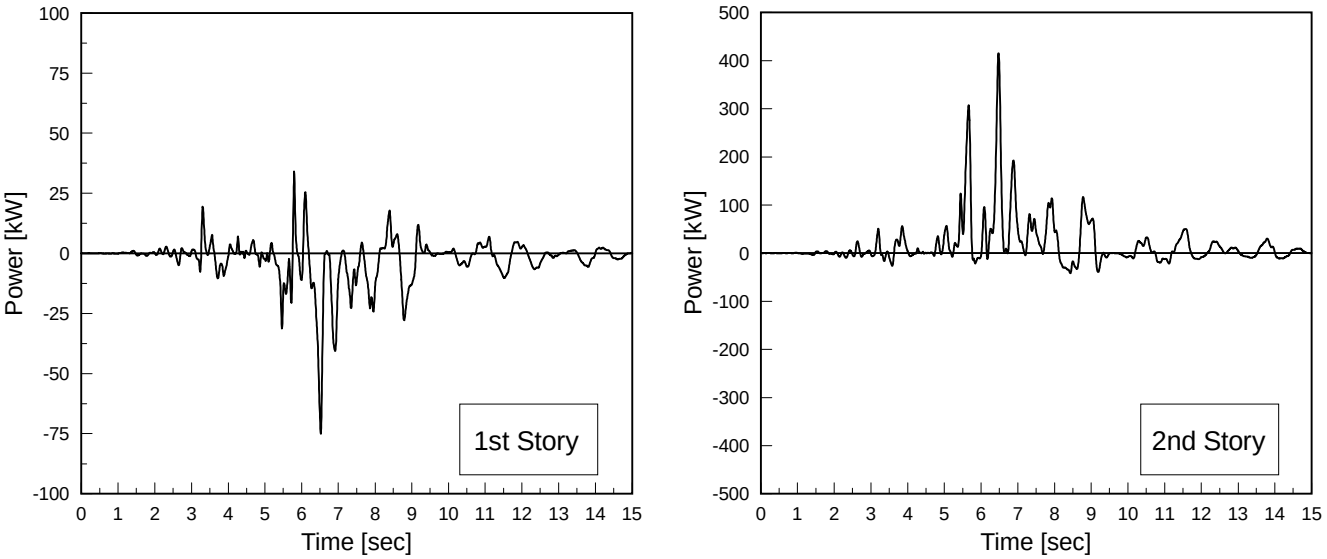

Figure 4.4: Mechanical power for San Fernando ground acceleration record (y2 weighting - number of measurements: 8).

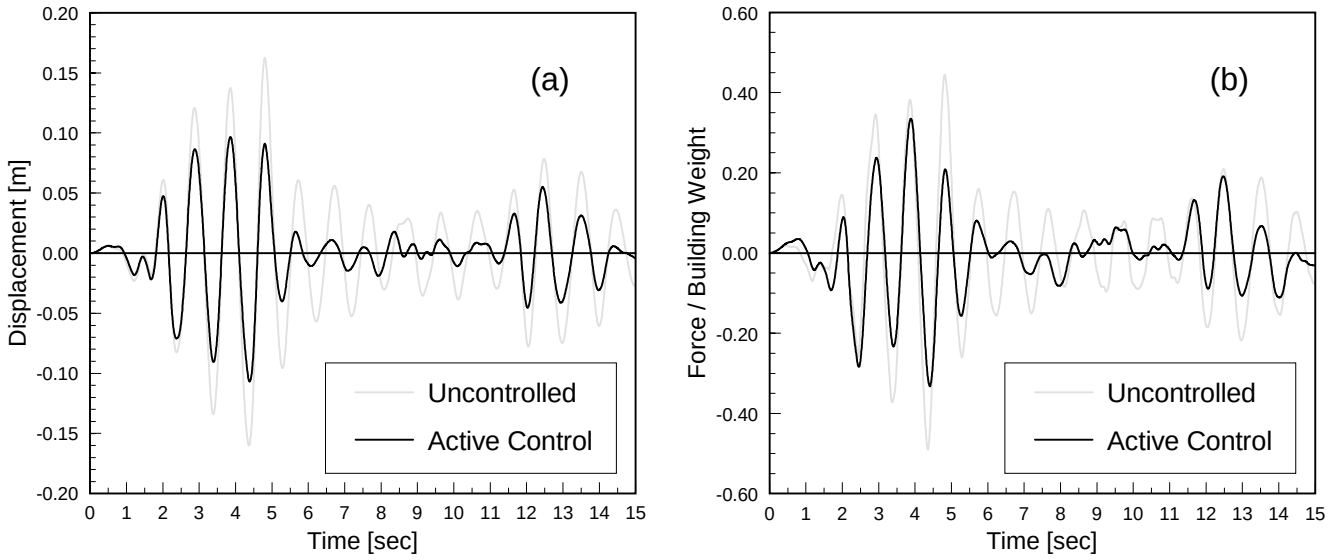

Figure 4.5: Comparison of uncontrolled and controlled top floor displacement and 1st story shear force for El Centro ground acceleration record (y1 weighting - number of measurements: 12).

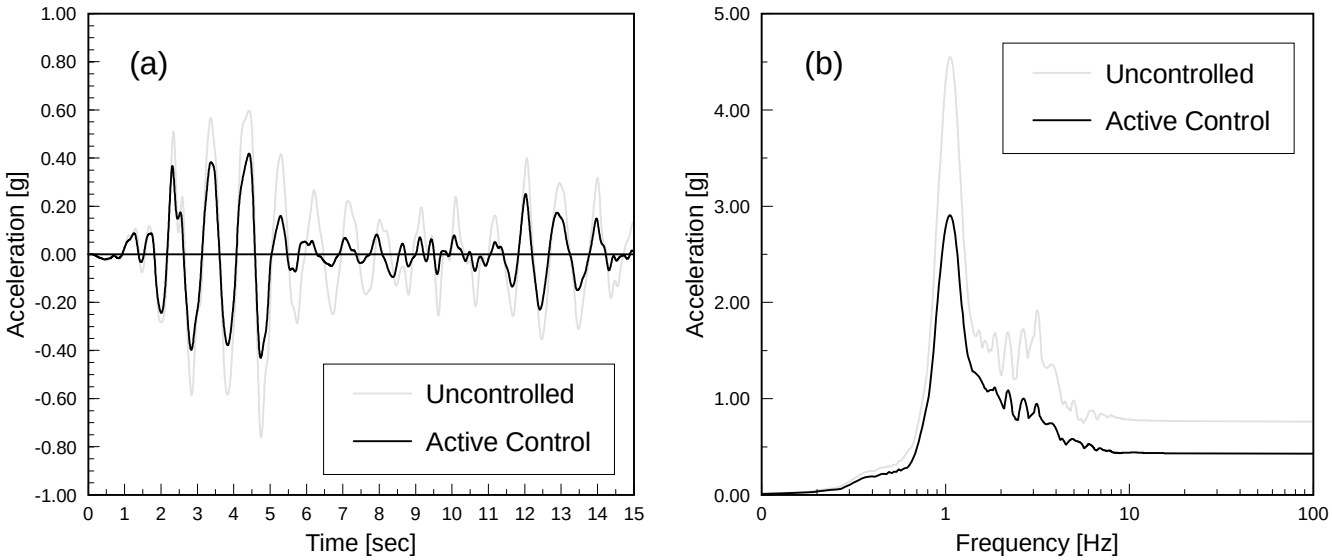

Figure 4.6: Comparison of uncontrolled and controlled top floor acceleration and top floor response spectra for El Centro ground acceleration record (y1 weighting - number of measurements: 12).

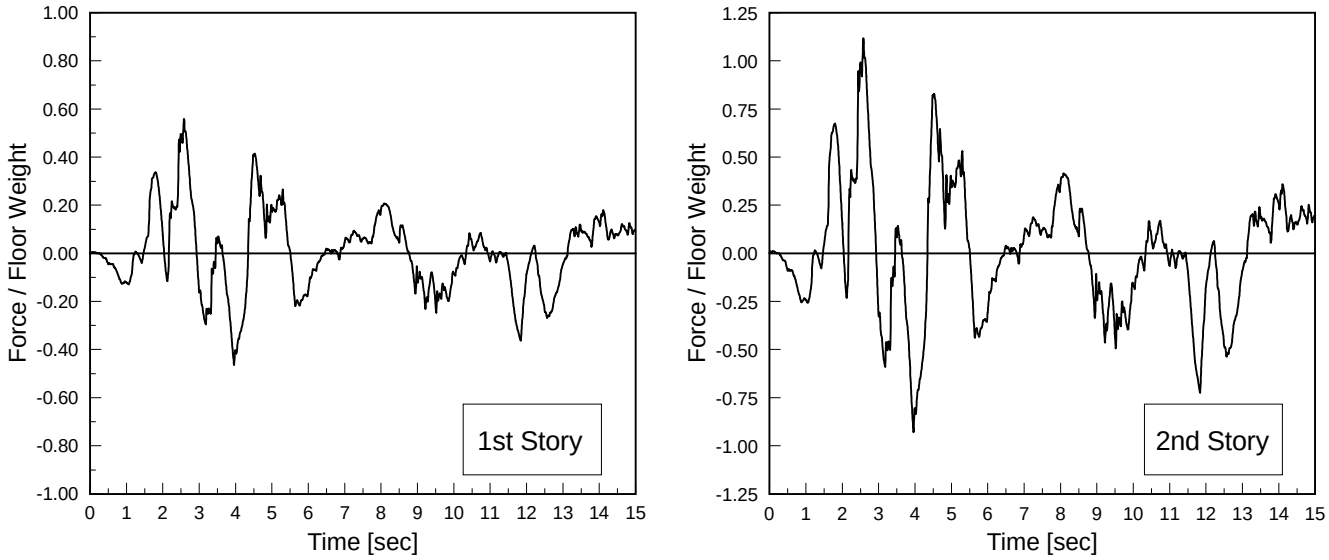

Figure 4.7: Control forces for El Centro ground acceleration record (y1 weighting - number of measurements: 12).

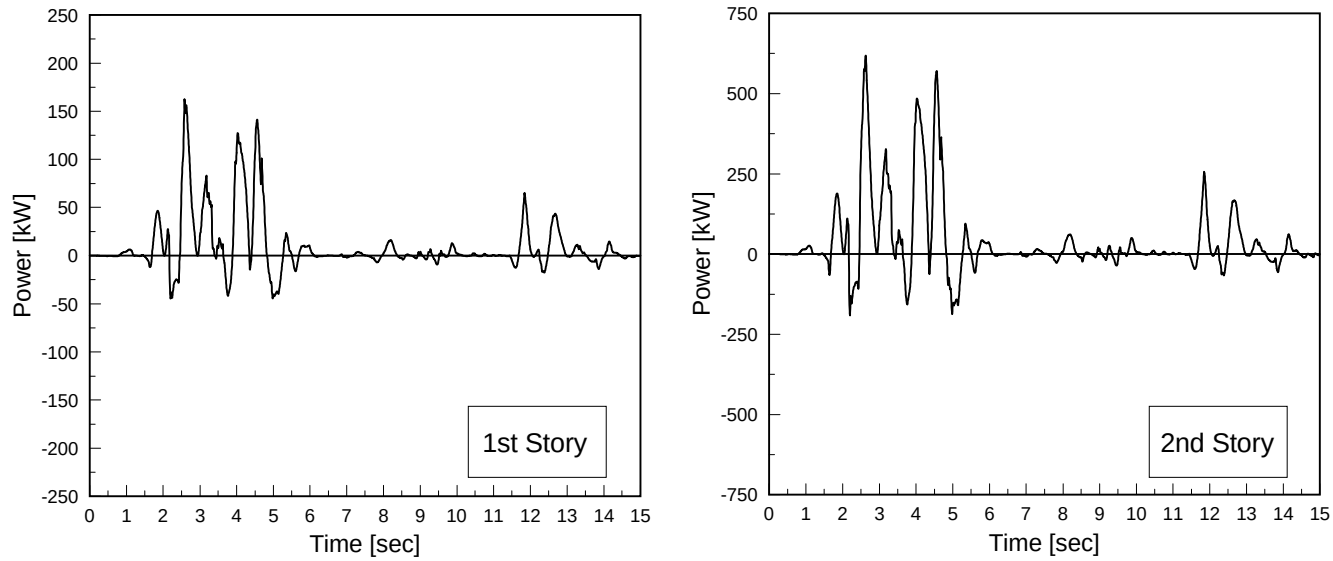

Figure 4.8: Mechanical power for El Centro ground acceleration record (y1 weighting - number of measurements: 12).

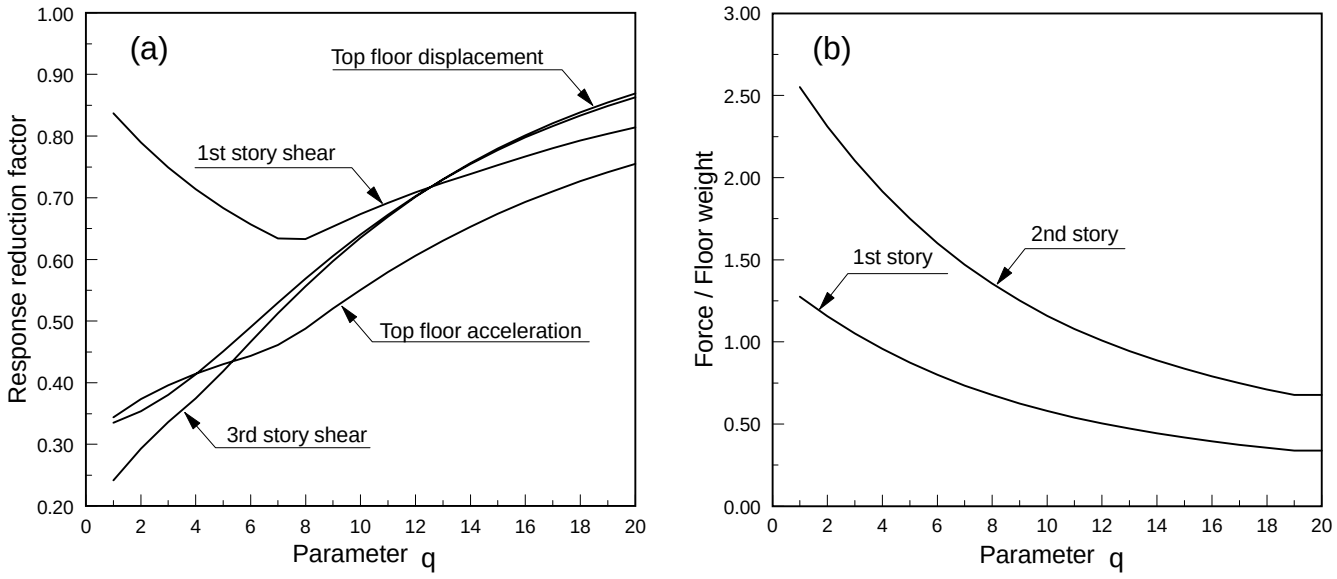

Figure 4.9: Maximum building responses and control requirements as a function of the parameter *q* for El Centro ground acceleration record (y1 weighting - number of measurements: 12).

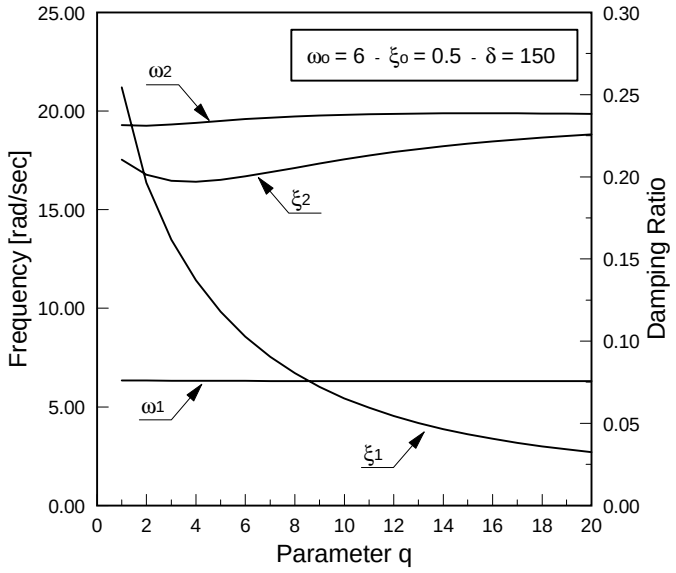

Figure 4.10: Natural frequencies and modal damping ratios as a function of the parameter *q* defining the sliding surface (y1 weighting - number of measurements: 12).

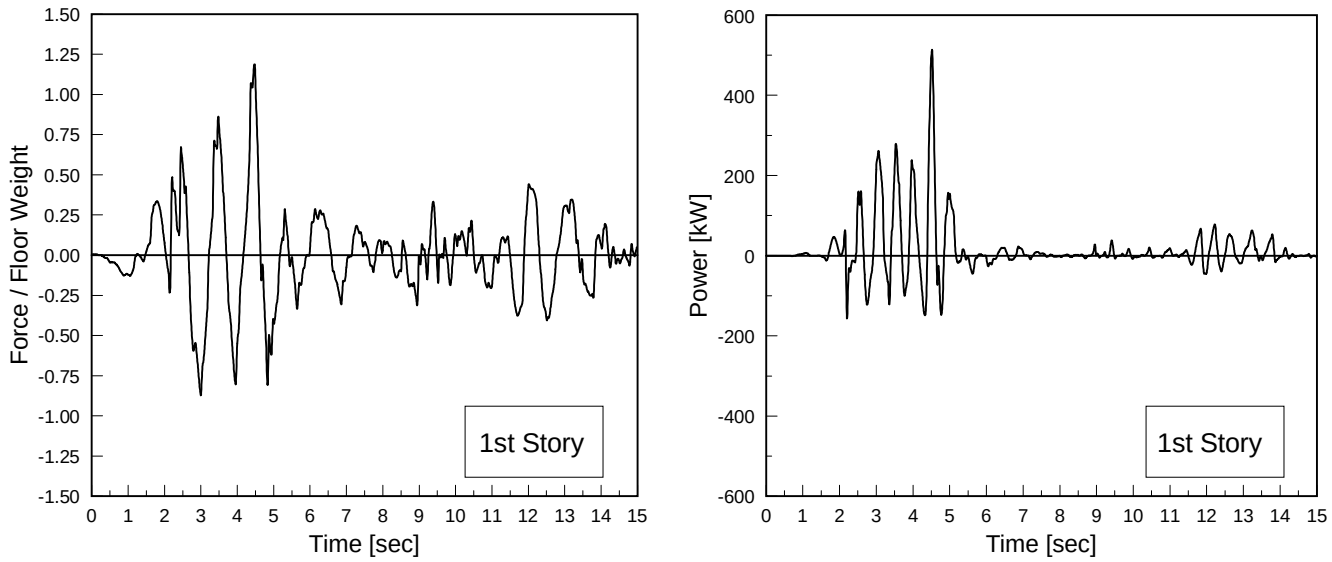

Figure 4.11: Control force and power for El Centro ground acceleration record in the event of failure of 2nd story actuation device (y1 weighting - number of measurements: 12).

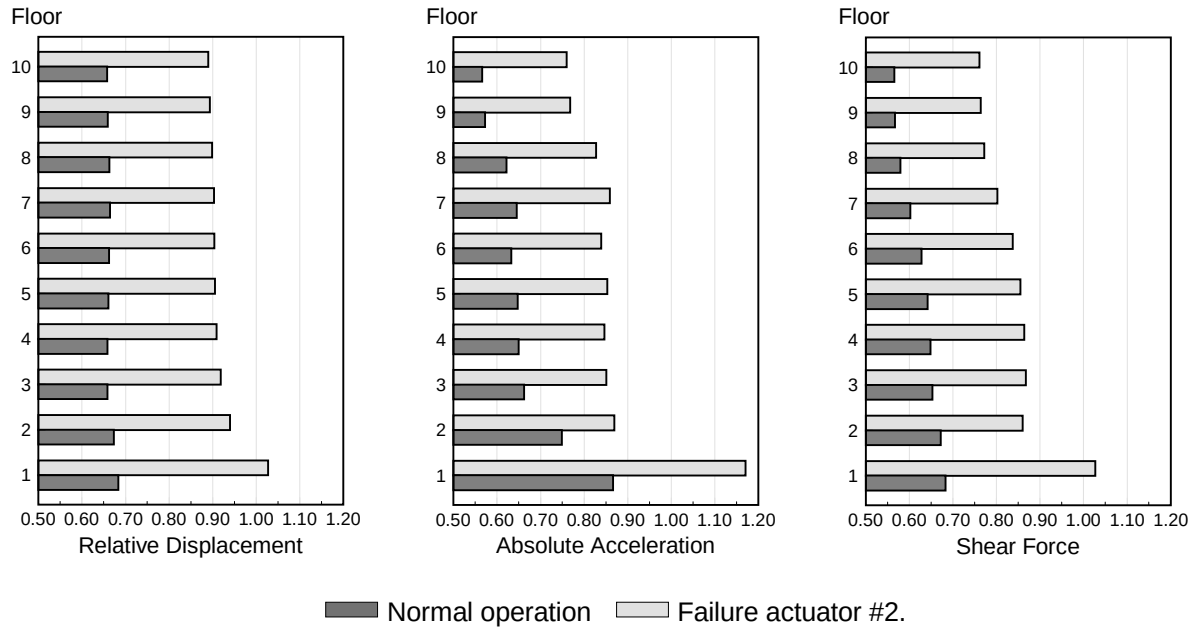

Figure 4.12: Comparison of response reduction factors during normal operation and the event of failure of 2nd story actuation device (y1 weighting - number of measurements: 12).

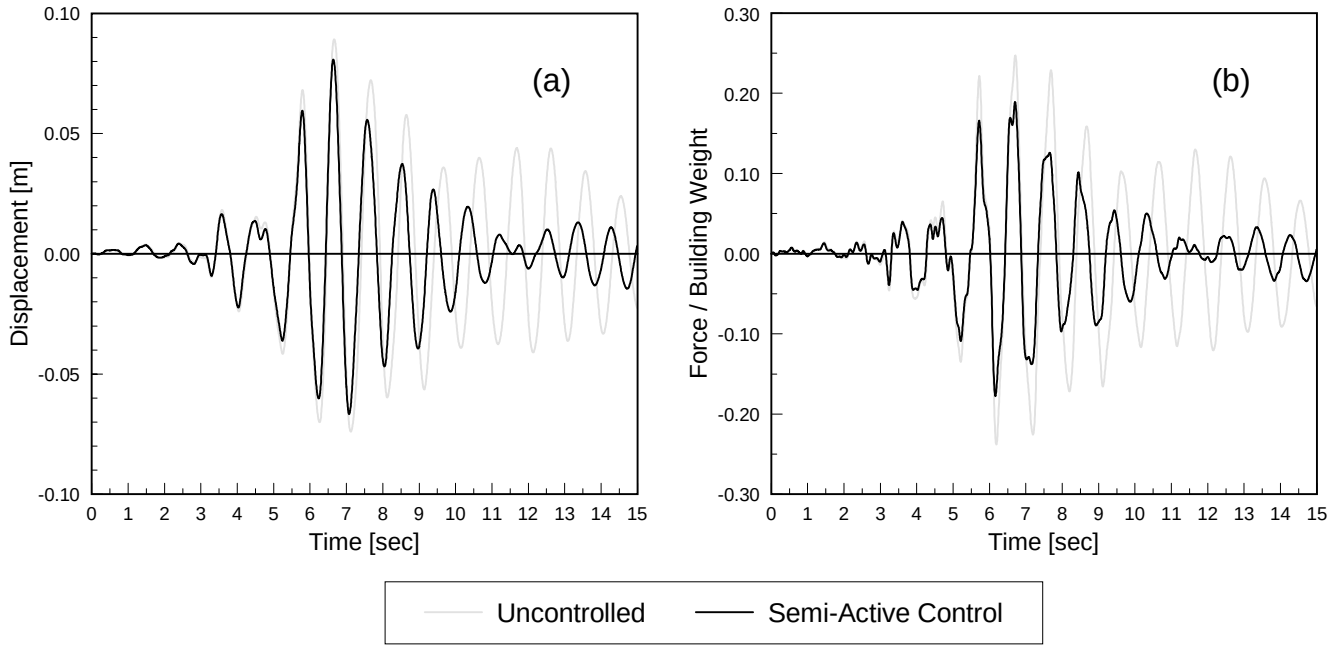

Figure 4.13: Comparison of uncontrolled and controlled top floor displacement and 1st story shear force for San Fernando ground acceleration record.

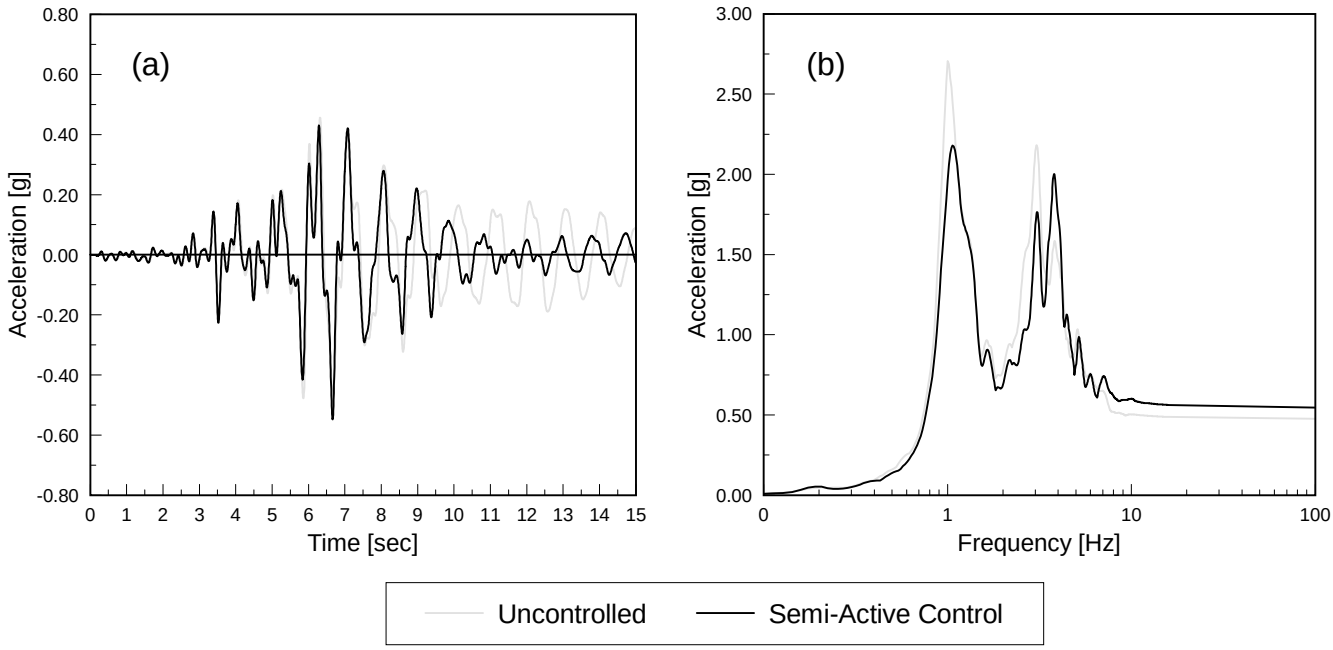

Figure 4.14: Comparison of uncontrolled and controlled top floor acceleration and top floor response spectra for San Fernando ground acceleration record.

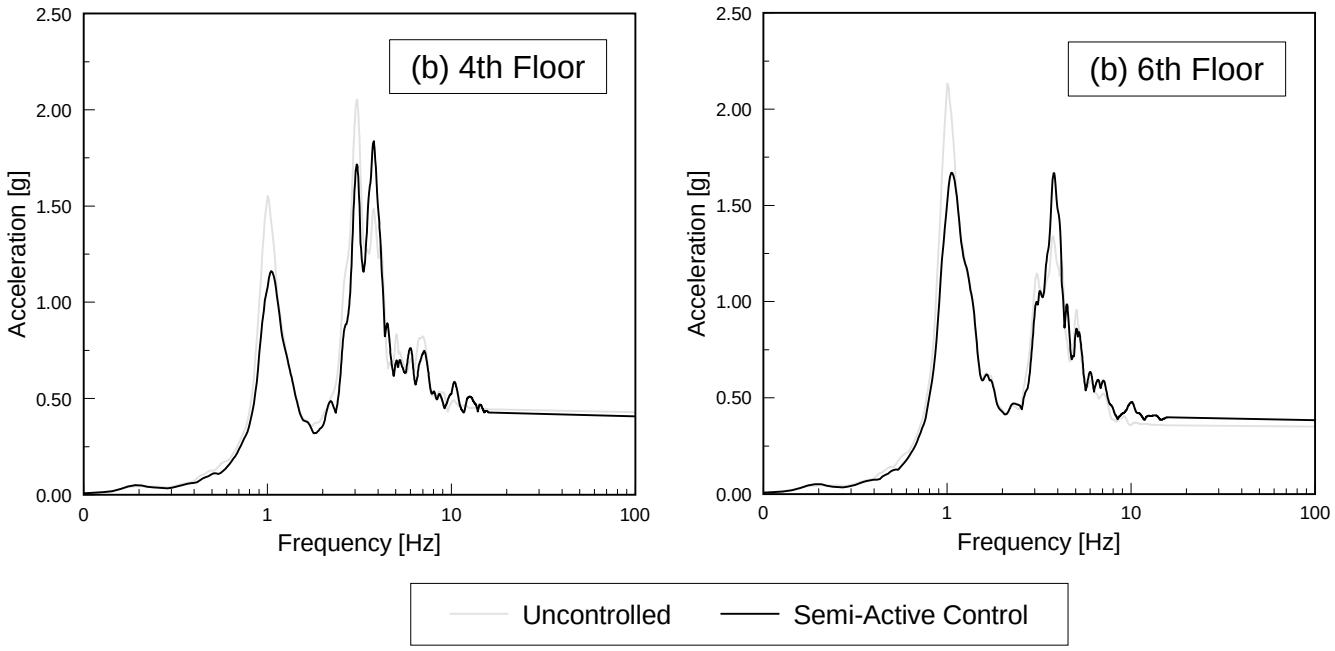

Figure 4.15: Comparison of uncontrolled and controlled floor acceleration and floor response spectra for San Fernando ground acceleration record.

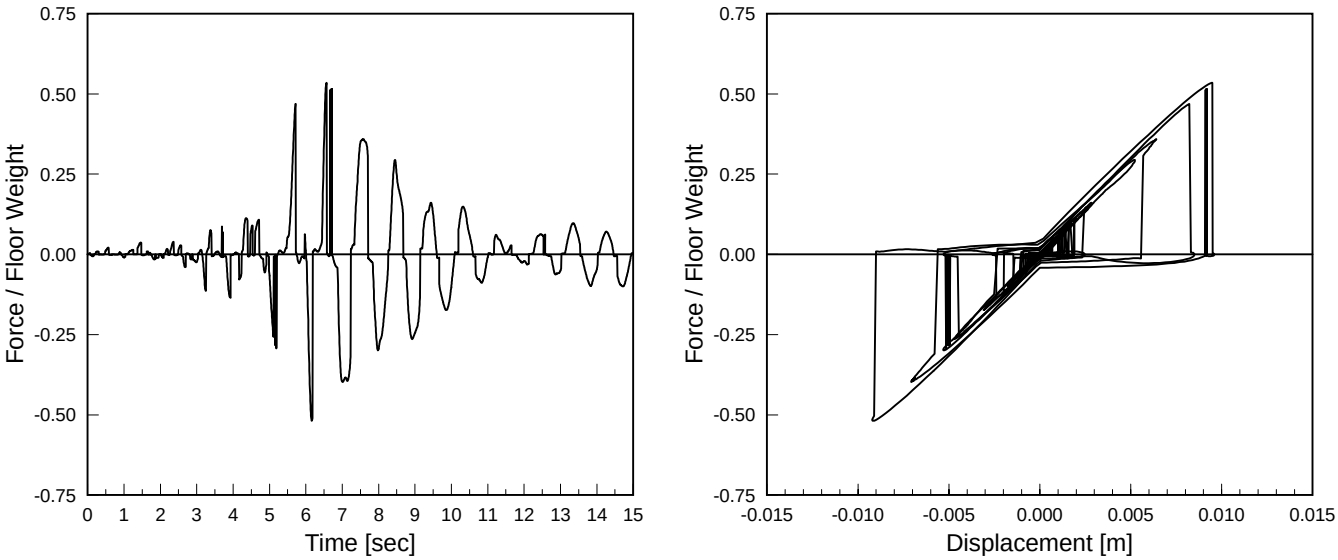

Figure 4.16: Semi-active control force for 2nd story device for San Fernando ground acceleration record.

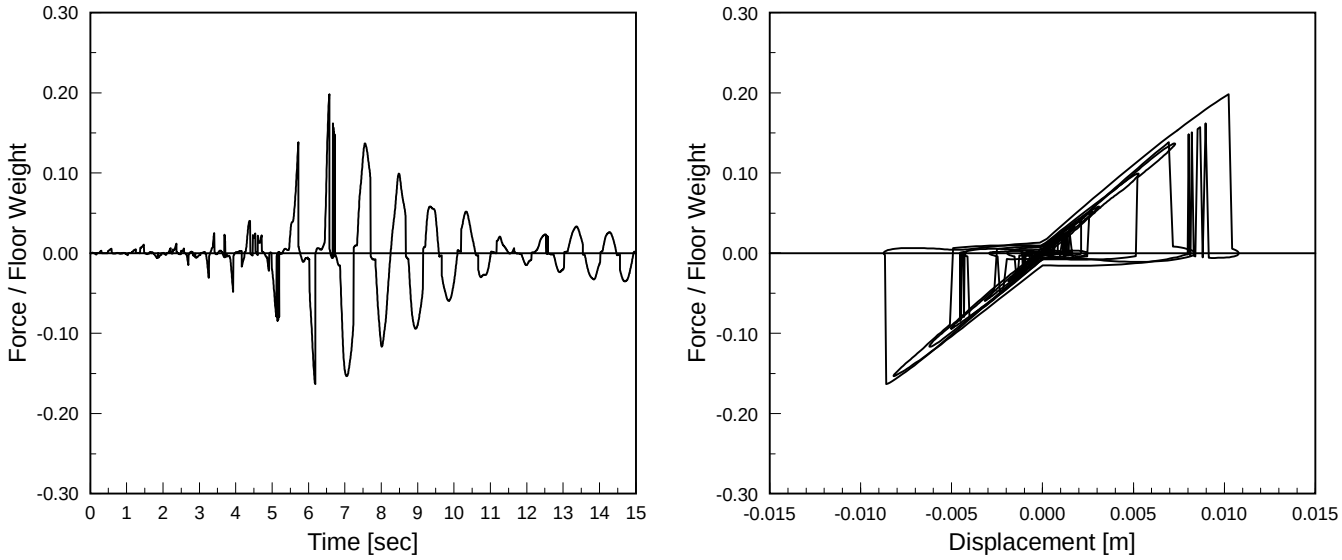

Figure 4.17: Semi-active control force for 4th story device for San Fernando ground acceleration record.

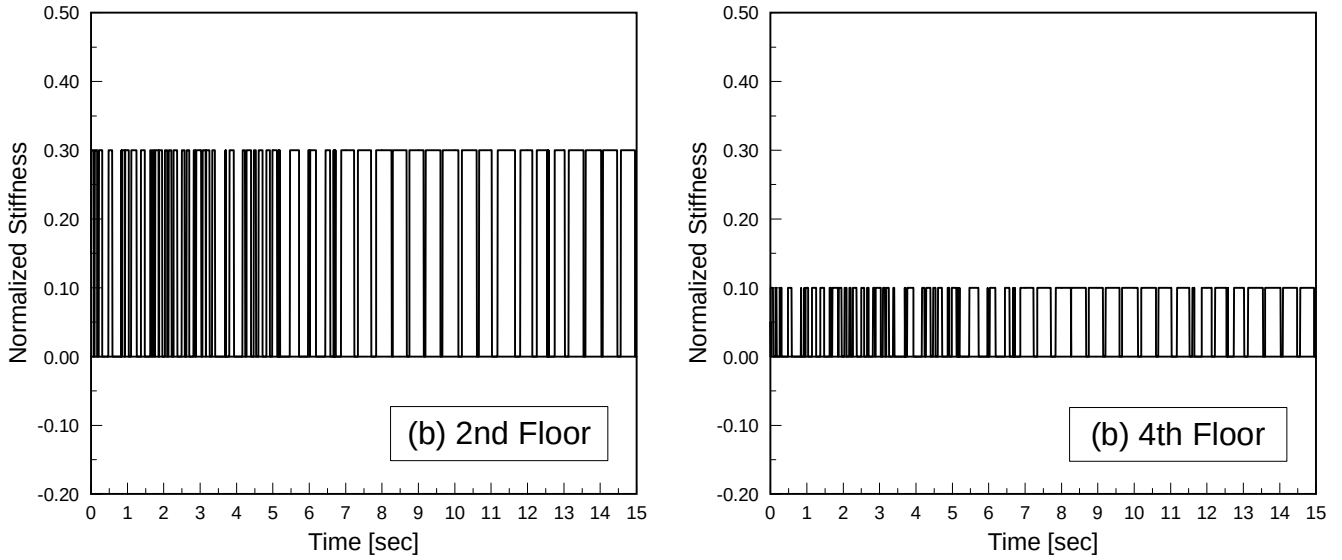

Figure 4.18: Variable stiffness coefficient time histories for 2nd and 4th story devices for San Fernando ground acceleration record.

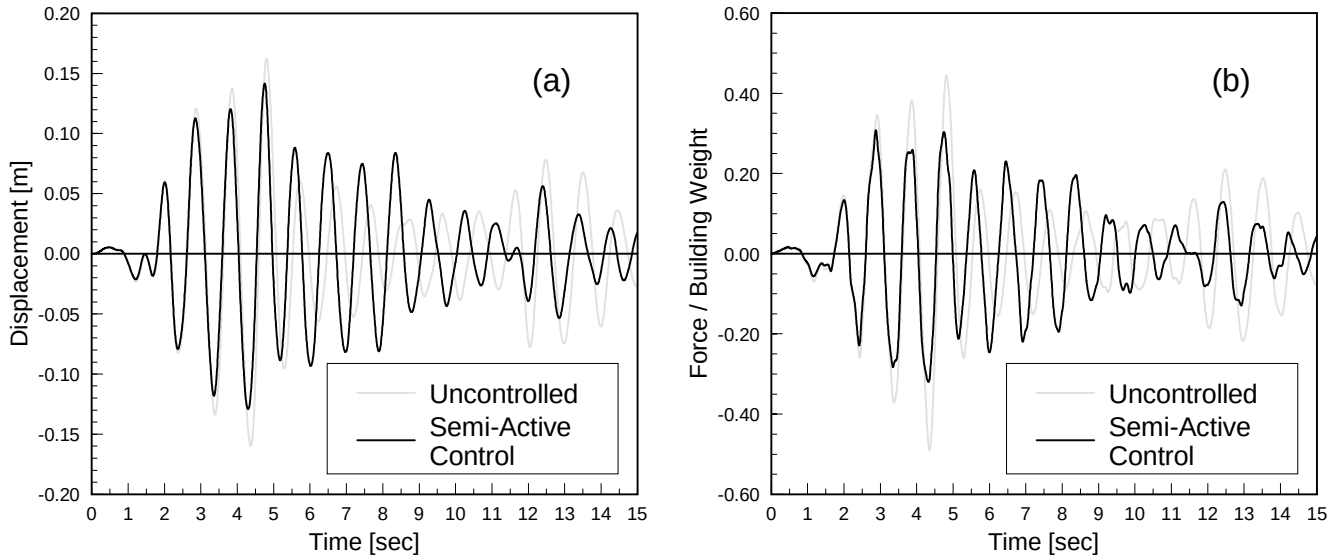

Figure 4.19: Comparison of uncontrolled and controlled top floor displacement and 1st story shear force for El Centro ground acceleration record.

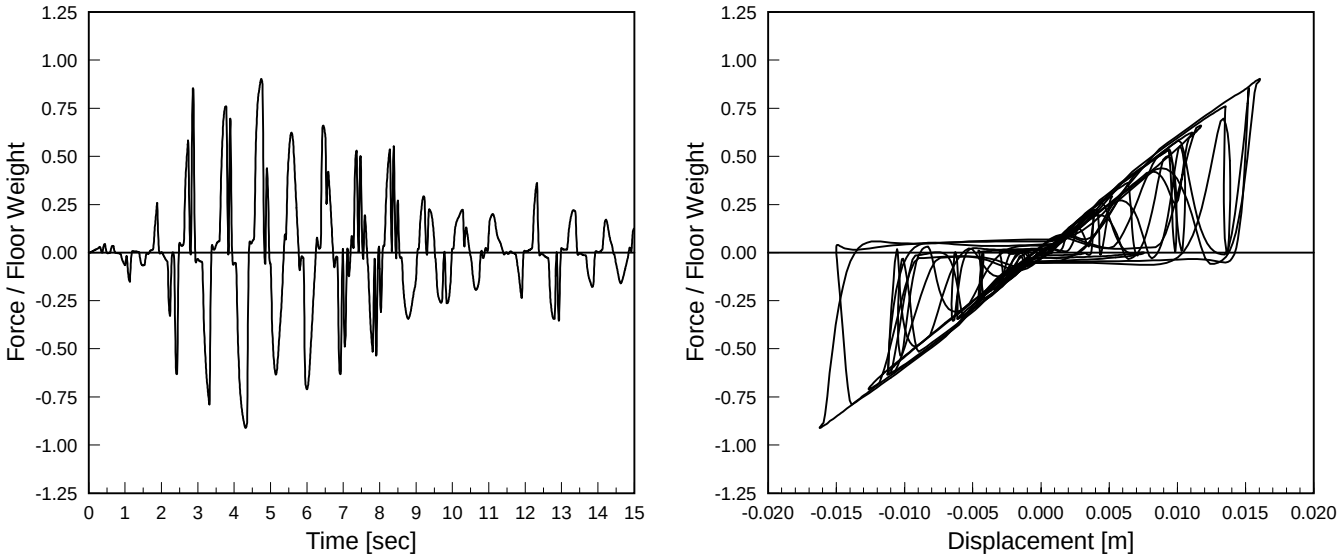

Figure 4.20: Semi-active control force for 2nd story device for El Centro ground acceleration record.

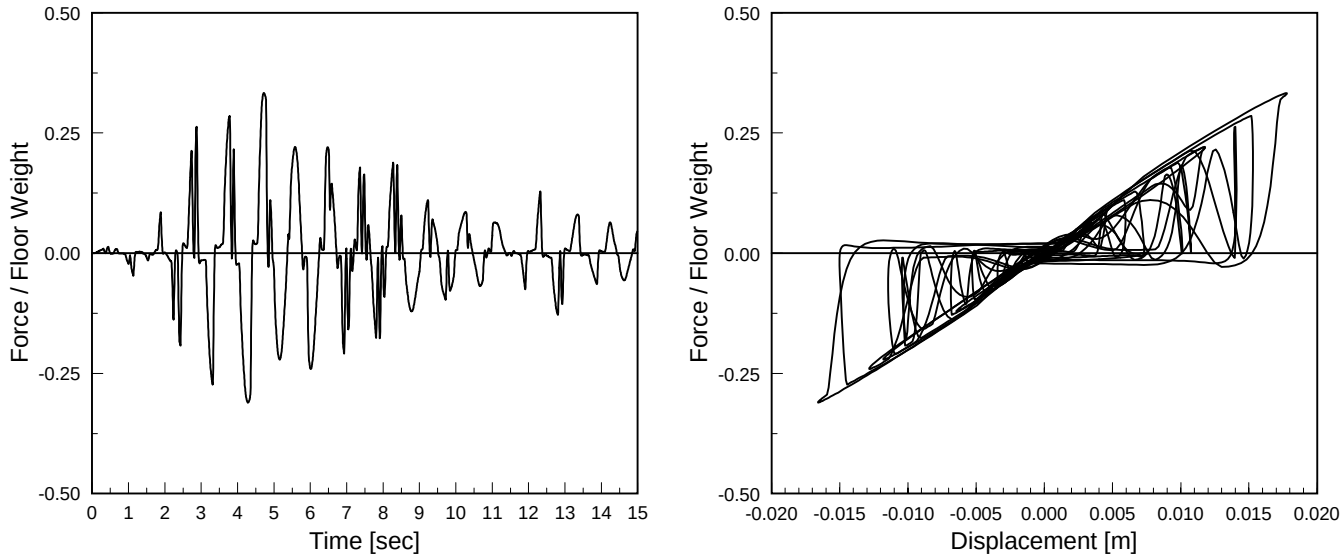

Figure 4.21: Semi-active control force for 4th story device for El Centro ground acceleration record.

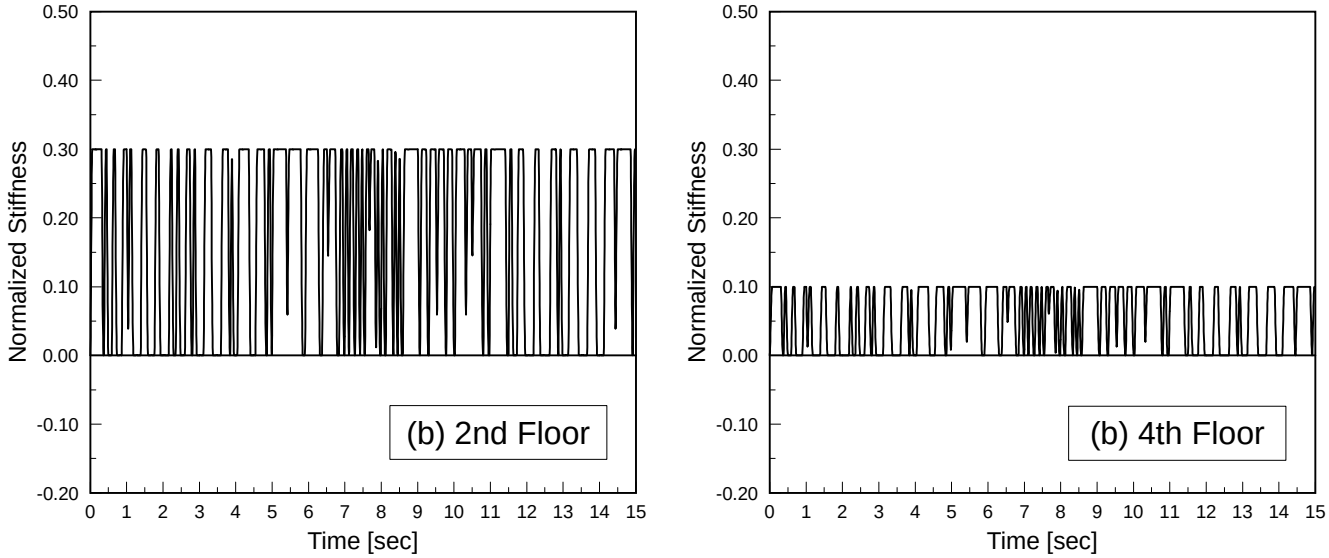

Figure 4.22: Variable stiffness coefficient time histories for 2nd and 4th story devices for El Centro ground acceleration record.

Floor	El Centro				San Fernando			
	Response	Response Reduction Factor			Response	Response Reduction Factor		
	[cm]	Full State	Output: Case a	Output: Case b	[cm]	Full State	Output: Case a	Output: Case b
[1]	[2]	[3]	[4]	[5]	[6]	[7]	[8]	[9]
10	**16.25**	0.66	0.66	0.66	**8.92**	0.73	0.73	0.71
9	**15.87**	0.66	0.66	0.66	**8.68**	0.72	0.73	0.71
8	**15.14**	0.66	0.66	0.66	**8.21**	0.72	0.73	0.70
7	**14.13**	0.67	0.67	0.66	**7.53**	0.72	0.72	0.70
6	**12.90**	0.67	0.66	0.66	**6.69**	0.71	0.72	0.70
5	**11.36**	0.67	0.66	0.66	**5.71**	0.71	0.71	0.72
4	**9.54**	0.67	0.66	0.66	**4.70**	0.70	0.70	0.74
3	**7.45**	0.67	0.66	0.66	**3.68**	0.70	0.70	0.74
2	**5.13**	0.68	0.65	0.67	**2.56**	0.70	0.69	0.78
1	**2.63**	0.69	0.63	0.68	**1.32**	0.69	0.65	0.79

Floor	Loma Prieta				Hollywood			
	Response	Response Reduction Factor			Response	Response Reduction Factor		
	[cm]	Full State	Output: Case a	Output: Case b	[cm]	Full State	Output: Case a	Output: Case b
[10]	[11]	[12]	[13]	[14]	[15]	[16]	[17]	[18]
10	**6.17**	0.89	0.88	0.85	**15.94**	0.66	0.67	0.64
9	**5.96**	0.90	0.89	0.85	**15.58**	0.66	0.67	0.64
8	**5.74**	0.88	0.87	0.83	**14.87**	0.66	0.66	0.64
7	**5.53**	0.83	0.82	0.79	**13.81**	0.66	0.66	0.64
6	**5.23**	0.77	0.79	0.73	**12.44**	0.66	0.66	0.64
5	**4.78**	0.75	0.76	0.69	**10.78**	0.66	0.66	0.64
4	**4.14**	0.73	0.74	0.66	**8.88**	0.65	0.65	0.65
3	**3.29**	0.69	0.70	0.64	**6.78**	0.65	0.64	0.67
2	**2.27**	0.66	0.66	0.64	**4.56**	0.64	0.64	0.71
1	**1.15**	0.68	0.67	0.63	**2.28**	0.67	0.63	0.74

Table 4.1: Maximum relative displacements using active control (generalized sliding surface / full state and output feedback).

Floor	El Centro				San Fernando			
	Response	Response Reduction Factor			Response	Response Reduction Factor		
	[g]	Full State	Output: Case a	Output: Case b	[g]	Full State	Output: Case a	Output: Case b
[1]	[2]	[3]	[4]	[5]	[6]	[7]	[8]	[9]
10	**0.76**	0.64	0.66	0.57	**0.48**	0.78	0.79	0.74
9	**0.72**	0.64	0.67	0.57	**0.44**	0.78	0.79	0.75
8	**0.64**	0.64	0.67	0.62	**0.39**	0.75	0.76	0.70
7	**0.60**	0.64	0.66	0.65	**0.35**	0.72	0.73	0.62
6	**0.58**	0.65	0.66	0.63	**0.35**	0.71	0.72	0.64
5	**0.54**	0.68	0.69	0.65	**0.41**	0.66	0.67	0.54
4	**0.50**	0.68	0.70	0.65	**0.43**	0.63	0.64	0.51
3	**0.44**	0.69	0.71	0.66	**0.37**	0.62	0.63	0.58
2	**0.35**	0.67	0.67	0.75	**0.33**	0.67	0.68	0.62
1	**0.26**	0.85	0.91	0.87	**0.31**	0.80	0.84	0.80

Floor	Loma Prieta				Hollywood			
	Response	Response Reduction Factor			Response	Response Reduction Factor		
	[g]	Full State	Output: Case a	Output: Case b	[g]	Full State	Output: Case a	Output: Case b
[10]	[11]	[12]	[13]	[14]	[15]	[16]	[17]	[18]
10	**0.49**	0.71	0.72	0.62	**0.69**	0.67	0.68	0.67
9	**0.42**	0.73	0.74	0.67	**0.67**	0.67	0.68	0.66
8	**0.33**	0.79	0.80	0.74	**0.64**	0.67	0.68	0.66
7	**0.28**	0.80	0.81	0.69	**0.60**	0.66	0.67	0.64
6	**0.36**	0.73	0.75	0.62	**0.55**	0.66	0.67	0.63
5	**0.42**	0.69	0.70	0.57	**0.48**	0.65	0.67	0.63
4	**0.43**	0.67	0.68	0.54	**0.42**	0.65	0.67	0.65
3	**0.37**	0.64	0.66	0.51	**0.36**	0.65	0.66	0.64
2	**0.28**	0.65	0.67	0.61	**0.29**	0.58	0.58	0.60
1	**0.29**	0.80	0.81	0.78	**0.21**	0.74	0.79	0.76

Table 4.2: Maximum absolute accelerations using active control (generalized sliding surface / full state and output feedback).

	Maximum control requirements					
	Full State Feedback		Output Feedback: (a)		Output Feedback: (b)	
	1st Story [Floor weight]	2nd Story [Floor weight]	1st Story [Floor weight]	2nd Story [Floor weight]	1st Story [Floor weight]	2nd Story [Floor weight]
	[1]	[2]	[3]	[4]	[5]	[6]
El Centro	0.45	0.98	0.59	1.31	0.56	1.12
San Fernando	0.33	0.66	0.39	0.84	0.40	0.80
Loma Prieta	0.28	0.49	0.30	0.58	0.29	0.58
Hollywood	0.39	0.99	0.40	1.23	0.50	1.00

Table 4.3: Maximum control force requirements (generalized sliding surface / full state and output feedback).

Floor	El Centro					San Fernando				
	Response	Response Reduction Factor				Response	Response Reduction Factor			
		Passive Control	Semi-Active Control				Passive Control	Semi-Active Control		
	[cm]		Full State	Output: Case a	Output: Case b	[cm]		Full State	Output: Case a	Output: Case b
[1]	[2]	[3]	[4]	[5]	[6]	[7]	[8]	[9]	[10]	[11]
10	**16.25**	0.97	0.85	0.85	0.87	**8.92**	0.95	0.91	0.91	0.91
9	**15.87**	0.97	0.84	0.84	0.86	**8.68**	0.95	0.91	0.90	0.91
8	**15.14**	0.95	0.83	0.83	0.85	**8.21**	0.96	0.91	0.90	0.91
7	**14.13**	0.93	0.80	0.80	0.83	**7.53**	0.97	0.92	0.89	0.91
6	**12.90**	0.89	0.77	0.77	0.79	**6.69**	0.97	0.93	0.89	0.92
5	**11.36**	0.84	0.73	0.73	0.75	**5.71**	0.96	0.93	0.88	0.91
4	**9.54**	0.78	0.68	0.68	0.70	**4.70**	0.92	0.90	0.84	0.88
3	**7.45**	0.73	0.64	0.65	0.67	**3.68**	0.86	0.84	0.78	0.82
2	**5.13**	0.71	0.62	0.63	0.65	**2.56**	0.79	0.78	0.75	0.77
1	**2.63**	0.71	0.62	0.63	0.65	**1.32**	0.75	0.75	0.76	0.75

Floor	Loma Prieta					Hollywood				
	Response	Response Reduction Factor				Response	Response Reduction Factor			
		Passive Control	Semi-Active Control				Passive Control	Semi-Active Control		
	[cm]		Full State	Output: Case a	Output: Case b	[cm]		Full State	Output: Case a	Output: Case b
[12]	[13]	[14]	[15]	[16]	[17]	[18]	[19]	[20]	[21]	[22]
10	**6.17**	1.03	1.01	0.99	1.00	**15.94**	0.89	0.79	0.83	0.83
9	**5.96**	1.04	1.01	1.01	1.01	**15.58**	0.89	0.79	0.83	0.83
8	**5.74**	1.05	1.00	1.01	1.01	**14.87**	0.88	0.78	0.82	0.82
7	**5.53**	1.05	1.00	0.99	1.00	**13.81**	0.87	0.77	0.81	0.81
6	**5.23**	1.04	0.99	0.97	0.98	**12.44**	0.85	0.75	0.80	0.80
5	**4.78**	1.01	0.98	0.94	0.95	**10.78**	0.82	0.73	0.80	0.80
4	**4.14**	0.98	0.95	0.90	0.92	**8.88**	0.79	0.71	0.79	0.80
3	**3.29**	0.95	0.93	0.87	0.89	**6.78**	0.76	0.69	0.79	0.80
2	**2.27**	0.93	0.91	0.85	0.87	**4.56**	0.74	0.67	0.80	0.80
1	**1.15**	0.93	0.92	0.85	0.88	**2.28**	0.75	0.67	0.80	0.81

Table 4.4: Maximum relative displacements using semi-active control (static sliding surface / full state feedback and generalized sliding surface / output feedback).

Floor	El Centro					San Fernando				
	Response	Response Reduction Factor				Response	Response Reduction Factor			
		Passive Control	Semi-Active Control				Passive Control	Semi-Active Control		
	[g]		Full State	Output: Case a	Output: Case b	[g]		Full State	Output: Case a	Output: Case b
[1]	[2]	[3]	[4]	[5]	[6]	[7]	[8]	[9]	[10]	[11]
10	**0.76**	1.16	1.11	1.10	1.10	**0.48**	1.05	1.11	1.15	1.17
9	**0.72**	1.17	1.07	1.06	1.07	**0.44**	1.05	1.09	1.11	1.13
8	**0.64**	1.18	1.02	1.00	1.04	**0.39**	1.05	1.02	1.04	1.05
7	**0.60**	1.08	0.98	0.95	1.02	**0.35**	1.14	1.11	1.06	1.11
6	**0.58**	0.88	0.93	0.88	0.93	**0.35**	1.15	1.20	1.09	1.19
5	**0.54**	0.88	0.89	0.83	0.83	**0.41**	1.03	1.05	0.97	1.00
4	**0.50**	0.87	0.83	1.02	0.80	**0.43**	1.03	1.06	0.95	1.01
3	**0.44**	0.88	0.81	1.04	1.00	**0.37**	1.03	1.07	0.95	1.04
2	**0.35**	0.91	0.91	1.16	1.14	**0.33**	0.96	0.96	0.97	0.95
1	**0.26**	0.96	0.96	1.05	1.28	**0.31**	0.99	0.99	0.97	1.00

Floor	Loma Prieta					Hollywood				
	Response	Response Reduction Factor				Response	Response Reduction Factor			
		Passive Control	Semi-Active Control				Passive Control	Semi-Active Control		
	[g]		Full State	Output: Case a	Output: Case b	[g]		Full State	Output: Case a	Output: Case b
[12]	[13]	[14]	[15]	[16]	[17]	[18]	[19]	[20]	[21]	[22]
10	**0.49**	1.07	1.12	1.01	1.08	**0.69**	1.12	1.04	1.06	1.04
9	**0.42**	1.08	1.11	1.00	1.08	**0.67**	1.07	0.99	1.02	1.00
8	**0.33**	1.09	1.07	0.96	1.03	**0.64**	1.00	0.91	0.94	0.95
7	**0.28**	1.18	1.19	1.13	1.15	**0.60**	0.94	0.86	0.84	0.89
6	**0.36**	1.15	1.18	1.07	1.10	**0.55**	0.89	0.93	0.74	0.89
5	**0.42**	1.12	1.16	1.02	1.05	**0.48**	0.86	0.97	0.80	1.01
4	**0.43**	1.09	1.16	0.99	1.03	**0.42**	0.86	1.00	1.24	1.08
3	**0.37**	1.08	1.16	0.99	1.04	**0.36**	0.83	1.05	1.43	1.32
2	**0.28**	1.09	1.18	1.05	1.15	**0.29**	0.86	1.08	1.70	1.44
1	**0.29**	1.01	1.01	0.92	1.02	**0.21**	0.98	1.12	0.99	1.47

Table 4.5: Maximum absolute accelerations using semi-active control (static sliding surface / full state feedback and generalized sliding surface / output feedback).

Chapter 5

Conclusions and Future Work

The main focus of this study is on the active and semi-active control of structures subjected to seismic excitations. In Chapter 1, a comprehensive review of various control approaches is presented, and their advantages and limitations are examined. Among different candidate control strategies, the sliding mode control approach emerges as a convenient alternative, because of its versatility for application to linear and nonlinear systems, and also its superb robustness under parametric and input uncertainties. The analytical developments and numerical results presented in this dissertation have, therefore, been directed to investigate the feasibility of application of the sliding mode control approach to civil structures.

The general formulation of the sliding mode control approach is presented in Chapter 2, using a unified treatment to include both active and semi-active implementations. This involved the introduction of a special coordinate transformation in the equations of motion which reduces the contribution of any semi-active device to a convenient diagonal form. A systematic procedure, based on a special state transformation, is also presented to obtain the regular form of the state equations to facilitate the design of the control system. The conditions under which this can be achieved in the general case of control redundancy are also defined. The regular form permits the separation of the design in two basic steps: (a)

design of the target sliding surface and (b) determination of the corresponding control actions. Several active and semi-active controllers with full state characteristics are proposed. Extensive numerical results are presented to investigate the performance of the proposed control designs and to examine the feasibility of application to real size civil structures. In particular, the magnitude of the control requirements in the active control scheme was examined considering several seismic inputs and two different actuation arrangements.

From the numerical studies presented in Chapter 2, it was concluded that the design of the sliding surface is perhaps, the most crucial step in the implementation of an effective sliding mode control scheme. It was found that, when the sliding surface is defined in the form of some static constraints between the state variables, it is not straightforward to achieve an appropriate selection of these constraints. Although these sliding constraints may be obtained by using some optimality criterion, the resulting sliding surface can lead to an improper design, where an increased control effort does not necessarily translate into a better control of the response. Thus, the selection of a proper sliding surface is quite important for achieving an efficient and flexible control design. This is facilitated by the developments presented in Chapter 3.

In Chapter 3, a generalized sliding surface definition is used, in which the sliding constraints are defined on the outputs of a two auxiliary dynamical systems. Therefore, the sliding surface is defined in an augmented state space. This was shown to provide additional flexibility for further tuning of the design to meet different performance specifications. This design flexibility becomes important if the active control system is part of an integrated protection system in which the response reduction responsibilities are distributed among structural members, passive devices and active systems. In this chapter, an alternative procedure is also introduced to obtain the regular form of the state equations. A general

active controller is proposed, composed of linear and nonlinear terms with full state feedback characteristics. The motivation for the incorporation of the nonlinear term was to increase the control authority when the system moves away from the target sliding surface. Some interesting characteristics of the closed-loop system corresponding to the linear version of the proposed controller have also been investigated. The performance of the control scheme is evaluated by numerical simulations. It is found that the generalized definition of the sliding surface allowed a easier tuning of the resulting design, when compared to the static sliding surface case.

From the point of view of practical feasibility of implementation, it is necessary to consider the situation in which the measurements on all the state variables may not be available for control purposes. Usually, only a subset of the physical variables, such as displacements and velocities, can be directly obtained. It is desirable, therefore, to design the controller based on such partial information. With this aim in mind, in Chapter 4, a general approach has been formulated to eliminate the explicit effect of the unmeasured states on the design of the sliding surface and the associated controller. This approach, based on a modification of the regular form transformation presented in the previous chapter, permits the utilization of different combinations of measured and unmeasured states. The sliding surface design problem is discussed within the framework of the classical optimal output feedback theory. In particular, the sliding surface is obtained by solving a system of nonlinear matrix equations. An efficient algorithm is proposed to solve these equations. The characteristics of this algorithm, based on a damped successive approximation scheme, are discussed in Appendix A. To verify the applicability of the formulation for various cases, several sets of numerical results have been obtained for the same example problem studied before. Both active and semi-active control schemes have been considered.

The broad conclusions of this study can be summarized as follows:

- In principle, active control schemes are feasible for application to civil structures. They, however, may require large forces and power for implementation, if significant reductions in the responses are desired. Semi-active control schemes are better suited as they do not require a significative input of external energy and a nominal power source can be used to operate the devices.

- The sliding mode control approach can be effectively used to design controllers with desirable performance characteristics, for full state and output feedback implementations.

Future Work: The sliding mode control approach is a powerful technique. Not all the features of this could be explored in this study. Lot more can be done with this approach for the control of structural systems. It is suggested that future studies focus on the application of this approach for nonlinear structural systems, on the use of continuous-state semi-active devices and on the implementation of acceleration feedback strategies. A comprehensive study for optimum selection of auxiliary systems to achieve desirable performance characteristics would also be very useful. Finally, the optimal integration of active and semi-active schemes with various passive systems, such as base isolators and energy dissipators, for cost-effective design of structural systems should be the ultimate goal of a control system.

Appendix A

Successive Substitution Algorithm

Most of the algorithms proposed to solve the set of nonlinear equations (4.69)-(4.71) representing the necessary conditions of the optimal output feedback problem can be classified as gradient/nongradient search techniques, homotopy methods or successive substitution procedures. In general, the latter methods, based on the sequential solution of the equations, are easier to implement than other techniques [80]. In the sequel, a procedure based on algorithms proposed by Broussard and Halyo [8] and Moerder and Calise [57] is briefly described.

Equations (4.69)-(4.71) constitute the necessary conditions for minimization of the performance index (or cost function)

$$J = \mathrm{tr}\,\{\mathbf{MY}\} \tag{A.1}$$

These necessary conditions can be written in the following form:

$$\mathbf{B}^T\mathbf{MLC}^T + \mathbf{W_2NCLC}^T = \mathbf{0} \tag{A.2}$$

$$[\mathbf{A} + \mathbf{BNC}]\ \mathbf{L} + \mathbf{L}\ [\mathbf{A} + \mathbf{BNC}]^T = -\mathbf{Y} \tag{A.3}$$

$$[\mathbf{A} + \mathbf{BNC}]^T\ \mathbf{M} + \mathbf{M}\ [\mathbf{A} + \mathbf{BNC}] + \mathbf{C}^T\mathbf{N}^T\mathbf{W_2NC} = -\mathbf{W_1} \tag{A.4}$$

where notation extraneous to our purpose here has been dropped.

For any matrix $\mathbf{N}$ such that $\mathbf{A}+\mathbf{BNC}$ is asymptotically stable, equation (A.3) may be viewed as determining $\mathbf{L}$ as a function of $\mathbf{N}$. Likewise, equation (A.4) can be regarded as determining $\mathbf{M}$ as a function of $\mathbf{N}$. These two equations can be rewritten as follows:

$$[\mathbf{A}+\mathbf{BNC}]\ \mathbf{L}(\mathbf{N})+\mathbf{L}(\mathbf{N})\ [\mathbf{A}+\mathbf{BNC}]^T=-\mathbf{Y} \tag{A.5}$$

$$[\mathbf{A}+\mathbf{BNC}]^T\,\mathbf{M}(\mathbf{N})+\mathbf{M}(\mathbf{N})\ [\mathbf{A}+\mathbf{BNC}]=-\mathbf{W_1}-\mathbf{C}^T\mathbf{N}^T\mathbf{W_2}\mathbf{NC} \tag{A.6}$$

in which the notation $\mathbf{L}(\mathbf{N})$ and $\mathbf{M}(\mathbf{N})$ denotes the dependence of these matrices on the matrix $\mathbf{N}$. Also, the $\mathbf{N}$-dependence of the cost function can be made explicit in the following form:

$$J(\mathbf{N})=\mathrm{tr}\,\{\mathbf{M}(\mathbf{N})\mathbf{Y}\} \tag{A.7}$$

in which $J(\mathbf{N})$ denotes the value of the cost function associated with such a matrix $\mathbf{N}$. Since equations (A.2)-(A.4) are first order necessary conditions, we know that any matrix $\mathbf{N}$ for which $J(\mathbf{N})$ is a minimum must enforce simultaneously these equations.

Now, let $\mathbf{N}_*$ denote a matrix such that $\mathbf{A}+\mathbf{BN}_*\mathbf{C}$ is asymptotically stable and that also satisfies equation (A.2),

$$\mathbf{B}^T\mathbf{M}(\mathbf{N}_*)\mathbf{L}(\mathbf{N}_*)\mathbf{C}^T+\mathbf{W_2}\mathbf{N}_*\mathbf{CL}(\mathbf{N}_*)\mathbf{C}^T=\mathbf{0} \tag{A.8}$$

where the matrices $\mathbf{L}(\mathbf{N}_*)$ and $\mathbf{M}(\mathbf{N}_*)$ are determined by using (A.5) and (A.6), respectively. That is, the matrix $\mathbf{N}_*$ and the associated $\mathbf{L}(\mathbf{N}_*)$ and $\mathbf{M}(\mathbf{N}_*)$ satisfy the necessary conditions for minimization of the performance index.

Equation (A.8) can be written as

$$\mathbf{N}_*=-\mathbf{W_2^{-1}}\mathbf{B}^T\mathbf{M}(\mathbf{N}_*)\mathbf{L}(\mathbf{N}_*)\mathbf{C}^T\left[\mathbf{CL}(\mathbf{N}_*)\mathbf{C}^T\right]^{-1}=\mathbf{F}(\mathbf{N}_*) \tag{A.9}$$

and hence the matrix $\mathbf{N}_*$ can be regarded as a fixed point of the function $\mathbf{F}$. Therefore, the search for a set of matrices $\mathbf{N}_*$, $\mathbf{L}(\mathbf{N}_*)$ and $\mathbf{M}(\mathbf{N}_*)$ that satisfy the conditions (A.2)-(A.4)

can be formulated as the problem of finding a fixed point of the function $\mathbf{F}$,

$$\mathbf{F}(\mathbf{N}) = -\mathbf{W_2^{-1}}\mathbf{B}^T\mathbf{M}(\mathbf{N})\mathbf{L}(\mathbf{N})\mathbf{C}^T\left[\mathbf{C}\mathbf{L}(\mathbf{N})\mathbf{C}^T\right]^{-1} \tag{A.10}$$

An obvious strategy is given by a direct successive substitution approach, in the form

$$\mathbf{N}_{k+1} = \mathbf{F}\left(\mathbf{N}_k\right) \tag{A.11}$$

Another alternative is a damped successive substitution procedure, in the form

$$\mathbf{N}_{k+1} = \mathbf{N}_k + \alpha\mathbf{P}_k \tag{A.12}$$

in which the increment direction $\mathbf{P}_k$ is defined by

$$\mathbf{P}_k = \mathbf{F}\left(\mathbf{N}_k\right) - \mathbf{N}_k \tag{A.13}$$

and where $\alpha \in [0,1]$ is a scaling parameter inducing a more conservative step selection. Note that the case $\alpha = 1$ corresponds to the direct successive substitution approach (A.11).

The iterative procedures indicated in (A.11) and (A.12) must be started by using an initial matrix $\mathbf{N}_0$ such that $\mathbf{A}+\mathbf{B}\mathbf{N}_0\mathbf{C}$ is asymptotically stable. If all eigenvalues of matrix $\mathbf{A}$ would have had strictly negative real parts, then $\mathbf{N}_0 = \mathbf{0}$ could have been selected as a convenient initial matrix. However, since for the problem consider here the matrix $\mathbf{A}$ is not asymptotically stable (as it was already shown in Chapter 4), then the procedure must be modified as indicated in the following.

A family of matrices $\mathbf{A}(\varepsilon)$ is defined in terms of a scalar parameter $\varepsilon \in [0,1]$ such that the matrix $\mathbf{A}(\varepsilon = 0)$ is asymptotically stable and the matrix $\mathbf{A}(\varepsilon = 1)$ corresponds to the original matrix $\mathbf{A}$. The idea is then to solve the necessary conditions (A.2)-(A.4) using $\mathbf{A}(\varepsilon)$ instead of $\mathbf{A}$ for a finite sequence of values of ε. For each value of the parameter ε, starting with $\varepsilon = 0$ and ending with $\varepsilon = 1$, the corresponding optimal matrix $\mathbf{N}_*(\varepsilon)$

is determined using the iterative procedure indicated in (A.12). This matrix is then used as the initial matrix for the iterations corresponding to the next value of ε. This can be done based on the fact that $\mathbf{N}_*(\varepsilon)$ stabilizes $\mathbf{A}(\varepsilon)$ for a neighborhood of ε. Therefore, it is sufficient to take the next value of ε within that neighborhood.

Note that, by construction of $\mathbf{A}(\varepsilon)$, the overall process can be started at $\varepsilon = 0$ by selecting a zero initial matrix. At the end of this procedure, a matrix $\mathbf{N}_*(\varepsilon = 1)$ is obtained that satisfies the necessary conditions (A.2)-(A.4).

Algorithm

- Let the matrix $\Delta\mathbf{A}$ be defined such that all the eigenvalues of $\mathbf{A}-\Delta\mathbf{A}$ have strictly negative real parts. In particular, and considering the stability characteristics of the matrix $\mathbf{A}$ for the problem studied here, the matrix $\Delta\mathbf{A}$ can be selected as the identity matrix. Define

$$\mathbf{A}(\varepsilon) = \mathbf{A} + (\varepsilon - 1)\,\Delta\mathbf{A} \tag{A.14}$$

- Take $\varepsilon = 0$ and starting with $\mathbf{N}_0(\varepsilon) = \mathbf{0}$, iterate according to (A.12) as follows:

$$\mathbf{N}_{k+1}(\varepsilon) = \mathbf{N}_k(\varepsilon) + \alpha\mathbf{P}_k(\varepsilon) \tag{A.15}$$

  in which

$$\mathbf{P}_k(\varepsilon) = \mathbf{F}\left(\mathbf{N}_k(\varepsilon)\right) - \mathbf{N}_k(\varepsilon) \tag{A.16}$$

  and where at each step k, the parameter α is determined by a line-search procedure so as to minimize $J\left(\mathbf{N}_k(\varepsilon) + \alpha\mathbf{P}_k(\varepsilon)\right)$. This procedure is discussed later in more detail.

- The iteration (A.15) continues until the following condition is satisfied:

$$\frac{\|\mathbf{P}_k(\varepsilon)\|_2}{\|\mathbf{N}_k(\varepsilon)\|_2} \leq \delta \tag{A.17}$$

for some $\delta > 0$. The matrix $\mathbf{N}_k(\varepsilon)$ satisfying this convergence criterion is denoted as $\mathbf{N}_*(\varepsilon)$ and while $\varepsilon < 1$, this matrix is used as the initial matrix for subsequent iterations.

- Repeat the procedure (A.14)-(A.17) for sequentally increasing values of the parameter ε, until $\varepsilon = 1$ is achieved.

Step Length Selection

For a given value of the parameter ε and at a given step k, the one-dimensional restriction of the performance index J to the increment direction $\mathbf{P}_k(\varepsilon)$ is given by

$$J_k(\alpha) = J\left(\mathbf{N}_k + \alpha \mathbf{P}_k\right) \tag{A.18}$$

where the dependence on ε has been dropped for simplicity and in which $J_k(\alpha)$ denotes the performance index as a function of the scalar parameter α. This can be written as follows:

$$J_k(\alpha) = \mathrm{tr}\left\{\mathbf{M}_k(\alpha)\mathbf{Y}\right\} \tag{A.19}$$

where $\mathbf{M}_k(\alpha)$ is the solution to

$$\begin{aligned}\left[\mathbf{A} + \mathbf{B}\left[\mathbf{N}_k + \alpha\mathbf{P}_k\right]\mathbf{C}\right]^T \mathbf{M}_k(\alpha) + \mathbf{M}_k(\alpha)\left[\mathbf{A} + \mathbf{B}\left[\mathbf{N}_k + \alpha\mathbf{P}_k\right]\mathbf{C}\right] = \\ = -\mathbf{W_1} - \mathbf{C}^T\left[\mathbf{N}_k + \alpha\mathbf{P}_k\right]^T \mathbf{W_2}\left[\mathbf{N}_k + \alpha\mathbf{P}_k\right]\mathbf{C}\end{aligned} \tag{A.20}$$

The parameter α is obtained by using a backtracking line-search algorithm [15]. The idea behind this algorithm is not to solve the one-dimensional optimization problem accurately, but to find a value of the parameter α that renders an acceptable reduction to the performance index. An outline of the procedure is presented below.

The procedure searches for a value of α that satisfies a sufficient-decrease condition (Armijo-Goldstein condition) of the form

$$J_k(\alpha) \leq J_k(0) + \alpha\rho J_k'(0) \tag{A.21}$$

where $\rho \in [0, 1/2]$ and in which

$$J_k^{'}(\alpha) = \frac{dJ_k(\alpha)}{d\alpha} \tag{A.22}$$

Note that this condition is stronger than the simple requirement $J_k(\alpha) < J_k(0)$, and it assures that the average rate of decrease of the performance index in a given step is at least a prescribed fraction of the initial rate of decrease, indicated by $J_k^{'}(0)$. Note also that since $J_k^{'}(0) < 0$ (as it is shown later) it is always possible to find a value of α that satisfies the condition (A.21).

Starting with $\alpha = 1$, if the above condition is not attained then $J_k(\alpha)$ is modeled as a quadratic function by using the values of the function at $\alpha = 0$ and $\alpha = 1$, and the value of its derivative at $\alpha = 0$. That is, a quadratic function $p_2(\alpha)$ is determined such that it satisfies

$$p_2(0) = J_k(0), \;\; p_2^{'}(0) = J_k^{'}(0) \;\; \text{and} \;\; p_2(1) = J_k(1) \tag{A.23}$$

The next value of α is then selected as $\alpha = \bar{\alpha}$, where $\bar{\alpha}$ minimizes the quadratic model. If the corresponding $J_k(\bar{\alpha})$ does not satisfy the condition (A.21), then for the next backtrack, $J_k(\alpha)$ is modeled as a cubic function using the information of the function at $\alpha = 0$ and the two values $J_k(1)$ and $J_k(\bar{\alpha})$. That is, a cubic function $p_3(\alpha)$ is determined such that it satisfies

$$p_3(0) = J_k(0), \;\; p_3^{'}(0) = J_k^{'}(0), \;\; p_3(1) = J_k(1) \;\; \text{and} \;\; p_3(\bar{\alpha}) = J_k(\bar{\alpha}) \tag{A.24}$$

The next value is then selected as the minimizer for the cubic model. This is done for any subsequent backtracks, for which the two most recent values of the function are used with the information at $\alpha = 0$ to define the corresponding cubic model.

Computation of $J_k^{'}(0)$

At step k, the derivative of the function J as a function of the parameter α is given by

$$J_k^{'}(\alpha) = \mathrm{tr}\left\{\mathbf{M}_k^{'}(\alpha)\mathbf{Y}\right\} \tag{A.25}$$

where $\mathbf{M}_k^{'}(\alpha)$ is the solution to

$$\begin{aligned}
&\left[\mathbf{A} + \mathbf{B}\left[\mathbf{N}_k + \alpha\mathbf{P}_k\right]\mathbf{C}\right]^T \mathbf{M}_k^{'}(\alpha) + \mathbf{M}_k^{'}(\alpha)\left[\mathbf{A} + \mathbf{B}\left[\mathbf{N}_k + \alpha\mathbf{P}_k\right]\mathbf{C}\right] = \\
&= -\mathbf{C}^T\left[\mathbf{P}_k^T\mathbf{W_2}\left[\mathbf{N}_k + \alpha\mathbf{P}_k\right] + \left[\mathbf{N}_k + \alpha\mathbf{P}_k\right]^T\mathbf{W_2}\mathbf{P}_k\right]\mathbf{C} - \\
&\quad -\mathbf{C}^T\mathbf{P}_k^T\mathbf{B}^T\mathbf{M}_k(\alpha) - \mathbf{M}_k(\alpha)\mathbf{B}\mathbf{P}_k\mathbf{C}
\end{aligned} \tag{A.26}$$

Evaluating at $\alpha = 0$, it follows that

$$J_k^{'}(0) = \mathrm{tr}\left\{\mathbf{M}_k^{'}\mathbf{Y}\right\} \tag{A.27}$$

where $\mathbf{M}_k^{'} = \mathbf{M}_k^{'}(0)$ is determined by solving the following Lyapunov equation:

$$\left[\mathbf{A} + \mathbf{B}\mathbf{N}_k\mathbf{C}\right]^T\mathbf{M}_k^{'} + \mathbf{M}_k^{'}\left[\mathbf{A} + \mathbf{B}\mathbf{N}_k\mathbf{C}\right] = \mathbf{R}_k \tag{A.28}$$

in which the matrix $\mathbf{R}_k$ is defined as

$$\mathbf{R}_k = -\mathbf{C}^T\left[\mathbf{P}_k^T\mathbf{W_2}\mathbf{N}_k + \mathbf{N}_k\mathbf{W_2}\mathbf{P}_k\right]\mathbf{C} - \mathbf{C}^T\mathbf{P}_k^T\mathbf{B}^T\mathbf{M}_k - \mathbf{M}_k\mathbf{B}\mathbf{P}_k\mathbf{C} \tag{A.29}$$

where $\mathbf{M}_k = \mathbf{M}_k(0)$.

In the sequel, it is shown that the evaluation of the derivative $J_k^{'}(0)$ does not require the solution of the equation (A.28). First it is noted that $J_k^{'}(0)$, given by equation (A.27), can also be expressed as follows:

$$J_k^{'}(0) = \mathrm{vec}\left\{\mathbf{M}_k^{'}\right\}^T\mathrm{vec}\left\{\mathbf{Y}\right\} \tag{A.30}$$

in which $\text{vec}\left\{\mathbf{M}_k^{'}\right\}$can be determined from the vectorized form of equation (A.28), given by

$$\left[\mathbf{I}\otimes\left[\mathbf{A}+\mathbf{B}\mathbf{N}_k\mathbf{C}\right]^T+\left[\mathbf{A}+\mathbf{B}\mathbf{N}_k\mathbf{C}\right]^T\otimes\mathbf{I}\right]\text{vec}\left\{\mathbf{M}_k^{'}\right\}=\text{vec}\left\{\mathbf{R}_k\right\} \tag{A.31}$$

and therefore

$$\text{vec}\left\{\mathbf{M}_k^{'}\right\}^T=\text{vec}\left\{\mathbf{R}_k\right\}^T\left[\mathbf{I}\otimes\left[\mathbf{A}+\mathbf{B}\mathbf{N}_k\mathbf{C}\right]+\left[\mathbf{A}+\mathbf{B}\mathbf{N}_k\mathbf{C}\right]\otimes\mathbf{I}\right]^{-1} \tag{A.32}$$

Next, equation (A.5) is also expressed in vectorized form to render

$$\left[\mathbf{I}\otimes\left[\mathbf{A}+\mathbf{B}\mathbf{N}_k\mathbf{C}\right]+\left[\mathbf{A}+\mathbf{B}\mathbf{N}_k\mathbf{C}\right]\otimes\mathbf{I}\right]\text{vec}\left\{\mathbf{L}_k\right\}=-\text{vec}\left\{\mathbf{Y}\right\} \tag{A.33}$$

Considering (A.32) and (A.33), it follows that

$$J_k^{'}(0)=-\text{vec}\left\{\mathbf{R}_k\right\}^T\text{vec}\left\{\mathbf{L}_k\right\} \tag{A.34}$$

and therefore $J_k^{'}(0)$ can be written as

$$J_k^{'}(0)=-\,\text{tr}\left\{\mathbf{R}_k^T\mathbf{L}_k\right\} \tag{A.35}$$

Sign of $J_k^{'}(0)$

By considering the definitions of the matrices $\mathbf{P}_k$ and $\mathbf{R}_k$, given by equations (A.13) and (A.29), respectively, it is possible to write the expression for the derivative $J^{'}(0)$ in expanded form as follows:

$$\begin{aligned}J_k^{'}(0)=-2\,\text{tr}\Big\{&\mathbf{\Pi}_k\mathbf{L}_k^{1/2}\left[\mathbf{M}_k\mathbf{B}\mathbf{N}_k\mathbf{C}+\mathbf{C}^T\mathbf{N}_k^T\mathbf{B}^T\mathbf{M}_k+\right.\\&\left.+\mathbf{M}_k\mathbf{B}^T\mathbf{W}_{\mathbf{2}}^{-1}\mathbf{B}\mathbf{M}_k+\mathbf{C}^T\mathbf{N}_k^T\mathbf{W}_{\mathbf{2}}\mathbf{N}_k\mathbf{C}\right]\mathbf{L}_k^{1/2}\mathbf{\Pi}_k\Big\}\end{aligned} \tag{A.36}$$

where the matrix $\mathbf{\Pi}_k$ is given by

$$\mathbf{\Pi}_k=\mathbf{L}_k^{1/2}\mathbf{C}^T\left[\mathbf{C}\mathbf{L}_k\mathbf{C}^T\right]^{-1}\mathbf{C}\mathbf{L}_k^{1/2} \tag{A.37}$$

If a matrix $\mathbf{V}_k$ is defined as

$$\mathbf{V}_k = \mathbf{M}_k\mathbf{B} + \mathbf{C}^T\mathbf{N}_k^T\mathbf{W_2} \tag{A.38}$$

then the derivative $J_k^{'}(0)$ can be written as

$$J_k^{'}(0) = -2\,\mathrm{tr}\left\{\mathbf{\Pi}_k\mathbf{L}_k^{1/2}\mathbf{V}_k\mathbf{W}_2^{-1}\left[\mathbf{\Pi}_k\mathbf{L}_k^{1/2}\mathbf{V}_k\right]^T\right\} \tag{A.39}$$

Since $\mathbf{W}_2$ is positive definite, so is $\mathbf{W}_2^{-1}$. Therefore, the matrix argument in the above expression is positive semi-definite, i.e.

$$\mathbf{\Pi}_k\mathbf{L}_k^{1/2}\mathbf{V}_k\mathbf{W}_2^{-1}\left[\mathbf{\Pi}_k\mathbf{L}_k^{1/2}\mathbf{V}_k\right]^T \geq 0 \tag{A.40}$$

and hence

$$J_k^{'}(0) \leq 0 \tag{A.41}$$

Furthermore, $J_k^{'}(0)$ is equal to zero if and only if

$$\mathbf{\Pi}_k\mathbf{L}_k^{1/2}\mathbf{V}_k = 0 \tag{A.42}$$

Considering the definition for $\mathbf{\Pi}_k$ given in equation (A.37), it is easy to show that the above condition is equivalent to

$$\mathbf{C}\mathbf{L}_k\mathbf{V}_k = 0 \tag{A.43}$$

and taking into account (A.38), it follows that $J_k^{'}(0)$ is equal to zero if and only if $\mathbf{N}_k$ satisfies exactly its defining equation, given by

$$\mathbf{N}_k = -\mathbf{W_2}^{-1}\mathbf{B}^T\mathbf{M}_k\mathbf{L}_k\mathbf{C}^T\left[\mathbf{C}\mathbf{L}_k\mathbf{C}^T\right]^{-1} \tag{A.44}$$

Therefore, considering (A.13), it follows that if $\mathbf{P}_k \neq \mathbf{0}$ then $J_k^{'}(0) < 0$.

Matrix $\mathbf{M}_k$

After some rearrangement, the governing equation for the matrix $\mathbf{M}_k$, given by (A.6), can be written in the following form:

$$\mathbf{M}_k\mathbf{B}\mathbf{N}_k\mathbf{C} + \mathbf{C}^T\mathbf{N}_k^T\mathbf{B}^T\mathbf{M}_k + \mathbf{C}^T\mathbf{N}_k^T\mathbf{W_2}\mathbf{N}_k\mathbf{C} = -\mathbf{A}^T\mathbf{M}_k - \mathbf{M}_k\mathbf{A} - \mathbf{W_1} \tag{A.45}$$

and considering the matrix $\mathbf{V}_k$, defined in (A.38), it is easy to see that

$$\mathbf{M}_k\mathbf{B}\mathbf{N}_k\mathbf{C} + \mathbf{C}^T\mathbf{N}_k^T\mathbf{B}^T\mathbf{M}_k + \mathbf{C}^T\mathbf{N}_k^T\mathbf{W_2}\mathbf{N}_k\mathbf{C} = \mathbf{V}_k\mathbf{W}_2^{-1}\mathbf{V}_k^T - \mathbf{M}_k\mathbf{B}^T\mathbf{W}_2^{-1}\mathbf{B}\mathbf{M}_k \tag{A.46}$$

Therefore, one can conclude that the matrix $\mathbf{M}_k$ satisfies the following equation:

$$\mathbf{A}^T\mathbf{M}_k + \mathbf{M}_k\mathbf{A} - \mathbf{M}_k\mathbf{B}^T\mathbf{W}_2^{-1}\mathbf{B}\mathbf{M}_k + \left[\mathbf{W_1} + \mathbf{V}_k\mathbf{W}_2^{-1}\mathbf{V}_k^T\right] = \mathbf{0} \tag{A.47}$$

which is the algebraic Ricatti equation corresponding to a full state feedback solution of the following problem:

- Minimize

$$\hat{J}_k = \int_0^\infty \left(\mathbf{y_c}^T\left[\mathbf{W_1} + \mathbf{V}_k\mathbf{W}_2^{-1}\mathbf{V}_k^T\right]\mathbf{y_c} + \mathbf{y_2}^T\mathbf{W_2}\mathbf{y_2}\right)dt \tag{A.48}$$

- Subject to the state equations

$$\dot{\mathbf{y}}_\mathbf{c} = \mathbf{A}\,\mathbf{y_c} + \mathbf{B}\,\mathbf{y_2} \tag{A.49}$$

References

[1] Ambrosino, G., Celentano, C. and Garofalo, F., "Variable Structure Model Reference Adaptive Control Systems", International Journal of Control, Vol. 39, pp. 1339-1349 (1984).

[2] Anderson, B.D.O. and Moore, J.B., *Optimal Control: Linear Quadratic Methods*, Prentice-Hall, Englewood-Cliffs, NJ (1990).

[3] Balas, M., "Active Control of Flexible Systems", Journal of Optimization Theory and Applications, Vol. 25, pp. 415-436 (1978).

[4] Balas, M., "Direct Output Feedback Control of Large Space Structures", Journal of the Astronautical Sciences, Vol. 27, No. 2, pp. 157-180 (1979).

[5] Balas, M., "Direct Velocity Feedback Control of Large Space Structures", Journal of Guidance and Control, Vol. 2, No. 3, pp. 252-253 (1979).

[6] Brandin, V.N. and Razorenov, G.N., "Decoupling of Nonlinear Dynamic Systems", Automation and Remote Control, No. 10, pp. 1405-1410 (1979).

[7] Brogan, W.L., *Modern Control Theory*, 3rd Ed., Prentice-Hall, Englewood-Cliffs, NJ (1991).

[8] Broussard, J.R. and Halyo, N., "Active Flutter Control using Discrete Optimal Constrained Dynamic Compensators", Proceedings of the American Control Conference, San Francisco, CA, pp. FA5 1026-1034 (1983).

[9] Burton, J. A. and Zinober, A., "Continuous Approximation of Variable Structure Control", International Journal of Systems Science, Vol. 17, No. 6, pp. 875-885 (1986).

[10] Chang, J.C. and Soong, T.T., "Structural Control using Active Tuned Mass Dampers", Journal of the Engineering Mechanics Division, ASCE, Vol. 106, No. 6, pp 1091-1098 (1980).

[11] Chung, L.L., Lin, R.C., Soong, T.T. and Reinhorn, A.M., "Experimental Study of Active Control for MDOF Seismic Structures," Journal of Engineering Mechanics, ASCE, Vol. 115, No. 8, pp. 1609-1627 (1989).

[12] Constantinou, M.C. and Symans, M.D., "Experimental and Analytical Investigation of Seismic Response of Structures with Supplemental Fluid Viscous Dampers", Technical Report NCEER-92-0032, National Center for Earthquake Engineering Research, State University of New York at Buffalo, Buffalo, NY (1992).

[13] Corless, M. and Leitmann, G., "Continuous State Feedback Guaranteeing Uniform Ultimate Boundedness for Uncertain Dynmic Systems", IEEE Transactions on Automatic Control, Vol. 26, pp. 1139-1144 (1981).

[14] DeCarlo, R.A., Zak, S.H. and Matthews, G.P., "Variable Structure Control of Nonlinear Multivariable Systems: A Tutorial", Proceedings IEEE, Vol. 76, pp. 212-232 (1988).

[15] Dennis, J and Schnabel, R., *Numerical Methods for Unconstrained Optimization and Nonlinear Equations*, Prentice-Hall, Englewood-Cliffs, NJ (1983).

[16] Dora, P., Abdall, C. and Cero, V., *Linear-Quadratic Control: An Introduction*, Prentice-Hall, Englewood-Cliffs, NJ (1995).

[17] Dorling, C.M. and Zinober, A., "Two Approaches to Hyperplane Design in Multivariable Variable Structure Control Systems", International Journal of Control, Vol. 44, pp. 65-82 (1986).

[18] Dorling, C.M. and Zinober, A., "Robust Hyperplane Design in Multivariable Variable Structure Control Systems", International Journal of Control, Vol. 48, pp. 2043-2054 (1988).

[19] Drazenovic, B., "The Invariance Conditions in Variable Structure Systems", Automatica, Vol. 5, pp. 287-295 (1969).

[20] Dyke, S.J., Spencer, B.F., Belknap, A.E., Ferrel, K.J., Quast, P. and Sain, M.K., "Absolute Acceleration Feedback Control Strategies for the Active Mass Driver", Proceedings of the 1st World Conference on Structural Control, August 3-5, Pasadena, CA (1994).

[21] Dyke, S.J., Spencer, B.F., Quast, P., Sain, M.K., Kaspari, D.C. and Soong, T.T., "Acceleration Feedback Control of MDOF Structures", Journal of Engineering Mechanics, ASCE, Vol. 122, No. 9, pp. 907-918 (1996).

[22] Dyke, S.J., Spencer, B.F., Sain, M.K. and Carlson, J.D., "A New Semi-Active Control Device for Seismic Response Reduction", Proceedings of the 11th Engineering Mechanics Conference, ASCE, May 19-22, Fort Lauderdale, FL, pp. 886-889 (1996).

[23] Faravelli, L and Venini, P., "Active Structural Control by Neural Networks", Journal of Structural Control, Vol. 1, pp. 79-101 (1994).

[24] Feng, M.Q., Shinozuka, M. and Fujii, S., "Experimental and Analytical Study of a Hybrid Isolation System using Friction Controllable Sliding Bearings", Technical Report NCEER-92-0009, National Center for Earthquake Engineering Research, State University of New York at Buffalo, Buffalo, NY (1992).

[25] Friedland, B., *Control System Design: An Introduction to State-Space Methods*, McGraw-Hill, New York, NY (1986).

[26] Gavin, H.P., Hanson, R.D. and McClamroch, N.H., "Control of Structures using ER Dampers", Proceedings of the 11th World Conference on Earthquake Engineering, June 23-28, Acapulco, Mexico, paper #, (1996).

[27] Golub, G.H. and Van Loan, C.F., *Matrix Computations*, 2nd Ed., Jonhs Hopkins University Press, Baltimore, MD (1989).

[28] Gupta, N.K., "Frequency-Shaped Cost Functionals: Extension of Linear-Quadratic-Gaussian Design Methods", Journal of Guidance and Control, Vol. 3, pp. 529-535 (1980).

[29] Hrovat, D., Barak, P. and Rabins, M., "Semi-Active versus Passive or Active Tuned Mass Dampers for Structural Control", Journal of Engineering Mechanics, ASCE, Vol. 109, No. 3, pp. 691-705 (1983).

[30] Igusa, T. and Xu, K., "Vibration Control using Multiple Tuned Mass Dampers", Journal of Sound and Vibration, (1994).

[31] Inaudi, J.A. and Kelly, J.M., "Variable-Structure Homogeneous Control Systems", Proceedings of the 1st International Workshop on Structural Control, August 5-7, Honolulu, HI, pp. 224-237 (1993).

[32] Inaudi, J.A. and Kelly, J.M., "Nonlinear Homogeneous Dynamical Systems", Technical Report UCB/EERC-93/11, Earthquake Engineering Research Center, University of California at Berkely, Berkeley, CA (1995).

[33] Itkis, U., *Control Systems of Variable Structure*, John Wiley & Sons, New York, NY (1976).

[34] Jabbari, F., Schmitendorf, W.E. and Yang, J.N., "H_∞ Control for Seismic-Excited Buildings with Acceleration Feedback", Journal of Engineering Mechanics, ASCE, Vol. 121, No. 9, pp. 994-1002 (1995).

[35] Jacobson, D.H., *Extensions of Linear Quadratic Control, Optimization and Matrix Theory*, Academic Press, New York (1977).

[36] Joghataie, A. and Ghaboussi, J., "A Comparative Study of Learning Methods and Mathematical Algorithms in Structural Control", Proceedings of the 11th World Conference on Earthquake Engineering, Paper No. 1432, Acapulco, Mexico, June 23-28 (1996).

[37] Kamagata, S. and Kobori, T. "Autonomous Adaptive Control of Active Variable Stiffness System for Seismic Ground Motion, Proceedings of the 1st World Conference on Structural Control, August 3-5, Los Angeles, CA, pp. TA4 33-42 (1994).

[38] Karnopp, D., "Design Principles for Vibration Control Systems using Semi-Active Dampers", ASME Journal of Dynamical Systems, Measurement and Control, Vol. 112, pp. 448-445 (1990).

[39] Kawashima, K. and Unjoh, S., "Variable Dampers and Variable Stiffness for Seismic Control of Bridges", Proceedings of the 1st International Workshop on Structural Control, August 5-7, Honolulu, HI, pp. 283-297 (1993).

[40] Kirk, D.E., *Optimal Control Theory*, Prentice-Hall, Englewood-Cliffs, NJ (1970).

[41] Kobori, T. and Minai, R., "Analytical Study on Active Seismic Response Control", Transactions of the Architectural Institute of Japan, No. 66, pp. 257-260 (1960).

[42] Kobori, T. and Kamagata, S., "Active Variable Stiffness System", Proceedings of the U.S.-Italy-Japan Workshop Symposium on Structural Control and Intelligent Systems, July 13-15, Sorrento, Italy, pp. 140-153 (1992).

[43] Kobori, T., Takahashi, M. Nasu, T. and Niwa, N., "Seismic Response Controlled Structure with Active Variable Stiffness System", Earthquake Engineering and Structural Dynamics, Vol. 22, pp. 925-941 (1993).

[44] Kobori, T., "Future Directions on Research and Development of Seismic-Response-Controlled Structures", Proceedings of the 1st World Conference on Structural Control, August 3-5, Los Angeles, CA, Vol. 1, pp. Panel_19-Panel_31 (1994).

[45] Kwakernaak, H. and Sivan, R., *Linear Optimal Control Systems*, John Wiley & Sons, New York, NY (1972).

[46] Lancaster, P. and Tismenetsky, M., *The Theory of Matrices with Applications*, 2nd Ed., Academic Press, Orlando, FL (1985).

[47] Leitmann, G., "Guaranteed asymptotic stability for some linear systems with bounded disturbances", ASME Journal of Dynamic Systems, Measurements and Control, Vol. 23, pp. 1079-1085 (1978).

[48] Levine, W.S. and Athans, M., "On the Determination of the Optimal Constant Output Feedback Gains for Linear Multivariable Systems", IEEE Transactions on Automatic Control, Vol. 15, No. 1, pp. 44-48 (1970).

[49] Lukyanov, A.G. and Utkin, V.I., "Methods of Reducing Equations for Dynamic Systems to a Regular Form", Automation and Remote Control, No. 4, pp. 413-420 (1981).

[50] McClamroch, N.H. and Gavin, H.P., "Closed-Loop Structural Control using ER Dampers", Proceedings of the American Control Conference, Seattle, WA, June, pp. 4173-4177 (1995).

[51] McClamroch, N.H. and Gavin, H.P., "ER Dampers and Semi-Active Structural Control", Proceedings of the 34th Conference on Decision and Control, New Orleans, LA, December, pp. 3528-3533 (1995).

[52] Martin, C.R. and Soong, T.T., "Modal Control of Multistorey Structures", Journal of the Engineering Mechanics Division, ASCE, Vol. 102, No. 4, pp. 613-632 (1976).

[53] Masri, S.F., Bekey, G. and Caughey, T.K., "Optimal Pulse Control of Flexible Structures", Journal of Applied Mechanics, Vol. 48, pp. 619-626 (1981).

[54] Meirovitch, L. and Oz, H., "Active Control of Structures by Modal Synthesis", *Structural Control*, Leipholz, H.H. (Ed.), North Holland, Armsterdam, pp. 505-521 (1980).

[55] Meirovitch, L., *Dynamics and Control of Structures*, John Wiley & Sons, New York (1990).

[56] Mendel, J.H., "A Concise Derivation of Optimal Constant Limited State Feedback Gains", IEEE Transactions on Automatic Control, Vol. 19, pp. 447-448 (1974).

[57] Moerder, D.D. and Calise, A.J., "Convergence of a Numerical Algorithm for Calculating Optimal Output Feedback Gains", IEEE Transactions on Automatic Control, Vol. AC-30, No. 9, pp. 900-903 (1984).

[58] Nagarajaiah, S., Feng, M. and Shinozuka, M., "Control of Structures with Friction Controllable Sliding Isolation Bearings", Soil Dynamics and Earthquake Engineering, Vol. 12, pp. 103-112 (1993).

[59] Nemir, D.C., Lin, Y. and Osegueda, R.A., "Semi-Active Motion Control using Variable Stiffness", Journal of Engineering Mechanics, ASCE, Vol. 120, No. 4, pp. 1291-1305 (1994).

[60] Pantelides, C.P. and Nelson, P.A., "Continuous Pulse Control of Structures with Material Nonlinearity", Earthquake Engineering and Structural Dynamics, Vol. 24, pp. 263-282 (1995).

[61] Patten, W.N., Kuo, C.C., He, Q., Liu, L. and Sack, R.L., "Seismic Structural Control via Hydraulic Semi-Active Vibration Dampers", Proceedings of the 1st World Conference on Structural Control, August 3-5, Los Angeles, CA, pp. FA2 83-89 (1994).

[62] Patten, W.N., Sack, R.L. and He, Q., "Controlled Semi-Active Hydraulic Vibration Absorber for Bridges", Journal of Structural Engineering, ASCE, Vol. 122, No. 2, pp. 187-192 (1996).

[63] Pong, W.S., Tsai, C.S. and Lee, G.C., "Seismic Study of Building Frames with Added Energy-Absorbing Devices", Technical Report NCEER-94-0016, National Center for Earthquake Engineering Research, State University of New York at Buffalo, Buffalo, NY (1994).

[64] Reinhorn, A.M., Manolis, G.D. and Wen, C.Y., "Active Control of Inelastic Structures", Journal of Engineering Mechanics, ASCE, Vol. 113, No. 3, pp. 315-333 (1987).

[65] Rodellar, J., Barbat, A.H. and Martin-Sanchez, J.M., "Predictive Control of Structures", Journal of Engineering Mechanics, ASCE, Vol. 113, No. 6, pp. 797-812 (1987).

[66] Rodellar, J., Chung, L.L., Soong, T.T. and Reinhorn, A.M., "Experimental Digital Control of Structures", Journal of Engineering Mechanics, ASCE, Vol. 115, No. 6, pp. 1245-1261 (1989).

[67] Roorda, J., "Tendon Control in Tall Structures", Journal of the Structural Division, ASCE, Vol. 101, No. 3, pp. 505-521 (1975).

[68] Ryan, E.P. and Corless, M., "Ultimate Boundedness and Asymptotic Stability of a Class of Uncertain Dynamical Systems via Continuous and Discontinuous Feedback Control", IMA Journal Math. Control and Optimization, Vol. 1, pp. 223-242 (1984).

[69] Sack, R.L. and Patten, W.N., "Semi-Active Hydraulic Structural Control", Proceedings of the 1st International Workshop on Structural Control, pp. 417-431 (1993).

[70] Sakamoto, M. and Kobori, T., "Practical Applications of Active and Hybrid Response Control Systems", Proceedings of the 1st International Workshop on Structural Control, August 5-7, Honolulu, Hawaii, pp. 432-446 (1993).

[71] Schmitendorf, W.E., Jabbari, F. and Yang, J.N., "Robust Control for Buildings under Earthquakes", Structural Engineering in Natural Hazards Mitigation, Proceedings of the ASCE Structures Congress 1993, April 19-21, Irvine, CA, Vol. 1, pp. 700-705 (1993).

[72] Schmitendorf, W.E., Jabbari, F. and Yang, J.N., "Robust Control Techniques for Buildings under Earthquake Excitation", Earthquake Engineering and Structural Dynamics, Vol. 23, pp. 539-552 (1994).

[73] Schmitendorf, W.E., Kose, I.E., Jabbari, F. and Yang, J.N., "H_∞ Control of Seismic-Excited Buildings using Direct Output Feedback", Proceedings of the 1st World Conference on Structural Control, August 3-5, Pasadena, CA, (1994).

[74] Slotine, J.J. and Sastry, S.S., "Tracking Control of Nonlinear Systems using Sliding Surfaces, with Applications to Robot Manipulators", International Journal of Control, Vol. 38, pp. 465-492 (1983).

[75] Soong, T.T., *Active Structural Control: Theory and Practice*, Longman Scientific and Technical, New York, NY (1990).

[76] Soong, T.T., "State-of-the-Art of Structural Control in USA", Proceedings of the US National Workshop on Structural Control Research, Los Angeles, October 25-26, pp. 48-65 (1990).

[77] Spencer, B.F., Suhardjo, J. and Sain, M.K., "Frequency Domain Control Algorithms for Civil Engineering Applications", Proceedings of the International Workshop on Technology for Hong Kong's Infrastructure Development, December 19-20, Hong Kong, pp. 169-178 (1991).

[78] Spencer, B.F., Dyke, S.J., Sain, M.K. and Quast, P., "Acceleration Feedback Control Strategies for Aseismic Protection", Proceedings of the American Control Conference, June 2-4, San Francisco, CA, pp. 1317-1321 (1993).

[79] Spencer, B.F., Suhardjo, J. and Sain, M.K., "Frequency Domain Optimal Control Strategies for Aseismic Protection", Journal of Engineering Mechanics, ASCE, Vol. 120, No. 1, pp. 135-158 (1994).

[80] Srinivasa, Y.G. and Rajogopalan, T., "Algorithms for the Computation of Optimal Output Feedback Gains", Proceedings of the 18th Conference on Decision and control, Fort Lauderdale, FL, pp. TP4 576-579 (1979).

[81] Strang, G., *Linear Algebra and its Applications*, 3rd Ed., Harcourt Brace Jovanovich Publishers, Orlando, FL (1988).

[82] Symans, M.D., Constantinou, M.C., Taylor, D.P. and Garnjost, K.D., "Semi-Active Fluid Viscous Dampers for Seismic Response Control", Proceedings of the 1st World Conference on Structural Control, August 3-5, Los Angeles, CA, pp. FA4 3-12 (1994).

[83] Symans, M.D. and Constantinou, M.C., "Development and Experimental Study of Semi-Active Fluid Damping Devices for Seismic Protection of Structures", Technical Report NCEER-95-0011, National Center for Earthquake Engineering Research, State University of New York at Buffalo, Buffalo, NY (1995).

[84] Tomasula, D.P., Spencer, B.F. and Sain, M.K., "Limiting Extreme Structural Responses using an Efficient Nonlinear Control Law", Proceedings of the 1st World Conference on Structural Control, August 3-5, Pasadena, CA, pp. (1994).

[85] Udwadia, F. and Tabaie, S., "Pulse Control of Single Degree-of-Freedom System", Journal of Engineering Mechanics, ASCE, Vol. 107, No. 6, pp. 997-1009 (1981).

[86] Udwadia, F. and Tabaie, S., "Pulse Control of Structural and Mechanical Systems", Journal of Engineering Mechanics, ASCE, Vol. 107, No. 6, pp. 1011-1028 (1981).

[87] Utkin, V.I., "Equations of the Sliding Regime in Discontinuous Systems - Part I", Automation and Remote Control, No. 12, pp. 42-54 (1971).

[88] Utkin, V.I., *Sliding Modes and their Application in Variable Structure Systems*, MIR Publishers, Moscow (1978).

[89] Utkin, V.I. and Young, K.D., "Methods for Constructing Discontinuous Planes in Multidimensional Variable Structure Systems", Automation and Remote Control, No. 31, pp. 1466-1470 (1978).

[90] Utkin, V.I., *Sliding Modes in Control and Optimization*, Springer-Verlag, Berlin (1992).

[91] Van de Vegte, J. and Hladun, A.R., "Design of Optimal Passive Beam Vibration Controls by Optimal Control Techniques", Journal of Dynamic Systems, Measurement and Control, pp. 427-434 (1973).

[92] Villaverde, R., "Reduction in Seismic Response with Heavily-Damped Vibration Absorbers", Earthquake Engineering and Structural Dynamics, Vol. 13, pp. 33-42 (1985).

[93] Wang, B.P., Kitis, L., Pilkey, W.D. and Palazzolo, A., "Synthesis of Dynamic Vibration Absorbers", Journal of Vibration, Acoustics, Stress, and Reliability in Design, Vol. 107, pp. 161-166 (1985).

[94] Warburton, G.B. and Ayorinde, E.O., "Optimum Absorber Parameters for Simple Systems", Earthquake Engineering and Structural Dynamics, Vol. 8, pp. 197-217 (1980).

[95] Wen, Y.-K., Ghaboussi, J., Venini, P. and Nikzad, K., "Control of Structures using Neural Networks", Proceedings of the US-Italy-Japan Workshop/Symposium on Structural Control and Intelligent Systems, Soorento, Italy, July 12-15, pp. 232-251 (1992).

[96] Wu, Z., Soong, T.T., Gattulli,V. and Lin, R.C., "Nonlinear Control Algorithms for Peak Response Reduction", Technical Report NCEER-95-0004, National Center for Earthquake Engineering Research, State University of New York at Buffalo, Buffalo, NY (1995).

[97] Wu, Z. and Soong, T.T., "Modified Bang-Bang Control Law for Structural Control Implementation", Journal of Engineering Mechanics, ASCE, Vol. 122, No. 8, pp. 771-777 (1996).

[98] Yang, J.N., "Aplications of Optimal Control Theory to Civil Engineering Structures", Journal of the Engineering Mechanics Division, ASCE, Vol. 101, No. 6, pp. 818-838 (1976).

[99] Yang, J.N. and Giannopoulos, F., "Active Tendon Control of Structures", Journal of the Engineering Mechanics Division, ASCE, Vol. 104, No. 3, pp. 551-568 (1978).

[100] Yang, J.N., Akbarpour, A. and Ghaemmaghami, P., "New Optimal Algorithms for Structural Control", Journal of Engineering Mechanics, ASCE, Vol. 113, No. 9, pp. 1369-1386 (1987).

[101] Yang, J.N., Long, F.X. and Wong, D., "Optimal Control of Nonlinear Structures", Journal of Applied Mechanics, ASME, Vol. 55, pp. 931-938 (1988).

[102] Yang, J.N. and Soong, T.T., "Recent Advances in Structural Control", Probabilistic Engineering Mechanics, Vol. 3, No. 4, pp. 179-188 (1989).

[103] Yang, J.N., Akbarpour, A., "Effect of System Uncertainty on Control of Seismic-Excited Buildings", Journal of Engineering Mechanics, ASCE, Vol. 116, No. 2, pp. 462-478 (1990).

[104] Yang, J.N., Li, Z. and Liu, S.C., "Stable Controllers for Instantaneous Optimal Control", Journal of Engineering Mechanics, ASCE, Vol. 118, No. 8, pp. 1612-1630 (1992).

[105] Yang, J.N., Li, Z. and Liu, S.C., "Control of Hysteretic Systems using Velocity and Acceleration Feedbacks", Journal of Engineering Mechanics, ASCE, Vol. 118, No. 11, pp. 2227-2245 (1992).

[106] Yang, J.N. and Li, Z., "Active Stiffness Control of Seismic-Excited Buildings", Proceedings of the 3rd PanAmerican Congress of Applied Mechanics, PACAM III, January 4-8, Sao Paulo, Brazil, pp. 568-571 (1993).

[107] Yang, J.N., Li, Z. and Vongchavalitkul, S., "Hybrid Control of Seismic-Excited Bridge Structures using Variable Dampers", Structural Engineering in Natural Hazards Mitigation, Proceedings of the ASCE Structures Congress 1993, April 19-21, Irvine, CA, Vol. 1, pp. 778-783 (1993).

[108] Yang, J.N., Li, Z., Wu, J.C. and Young, K.K.D., "A Discontinuous Control Method for Civil Engineering Structures", Proceedings of the 9th VPI&SU Symposium on

Dynamics and Control of Large Structures, May 10-12, Blacksburg, VA, pp. 167-180 (1993).

[109] Yang, J.N., Li, Z. and Wu, J.C., "Discontinuous Nonlinear Control of Base-Isolated Buildings", Proceedings of the 1st International Workshop on Structural Control, August 5-7, Honolulu, HI, pp. 551-553 (1993).

[110] Yang, J.N., Li, Z. and Wu, J.C., "Control of Seismic-Excited Buildings using Active Variable Stiffness Systems", Proceedings of the American Control Conference, Baltimore, MD, pp. 1083-1088 (1994).

[111] Yang, J.N., Wu, J.C., Agrawal, A.K. and Li, Z., "Sliding Mode Control for Seismic-Excited Linear and Nonlinear Civil Engineering Structures", Technical Report NCEER-94-0017, National Center for Earthquake Engineering Research, State University of New York at Buffalo, Buffalo, NY (1994).

[112] Yang, J.N., Agrawal, A.K. and Wu, J.C., "Sliding Mode Control of Structures subjected to Seismic Loads", Proceedings of the 1st World Conference on Structural Control, August 3-5, Los Angeles, CA, pp. WA1 13-22 (1994).

[113] Yang, J.N., Wu, J.C., Reinhorn, A.M., Riley, M., Schmitendorf, W.E. and Jabbari, F., "Experimental Verifications of H_∞ and Sliding Mode Control for Seismic-Excited Buildings", Proceedings of the 1st World Conference on Structural Control, August 3-5, Los Angeles, CA, pp. TP4 63-72 (1994).

[114] Yang, J.N., Wu, J.C. and Hsu, S.Y., "Parametric Control of Seismic-Excited Structures", Proceedings of the 1st World Conference on Structural Control, August 3-5, Los Angeles, CA, pp. WP1 88-97 (1994).

[115] Yang, J.N., Wu, J.C., Kawashima, K. and Unjoh, S., "Hybrid Control of Seismic-Excited Bridge Structures", Earthquake Engineering and Structural Dynamics, Vol. 24, pp. 1437-1452 (1995).

[116] Yang, J.N., Wu, J.C. and Agrawal, A.K., "Sliding Mode Control for Seismically Excited Linear Structures", Journal of the Engineering Mechanics Division, ASCE, Vol. 121, No. 12, pp. 1386-1390 (1995).

[117] Yang, J.N., Wu, J.C., Reinhorn, A.M., Riley, M., Schmitendorf, W.E. and Jabbari, F.,"Experimental Verifications of H_∞ and Sliding Mode Control for Seismically Excited Buildings", Journal of Structural Engineering, ASCE, Vol. 122, No. 1, pp. 69-75 (1996).

[118] Yang, J.N., Wu, J.C., Reinhorn, A.M. and Riley, M., "Control of Sliding-Isolated Buildings using Sliding Mode Control", Journal of Structural Engineering, ASCE, Vol. 122, No. 2, pp. 179-186 (1996).

[119] Yao, J.T.P., "Concept of Structural Control", Journal of the Structural Division, ASCE, Vol. 98, No. 7, pp. 1567-1574 (1972).

[120] Yao, J.T.P. and Sae-Ung, S., "Active Control of Building Structures", Journal of the Engineering Mechanics Division, ASCE, Vol. 104, No. 2, pp. 335-350 (1978).

[121] Young, K.D. and Ozguner, U., "Frequency Shaping Compensator Design for Sliding Mode", International Journal of Control, Vol. 57, No. 5, pp. 1005-1019 (1993).

[122] Zhou, F. and Fisher, D.G., "Continuous Sliding Mode Control", International Journal of Control, Vol. 55, pp. 313-327 (1992).

Vita

Enrique Eduardo Matheu was born on March 20, 1964 in the city of Cordoba, Republic of Argentina, the youngest of three children of Chiche and Carlos Matheu. During his high school years, he attended the Colegio Nacional de Monserrat in Cordoba, where he was awarded the Gold Medal for graduating with the highest GPA of his class in 1981. He attended the National University of Cordoba (UNC), where he received a Bachelor of Science in Civil Engineering in March, 1988, and was awarded the University Award for being the student with the highest GPA among his graduating class. Among other awards, he received a two-year research fellowship granted by the National Council for Scientific and Technological Research (CONICET). He also taught as an instructor in the College of Engineering at the UNC. In January, 1991, he went to pursue graduate studies at the University of Puerto Rico at Mayaguez, in Mayaguez, Puerto Rico. After receiving the degree of Master of Science in Civil Engineering in June, 1992, he joined the graduate school of the Virginia Polytechnic Institute & State University, in Blacksburg, Virginia, where he worked under the tutelage of Prof. M. P. Singh. During the last summer of his graduate studies, he worked as a contractor for the Structures Laboratory of the US Army Engineer Waterways Experiment Station located in Vicksburg, Mississippi. He received the degree of Doctor of Philosophy in Engineering Mechanics in May, 1997. Upon graduating, he will join the Structural Mechanics Division at the Waterways Experiment Station as a research structural engineer.